

**Structural and functional  
characterization of  
G protein-coupled adenosine receptors  
and the orphan receptor GPR143**

Dissertation

zur

Erlangung des Doktorgrades (Dr. rer. nat.)

der

Mathematisch-Naturwissenschaftlichen Fakultät

der

Rheinischen Friedrich-Wilhelms-Universität Bonn

vorgelegt von

Elisabetta De Filippo

aus

Brescia

Bonn 2015



Angefertigt mit Genehmigung der Mathematisch-Naturwissenschaftlichen Fakultät  
der Rheinischen Friedrich-Wilhelms-Universität Bonn

1. Gutachter: Prof. Dr. Christa E. Müller

2. Gutachter: PD Dr. Anke C. Schiedel

Tag der Promotion: 20.04.2016

Erscheinungsjahr: 2016



Die vorliegende Arbeit wurde in der Zeit von März 2012 bis Dezember 2015 am Pharmazeutischen Institut, Pharmazeutische Chemie I, Bonn unter der Leitung von Frau Prof. Dr. Christa E. Müller und von Frau PD Dr. Anke C. Schiedel durchgeführt.

## Table of contents

<b>1. Introduction.....</b>	<b>3</b>
<b>1.1 G protein-coupled receptors .....</b>	<b>3</b>
<b>2. Characterization of adenosine A<sub>2A</sub> and A<sub>2B</sub> receptor subtypes .....</b>	<b>10</b>
<b>2.1 Purinergic receptors .....</b>	<b>10</b>
<b>2.2 Adenosine receptors .....</b>	<b>11</b>
<b>2.3 Cristallographic structures and structural insight.....</b>	<b>12</b>
<b>2.4 Aim of the project.....</b>	<b>17</b>
<b>2.5 Part I: the human adenosine A<sub>2A</sub>(ECL2 A<sub>2B</sub>) chimera .....</b>	<b>20</b>
2.5.1 Generation and characterization of the loop exchange mutant.....	20
2.5.2 Radioligand binding studies .....	21
2.5.3 Functional studies .....	26
2.5.4 Discussion .....	30
<b>2.6 Part II: the cysteine mutant adenosine A<sub>2A</sub> receptors.....</b>	<b>35</b>
2.6.1 Potential role of disulfide bonds in the adenosine A <sub>2A</sub> receptor .....	35
2.6.2 Generation and characterization of mutant cell lines.....	36
2.6.3 Functional studies .....	38
2.6.4 Binding studies .....	41
2.6.5 Binding mode and interactions .....	44
2.6.6 Models of cysteine mutant adenosine A <sub>2A</sub> receptors .....	46
2.6.7 Discussion .....	48
<b>3. Characterization of the G protein coupled-receptor GPR143.....</b>	<b>55</b>
<b>3.1 Albinism .....</b>	<b>55</b>
<b>3.2 Ocular Albinism type I.....</b>	<b>56</b>
<b>3.3 GPR143 receptor .....</b>	<b>56</b>
<b>3.4 Subcellular localization debate .....</b>	<b>59</b>
<b>3.5 Intracellular signaling pathway and ligands .....</b>	<b>60</b>
<b>3.6 Tyrosinase .....</b>	<b>61</b>
<b>3.7 GPR143 functions.....</b>	<b>64</b>
<b>3.8 Aim of the project.....</b>	<b>65</b>
<b>3.9 Part I: GPR143 ligands as pharmacological tools to analyze receptor function .....</b>	<b>67</b>
3.9.1 Characterization of wildtype and mutant GPR143 in CHO cells .....	67
3.9.2 GPR143 stimulation with levodopa.....	70
3.9.3 Compound library screening.....	71
3.9.4 Validation of hit compounds.....	74
3.9.5 Tyrosinase activity.....	75
3.9.6 Discussion .....	77
<b>3.10 Part II: investigation of GPR143-tyrosinase interaction .....</b>	<b>82</b>
3.10.1 Characterization of GPR143 in COS7 and melan-a cells .....	82
3.10.2 Colocalization of GPR143 and tyrosinase in COS7 and melan-a cells .....	84
3.10.3 Immunoprecipitation of GPR143 and tyrosinase .....	85
3.10.4 Fluorescence Resonance Energy Transfer (FRET).....	87
3.10.5 Discussion .....	92
<b>4. Summary .....</b>	<b>99</b>
<b>5. Materials .....</b>	<b>105</b>
<b>5.1 Chemicals and tested compounds .....</b>	<b>105</b>
<b>5.2 Instruments.....</b>	<b>107</b>
<b>5.3 Cell lines and culture media .....</b>	<b>108</b>
<b>5.4 Radioligands .....</b>	<b>109</b>
<b>5.5 Buffers.....</b>	<b>109</b>

<b>5.6 Antibodies</b> .....	<b>110</b>
<b>5.7 Mutagenesis primers</b> .....	<b>111</b>
<b>5.8 Materials for molecular biology</b> .....	<b>112</b>
<b>6. Methods</b> .....	<b>113</b>
<b>6.1 Cell culture</b> .....	<b>113</b>
6.1.1 General conditions and handling .....	113
6.1.2 Transient transfection .....	113
6.1.3 Stable transfection.....	114
<b>6.2 Membrane preparation</b> .....	<b>115</b>
<b>6.3 Molecular biology</b> .....	<b>115</b>
6.3.1 Cloning.....	115
6.3.1.1 Polymerase Chain Reaction (PCR).....	115
6.3.1.2 Analysis and separation of PCR products.....	116
6.3.1.3 Enzymatic digestion .....	116
6.3.1.4 Ligation.....	117
6.3.1.5 Production of competent E.coli with Calcium Chloride.....	117
6.3.1.6 Transformation of chemocompetent bacteria.....	117
6.3.1.7 Colony screening and MiniPreps .....	118
6.3.1.8 Plasmid preparation by Midipreps.....	118
6.3.1.9 Site-directed mutagenesis .....	119
6.3.1.10 Gibson assembly master mix.....	120
6.3.2 Quantitative PCR (qPCR) .....	121
6.3.2.1 mRNA extraction .....	121
6.3.2.2 DNaseI digestion.....	122
6.3.2.3 Reverse transcription.....	122
6.3.2.4 Real Time PCR.....	122
<b>6.4 Immunohistochemistry</b> .....	<b>123</b>
<b>6.5 Bradford protein assay</b> .....	<b>124</b>
<b>6.6 Western Blot</b> .....	<b>124</b>
<b>6.7 Immunoprecipitation</b> .....	<b>125</b>
<b>6.8 Glycosylation studies</b> .....	<b>126</b>
<b>6.9 Fluorescence Resonance Energy Transfer (FRET)</b> .....	<b>127</b>
<b>6.10 Enzyme-linked immunosorbent assay (ELISA)</b> .....	<b>130</b>
<b>6.11 MTT assay</b> .....	<b>130</b>
<b>6.12 Melanin assay</b> .....	<b>131</b>
<b>6.13 Tyrosinase activity in cell lysates</b> .....	<b>131</b>
<b>6.14 Functional assays</b> .....	<b>132</b>
6.14.1 $\beta$ -arrestin recruitment assay.....	132
6.14.2 Calcium mobilization assay.....	133
6.14.3 cAMP accumulation assay.....	134
<b>6.15 Radioligand binding</b> .....	<b>136</b>
<b>6.16 Molecular Docking</b> .....	<b>137</b>
<b>7. References</b> .....	<b>138</b>
<b>8. Appendices</b> .....	<b>148</b>
<b>9. Abbreviations</b> .....	<b>151</b>
<b>10. Curriculum vitae</b> .....	<b>155</b>
<b>11. Acknowledgments</b> .....	<b>157</b>

# 1. Introduction

## 1.1 G protein-coupled receptors

The G protein coupled-receptors (GPCRs) form one of the largest superfamily of proteins in the mammalian genome, including more than 800 human genes [1]. Two main features characterize a receptor as a GPCR. The first requirement is the presence of seven amino acid sequences with high degree of hydrophobicity which represent seven  $\alpha$ -helices spanning the cell plasma membrane. Because of this element, GPCRs are also termed “seven transmembrane (7TM) receptors” [2]. The second requirement is the ability of the receptor to bind to heterotrimeric G proteins. The interaction between GPCRs and different subunits of G proteins is responsible for a large variety of alternative signaling pathways. The ligands of GPCRs cover a wide spectrum of extracellular signals including photons, ions, lipids, nucleotides, amines, peptides and entire proteins [2]. Therefore, GPCRs are one of the essential junction for the communication between external and internal environment of the cell. After ligand binding, the receptor is subjected to conformational changes which activate the complex cytosolic signaling network resulting in a cellular response [3].

Due to the large variety of biological functions and human diseases associated with GPCRs, these receptors are among the most pursued targets for drug development. It has been estimated that about 30% of all drugs currently on the market target GPCRs and since the knowledge about those receptors and their signalling pathways is constantly increasing the potential for drug discovery in this field is also immense [2].

Several classification systems have been used for the GPCR superfamily, including grouping of the receptors by their ligand binding mode or by structural features. The International Union of Basic and Clinical Pharmacology (IUPHAR) recommends one of the most frequently used systems which covers all GPCRs, in both vertebrates and invertebrates, and divides them in classes from A to F [4]. Some of those families do not exist in human, such as classes D and E, which correspond to fungal pheromone receptors, and class F, which contains archaebacterial opsin. Furthermore, vertebrates GPCRs can be classified into five main families (Fig 1) according to their pharmacological properties and to which the acronym GRAFS has been applied [3]:

- G: Glutamate or class C receptors
- R: Rhodopsin or class A receptors



- A: Adhesion or class B receptors
- F: Frizzled/TAS2 or class F receptors
- S: Secretin receptors, included in class B.

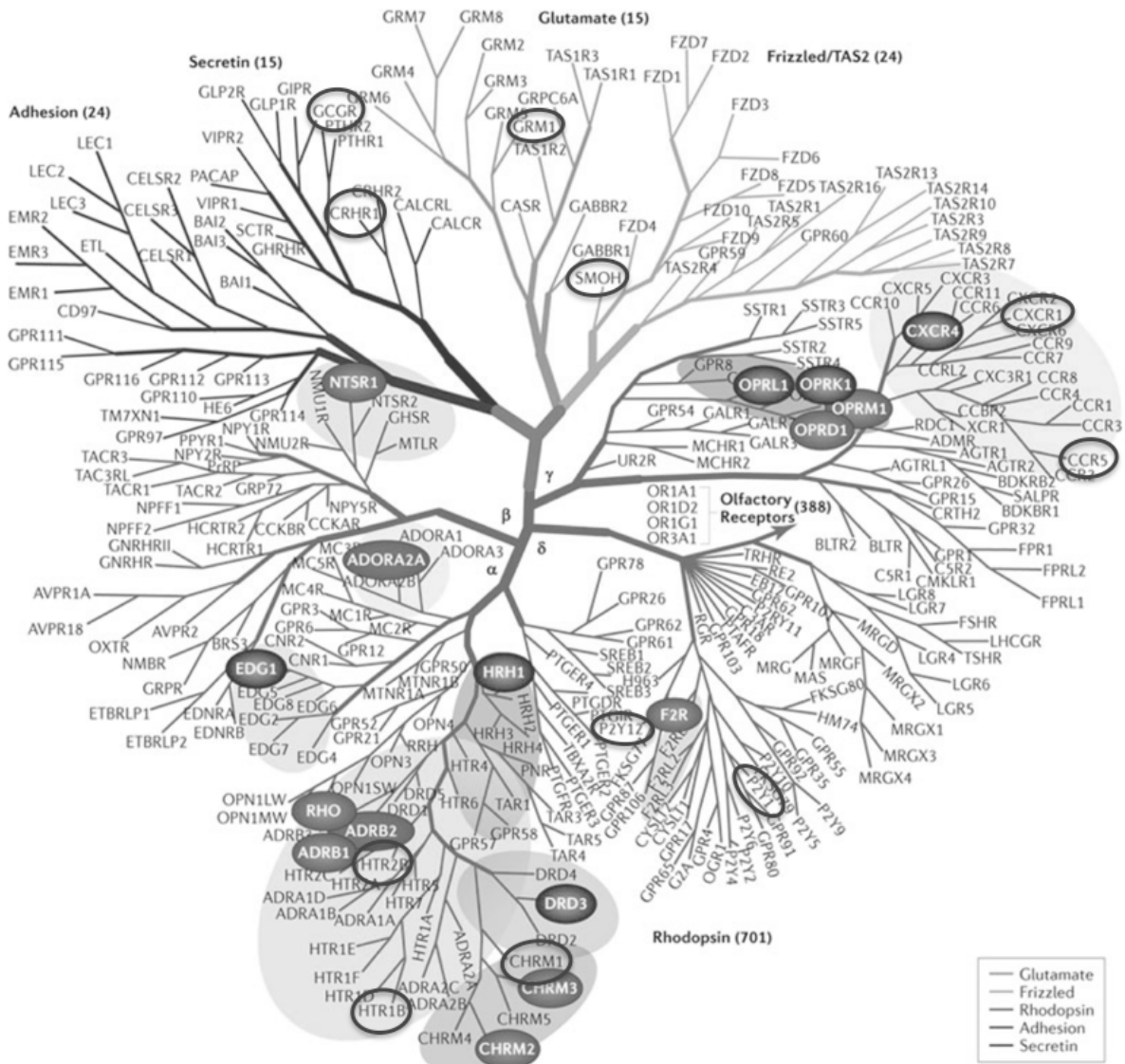


**Figure 1. Phylogenetic tree of the human GPCR superfamily.** The GPCRs can be classified into five families: Rhodopsin (class A), Secretin and Adhesion (class B), Glutamate (class C) and Frizzled/taste receptor 2. These families can be further divided into subfamilies according to their sequence similarity. The receptors are named according to their gene name, as used in UniProt database. Receptors whose crystal structure is solved are circled in red and blue. Adapted from [5].

The rhodopsin family is the largest and the most diverse class of GPCRs and the members are characterized by similar structural features and activation mechanisms. On the other hand, individual GPCRs are associated with unique signal transduction pathways involving multiple G protein subtypes and G protein-independent signalling processes [6].

Heterotrimeric G proteins are composed of an  $\alpha$ -,  $\beta$ - and  $\gamma$ -subunit and they are subjected to conformational changes leading to the exchange of GDP for GTP bound to the  $\alpha$ -subunit after receptor activation. Consequently, the heterotrimeric complex is dissociated into the  $G\alpha$ - and  $G\beta\gamma$ -subunits, which promote the stimulation of effector molecules (Fig 2), such as adenylate cyclases (AC), phosphodiesterases, phospholipase A<sub>2</sub> (PLA<sub>2</sub>), phospholipase C (PLC) and phosphoinositide 3-kinases (PI3Ks). Finally, they activate or inhibit the production of different second messengers (cAMP, cGMP, diacylglycerol, inositol (1,4,5)-triphosphate, arachidonic acid and intracellular calcium ions) [7].

The signaling of the activated GPCR is terminated by phosphorylation of the cytoplasmatic loops and tail of the receptor catalyzed by GPCR kinases (GRKs). As consequence, the arrestins ( $\beta$ -arrestin 1 and 2, mainly) are recruited and bind to the receptor which is internalized in clathrin-coated vesicles. Thus, in the classical GPCR model, heterotrimeric G proteins mediate the signal transduction while  $\beta$ -arrestins mediate receptor desensitization [8].

This classical model for GPCR mechanism of action is considered over-simplified and incomplete. Over the last decade, there has been evidence regarding the ability of  $\beta$ -arrestins to act not only as regulators of GPCR desensitization but also as adaptor proteins which have the ability to signal through multiple mediators, such as mitogen-activated protein kinases (MAPKs), nuclear factor- $\kappa$ B (NF- $\kappa$ B) and phosphoinositide 3-kinase (PI3K). In this new perspective, both heterotrimeric G proteins and  $\beta$ -arrestins are able of interacting with intracellular signaling molecules mediating distinct functional and physiological consequences [9].

The original model was based on the idea that most ligands binding to GPCRs have balanced or unbiased activity activity for signaling through  $\beta$ -arrestins or G proteins meaning that they can signal equally through both. However, for some GPCRs it has been found that depending on the ligand the receptor display bias toward one pathway over the other thus, it preferentially signal through the G protein- or  $\beta$ -arrestin-mediated pathway [8]. This behaviour is named biased agonism and it has important implications for the design of drugs

that target GPCRs because the signalling derived by these parallel pathways might have distinct functional consequences [8].

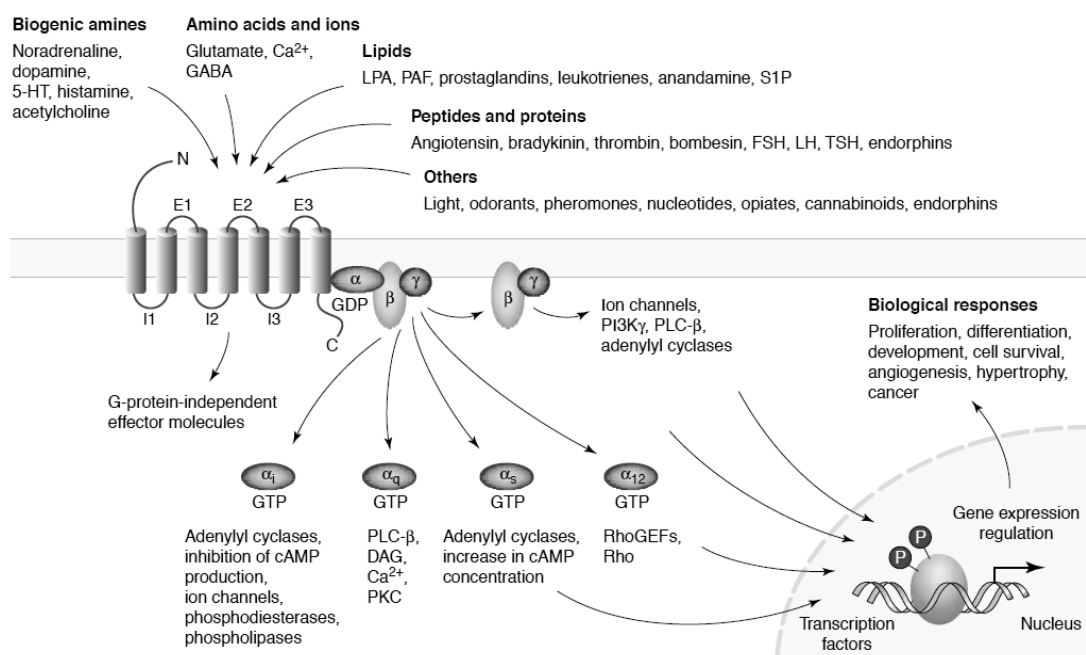


**Figure 2. Diversity of signaling pathways involved in the activation of GPCRs.** A large variety of ligands stimulate the receptors, activating heterotrimeric G protein-dependent and –independent pathways. The principal effector molecules are listed under the corresponding G protein subunit. GPCR activation regulates key biological functions, such as cell proliferation, cell survival and angiogenesis [7].

Since GPCRs have a fundamental role in health and disease, a detailed understanding of their structure and function is critical for new drug discovery. However, the characteristic flexibility of these receptors, important for their activity in physiological conditions, interferes with the traditional methods of crystallization and structure determination [5]. In 2000, the first crystal structure of a mammalian GPCR, the bovine rhodopsin, was solved and since then, rapid progresses in protein engineering and crystallography allowed an exponential growth in GPCR structure determination [10,11].

So far, three-dimensional structures of more than 20 different GPCRs have been solved, giving progressively new insights into protein function and their interaction with ligands or drugs [12,13]. Most of the solved structures belong to class A GPCRs, in particular to the cluster of aminergic receptors, of which many are relevant in pharmacology. Beyond the class A receptors, at least one crystal structure for each of the other classes of GPCRs have been

solved as well. Two structures of the secretin receptor family (class B) have been published, corticotropin releasing factor receptor 1 (CRF<sub>1</sub>R, [14]) and glucagone (GCGR, [15]), while for the metabotropic family (class C), the structures of the glutamate receptor 1 (mGluR1, [16]) and 5 (mGluR5, [17]) have been solved. For the adhesion family, several crystal structures of the neurotensin receptor (NTSR1, [18,19]) are available and for the smoothed receptor (SMOH, [20,21]) belonging to the Frizzled/TAS2 family, as well.

Several GPCRs have been co-crystallized in complexes with different ligands (agonists, antagonists, inverse agonists or allosteric compounds), different crystallization methods (i.e. lipidic cubic phase or with new detergents) or using different approaches for the receptor stabilization (i.e. generation of receptor-T4 lysozyme and receptor-apocytochrome chimeras, co-crystallization with monoclonal antibody fragments from mouse or camelids, receptor thermostabilization by scanning mutagenesis or engineering disulphide bonds) [3,11].

The structure of a GPCR can be divided in three main parts: the extracellular region, which consists in the N terminal tail and in three extracellular loops (ECL1-3), the transmembrane (TM) region, including the seven  $\alpha$ -helices, and the intracellular region, which consists in the C terminal tail and three intracellular loops (ICL1-3). The extracellular domain modulates the ligand access and sequence analysis shows that this region is characterized by a large diversity in lengths and sequence composition. The TM region forms the structural core, binds the ligand and transduce this information to the intracellular domain by conformational changes. Despite the sequence diversity between TM domains of different GPCRs, they share a similar three-dimensional architecture of seven helices held together by tertiary contacts [3]. Comparing the ligand positions from class B, class F and across subgroups of class A, all ligands have been observed to bind in an extracellular pocket of the TM domain, however they have access to different depths within this pocket [22]. Most of the residues in contact with the ligand are present in the TM regions (Fig 3), except for ligands of some receptors (e.g. chemokine receptor 4, CXCR4; neurotensin receptor 1, NTSR1; adenosine A<sub>2A</sub> receptor; smoothed receptor, SMO) in which the extracellular domains are involved as well. An unexpected exception is represented by a class B receptor, corticotropin-releasing hormone receptor 1 (CRF1), in which the small antagonist CP-376395 was found in an allosteric pocket close to the intracellular boundary, the deepest binding site discovered in GPCRs to date [22]. The ligand binding position provides a potential handle for drug design targeting

GPCRs. Finally, the intracellular region binds the cytosolic signalling proteins, such as G proteins, GPCR kinases and arrestins [3].

These multiple crystal structures provide unprecedented insights into the structural diversity of the GPCR family. This knowledge combined with the biochemical, biophysical and computational studies gives us the molecular basis to understand the relationship between GPCR structure and function [3].

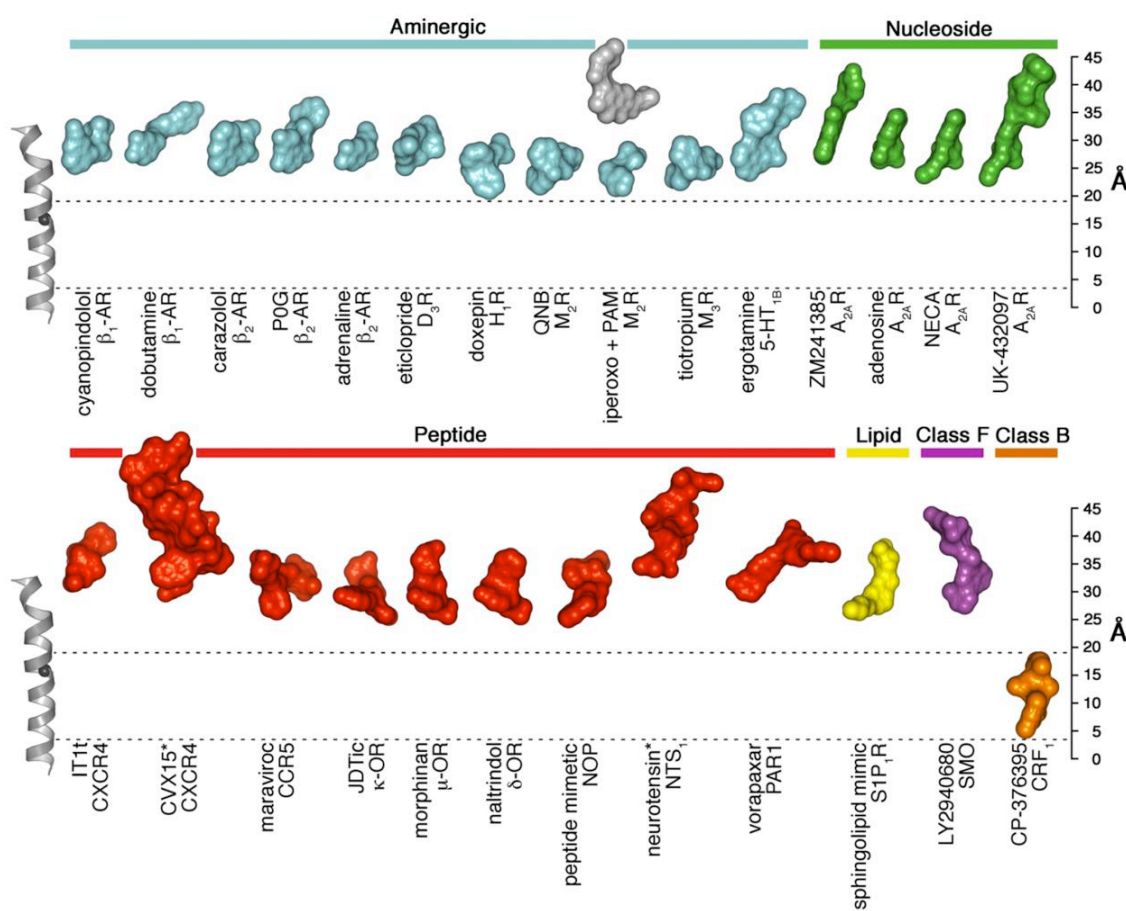


**Figure 3. Position of ligand binding sites in GPCRs of solved structure.** The structures include a selected set of class A, B and F receptor-ligand complexes which were superimposed and the ligand is shown to represent the location of the ligand binding site. The TMD4 from bovine rhodopsin (PDB ID 1HZX) is shown as a reference on the left side, with the C $\alpha$ -carbon of the highly conserved W4.50 (Ballesteros-Weinstein numbering [23]) displayed as a black sphere. Peptide-ligands are marked with an asterisk. [22]

This research project focuses on the characterization of different GPCRs covering structural and functional aspects.

- The first part contains a structural study of adenosine  $A_{2A}$  and  $A_{2B}$  receptor subtypes, in particular regarding the role of their extracellular loops for receptor function and with regard to subtype diversity. Furthermore, the extracellular disulfide bond network of the  $A_{2A}$  adenosine receptor has been studied to obtain insight into the structural differences involved in receptor subtype selectivity.
- In the second part an uncommon intracellular GPCR, GPR143, associated with a particular type of albinism is investigated. The signalling pathway and the function of this receptor in patho-physiological conditions are still unknown. Thus, this study focuses on the investigation of a much needed pharmacological tool to analyze GPR143 function and on the identification of potential interaction partners.

## 2. Characterization of adenosine A<sub>2A</sub> and A<sub>2B</sub> receptor subtypes

### 2.1 Purinergic receptors

After the release in the extracellular environment, adenosine 5'-triphosphate (ATP) and other nucleotides are subjected to enzymatic degradation by ectonucleotidases, which is important because ATP metabolites are physiological ligands for the different purinergic receptors (Fig 4). The ectonucleotidase family includes the E-NTPDase (ectonucleoside triphosphate diphosphohydrolases) and the E-NPPs (ectonucleotide pyrophosphatase and/or phosphodiesterases) which hydrolyze ATP and ADP to AMP, while ecto-5'-nucleotidase hydrolyzes AMP to adenosine [24].

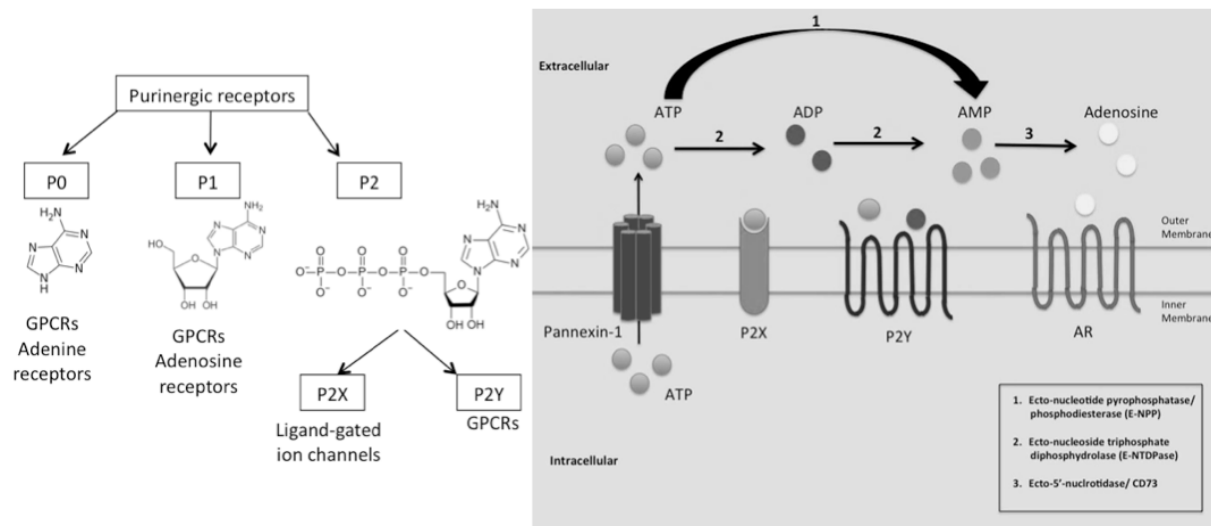


**Figure 4. Schematic representation of the elements involved in purinergic signaling.** The ATP/ADP/AMP present in the extracellular environment can bind to P2X and P2Y receptors. E-NTPDases (1 and 2 in the right panel) promote the hydrolysis of ATP to ADP or from ADP to AMP. AMP is further hydrolyzed by ecto-5'-nucleotidase (3 in the right panel) to adenosine, which activates adenosine receptors [25].

Purinergic receptors are divided into two groups: P1 or adenosine receptors (ARs) activated by adenosine and P2 receptors for ATP/ADP [26]. P2 receptors are subdivided into ionotropic P2X and metabotropic P2Y receptors. P2X receptors are ligand gated ion channels which form trimeric structures using individual subunits (P2X<sub>1-7</sub>). On the other hand, P2Y receptors are GPCRs with eight subtypes (P2Y<sub>1</sub>, P2Y<sub>2</sub>, P2Y<sub>4</sub>, P2Y<sub>6</sub>, P2Y<sub>11-14</sub>). Purinoceptors might be

the most abundant receptors in mammalian tissues thus, they can be found in all types of cells including those of neural origin [24,26].

Recently, a third family of purinergic receptors has been characterized as GPCRs activated by adenine, adenine receptors, for which the classification as “P0 receptors” has been suggested [27].

## **2.2 Adenosine receptors**

Adenosine receptors (ARs) belong to the rhodopsin-like (class A) family of GPCRs and are divided into four subtypes: A<sub>1</sub>, A<sub>2A</sub>, A<sub>2B</sub> and A<sub>3</sub>. They are ubiquitously expressed in the human body and respond to the same endogenous ligand, adenosine, however they activate different intracellular signalling pathways (Table 1) [26]. A<sub>1</sub> and A<sub>3</sub> receptors are coupled to G<sub>i</sub> proteins thereby inhibiting adenylate cyclase and decreasing the intracellular cAMP level. A<sub>2A</sub> and A<sub>2B</sub> receptors are coupled to G<sub>s</sub> proteins mediating an increase in intracellular cAMP through adenylate cyclase activation [28]. For the A<sub>2B</sub>AR G<sub>q</sub> coupling has also been shown [29]. The latter two subtypes share a higher sequence identity of 59%, while the human A<sub>1</sub> and A<sub>3</sub>ARs only show an identity of 49%.

ARs are promising therapeutical drug targets due to their involvement in a wide range of conditions and diseases [30]. The A<sub>2A</sub>AR subtype plays a role in anti-inflammatory and immunosuppressive effects [31]. A<sub>2A</sub>AR antagonists are candidates for the treatment of Parkinson’s and Alzheimer’s diseases as well as for the treatment of addiction and depression [32,33]. Recently, pharmaceutical companies have been investing in the development of A<sub>2A</sub>AR antagonists in combination with antibodies blocking inhibitory receptors, such as PD-1 and CTLA-4, for an improved immunochemotherapy [32]. On the other hand, the involvement of the A<sub>2B</sub>AR subtype is being evaluated for asthma, bronchial inflammation, cancer, diabetes, neuroinflammation and Alzheimer’s diseases [33–37]. Partial agonists A<sub>1</sub>-selective have been evaluated for the treatment of tachycardia, atrial fibrillation, type II diabetes and neuropathic pain while various A<sub>1</sub>AR antagonists have been explored for improving renal function and for the treatment of heart failure [30]. A<sub>3</sub>AR agonists have been tested for treatment of autoimmune inflammatory disorders, liver cancer, rheumatoid arthritis, psoriasis and they seemed to have also cardioprotective effects while A<sub>3</sub>AR antagonists are being studied to cure glaucoma [30].



**Table 1.** Important signaling pathways, selective agonists and body distribution of the human adenosine receptor subtypes [38].

	<b>A<sub>1</sub>AR</b>	<b>A<sub>2A</sub>AR</b>	<b>A<sub>2B</sub>AR</b>	<b>A<sub>3</sub>AR</b>
<b>G protein</b>	G <sub>i</sub> / G <sub>o</sub>	G <sub>s</sub> / G <sub>olf</sub>	G <sub>s</sub> / G <sub>q/11</sub>	G <sub>i</sub> / G <sub>q/11</sub>
<b>Affinity for adenosine – K<sub>i</sub></b> [30]	ca. 100 nM	310 nM	15 000 nM	290 nM
<b>Selective agonists</b>	CPA, CCPA	CGS21680	BAY60-6583	CI-IB-MECA
<b>High expressing tissues</b>	Brain (cortex, cerebellum, hippocampus), dorsal horn of spinal cord, eye, adrenal gland, atria	Spleen, thymus, leukocytes, blood platelets, striatopallidal GABAergic neurons, olfactory bulb	Cecum, colon, bladder	Testis (rat), mast cells (rat)

### 2.3 Crystallographic structures and structural insight

Despite the high sequence identity between A<sub>2B</sub>AR and its close homolog the A<sub>2A</sub>AR, the endogenous ligand, adenosine (Fig 5, **1**), and its derivatives, NECA (**2**) and CGS21680 (**3**), show higher affinity for A<sub>2A</sub>AR. The structural reason for this distinction is unknown. The functional knowledge about the A<sub>2B</sub>AR is increasing in the last years, mostly due to mutagenesis studies [39–48], but a clear view about the structure of this receptor is still missing.

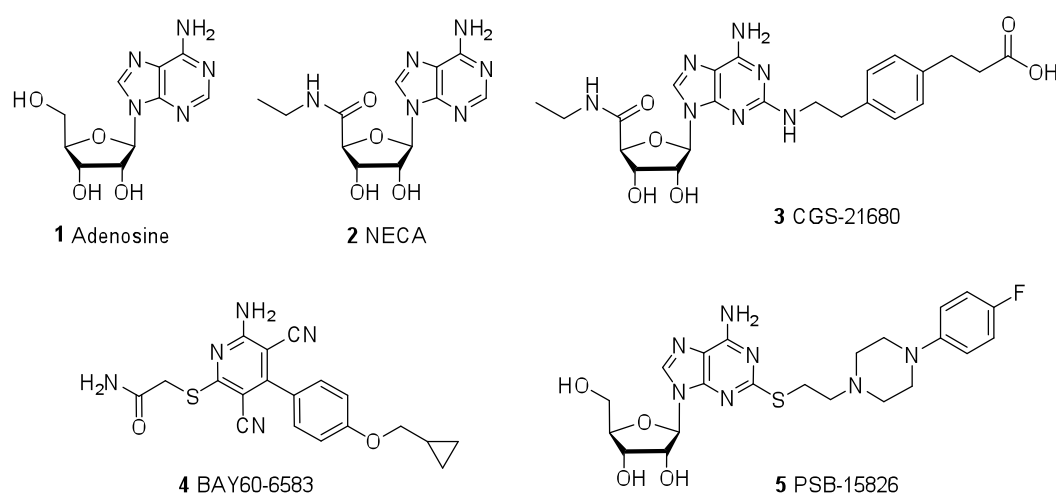


**Figure 5.** Selected adenosine A<sub>2A</sub> and A<sub>2B</sub> receptor agonists.

The so far available A<sub>2A</sub>AR X-ray structures reveal different snapshots of the receptor conformations in complex with different ligands: the inactive conformation bound to ZM241385 (3EML, [49] and 4EIY, [50]), XAC (3REY) and caffeine (3RFM, [51]), then the intermediate state (NECA, 2YDV, and adenosine, 2YDO, [52]) and the fully activated conformation (UK-432097, 3QAK, [53] and CGS21680, 4UG2 and 4UHR, [54]). The published crystal structures are summarized in Table 2.

**Table 2.** Crystal structures of the adenosine A<sub>2A</sub> receptor. The ligands co-crystallized with the receptor are listed together with the resolution of the solved structure and the authors. The identification code corresponding to the structure deposited in Protein Data Bank (PDB ID) is listed as well.

PDB ID	Ligand	resolution	author
3EML	ZM241385, inverse agonist	2.6 Å	<i>Jaakola et al, 2008</i>
3QAK	UK432097, full agonist	2.7 Å	<i>Xu et al, 2011</i>
2YDO	Adenosine, full agonist	3.0 Å	<i>Lebon et al, 2011</i>
2YDV	NECA, full agonist	2.6 Å	<i>Lebon et al, 2011</i>
3PWH	ZM241385, inverse agonist	3.3 Å	<i>Doré et al, 2011</i>
3REY	XAC, xanthine amine congener, antagonist	3.31 Å	<i>Doré et al, 2011</i>
3RFM	Caffeine, antagonist	3.6 Å	<i>Doré et al, 2011</i>
3VG9	Allosteric inverse-agonist antibody	2.7 Å	<i>Hino et al, 2012</i>
3VGA	Allosteric inverse-agonist antibody	3.1 Å	<i>Hino et al, 2012</i>
3UZA	6-(2,6-dimethylpyridin-4-yl)-5-phenyl-1,2,4-triazin-3-amine	3.27 Å	<i>Congreve et al, 2012</i>
3UZC	4-(3-amino-5-phenyl-1,2,4-triazin-6-yl)-2-chlorophenol	3.34 Å	<i>Congreve et al, 2012</i>
4EIY	ZM241385, inverse agonist (Na <sup>+</sup> allosteric modulation)	1.8 Å	<i>Liu et al, 2012</i>
4UG2	CGS21680, selective A <sub>2A</sub> agonist (monoclinic crystal)	2.6 Å	<i>Lebon et al, 2015</i>
4UHR	CGS21680, selective A <sub>2A</sub> agonist (orthorhombic crystal)	2.6 Å	<i>Lebon et al, 2015</i>

Since there is no A<sub>2B</sub>AR crystal structure available yet, some of the solved A<sub>2A</sub> structures have been used to construct a homology models of the closely related A<sub>2B</sub>AR [55,56]. The most difficult structural elements to model are the extracellular loops (ECLs) of the receptors because of their high flexibility and their great variability in terms of sequence and length. Over the last decade, it has been proven that the ECLs, in particular the ECL2, have a critical role in receptor activation and ligand binding. In class A GPCRs, the ECL2 is associated with ligand selectivity, that would explain their large variety [57]. The EL2 is one of the least conserved regions between the A<sub>2A</sub> and A<sub>2B</sub> receptor subtypes, showing 34% identity and 46% similarity [39]. The ECL2 of A<sub>2B</sub>AR is the longest of all four receptor subtypes (Fig 6) and possesses four cysteine residues, only one of which is involved in disulfide bond formation [55]. Only in four A<sub>2A</sub>AR crystal structures (the two intermediate state 2YDV and 2YDO, the inactive conformation 4EIIY and the active structure 4UHR) the ECL2 is completely solved, while in the other structures the loop resolution is very low and the models lack parts of the ECL regions. This underlines the fact that the loops are highly flexible. The solved ECL2 in A<sub>2A</sub> shows a random coil structure including a short  $\alpha$ -helix close to the transmembrane domain 5 (TMD5) and an anti-parallel  $\beta$ -sheet with the ECL1, that is mainly constrained by the three disulfide bonds between the two ECLs [49,51,57].

The ECL2 might contribute to the specificity of ligand binding by directly forming part of the binding cavity. Several A<sub>2A</sub>AR crystal structures show direct interactions of residues in ECL2 (i.e. Phe168<sup>5,29</sup> and Glu169<sup>5,30</sup>) with the bound ligand in the binding pocket [49,51–54,58], which were also proven by mutagenesis studies [59,60]. The binding pocket at the extracellular surface is influenced by the ligand structure [54], indeed when small molecules (NECA) are bound the entrance of the binding pocket is narrow [52], while it widens appreciably with ligands with bulky extensions at the adenosine moiety (UK432097) [53]. The ECL2 seems also to be an important element for the subtype selectivity of ligands. Both ZM241385- and CGS21680-bound crystal structures of A<sub>2A</sub> receptor clearly show that the long side chain of the two ligands is protruding out of the transmembrane regions creating interactions with the ECL2. Some of these interactions can be determinant for the receptor subtype specificity [54]. Structure-activity relationship studies have already shown that small substituents in position 2 of the adenosine moiety reduce the A<sub>2A</sub> selectivity [61].

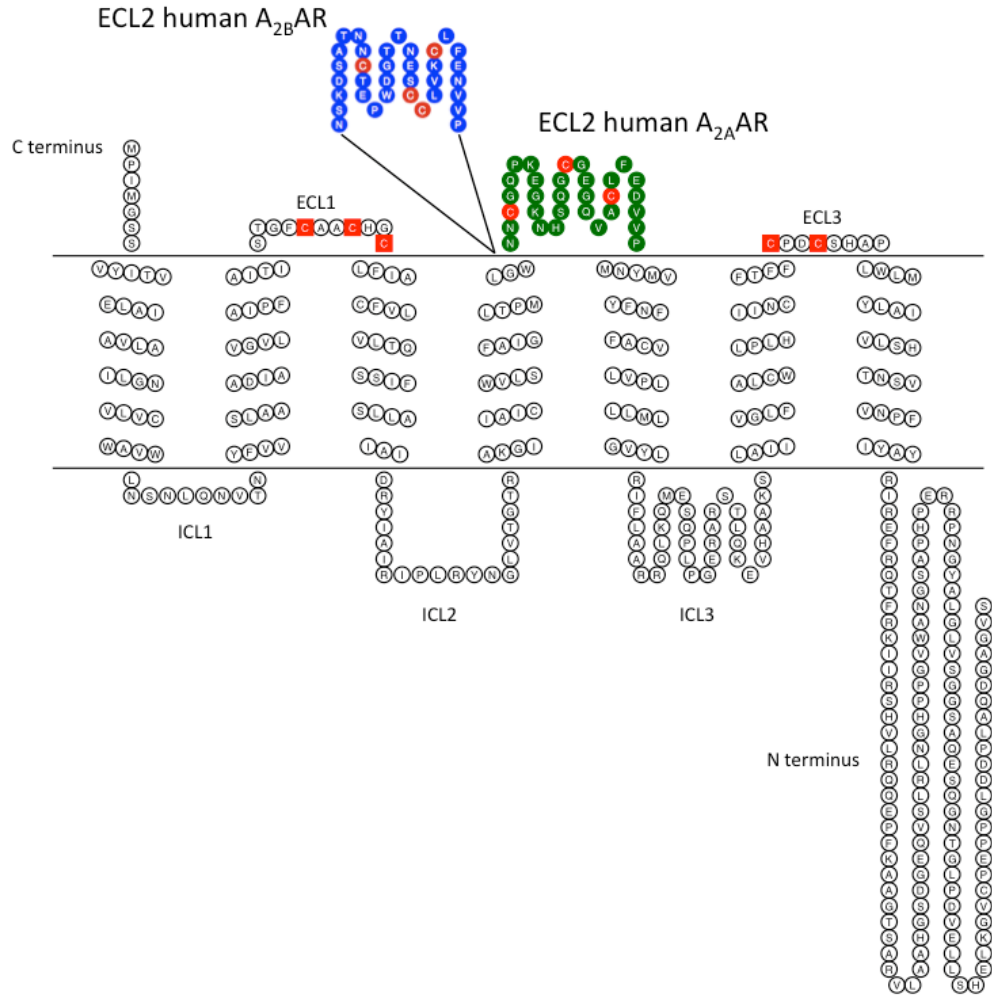


**Figure 6. Topology model of the human A<sub>2A</sub> receptor where its extracellular loop 2 is compared to the one of the human A<sub>2B</sub> receptor.** The residues included in the human A<sub>2A</sub>AR extracellular loop 2 (ECL2) are highlighted in green, while the residues of the human A<sub>2B</sub>AR ECL2 are shown in blue. The extracellular cysteine residues are represented in red. The extracellular and intracellular loops of the human A<sub>2A</sub>AR are indicated as ECL and ICL, respectively. The structure represents the chimera receptor generated in this project: the ECL2 of the human A<sub>2A</sub>AR was exchanged with the ECL2 of the human A<sub>2B</sub>AR creating the hA<sub>2A</sub>(ECL2 hA<sub>2B</sub>) receptor. Image realized with TOPO2 software [62].

Recently, we investigated the hypothesis of the ECL2 as being critical for ligand recognition and receptor activation in ARs [39]. The complete ECL2 of the human A<sub>2B</sub> receptor was exchanged for the corresponding loop in A<sub>2A</sub>AR subtype generating the A<sub>2B</sub>(ECL2-A<sub>2A</sub>) mutant. This loop exchange had significant effects on ligand binding and receptor function [39]. The A<sub>2A</sub>-selective agonist CGS21680 was able to activate the A<sub>2B</sub>(ECL2-A<sub>2A</sub>) mutant, but did not show any activation of the wildtype (wt) A<sub>2B</sub>AR. Moreover, the maximal effect of

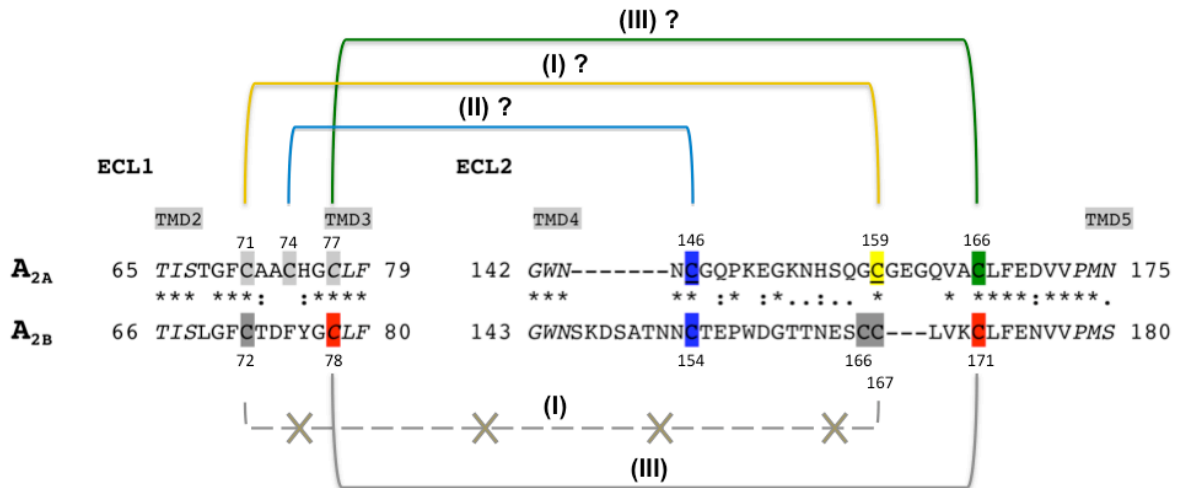
all agonists tested in cAMP accumulation assays of the G<sub>s</sub>-coupled receptor was significantly increased in the loop exchange mutant as compared to the wt receptor. These results showed that the ECL2 does not only contribute to ligand selectivity but, in addition, appears to stabilize agonist-bound active conformations of the receptor [39].

Most class A GPCRs contain disulfide bonds in their extracellular domains rigidifying the structure. In addition, several mutagenesis studies and X-ray structures [63–66], showed that the ECL2 adopts different conformations during the activation mechanism, switching between an open and closed state. In a previous study by *de Graaf et al.* the ECL2 sequences of 365 human non-olfactory GPCRs were aligned and the number of cysteine residues were analyzed [67]. The A<sub>2A</sub> and A<sub>2B</sub> AR subtypes were found to have the highest number of cysteine residues in the ECL2, three and four, respectively (Fig 7). In most rhodopsin-like GPCRs two highly conserved cysteine residues are present in the extracellular surface, forming a disulfide bond which has been shown to be essential for receptor structure and activation [11,68]. Both A<sub>2A</sub> and A<sub>2B</sub> AR subtypes possess two cysteine residues which were found to be highly conserved in most class A GPCRs: Cys<sup>45.50</sup> in the ECL2 and Cys<sup>3.25</sup> located at the extracellular end of the transmembrane domain 3 (TMD3) (Ballesteros Weinstein nomenclature [23] and ECL nomenclature defined by *de Graaf et al* [67]).

Mutagenesis studies have previously shown that in A<sub>2B</sub>AR the two conserved cysteine residues (Cys78<sup>3.25</sup> in TM3 and Cys171<sup>45.50</sup> in ECL2) form a disulfide bond which plays an essential role in ligand binding and receptor activation [55]. On the contrary, mutations in the other three cysteine residues present in the ECL2 of the A<sub>2B</sub>AR (Cys154, Cys166 and Cys167) slightly affect the receptor activation indicating that the potential disulfide bonds formed by those cysteine residues are not critical for the A<sub>2B</sub>AR function [55].

On the other hand, crystal structures of the closely related A<sub>2A</sub>AR as well as a molecular modeling study, indicated that four disulfide bonds are formed in that receptor (Fig 7): three of them linking the ECL2 with the ECL1 (Cys71<sup>2.69</sup>-Cys159<sup>45.43</sup>, Cys74<sup>3.22</sup>-Cys146<sup>45.30</sup> and Cys77<sup>3.25</sup>-Cys166<sup>45.50</sup>), and the fourth one forming an intra-loop bond in the ECL3 (Cys259<sup>6.61</sup>-Cys262<sup>6.64</sup>) [49,50,52,54,69,70]. A recent mutagenesis study suggested that the conserved disulfide bond in A<sub>2A</sub>AR (Cys77<sup>3.25</sup>-Cys166<sup>45.50</sup>) is not essential for [<sup>3</sup>H]CGS21680 binding and for its plasma membrane expression [70].

a



b

disulfide bond number	A <sub>2A</sub>	A <sub>2B</sub>
I	C71-C159	C72-C167
II	C74-C146	
III	C77-C166	C78-C171

**Figure 7. Cysteine residues and disulfide bonds in the extracellular loop 1 and 2 of the human A<sub>2A</sub> and A<sub>2B</sub> ARs.** The amino acid sequence alignment (a) of ECL1 and 2 of A<sub>2A</sub> and A<sub>2B</sub> ARs was done using ClustalW. The following cysteine residues in ECL2 of A<sub>2A</sub>AR are highlighted accordingly to the colors of cysteine residue mutants: blue C146<sup>A2A</sup>, yellow C159<sup>A2A</sup>, green the conserved C166<sup>A2A</sup>. The other extracellular cysteine residues in A<sub>2A</sub>AR are highlighted in light grey. In A<sub>2B</sub>AR the essential cysteine residues found by mutagenesis study [55] are indicated in red. The residues included in transmembrane domains are shown in italics. The identical amino acid residues (\*), the conserved amino acid substitutions (:), and the semi-conserved amino acid substitutions (.) are indicated. The positions of the cysteine residues are given for the A<sub>2A</sub> and A<sub>2B</sub> ARs. (b) The disulfide bonds found in the crystal structure of A<sub>2A</sub>AR and the predicted disulfide bonds in the A<sub>2B</sub>AR [55] have been assigned to arbitrary numbers (I-III) based on the progressive cysteine residues in ECL1 of the human A<sub>2A</sub>AR. The disulfide bonds are represented in (a).

## 2.4 Aim of the project

The project focused on the extracellular loops (ECLs) of GPCRs, as they might be involved in ligand binding and receptor activation [57]. In class A GPCRs, including adenosine receptors (ARs), the ECL2 is the largest and most diverse of the three ECLs. Its high variety even within subfamilies has been associated with ligand selectivity [39,71–74]. Among the four AR subtypes, the human A<sub>2A</sub> and A<sub>2B</sub> AR are the closest homologs and sequence analysis of

the two subtypes revealed the largest differences in the loop regions, especially in the extracellular loop 2 (ECL2) [55]. The endogenous ligand adenosine and its derivatives NECA and CGS21680 show higher affinity for A<sub>2A</sub>AR than for A<sub>2B</sub> subtype, despite very similar ligand binding sites. The structural reason for this striking difference is still unknown.

Recently, the complete ECL2 of the human A<sub>2B</sub>AR was exchanged for the corresponding loop of the A<sub>2A</sub>AR subtype (resulting in the mutant receptor A<sub>2B</sub>(ECL2-A<sub>2A</sub>)) and this led to significant effects on ligand binding and receptor function. The results showed that the ECL2 does not only contribute to ligand selectivity but, in addition, can stabilize agonist-bound active conformations of the receptor [39].

The aim of the first part of this study was to investigate the complementary **chimera of the human A<sub>2A</sub>AR**, in which the ECL2 was exchanged for that of the human A<sub>2B</sub>AR (resulting in A<sub>2A</sub>(ECL2-A<sub>2B</sub>)), in order to clarify the role of the ECL2 in the two AR subtypes. Several AR agonists were tested in functional assay and their binding to the wildtype and the chimera receptors was evaluated with radioligand binding experiments.

The second part of the study concerns the investigation of the role of **extracellular cysteine residues of the human A<sub>2A</sub>AR** in the ligand binding and receptor activation using various agonists including the endogenous ligand adenosine.

Recently, a mutagenesis study was published in which extracellular cysteine residues of the A<sub>2A</sub>AR were mutated to alanine [70]. The authors suggested that the formation of the conserved disulfide bond Cys77-Cys166 was not essential for receptor localization at the cell surface and for ligand binding [70]. Their investigation was based on ligand binding utilizing a single adenosine derivative, CGS21680, but functional data of the cysteine mutant receptors were not included. Here, we present a comprehensive study on the role of extracellular disulfide bonds in A<sub>2A</sub>AR. We generated three A<sub>2A</sub>AR mutants replacing each cysteine residue present in the ECL2 (Cys146<sup>45.30</sup>, Cys159<sup>45.43</sup> and Cys166<sup>45.50</sup>) by serine, sterically and electronically similar amino acids, thereby disrupting one of the potential single disulfide bonds in each mutant receptor. In addition, considering the high homology to the closely related A<sub>2B</sub>AR subtype, we created an A<sub>2A</sub>AR double mutant exchanging the two cysteine residues in ECL2 (Cys146<sup>45.30</sup> and Cys159<sup>45.43</sup>) which were supposed to be involved in disulfide bonds with the ECL1, thereby disrupting two potential disulfide bonds in a single mutant receptor. Finally, the results obtained experimentally by testing the ligands on

functional assays and binding studies were supported by molecular modeling based on recently published crystal structures.

The work shown in the following result sections is included in two manuscripts:

- **De Filippo E.**, El-Tayeb A., Schiedel A.C. and Müller C.E. (*in preparation*). Characterization of the extracellular loop 2 of adenosine A<sub>2A</sub> and A<sub>2B</sub> receptors.
- **De Filippo E.**, Namasivayam V., Zappe L., El-Tayeb A., Schiedel A.C. and Müller C.E. (*in preparation*). Role of extracellular cysteine residues in the adenosine A<sub>2A</sub> receptor.



## 2.5 Part I: the human adenosine A<sub>2A</sub>(ECL2 A<sub>2B</sub>) chimera

### 2.5.1 Generation and characterization of the loop exchange mutant

The complete extracellular loop 2 (ECL2) of the human A<sub>2A</sub> receptor was exchanged to the corresponding one of the human A<sub>2B</sub> receptor using the Gibson Assembly method [75], obtaining the hA<sub>2A</sub>(ECL2 hA<sub>2B</sub>) mutant receptor. Chinese Hamster Ovary (CHO) cells were stably transfected either with the loop mutant, the wildtype (wt) hA<sub>2A</sub> or the wt hA<sub>2B</sub>AR. To compare the loop mutant with the wt receptors, the cell surface expression was quantified by ELISA. Therefore, the human influenza hemagglutinin (HA) tag was linked to the N terminus of the coding sequence of each gene, which had already been shown not to interfere with the ligand binding and function of other GPCRs [55,76]. The surface expression level of the wt hA<sub>2A</sub> receptor was set as 100% while untransfected CHO cells were used as 0% (Fig 8 and values are listed in Table 3). The cell surface expression level of the three receptors was similar and not significantly different from each other.

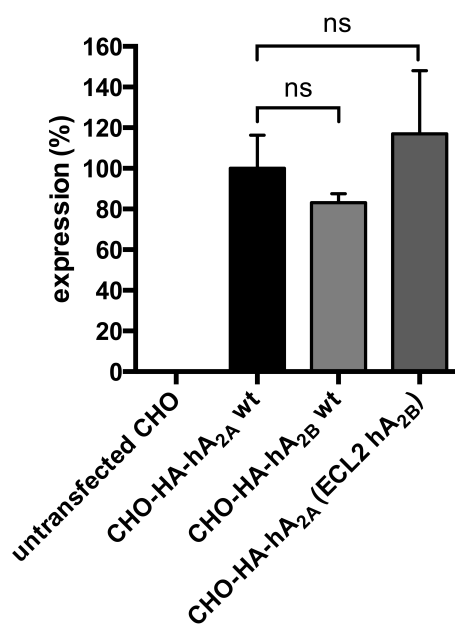


**Figure 8. Cell surface expression levels of the human A<sub>2A</sub>AR, the human A<sub>2B</sub>AR and the hA<sub>2A</sub>(ECL2 hA<sub>2B</sub>) receptor determined by ELISA.** Values were normalized to the untransfected CHO cells, set as 0%, and to the hA<sub>2A</sub>AR, set as 100%. Data represent the mean values  $\pm$  SEM of three (hA<sub>2B</sub>AR), four (hA<sub>2A</sub>AR) or five (hA<sub>2A</sub>(ECL2 hA<sub>2B</sub>)) independent experiments performed in triplicates. Two-tailed *t*-test was performed comparing the hA<sub>2A</sub>AR with the hA<sub>2B</sub>AR and the hA<sub>2A</sub>(ECL2 hA<sub>2B</sub>): both comparisons were not significantly different (ns) from the hA<sub>2A</sub>AR ( $p = 0.507$  and  $p = 0.250$ , respectively).

The wt hA<sub>2A</sub> receptor and the hA<sub>2A</sub> (ECL2 hA<sub>2B</sub>) receptor were then analyzed with homologous competition binding using the A<sub>2A</sub> agonist radioligand [<sup>3</sup>H]CGS21680, obtaining K<sub>D</sub> values, indicating the affinity of the compound for the receptors, and B<sub>max</sub> values, the maximal number of receptor binding sites (Table 3). The affinity of the mutant receptor for the A<sub>2A</sub> selective agonist CGS21680 (**3**, Fig 5) was 3-fold decreased in comparison to the wt hA<sub>2A</sub>AR. The B<sub>max</sub> ratio between the mutant and the wt hA<sub>2A</sub> receptor was in agreement with the percentage of the cell surface expression determined by ELISA.

**Table 3.** Expression levels (B<sub>max</sub>) and K<sub>D</sub> values of the hA<sub>2A</sub>AR and the hA<sub>2A</sub>(ECL2 hA<sub>2B</sub>) receptor determined by homologous competition binding versus [<sup>3</sup>H]CGS21680. The cell surface expression levels determined by ELISA are shown for comparison. Data represent mean ± SEM of three independent experiments, unless otherwise noted.

receptor	B <sub>max</sub> ± SEM (fmol/mg of protein)	K <sub>D</sub> ± SEM (nM)	ELISA % expression level
hA <sub>2A</sub> AR	480 ± 110	72.1 ± 18.0	100 ± 16
hA <sub>2A</sub> (ECL2 hA <sub>2B</sub> )	799 ± 126 <sup>ns, p = 0.179</sup>	194 ± 29 <sup>ns, p = 0.056</sup>	117 ± 31 <sup>a, ns</sup>

Results of two-tailed *t*-test: <sup>ns</sup> not significantly different from the wildtype human A<sub>2A</sub>AR.

<sup>a</sup> n = 5.

### 2.5.2 Radioligand binding studies

Competition radioligand binding studies were performed to characterize the loop exchange testing different A<sub>2A</sub> and A<sub>2B</sub> agonists: the endogenous ligand adenosine (**1**, Fig 5), the analog NECA (**2**), the A<sub>2A</sub> selective agonist CGS21680 (**3**), the A<sub>2B</sub> selective partial agonist BAY60-6583 (**4**) and a bulky 2-substituted adenosine derivative PSB-15826 (**5**). For binding assays membrane preparations of cells stably expressing either the wt or the mutant receptor were used. Adenosine deaminase was added for all tested compounds, except for adenosine, therefore the values obtained for this particular compound are an underestimation of its real affinity for the binding site of the receptor.

As first, the A<sub>2A</sub> agonist [<sup>3</sup>H]CGS21680 was used as radioligand for binding assays. Adenosine lost affinity (22-fold) at the loop mutant in comparison to the wt hA<sub>2A</sub>AR (Fig 9 A,

Table 4), while the analog NECA displayed similar affinity for both receptors (Fig 9 B). The compounds with a long substituent in position 2 of adenosine show a large loss in affinity at the chimeric mutant in comparison to the wt  $A_{2A}$  receptor (Fig 9 C-D). The partial  $A_{2B}$  agonist BAY60-6583 has no affinity to both wt  $hA_{2A}AR$  and loop mutant (data not shown).

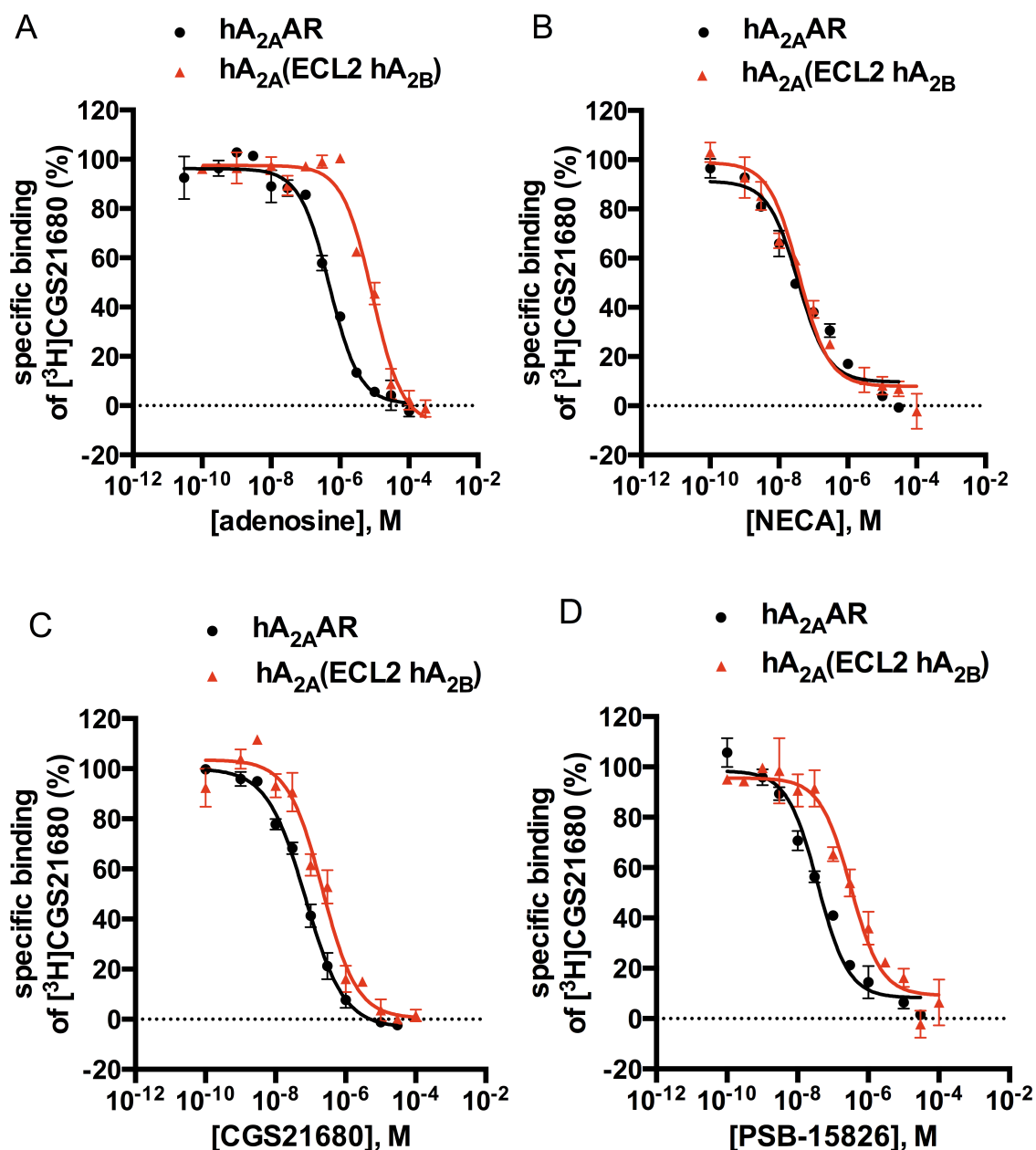


Figure 9. Competition binding studies at the human  $A_{2A}AR$  and at the human  $A_{2A}(ECL2 hA_{2B})$  receptor versus  $[^3H]CGS21680$  (5 nM) using (A) adenosine, (B) NECA, (C) CGS21680 and (D) PSB-15826. Membrane preparations from CHO cells stably expressing the receptors were used. Data points represent means  $\pm$  SEM of three independent experiments performed in duplicates.  $K_i$  values are listed in Table 4.

The results obtained with the opposite loop exchange mutant, hA<sub>2B</sub>(ECL2 hA<sub>2A</sub>), suggested that the ECL2 has a role in the conformation changes in A<sub>2A</sub> and A<sub>2B</sub> subtypes [39]. For this reason an A<sub>2A</sub> antagonist radioligand, [<sup>3</sup>H]MSX-2, was also tested in binding assays versus *cold* agonists. Antagonists have virtually equal affinity for active and inactive state of the receptors, while agonists have higher affinity for the active state. The inhibition binding curves (Fig 10) show a biphasic behavior, which is more evident in the hA<sub>2A</sub>(ECL2 hA<sub>2B</sub>) mutant than the wt hA<sub>2A</sub>AR. Two conformational states are labeled by the antagonist radioligand [<sup>3</sup>H]MSX-2, the active state at lower agonist concentrations and the inactive one at a higher concentration range. The difference between the two conformational states is larger in the loop mutant than in the wt hA<sub>2A</sub>AR. NECA and CGS21680 showed an increase in affinity at the active state of the loop mutant in comparison with the wt hA<sub>2A</sub>AR (Fig 10 A-B, IC<sub>50</sub> values in Table 4), while the bulky 2-substituted PSB-15826 (Fig 10 C, Table 4) displayed a decreased affinity at the active state than the wt hA<sub>2A</sub>AR. The percentage of the two conformational species for NECA and CGS21680 are similar in the loop mutant and in the wt hA<sub>2A</sub>AR, where the active state represents the most prevalent receptor state. In PSB-15826 the opposite situation is noticeable, the higher percentage is represented by the inactive state of the receptors. The A<sub>2B</sub> partial agonist BAY60-6583 seems to modulate [<sup>3</sup>H]MSX-2 binding at the loop mutant (Fig 10 D), this compound showed a significant increase in affinity in comparison to the wt hA<sub>2A</sub>AR.

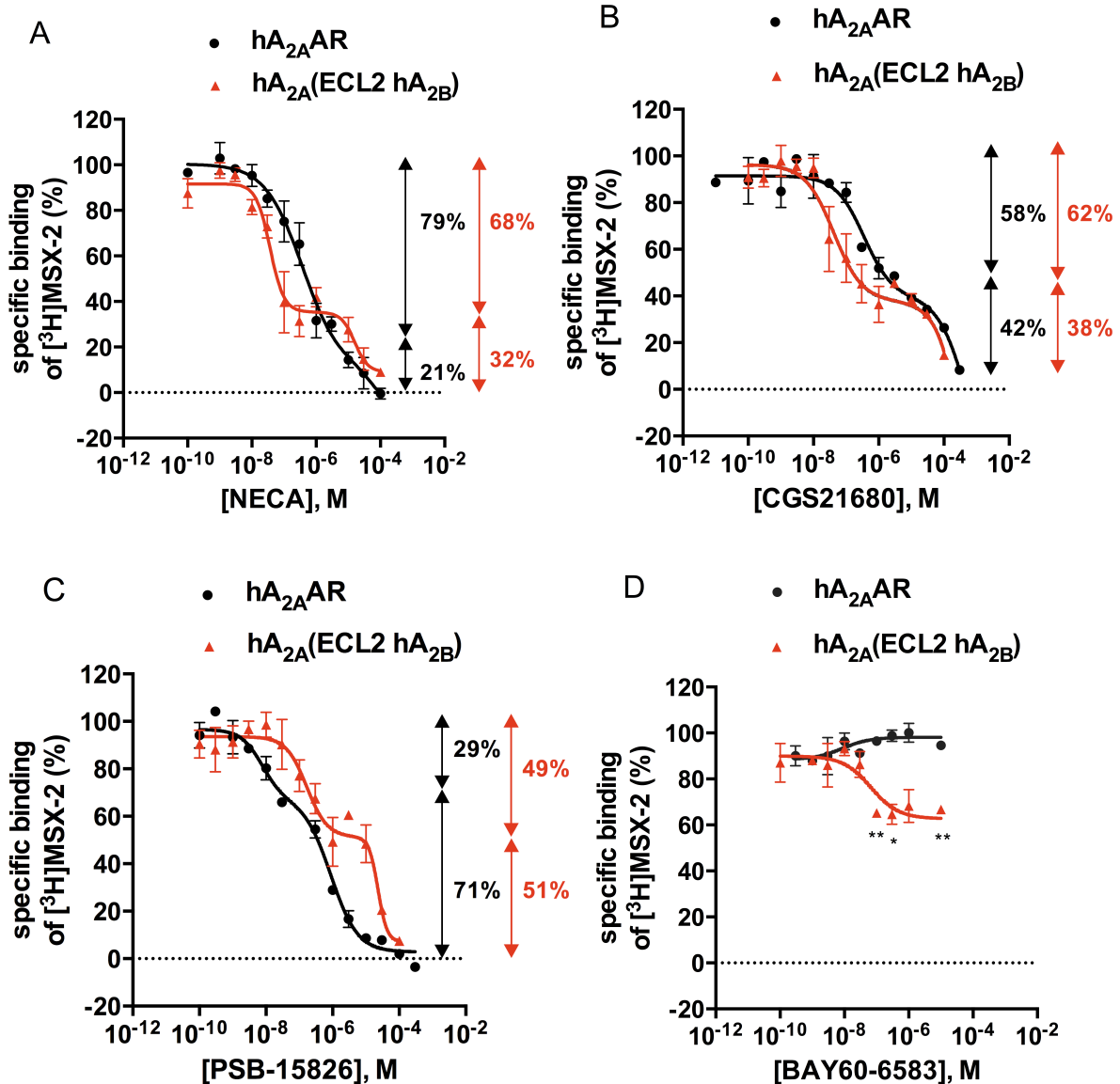


Figure 10. Competition binding studies at the human  $A_{2A}AR$  and at the  $hA_{2A}(ECL2 hA_{2B})$  receptor versus  $[^3H]MSX-2$  (1 nM) using (A) NECA, (B) CGS21680, (C) PSB-15826 and (D) BAY60-6583. Membrane preparations from CHO cells stably expressing the receptor were used. Data points represent means  $\pm$  SEM of three independent experiments performed in duplicates. The arrows located at the graph side correspond to the two different conformational states of the receptor (black:  $hA_{2A}AR$  and red:  $hA_{2A}(ECL2 hA_{2B})$  receptor). Two-tailed  $t$ -test was performed for each data point in graph D: <sup>ns</sup> not significantly different from the  $hA_{2A}AR$ , \*  $p < 0.05$ , \*\*  $p < 0.01$ , \*\*\*  $p < 0.001$ .

**Table 4.** Affinities of A<sub>2A</sub> agonists and A<sub>2B</sub> partial agonist at the human A<sub>2A</sub>AR and the hA<sub>2A</sub>(ECL2 hA<sub>2B</sub>) receptors defined by radioligand binding studies versus [<sup>3</sup>H]CGS21680 (5 nM) or [<sup>3</sup>H]MSX-2 (1 nM). “Low” refers to the IC<sub>50</sub> value of the biphasic curve at the lower agonist concentration, while “high” refers to the one at higher agonist concentration. Data represent mean ± SEM of three independent experiments, unless otherwise noted.

K <sub>i</sub> values ± SEM (nM) – [ <sup>3</sup> H]CGS21680							
receptor	adenosine		NECA	CGS21680	PSB-15826		
A <sub>2A</sub> AR	437 ± 15 <sup>a</sup>		37.3 ± 5.9	72.6 ± 16.3	33.2 ± 3.7		
A <sub>2A</sub> (ECL2 A <sub>2B</sub> )	9540 ± 550 <sup>a,***</sup>		24.7 ± 6.0 <sup>ns, p=0.379</sup>	204 ± 45 <sup>ns, p=0.119</sup>	384 ± 26 <sup>**</sup>		
IC <sub>50</sub> values ± SEM (nM) – [ <sup>3</sup> H]MSX-2							
receptor	NECA		CGS21680		PSB-15826		BAY60-6583
	<i>low</i>	<i>high</i>	<i>low</i>	<i>high</i>	<i>low</i>	<i>high</i>	
A <sub>2A</sub> AR	118 ± 6	7870 ± 276	458±239	>10 000	8.28 ± 0.12	357 ± 164	n.d.
A <sub>2A</sub> (ECL2 hA <sub>2B</sub> )	33 ± 1.5 <sup>***</sup>	>10 000	42.1±3.3 <sup>ns</sup>	>10 000	175 ± 97 <sup>ns</sup>	>10 000	39.0 ± 13.9

Results of two-tailed *t*-test: <sup>ns</sup> not significantly different from wildtype human A<sub>2A</sub>AR, \*\* p<0.01, \*\*\* p<0.001.

n.d., not determined. The IC<sub>50</sub> value could not be determined since BAY60-6583 has no affinity for the hA<sub>2A</sub>AR.

<sup>a</sup> the affinity of adenosine for the receptors is underestimated because adenosine deaminase could not be used in the assay.

### 2.5.3 Functional studies

cAMP accumulation assays induced by A<sub>2A</sub> agonists (1-3 and 5) and an A<sub>2B</sub> partial agonist (4) were performed to investigate the activation of the wt hA<sub>2A</sub>AR and hA<sub>2B</sub>AR in comparison to the hA<sub>2A</sub>(ECL2 hA<sub>2B</sub>) mutant receptor.

As expected, adenosine was more potent at the hA<sub>2A</sub>AR as compared to the hA<sub>2B</sub>AR (Fig 11 A, EC<sub>50</sub>: 170 ± 29 nM and 12 000 ± 670 nM, respectively; see Table 5) showing similar efficacy at both wt receptors. Adenosine lost 70-fold potency at the loop mutant in comparison to the wt hA<sub>2A</sub>AR, achieving similar A<sub>2B</sub> potency (mutant EC<sub>50</sub>: 15 300 ± 6130 nM, Table 5).

The non-selective adenosine derivative NECA was 10-fold more potent at the A<sub>2A</sub>AR than the A<sub>2B</sub>AR and no significant differences were noted neither in potency nor efficacy between the wt hA<sub>2A</sub>AR and the loop mutant (Fig 11 B and values in Table 4).

The A<sub>2A</sub> selective nucleosidic agonist CGS21680 (Fig 11 C) is active at A<sub>2B</sub>AR only at high concentrations (>10 000 nM), while it showed similar potency and efficacy at the wt hA<sub>2A</sub>AR (EC<sub>50</sub> 16.6 ± 0.9 nM, efficacy 49 ± 2%) and the loop mutant (EC<sub>50</sub> 27.1 ± 11.3 nM, efficacy 64 ± 6%).

The bulky substituted adenosine derivative PSB-15826 (Fig 11 D) is inactive at the wt hA<sub>2B</sub>AR and showed similar potency at the wt hA<sub>2A</sub>AR and at the loop mutant (EC<sub>50</sub> 53.5 ± 17.9 nM and 65.7 ± 6.2 nM, respectively). PSB-15826 displayed a significant decrease in efficacy at the loop mutant in comparison to the wt hA<sub>2A</sub>AR (84 ± 4% and 58 ± 2%, respectively).

The A<sub>2B</sub> partial agonist BAY60-6583 (Fig 12 A, Table 5) showed no activity at the wt hA<sub>2A</sub>AR and a potency of 195 ± 40 nM at the wt hA<sub>2B</sub>AR. On the other hand, BAY60-6583 at the loop mutant displayed a small reduction in cAMP accumulation, considering that the loop mutant showed a slight basal activity. To analyze the hypothetical function of BAY60-6583 as antagonist at the loop mutant receptor, a cAMP assay with BAY60-6583 preincubation (10 μM) and then agonist stimulation (adenosine or NECA, Fig 12 inset) was performed. BAY60-6583 has no inhibitory function at the loop mutant receptor, since no reduction in cAMP production was observed.

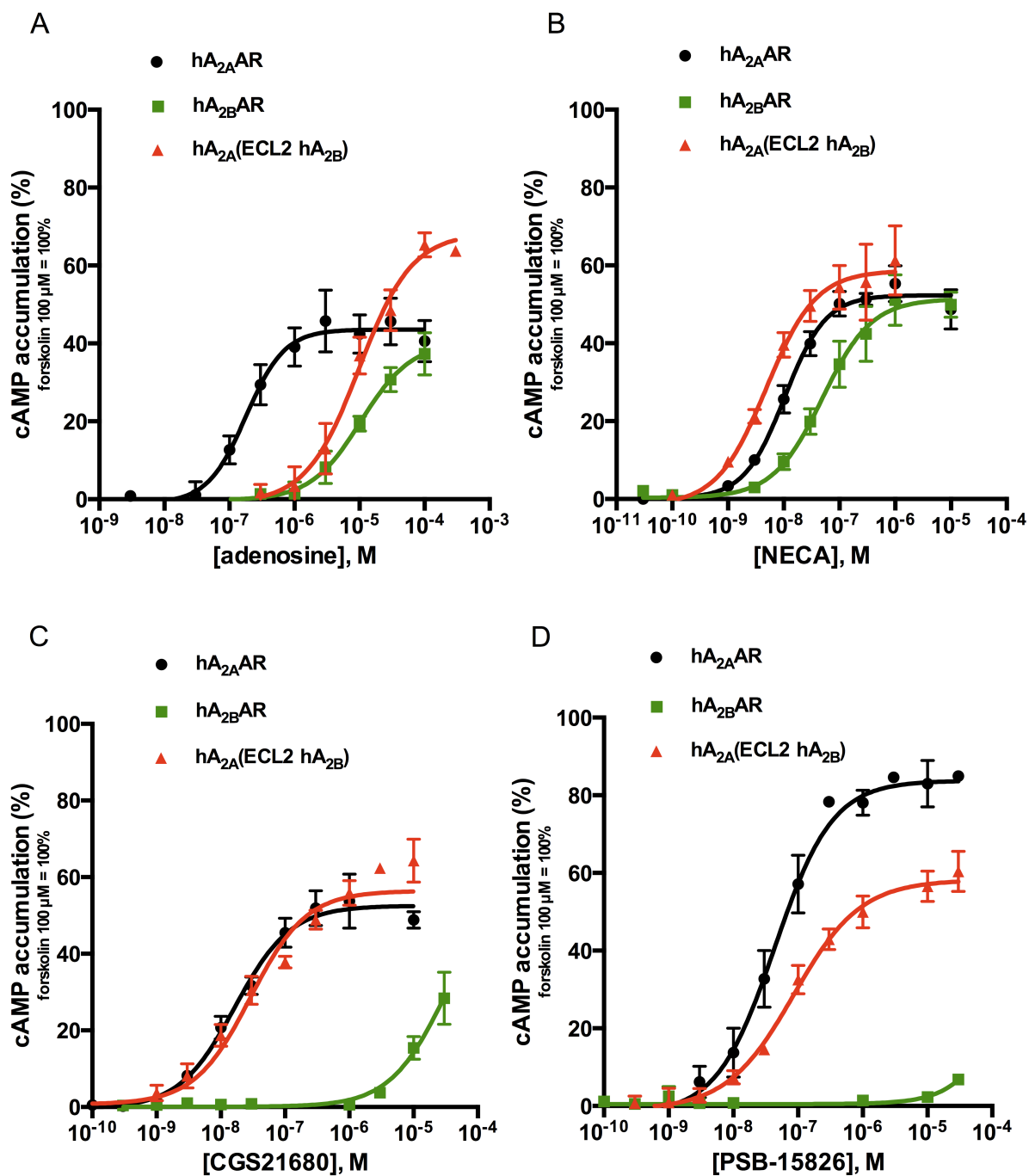


Figure 11. Agonist-induced cAMP accumulation studies at CHO cells stably expressing the human A<sub>2A</sub>AR, the human A<sub>2B</sub>AR and the mutant hA<sub>2A</sub>(ECL2 hA<sub>2B</sub>) AR using (A) adenosine, (B) NECA, (C) CGS21680 or (D) PSB-15826 as agonist. Data represent mean ± SEM from three to five independent experiments performed in duplicates. Data are normalized to the effect of 100 μM forskolin, set as 100%. Corresponding EC<sub>50</sub> and maximal effects are listed in Table 5.



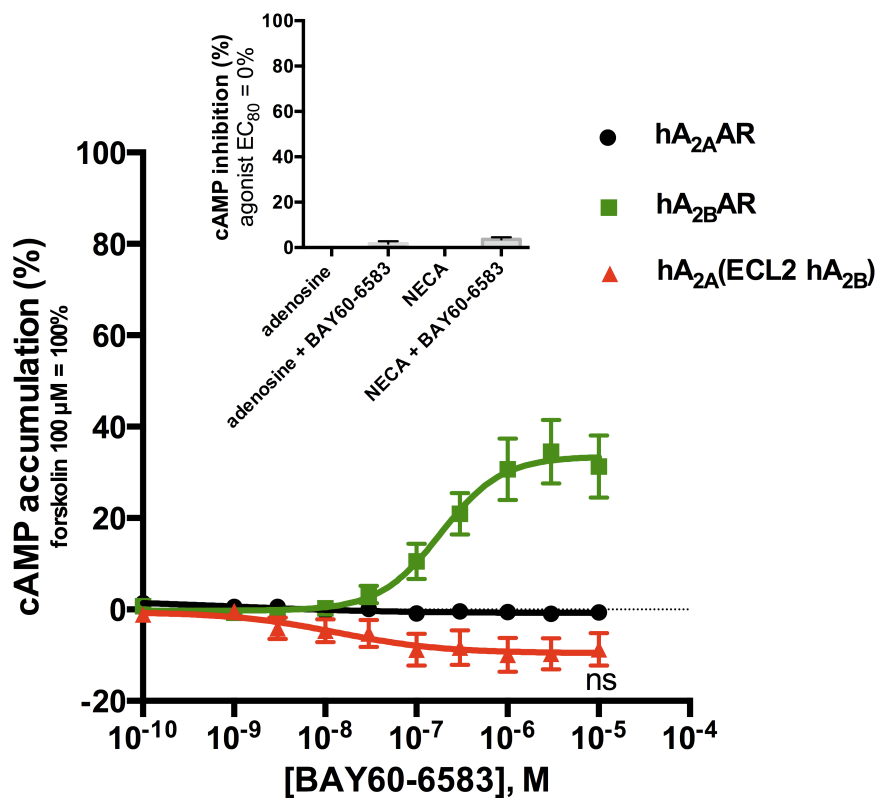


Figure 12. cAMP accumulation studies at CHO cells stably expressing the human A<sub>2A</sub>AR, the human A<sub>2B</sub>AR and the mutant hA<sub>2A</sub>(ECL2 hA<sub>2B</sub>) receptor using a partial A<sub>2B</sub> selective agonist, BAY60-6583. The agonist-induced cAMP production was normalized to the effect of 100 μM forskolin (set as 100%) and a two-tailed *t*-test was performed comparing point by point the effect of the hA<sub>2A</sub>AR and the mutant hA<sub>2A</sub>(ECL2 hA<sub>2B</sub>) receptor (<sup>ns</sup> not significantly different from the hA<sub>2A</sub>AR). In the inset, comparison of the cAMP inhibition induced by BAY60-6583 (10 μM) at the loop mutant before treatment with adenosine and NECA. Data are normalized to the effect of the EC<sub>80</sub> of the agonist (adenosine or NECA), set as 0%.

**Table 5.** EC<sub>50</sub> values and maximal effects of selected agonists determined in cAMP accumulation assays at the human A<sub>2A</sub>AR, the human A<sub>2B</sub>AR and the mutant hA<sub>2A</sub>(ECL2 hA<sub>2B</sub>) receptors. Data are normalized to the effect of forskolin (100 μM), set as 100%. Data are mean ± SEM of three to five independent experiments.

agonist	human A <sub>2A</sub>		human A <sub>2B</sub>		human A <sub>2A</sub> (ECL2 A <sub>2B</sub> )	
	EC <sub>50</sub> ± SEM (nM)	Efficacy ± SEM (%)	EC <sub>50</sub> ± SEM (nM)	Efficacy ± SEM (%)	EC <sub>50</sub> ± SEM (nM)	Efficacy ± SEM (%)
Adenosine	170 ± 29	44 ± 2	12,000 ± 670 ***	40 ± 6 <sup>ns</sup>	15,300 ± 6130 ***	68 ± 8 **
NECA	10.5 ± 0.8	52 ± 2	109 ± 37 **	51 ± 4 <sup>ns</sup>	7.21 ± 0.89 <sup>ns</sup>	59 ± 4 <sup>ns</sup>
CGS21680	16.6 ± 0.9	49 ± 2	31,100 ± 7130 ***	28 ± 7 *	27.1 ± 11.3 <sup>ns</sup>	64 ± 6 <sup>ns</sup>
PSB-15826	53.5 ± 17.9	84 ± 4	> 100,000 <sup>b</sup>	n.d.	65.7 ± 6.2 <sup>ns</sup>	58 ± 2 **
BAY60-6583	> 100,000 <sup>b</sup>	n.d.	195 ± 40	34 ± 3	22.9 ± 18.6 <sup>a</sup>	- 9 ± 4 <sup>ns</sup>

n.d., not determined.

<sup>a</sup> IC<sub>50</sub> value ± SEM.

<sup>b</sup> no EC<sub>50</sub> value could be determined since the agonist is inactive at the receptor.

Results of two-tailed *t*-test: <sup>ns</sup> not significantly different from wildtype human A<sub>2A</sub>AR, \* *p* < 0.05,

\*\* *p* < 0.01, \*\*\* *p* < 0.001.

#### 2.5.4 Discussion

Adenosine receptors (ARs) belong to the rhodopsin-like family (class A) of G protein-coupled receptors (GPCRs) and are among the most important pharmacological targets for drug development due to their involvement in most of the physiological and pathophysiological pathways [30]. Despite the increasing number of solved GPCR crystal structures, several aspects of the ligand-receptor modulation are unclear. Three-dimensional models based on the several A<sub>2A</sub> crystal structures and ligand docking studies showed that, among the four AR subtypes, A<sub>2A</sub> and A<sub>2B</sub>ARs have the highest sequence conservation (identity of 59%), especially in the helices involving the binding pocket [55,77]. However, their response to the endogenous ligand, adenosine (**1**, Fig 5), and its nucleosidic derivatives considerably differ, these compounds have a higher affinity for the A<sub>2A</sub> subtype than for the A<sub>2B</sub>AR. The explanation of this discrepancy is still unknown but the investigation is in progress. In the last decade, it has become clear that not only the most conserved transmembrane domains (TMDs) but also the extracellular loops (ECLs) have important roles in receptor activation. The ECLs, in particular the ECL2, show low sequence homology even within GPCRs of the same subfamily, therefore this diversity might be one of the explanations of the receptor subtype specificity [57].

Recently we generated a mutant receptor exchanging the ECL2 of the human A<sub>2B</sub>AR for the one of the human A<sub>2A</sub>AR [39]. We showed with radioligand binding and functional studies that the ECL2 in A<sub>2A</sub> and A<sub>2B</sub> subtypes contributes to ligand affinity and selectivity. The A<sub>2B</sub>AR is not activated by the A<sub>2A</sub> selective agonist CGS21680 while the loop mutant, containing the A<sub>2A</sub>AR ECL2, gains affinity for this compound. Functional experiments confirmed the increased activity of CGS21680 at the loop mutant as well. In addition we noticed that the ECL2 exchange also led to the stabilization of the receptor's active conformation, since the maximal effect of all agonists was dramatically increased in the loop mutant as compared to the wt receptors.

In order to have a comprehensive overview about the ECL2 in A<sub>2A</sub> and A<sub>2B</sub>AR subtypes, we exchanged the whole ECL2 of the human A<sub>2A</sub>AR to the one of the human A<sub>2B</sub>AR, obtaining the opposite chimera, the hA<sub>2A</sub>(ECL2 hA<sub>2B</sub>) receptor. CHO cells were stably transfected with either the wt hA<sub>2A</sub>AR, the wt hA<sub>2B</sub>AR or the loop mutant, using retroviral transfection. The expression level of the receptors was determined with ELISA, detecting the receptor population at the cell surface, and with homologous binding experiments, estimating the

number of receptor binding sites in the membrane preparation. The loop mutant receptor appears to be efficiently transported to the cell surface since the values obtained from the ELISA and the homologous binding were similar. The expression level of the loop mutant and the wt hA<sub>2B</sub>AR were similar and not significantly different to the wt hA<sub>2A</sub>AR, therefore the data obtained from the three cell lines were comparable to each other.

Since previous studies suggested that the ECL2 is involved in the stabilization of certain receptor conformations [39,66], binding studies were performed with the A<sub>2A</sub> agonist, [<sup>3</sup>H]CGS21680, which label only the active state of the receptor, as well as with the antagonist, [<sup>3</sup>H]MSX-2, thus labeling both the active and inactive receptor population.

The K<sub>i</sub> values of the tested agonists determined in binding assay versus [<sup>3</sup>H]CGS21680 were in the expected rank-order of affinity for A<sub>2A</sub>AR but slightly higher than previously reported [30]. Former studies defined different reasons for these results. Firstly, this outcome depends on the low level of G<sub>αs</sub> proteins present in mammalian cells relative to the overexpressed A<sub>2A</sub>AR, so only a low percentage of receptors couples to the G protein, resulting in the active state [78]. It was also demonstrated that the composition of the G<sub>β</sub> subunit changes the coupling ability of receptors to G<sub>s</sub> proteins [79]. Our experimental conditions reflect the overexpression system, indeed the obtained B<sub>max</sub> values indicate that both wt A<sub>2A</sub>AR and the loop exchange mutant are higher expressed in CHO cells than in native tissues (B<sub>max</sub>: 480 ± 110 and 799 ± 126 fmol/mg of protein for the wt A<sub>2A</sub>AR and the loop mutant, respectively) [80]. Therefore, the high K<sub>i</sub> values obtained with [<sup>3</sup>H]CGS21680 are caused by the inability of a certain percentage of receptor to switch to the high-affinity agonist conformation.

Using [<sup>3</sup>H]CGS21680, we found that compounds with a long substituent in position 2 of adenosine (CGS21680 and PSB-15826) showed a 3-fold and 12-fold loss in affinity at the loop mutant in comparison to the wt A<sub>2A</sub> receptor, respectively. Previous studies showed that long substituents in position 2 of adenosine lead to A<sub>2A</sub> selectivity [61], therefore we could confirm that the A<sub>2A</sub> ECL2 is involved in binding the long 2-substituent, as the recent A<sub>2A</sub>AR crystal structures demonstrated [54]. ECL2 also contributes to A<sub>2A</sub> selectivity of 2-substituted adenosine derivatives, like CGS21680 and PSB-15826. On the other hand, a 22-fold loss in affinity of adenosine was detected in comparison with the wt hA<sub>2A</sub>AR, while no significant changes were noticed for the structurally similar adenosine analog, NECA. An hypothesis might involve the meta-binding site found in the ECL2 of the human A<sub>2A</sub>AR by *Moro et al.* [81]. Since in the chimeric receptor the A<sub>2B</sub> ECL2 was present, adenosine might show less

affinity to the putative meta-binding site present in the ECL2. However, the ECL2 replacement might have changed the conformation of the orthosteric binding site thereby reducing the interactions with adenosine. The differences found between adenosine and NECA might be due to the N-ethylcarboxamido group present in NECA which contributes to the stabilization of the ligand-receptor complex by additional interaction with the A<sub>2A</sub>AR.

Binding studies versus the A<sub>2A</sub> antagonist [<sup>3</sup>H]MSX-2 were performed to analyze the involvement of the ECL2 in conformational changes. A biphasic behaviour describing the active and inactive receptor species was more marked in the hA<sub>2A</sub>(ECL2 hA<sub>2B</sub>) mutant than the wt hA<sub>2A</sub>AR. The ECL2 exchange seems to stabilize the active conformation of the receptor for compounds such as NECA and CGS21680, maybe the introduction of the A<sub>2B</sub> ECL2 has changed the twists of the transmembrane domains, promoting the active conformation. The same effect was not visible for the bulky 2-substituted PSB-15826, maybe because of different interactions with the ECL2. By comparing the active and inactive populations of receptors bound to different agonists, it was noticed that the longer the substituent in position 2 of adenosine the smaller the percentage of receptor in the active state (29% for PSB-15826, 58% for CGS21680 and 79% for NECA; Fig 10). The same tendency is observed at the loop mutant receptor.

Functional studies highlighted the dramatic loss in potency (70-fold) for adenosine at the mutant receptor in comparison with the wt A<sub>2A</sub>AR, becoming similar to the wt A<sub>2B</sub>AR potency. This finding is consistent with the loss in affinity (22-fold) observed in binding studies. These results suggest that the ECL2 is important for the endogenous ligand recognition and for the subtype selectivity as well. The putative meta-binding site present in the A<sub>2A</sub> ECL2 might be lost in the loop exchange mutant.

The other ligands (NECA, CGS21680 and PSB-15826) showed only little changes in potency at the loop mutant receptor if compared to the wt hA<sub>2A</sub>AR. A reduction in the maximal effect of PSB-15826 at the loop mutant is visible, probably due to lost interactions with the A<sub>2A</sub> ECL2 and the flexibility of the A<sub>2B</sub> ECL2. The A<sub>2A</sub> loop exchange did not influence neither the potency or the efficacy of the A<sub>2A</sub> agonists as much as the opposite chimera, hA<sub>2B</sub>(ECL2 hA<sub>2A</sub>), showed in the previous study [39]. An hypothesis could be that the interactions formed between the agonists and the A<sub>2A</sub> ECL2 were replaced by similar residues present in the A<sub>2B</sub> ECL2. Some A<sub>2A</sub>AR crystal structures showed interaction with residues present in ECL2. Some of those residues are also present in the A<sub>2B</sub> ECL2 in similar positions, for example the

role of Glu169<sup>ECL2</sup> of A<sub>2A</sub>AR could be replaced by Glu174<sup>ECL2</sup> in A<sub>2B</sub>AR, since both residues are close to the TM5 and to the ECL3, and the role of Phe168<sup>ECL2</sup> of A<sub>2A</sub> could be replaced by Phe173<sup>ECL2</sup> in A<sub>2B</sub>AR.

Since we were testing the ability of ECLs to recognize subtype-selective ligands, the partial A<sub>2B</sub>AR agonist BAY60-6583 was tested at the loop mutant as well. This compound slightly modulates the binding affinity of the A<sub>2A</sub> antagonist [<sup>3</sup>H]MSX-2 (30% of competitive replacement) but no competition is detected versus the A<sub>2A</sub> agonist [<sup>3</sup>H]CGS21680. Functional studies showed that the reduction of the loop mutant receptor's basal activity induced by BAY60-6583 is not significant and the compound has no antagonistic activity against adenosine or NECA.

In conclusion, we found that the ECL2 in A<sub>2A</sub> and A<sub>2B</sub> receptor is involved in subtype selectivity and ligand recognition. Adenosine lost affinity and potency at the loop mutant as compared to the wt A<sub>2A</sub>AR, indicating that the ECL2 has a role in the binding of endogenous agonist and in the activation of the receptor. The presence of a putative meta-binding site in the ECL2 of the A<sub>2A</sub>AR could explain the lost in affinity displayed by adenosine at the loop mutant containing the A<sub>2B</sub>AR ECL2. Furthermore, the loop mutant receptor lost affinity for CGS21680 and PSB-15826 which are characterized by a long acidic 2-substituted group at the adenosine molecule. This confirms that the A<sub>2A</sub>AR ECL2 is involved in binding of the long 2-substituent of adenosine derivatives as suggested previously [54,61].

In addition, we verified that the ECL2 of the A<sub>2A</sub> and A<sub>2B</sub> AR is associated with conformational changes. In the A<sub>2B</sub>(ECL2 A<sub>2A</sub>) mutant, the loop exchange stabilized the active conformation increasing the efficacy of the AR agonists as compared to wt human A<sub>2B</sub>AR [39]. In the A<sub>2A</sub>(ECL2 A<sub>2B</sub>) mutant, the binding experiments with the A<sub>2A</sub> antagonist [<sup>3</sup>H]MSX-2 showed that the loop exchange stabilized the active conformation at NECA and CGS21680 as compared to the wt A<sub>2A</sub>AR. This stabilization might compensate the loss of the structured A<sub>2A</sub>AR ECL2 containing the meta-binding site and resulting in similar efficacies for those AR agonists as the wt A<sub>2A</sub>AR. The conformational stabilization was not observed for PSB-15826 which lost affinity at the active state of the loop mutant and its efficacy decreased in comparison to the wt A<sub>2A</sub>AR.

These findings were in agreement with former studies indicating that the ECL2 is involved in conformational changes in several GPCRs, such as the ECL2 of the complement factor 5a (C5a) receptor was found to stabilizes its inactive conformation [66], in angiotensin II (Ang

II) type 1 receptor (AT1R) ECL2 is an important regulator of the functional states [82] and in the muscarinic M3 receptor the ECL2 stabilize its active conformation [83].

## 2.6 Part II: the cysteine mutant adenosine A<sub>2A</sub> receptors

### 2.6.1 Potential role of disulfide bonds in the adenosine A<sub>2A</sub> receptor

The relevance of disulfide bond formation for the function of the A<sub>2A</sub>AR was experimentally observed by treating A<sub>2A</sub>-expressing CHO cells with a reducing agent, dithiothreitol (DTT), followed by agonist-induced cAMP accumulation assay. As shown in Fig 13, reducing of the disulfide bonds accessible to DTT caused a rightward shift of the dose-response curves obtained by NECA or CGS21680 stimulation, respectively, in comparison with untreated cells. NECA-induced cAMP production was more affected than the CGS21680-induced accumulation. After DTT treatment, the NECA potency at the A<sub>2A</sub>AR was 100-fold lower (EC<sub>50</sub> values: 6.81 ± 1.27 nM vs. 606 ± 12 nM) and the potency of CGS21680 was reduced by 6-fold (EC<sub>50</sub> values: 22.6 ± 3.6 nM vs. 119 ± 6 nM).

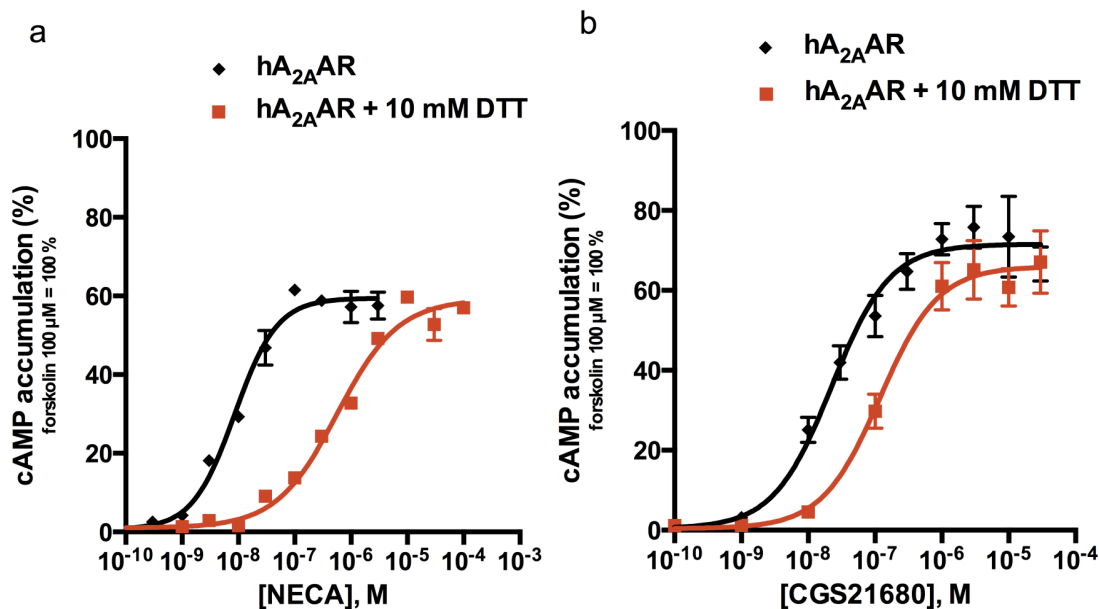


**Figure 13. Effect of DTT on the human A<sub>2A</sub>AR activity.** cAMP accumulation induced by NECA (a) or CGS21680 (b) in CHO cells stably expressing the human A<sub>2A</sub>AR in presence and absence of DTT pretreatment (10 mM, 2 h, 37 °C). Data represent mean ± SEM of two independent experiments performed in duplicates. Determined EC<sub>50</sub> values for NECA: A<sub>2A</sub> without DTT: 6.81 ± 1.27 nM; A<sub>2A</sub> with DTT: 606 ± 12 nM<sup>\*\*\*</sup>. EC<sub>50</sub> values for CGS21680: A<sub>2A</sub> without DTT: 22.6 ± 3.6 nM; A<sub>2A</sub> with DTT: 119 ± 6 nM<sup>\*\*</sup>. (Two-tailed *t*-test: <sup>\*\*</sup> *p* < 0.01 and <sup>\*\*\*</sup> *p* < 0.001).



## 2.6.2 Generation and characterization of mutant cell lines

Since the initial DTT experiments suggested that disulfide bonds play an important role in A<sub>2A</sub>AR function, the next step was to generate A<sub>2A</sub> mutant receptors by site-directed mutagenesis, exchanging a single cysteine residue present in the ECL2 (C146, C159, or C166) for a serine residue. This led to the disruption of a single disulfide bond between ECL1 and ECL2 in each cysteine mutant (C146S, C159S and C166S), see Fig 7. A fourth A<sub>2A</sub> receptor mutant was generated by replacing both cysteine residues, that are not conserved in class A GPCRs, in the ECL2 (C146S-C159S) thereby disrupting two disulfide bonds at the same time.

After the CHO cell lines that stably express the cysteine A<sub>2A</sub> mutant receptors had been established, their cell surface expression was compared to that of the wildtype (wt) A<sub>2A</sub>AR by enzyme-linked immunosorbent assay (ELISA; see Table 6). For this purpose, each receptor had been linked at the N terminus to an HA-tag, which had previously been shown not to interfere with receptor function or ligand binding [55,84]. In addition, cysteine mutant receptors were analyzed by homologous competition binding using CGS21680 versus the agonist radioligand [<sup>3</sup>H]CGS21680 and calculating B<sub>max</sub> and K<sub>D</sub> values (Table 6). Differently from the ELISA which was performed with intact cells to detect only the receptor surface expression, this method was performed with cell membranes thereby quantifying the density of receptors present in all membranes, including the intracellular ones. The mutant C159S A<sub>2A</sub> receptor showed a significant gain in affinity (3-fold) for CGS21680 and a higher cell surface expression level (227%) than the wt A<sub>2A</sub>AR (100%). Both, the single mutant C166S and the double mutant C146S-C159S receptors, displayed somewhat lower expression levels than the wt A<sub>2A</sub>AR as determined by ELISA (40% and 87% of the wt expression, respectively) and homologous binding experiments (48% and 74% of the wt expression, respectively). A different radioligand, [<sup>3</sup>H]NECA (3 nM), was used to determine K<sub>D</sub> and B<sub>max</sub> values of the C146S mutant, because of the narrow window between total binding and non-specific binding values obtained with the radioligand [<sup>3</sup>H]CGS21680. While the cell surface expression of the C146S mutant receptor was found to be significantly decreased in comparison to the wt A<sub>2A</sub>AR (23% of the wt expression determined by ELISA), the B<sub>max</sub> value was not significantly different from that of the wt receptor.

**Table 6.** Expression levels ( $B_{\max}$ ) and  $K_D$  values of the wt human  $A_{2A}$  receptor and the  $A_{2A}$  cysteine mutants. Data are obtained by homologous binding versus [ $^3H$ ]CGS21680 (5 nM; upper table) and [ $^3H$ ]NECA (3 nM; lower table). Data are means  $\pm$  SEM of three independent experiments, unless otherwise noted. ELISA data are shown for comparison between the wt hA $_{2A}$ AR and the mutants.

<i>[<math>^3H</math>]CGS21680</i>	$K_D \pm SEM$ (nM)	$B_{\max} \pm SEM$ (fmol/mg of protein)	ELISA (%)
hA $_{2A}$ wt	127 $\pm$ 3	478 $\pm$ 70	100 $\pm$ 16
hA $_{2A}$ C146S	n.d.	n.d.	23.0 $\pm$ 6.5 ***
hA $_{2A}$ C166S	110 $\pm$ 4 <sup>b, ns</sup>	230 $\pm$ 38 <sup>a, **</sup>	40.1 $\pm$ 12.4 ***
hA $_{2A}$ C159S	46.2 $\pm$ 6.5 <sup>a, ***</sup>	421 $\pm$ 51 <sup>ns</sup>	227 $\pm$ 4 ***
hA $_{2A}$ C146S – C159S	124 $\pm$ 10 <sup>b, ns</sup>	352 $\pm$ 78 <sup>b, ns</sup>	87.4 $\pm$ 15.2 *
<i>[<math>^3H</math>]NECA</i>			
hA $_{2A}$ wt	6.33 $\pm$ 1.42	129 $\pm$ 13	100 $\pm$ 16
hA $_{2A}$ C146S	25.8 $\pm$ 5.9 *	152 $\pm$ 17 <sup>ns</sup>	23.0 $\pm$ 6.5 ***

<sup>n.d.</sup> not determined, because of the low expression of the hA $_{2A}$  C146S mutant

<sup>a</sup> n = 4

<sup>b</sup> n = 5

<sup>ns</sup> Not significantly different from wt hA $_{2A}$ AR (determined using the two tailed *t*-test)

\* p < 0.05

\*\* p < 0.01

\*\*\* p < 0.001

### 2.6.3 Functional studies

The function of the cysteine A<sub>2A</sub> mutant receptors was investigated by agonist-induced cAMP accumulation assays (Fig 14) and compared to that of the wt A<sub>2A</sub>AR as well as the homologous A<sub>2B</sub>AR. Structurally diverse agonists were tested: the endogenous agonist adenosine (**1**, Fig 5), its close analog NECA (**2**), the 2-substituted acidic agonist CGS21680 (**3**), and the 2-substituted uncharged adenosine derivative PSB-15826 (**5**).

The response of all cysteine mutant receptors to the endogenous agonist adenosine was significantly altered in comparison with the wt A<sub>2A</sub>AR (EC<sub>50</sub> values and efficacies listed in Table 7). At three cysteine mutants adenosine displayed significantly reduced potency (22-fold at C159S, 30-fold at C166S and 253-fold at C146S-C159S) while the C146S mutant receptor showed almost no activation by adenosine (maximal effects: 4 ± 1% vs 44 ± 3% of forskolin activation).

Analyzing the receptors' activation by other agonists, we noticed that the C166S mutant receptor showed only minor potency changes for the adenosine derivatives NECA, CGS21680 and PSB-15826 compared to the wt A<sub>2A</sub>AR (Table 7). The C146S mutant receptor could be moderately activated by NECA and CGS21680 (efficacies: 20% and 18% vs. 55% and 52%, respectively) while it showed no activation by the bulky 2-substituted PSB-15826. A gain in potency was found at the C159S mutant receptor for all adenosine derivatives (10-fold for NECA, 6-fold for CGS21680 and 21-fold for PSB-15826).

The activity of the double mutant C146S-C159S was more affected by smaller agonists (potency loss: 253-fold for adenosine and 87-fold for NECA) than large ones (similar to wt A<sub>2A</sub>AR EC<sub>50</sub> values for CGS21680 and PSB-15826, Table 7).

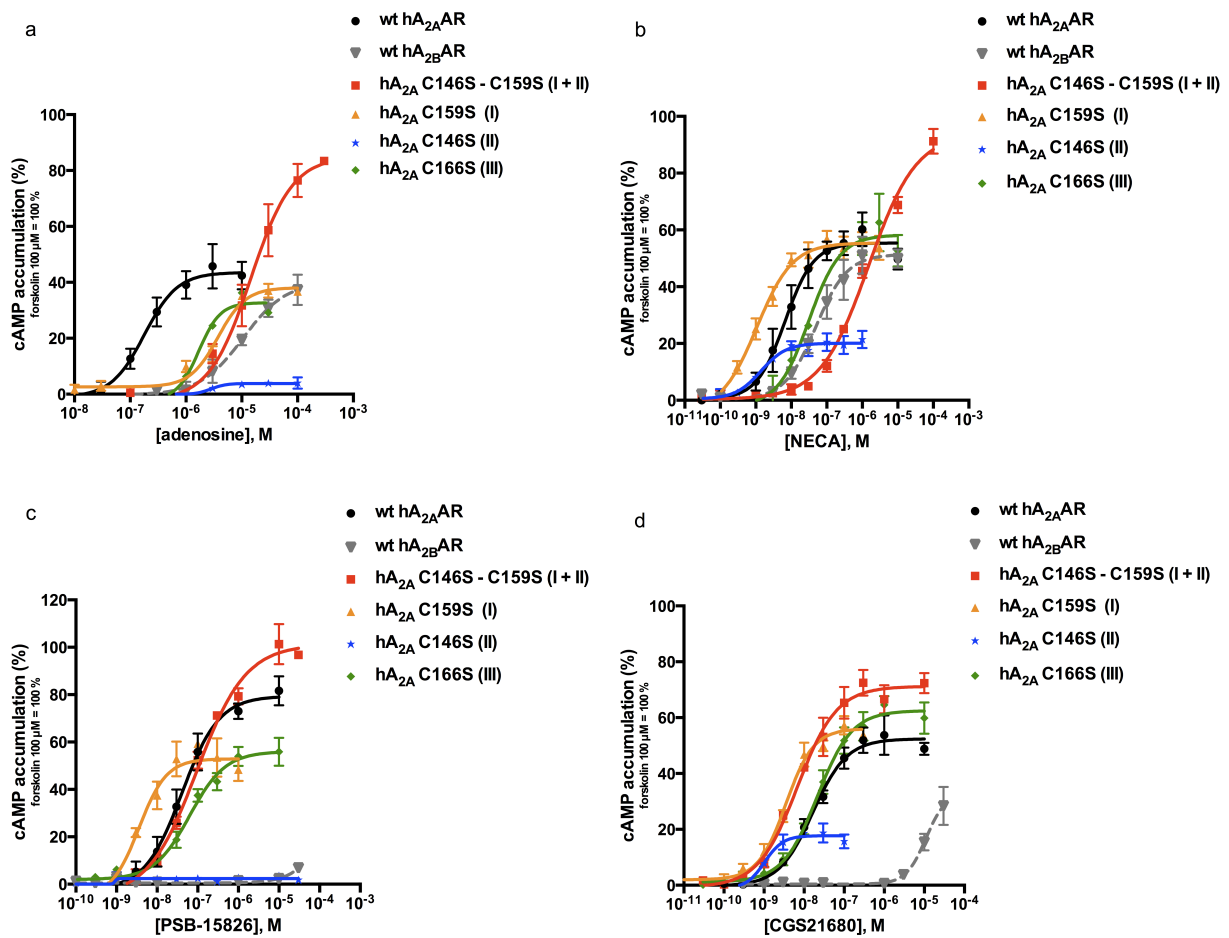


**Figure 14.** Agonist-induced cAMP accumulation studies in CHO cells stably expressing the human wt A<sub>2A</sub>AR, wt A<sub>2B</sub>AR and A<sub>2A</sub> cysteine mutant receptors. Cells were stimulated with different concentrations of selected A<sub>2A</sub> agonists: **(a)** adenosine, **(b)** NECA, **(c)** PSB-15826 or **(d)** CGS21680. The disrupted disulfide bond is indicated in brackets. Data are normalized to forskolin (100 μM), set as 100%. Data represent mean ± SEM of at least three independent experiments performed in duplicates. EC<sub>50</sub> values and maximal effects are listed in Table 7.

**Table 7.** EC<sub>50</sub> values and efficacies of selected A<sub>2A</sub> agonists determined in cAMP accumulation assays at the wt hA<sub>2A</sub>AR, the wt hA<sub>2B</sub>AR and the A<sub>2A</sub> cysteine mutant receptors. Data are normalized to 100 μM forskolin, set as 100%, and represent mean ± SEM of three independent experiments, unless otherwise noted.

compounds		<i>hA<sub>2A</sub> wt</i>	<i>hA<sub>2B</sub> wt</i>	<i>hA<sub>2A</sub> C146S</i>	<i>hA<sub>2A</sub> C166S</i>	<i>hA<sub>2A</sub> C159S</i>	<i>hA<sub>2A</sub> C146S – C159S</i>
<b>adenosine</b>	EC <sub>50</sub> ± SEM (nM)	170 ± 29	11,900 ± 670 <sup>***</sup>	n.d.	5110 ± 32 <sup>a,***</sup>	3670 ± 719 <sup>**</sup>	43,100 ± 8090 <sup>a,**</sup>
	Efficacy ± SEM (%)	44 ± 3	40 ± 6 <sup>ns</sup>	4 ± 1 <sup>**</sup>	33 ± 2 <sup>ns</sup>	38 ± 2 <sup>ns</sup>	85 ± 8 <sup>**</sup>
<b>NECA</b>	EC <sub>50</sub> ± SEM (nM)	10.5 ± 0.8	109 ± 37 <sup>**</sup>	1.43 ± 0.43 <sup>***</sup>	31.4 ± 7.4 <sup>a,ns</sup>	1.27 ± 0.24 <sup>***</sup>	870 ± 107 <sup>**</sup>
	Efficacy ± SEM (%)	55 ± 3	51 ± 4 <sup>ns</sup>	20 ± 1 <sup>**</sup>	58 ± 3 <sup>ns</sup>	55 ± 2 <sup>ns</sup>	94 ± 4 <sup>**</sup>
<b>CGS21680</b>	EC <sub>50</sub> ± SEM (nM)	16.6 ± 0.1	31,100 ± 7130 <sup>***</sup>	0.653 ± 0.055 <sup>***</sup>	25.9 ± 1.1 <sup>a,**</sup>	3.05 ± 0.15 <sup>***</sup>	7.16 ± 1.59 <sup>**</sup>
	Efficacy ± SEM (%)	52 ± 2	33 ± 7 <sup>ns</sup>	18 ± 1 <sup>*</sup>	62 ± 2 <sup>ns</sup>	56 ± 2 <sup>ns</sup>	71 ± 2 <sup>*</sup>
<b>PSB-15826</b>	EC <sub>50</sub> ± SEM (nM)	62.0 ± 14.8	n.d.	n.d.	75.0 ± 16.6 <sup>ns</sup>	2.41 ± 0.79 <sup>*</sup>	83.5 ± 4.1 <sup>ns</sup>
	Efficacy ± SEM (%)	79 ± 4	n.d.	2 ± 1 <sup>***</sup>	56 ± 3 <sup>**</sup>	53 ± 3 <sup>**</sup>	101 ± 4 <sup>*</sup>

n.d. not determined

<sup>a</sup> n = 4

<sup>ns</sup> Not significantly different from wt hA<sub>2A</sub>AR (determined using the two tailed *t*-test)

<sup>\*</sup> p < 0.05

<sup>\*\*</sup> p < 0.01

<sup>\*\*\*</sup> p < 0.001

#### 2.6.4 Binding studies

Competitive binding versus the radioligand [<sup>3</sup>H]CGS21680 (Fig 15) was used to determine the affinity of the cysteine A<sub>2A</sub> mutant receptors for the selected agonists.

The increase in potency noticed in cAMP accumulation assays for the adenosine derivatives at the A<sub>2A</sub> C159S receptor was consistent with the relative gain in affinity found in comparison to the wt A<sub>2A</sub>AR (K<sub>i</sub> values listed in Table 8). Adenosine was not tested in binding experiments since cell membrane preparations already contain endogenous adenosine and cannot be treated with adenosine deaminase, which would hydrolyze endogenous as well as added adenosine. A biphasic behaviour was observed for NECA binding at the C159S mutant receptor, where the low K<sub>i</sub> value (4.92 ± 0.68 nM) was significantly decreased in comparison to the wt A<sub>2A</sub>AR (81.2 ± 11.4 nM).

The A<sub>2A</sub> C166S mutant receptor characterized by a disruption of the “conserved” disulfide bond, showed similar affinity for the adenosine derivatives NECA and CGS21680 and a slight but significant reduction in affinity (1.7-fold) for PSB-15826 (see Table 8).

The double mutant receptor C146S-C159S significantly lost affinity (30-fold) for the small ligand NECA while only a slight decrease (2-fold) was observed for PSB-15826 in comparison with the wt A<sub>2A</sub>AR.

The agonist radioligand [<sup>3</sup>H]NECA has been used only for the A<sub>2A</sub> C146S mutant receptor and a significant loss in affinity was noticed for NECA itself in comparison to the wt A<sub>2A</sub>AR (K<sub>i</sub> values: 7.06 ± 1.27 nM vs. 39.1 ± 1.3 nM, see Table 8).

**Table 8.** Affinities of selected ligands for the wt human A<sub>2A</sub>AR compared to the cysteine mutant receptors determined in radioligand binding studies versus [<sup>3</sup>H]CGS21680 (5 nM) or [<sup>3</sup>H]NECA (3 nM). K<sub>i</sub> values were calculated based on the K<sub>D</sub> values obtained in homologous competition experiments (see Table 6). Data are mean ± SEM of three independent experiments, otherwise noted.

K <sub>i</sub> ± SEM (nM)						
[ <sup>3</sup> H]CGS21680	NECA	Fold shift <sup>d</sup>	CGS21680	Fold shift <sup>d</sup>	PSB-15826	Fold shift <sup>d</sup>
hA <sub>2A</sub> wt	81.2 ± 11.4 <sup>a</sup>		130 ± 1 <sup>a</sup>		118 ± 1	
hA <sub>2A</sub> C166S	99.4 ± 15.2 <sup>ns</sup>	1.2	114 ± 4 <sup>b, ns</sup>	0.9	196 ± 1 <sup>***</sup>	1.7
hA <sub>2A</sub> C159S	<i>low</i> <sup>c</sup> 4.92 ± 0.68 <sup>*</sup>	0.1	50.1 ± 0.7 <sup>b, ***</sup>	0.4	29.2 ± 3.6 <sup>a, ***</sup>	0.3
	<i>high</i> 467 ± 119 <sup>*</sup>	5.8				
	<i>one-site</i> 20.2 ± 0.8	0.3				
hA <sub>2A</sub> C146S – C159S	2490 ± 3 <sup>b, ***</sup>	31	128 ± 10 <sup>a, ns</sup>	1.0	278 ± 8 <sup>a, ***</sup>	2.4
[ <sup>3</sup> H]NECA						
hA <sub>2A</sub> wt	7.06 ± 1.27		17.8 ± 3.5		43.5 ± 5.3	
hA <sub>2A</sub> C146S	39.1 ± 1.3 <sup>***</sup>	5.5	19.5 ± 3.4 <sup>ns</sup>	1.1	33.9 ± 2.2 <sup>ns</sup>	0.8

<sup>a</sup> n = 4

<sup>b</sup> n = 5

<sup>c</sup> *low* and *high* refer to the two K<sub>i</sub> values of the biphasic curve of the C159S mutant, while *one-site* refer to the single K<sub>i</sub> value calculated with one-site competition fit

<sup>d</sup> The shift represents the ratio K<sub>i</sub> (mutant): K<sub>i</sub> (wt)

<sup>ns</sup> Not significantly different from wt hA<sub>2A</sub>AR (determined using the two tailed *t*-test)

<sup>\*</sup> p < 0.05

<sup>\*\*\*</sup> p < 0.001

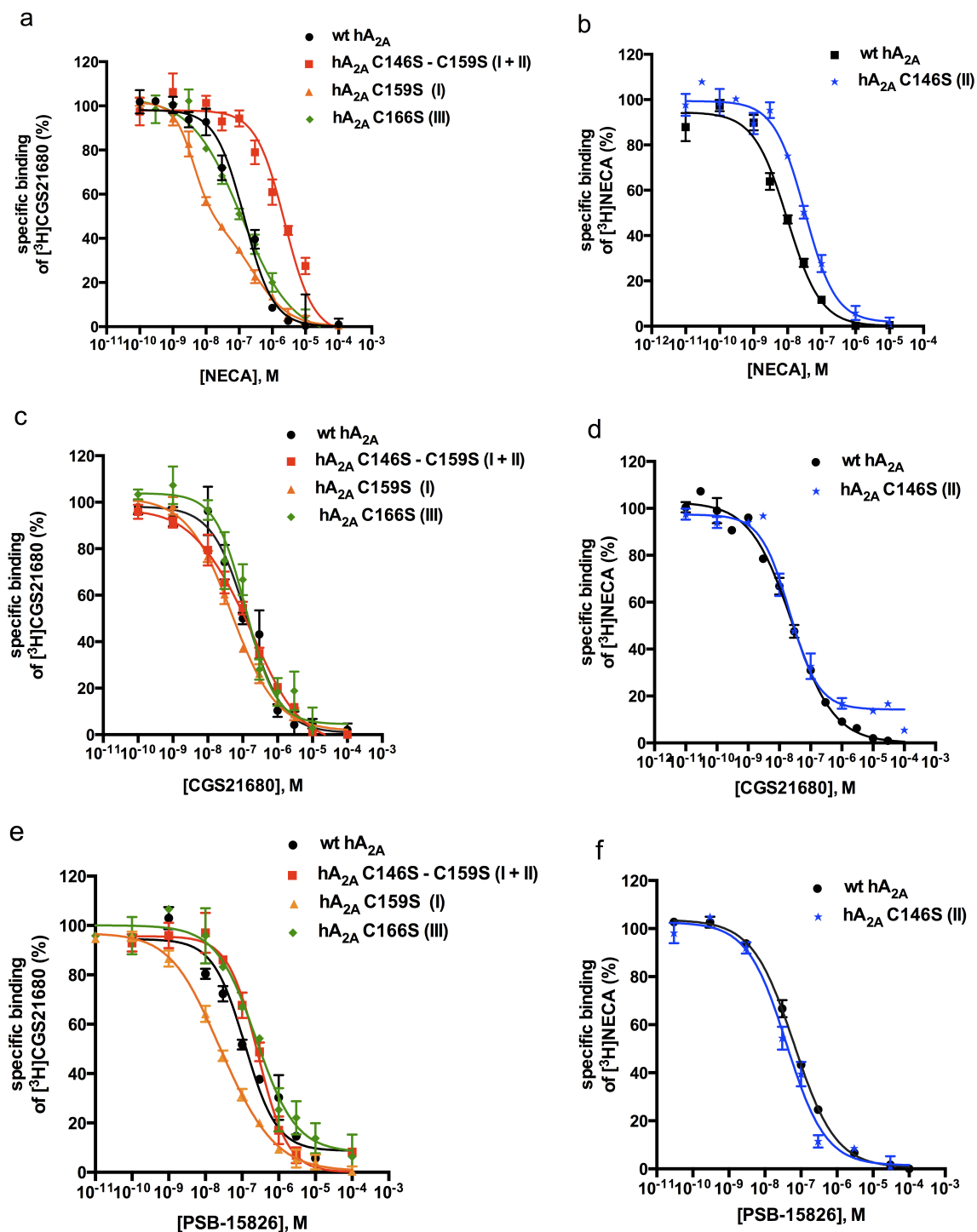


**Figure 15.** Competition binding studies at the wildtype (wt) human A<sub>2A</sub>AR and the A<sub>2A</sub> cysteine mutants versus [<sup>3</sup>H]CGS21680 (5 nM; a, c, e) or [<sup>3</sup>H]NECA (3 nM; b, d, f) testing selected agonists, NECA (a, b), CGS21680 (c, d) and PSB-15826 (e, f). The affinity for the tested agonists at the hA<sub>2A</sub> C146S mutant receptor could be defined only through [<sup>3</sup>H]NECA binding, due to the low mutant expression. The disrupted disulfide bond is indicated in brackets. Data points represent means ± SEM of at least three independent experiments performed in duplicates. The correspondent K<sub>i</sub> values are listed in Table 8.



### 2.6.5 Binding mode and interactions

To understand the significance of the potential extracellular disulfide bonds for receptor function, and to find possible explanations for the results obtained with the mutagenesis experiments, we explored the X-ray crystal structures available for A<sub>2A</sub>AR co-crystallized with the ligands used in this study.

The recent structure co-crystallized with the agonist CGS21680 (4UHR.pdb) was considered as a reference, and the other two structures crystallized with the ligands NECA (2YDV.pdb) and adenosine (2YDO.pdb) were superimposed. For PSB-15826, a putative binding mode was predicted by docking the compound into the known orthosteric binding site of the A<sub>2A</sub>AR (Fig 16). The docking calculation was evaluated by redocking the co-crystallized ligand, CGS21680 which obtained an RMSD value of 0.90 Å. The output for PSB-15826 showed that the lowest binding energy binding pose was well correlated with the binding conformation of CGS21680.

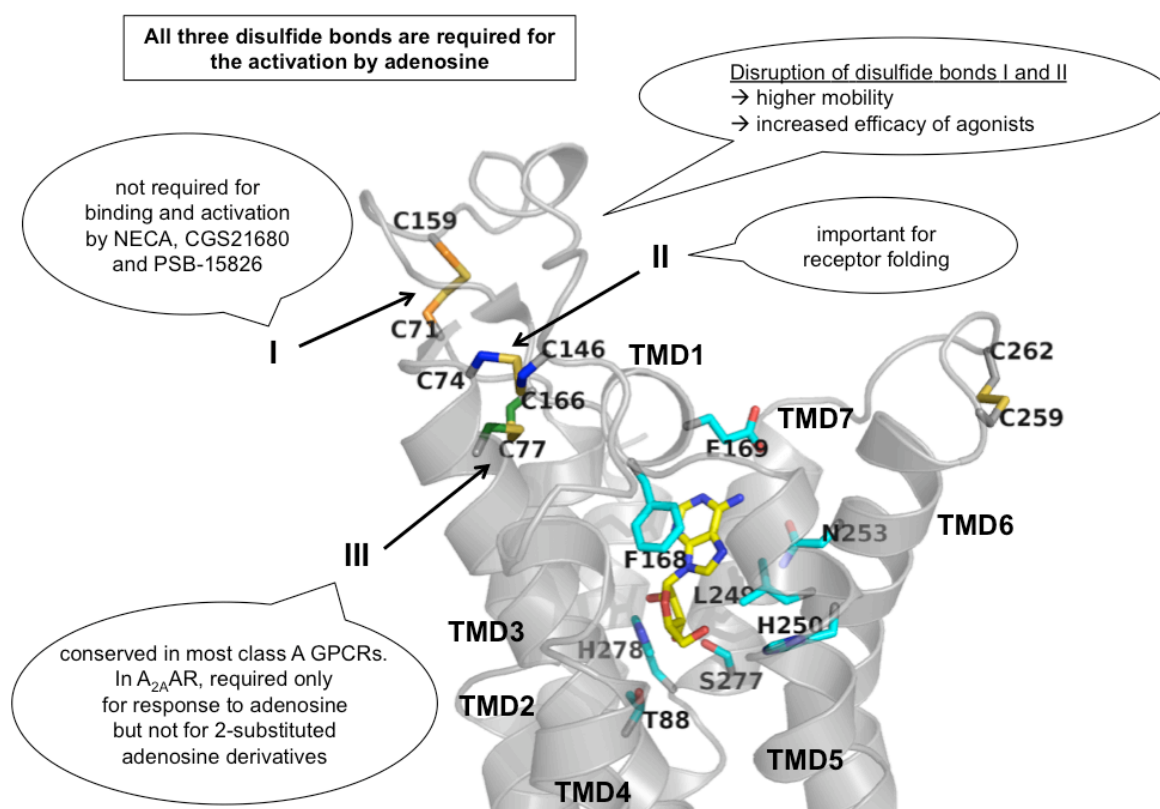


**Figure 16. Binding modes of adenosine.** Crystallographic binding poses of the agonist adenosine, (represented in stick, carbon atoms in yellow) in the active sites of A<sub>2A</sub>AR (represented in ribbon in grey color) with the important residues in the binding pocket (represented in stick, carbon atoms in green color) are shown. Oxygen atoms are colored in red, nitrogen atoms in blue, hydrogen in silver white and sulfur atoms in yellow. Figure credit to Dr. V. Namasivayam and PD Dr. A. Schiedel.

Similar to the binding interactions of adenosine (Fig 16 and 18a), NECA (Fig 17a and 18b) and CGS21680 (Fig 17b and 18c), the adenine moiety forms a  $\pi$ - $\pi$  interaction with Phe168, a hydrophobic interaction with Leu249 and hydrogen bond interactions with the amino acids residues Asn253 and Glu169 (Fig 17c and Fig 18d). The 2-OH function of the ribose interacts with Ser277 and the 3-OH group possibly forms interactions with His278 (Fig 17c). The N-ethylcarboxamido group of NECA and CGS21680 was replaced with a hydroxymethylene group in PSB-15826 which forms interactions with Thr88 (Fig 17c). In comparison, the N-ethylcarboxamido group forms interactions with Thr88 and His250 (Fig 17b). The 2-(4-(4-fluorophenyl)piperazin-1-yl)ethylthio group of PSB-15826 might form hydrophobic interactions with the residues Ile66 and Leu167 similar to the (2-carboxyethyl)phenylethylamino group in CGS21680. On the other hand, the negatively charged carboxy group of CGS21680 and the fluorophenyl group of PSB-15826, which acquires a partial negative charge, might be similarly hydrated in the extracellular space (Fig 18 c-d). This network might stabilize the receptor-ligand complex beyond the interactions with the core adenosine group into the orthosteric binding site of the receptor.

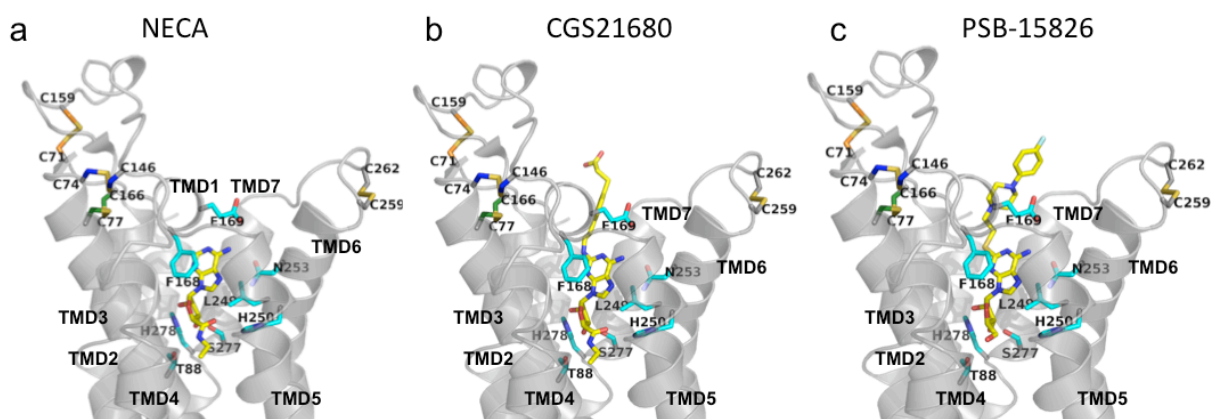


**Figure 17. Binding modes of agonists.** Crystallographic binding poses of the agonist (a) NECA, (b) CGS21680 and (c) PSB-15826 in the binding pocket of A<sub>2A</sub>AR (represented as grey ribbon) are shown. All ligands are shown as sticks with carbons in yellow. The sidechains of important residues in the binding pocket are shown as sticks with carbons in cyan. The cysteine residues involved in disulfide bonds are shown as sticks and the carbon atoms are color coded as follows: Cys74<sup>3,22</sup>-Cys146<sup>45,30</sup> blue, Cys71<sup>2,69</sup>-Cys159<sup>45,43</sup> orange and Cys77<sup>3,25</sup>-Cys166<sup>45,50</sup> green. Figure credit to Dr. V. Namasivayam and PD Dr. A. Schiedel.

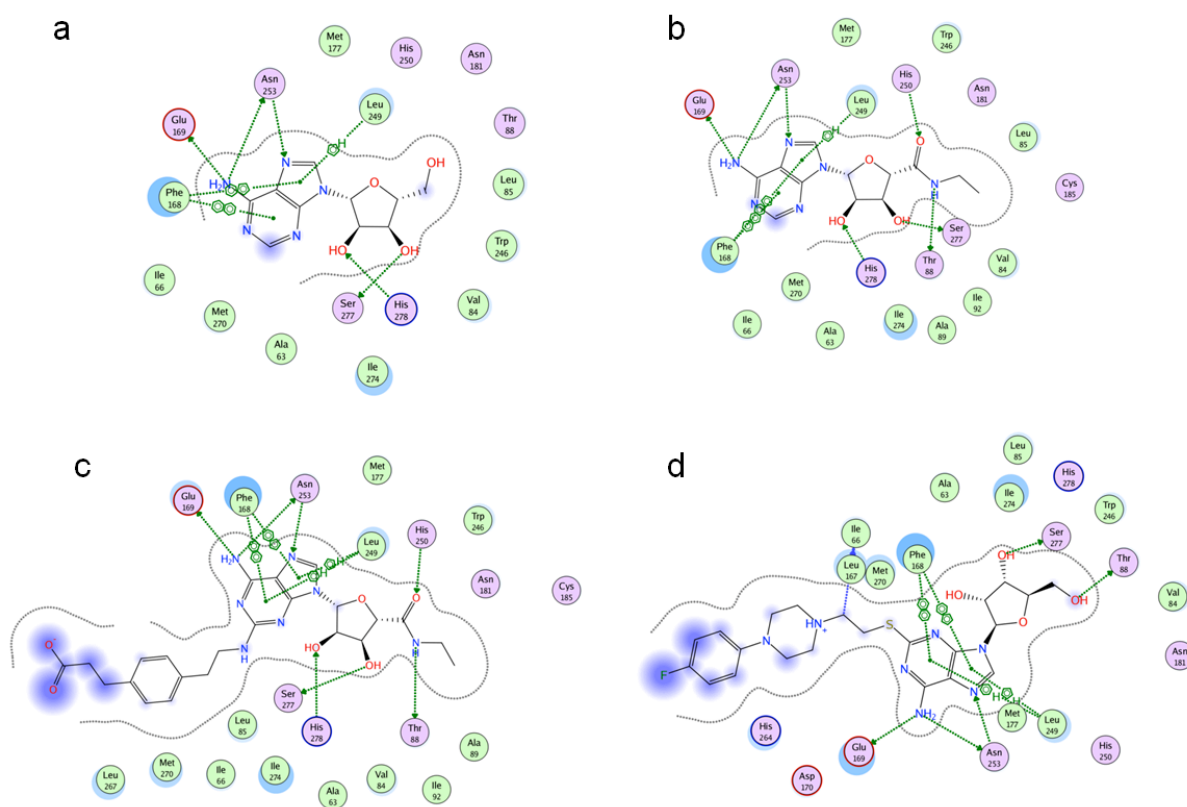


**Figure 18.** 2D interaction diagram for agonists of  $A_{2A}AR$ . The interaction diagrams of the selected agonists (a) adenosine, (b) NECA, (c) CGS21680, (d) PSB-15826 and human  $A_{2A}AR$  are reported.

### 2.6.6 Models of cysteine mutant adenosine $A_{2A}$ receptors

Models of each cysteine mutant  $A_{2A}$  receptor have been generated using the crystallographic structure of the human  $A_{2A}AR$  bound to CGS21680 (4UHR.pdb) as reference. The disulfide bond I (Cys71-Cys159) was formed in the middle of the ECL2 and its disruption could increase the flexibility of the entire loop, in particular the two charged amino acids close to Cys159 such as Gln157 and Gln163, which might then form interactions with the distant residues in the receptor (Fig 19a). When the disulfide bond II (Cys74-Cys146) was disrupted (Fig 19b) by the C146S mutation, the Ser146 was found close to polar residues such as His75 and Asn144 and possibly form intramolecular interactions. In the wildtype  $A_{2A}AR$ , the Cys166 residue was found in proximity of two residues involved in ligand binding, Phe168 and Glu169. The C166S mutation in  $A_{2A}AR$  causing the disruption of the disulfide bond III (Cys77-Cys166) might cause a rearrangement of the two specified amino acids (Fig 19c).

Finally in the double mutant  $A_{2A}AR$ , the disulfide bonds I and II disruption was characterized by a high flexibility of ECL1 and 2 (Fig 19d) influence the orthosteric binding pocket of the receptor. Several charged amino acids close to the mutated Cys146 and Cys159 such as Lys150 and Lys153, induces large flexible movement and accessible to form new interactions.

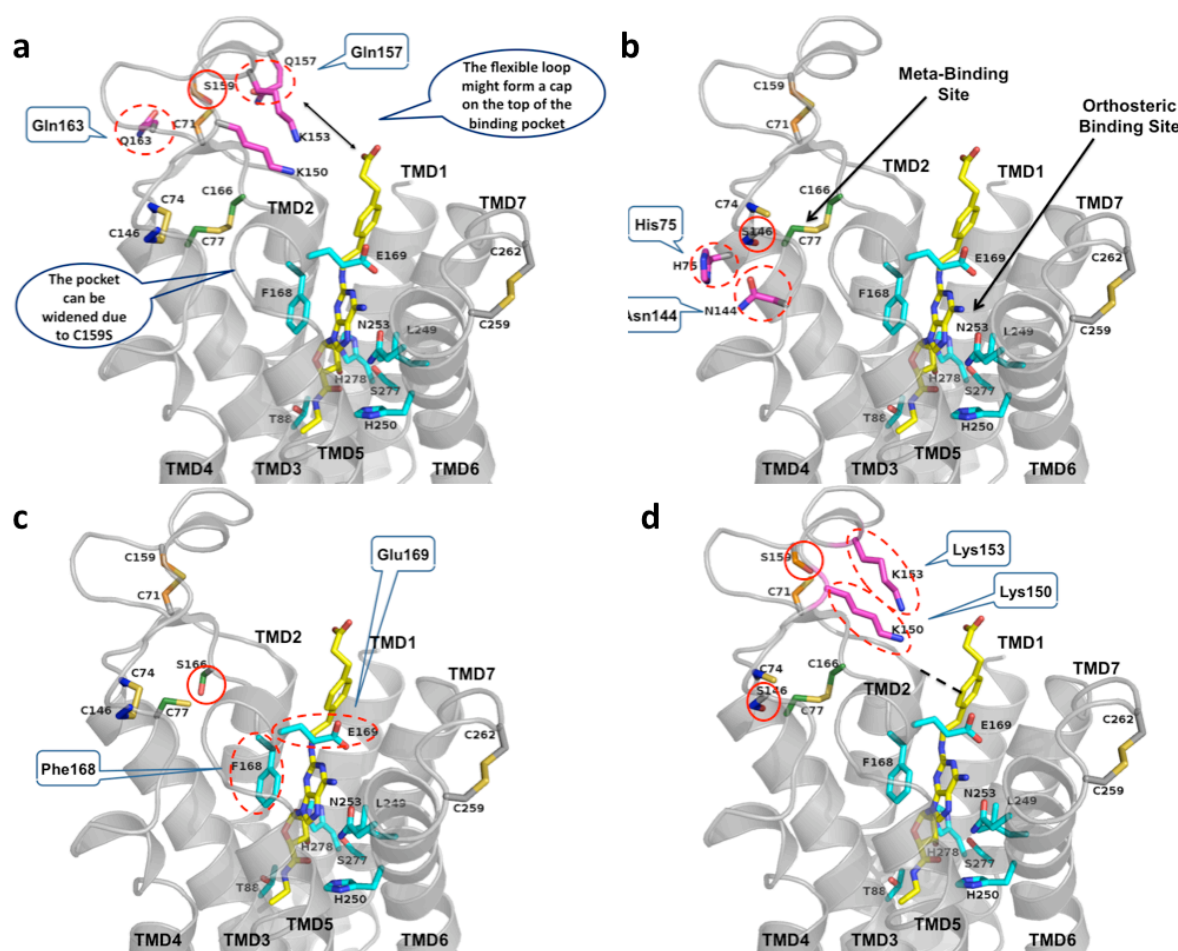


**Figure 19. Mutated models of  $A_{2A}AR$ .** All four models are shown with the ligand CGS21680 (stick representation with carbons in yellow). The sidechains of important residues in the orthosteric binding pocket are shown as sticks with carbons in cyan. The cysteine residues involved in disulfide bonds are shown as sticks and the carbon atoms are color coded as before (Cys74<sup>3,22</sup>-Cys146<sup>45,30</sup> blue, Cys71<sup>2,69</sup>-Cys159<sup>45,43</sup> orange and Cys77<sup>3,25</sup>-Cys166<sup>45,50</sup> green). The mutated residues serine are shown in the respective color code as well. Amino acids which play an important role in the mutated receptors are highlighted as sticks with carbons in magenta and predicted interactions are circled with dotted lines. (a) Disruption of disulfide bond I (C159S). (b) Disruption of disulfide bond II (C146S). (c) Disruption of disulfide bond III (C166S). (d) Disruption of disulfide bonds I and II (C146S-C159S). Figure credit to Dr. V. Namasivayam and PD Dr. A. Schiedel.

### 2.6.7 Discussion

Structural investigation of adenosine receptors (ARs) is critical for rational drug discovery. The four subtypes of ARs ( $A_1$ ,  $A_{2A}$ ,  $A_{2B}$  and  $A_3$ ) respond to a single endogenous agonist, adenosine, and they are ubiquitously expressed in the human body, thereby involved in several pathological conditions [30]. The similarity in the orthosteric binding pockets interferes with the discovery of subtype selective drugs [77]. Therefore, crystal structures with different ligands bound to the ARs and mutagenesis studies are both essential for the investigation of structural and conformational dynamics.

Due to their high flexibility and conformational diversity, the extracellular loops (ECLs) of the  $A_{2A}$ AR have been resolved only in a few of the available crystal structures but the presence of disulfide bonds between ECLs is consistently identified in each of these X-ray structures [50,52,54]. Three disulfide bonds constrain the ECL1 and ECL2, Cys71<sup>2.69</sup>-Cys159<sup>45.43</sup> (I), Cys74<sup>3.22</sup>-Cys146<sup>45.30</sup> (II) and Cys77<sup>3.25</sup>-Cys166<sup>45.50</sup> (III). The latter is conserved among most of the class A GPCRs [11]. The fourth intraloop disulfide bond is present within the ECL3 (Cys259<sup>6.61</sup>-Cys262<sup>6.64</sup>).

The two closely related  $A_{2A}$  and  $A_{2B}$ AR subtypes are characterized by a high sequence identity (58%) however the endogenous ligand adenosine and its derivatives have higher affinity for  $A_{2A}$ AR than for  $A_{2B}$ AR. Contradictory data were also found regarding the essential cysteine residues and extracellular disulfide bonds present in the two AR subtypes. While crystal structures and a molecular modeling study indicated that four extracellular disulfide bonds are formed in  $A_{2A}$ AR [49,50,52,54,69], mutagenesis studies on extracellular cysteine residues have been performed on the  $A_{2B}$ AR subtype [55]. They demonstrated that for  $A_{2B}$  subtype only the two conserved cysteine residues (Cys78<sup>3.25</sup>-Cys171<sup>45.50</sup>) located at the extracellular end of transmembrane domain 3 (TMD3) and in the ECL2 form a disulfide bond which is essential for the ligand binding and receptor folding [55].

Several hypotheses might explain those discrepancies, such as the disulfide bonds solved in the  $A_{2A}$ AR crystal structures are artefacts due to artificial conditions of the crystallization process. Another possibility includes that the cysteine residues found to be not essential for the function of  $A_{2B}$ AR might possess a different role. Therefore, a focused investigation to evaluate the role of the extracellular cysteine residues in the  $A_{2A}$ AR is critical.

The relevance of  $A_{2A}$ AR disulfide bonds for [<sup>3</sup>H]CGS21680 binding was first shown using reducing agents, such as tris(2-carboxyethyl)phosphine (TCEP) and dithiothreitol (DTT)

[85,86]. A recent mutagenesis approach suggested that the conserved disulfide bond in A<sub>2A</sub>AR is not essential for [<sup>3</sup>H]CGS21680 binding and for its plasma membrane expression [70] indicating that the mentioned disulfide bonds found in the A<sub>2A</sub>AR crystal structure might be an artefact. However, the mutagenesis study focused on ligand binding of cysteine residue A<sub>2A</sub>AR mutants utilizing one adenosine derivative, CGS21680, while functional data were not available. Our investigation addressed structural and functional issues involving the A<sub>2A</sub>AR extracellular cysteine residues and the corresponding disulfide bonds.

### **Extracellular disulfide bonds are important for A<sub>2A</sub>AR function**

The first hint of the relevance of disulfide bonds for the function of A<sub>2A</sub>AR was observed by the loss in potency of NECA and CGS21680 in cAMP accumulation assay at the wt receptor after DTT pre-incubation. The treatment caused the disruption of multiple disulfide bonds present in the extracellular surface of the A<sub>2A</sub>AR, therefore, a precise understanding of the importance of single disulfide bonds in the stability and activation of the receptor was not feasible at that point.

### **Role of single extracellular disulfide bonds in A<sub>2A</sub>AR**

In order to get a more complete view about the role of extracellular disulfide bonds of the A<sub>2A</sub>AR, we generated mutant A<sub>2A</sub> receptors in which cysteine residues were exchanged with serine (C146S, C159S, C166S and a double mutant C146S-C159S) focusing on ligand binding and receptor function with a variety of ligands (Fig 5). We tested A<sub>2A</sub>AR agonists with different substituents evaluating their effects on the mutant receptors: as first the endogenous ligand adenosine (**1**), then the derivatives NECA (**2**), the A<sub>2A</sub> selective CGS21680 (**3**) and a bulky 2-substituted derivative PSB-15826 (**5**), which is also selective for the A<sub>2A</sub>AR. When the CHO cell lines stably expressing the mutant receptors were established, two approaches were used to define their expression: by ELISA we characterized the amount of receptors transported to the cell surface and by ligand binding with cell membranes we defined the density of receptors in the preparation (B<sub>max</sub> value).

### **The three extracellular disulfide bonds are critical for A<sub>2A</sub>AR activation by adenosine**

The involvement of the three disulfide bonds between the ECLs in A<sub>2A</sub>AR activation is one of the main foci of the current study. The results obtained with the adenosine-stimulated cAMP accumulation assay showed that all cysteine A<sub>2A</sub> mutant receptors lost potency as compared to the wt A<sub>2A</sub>AR, reaching EC<sub>50</sub> values in the micromolar range, similar to the wt A<sub>2B</sub>AR. All

three disulfide bonds seem to be critical for the response of the A<sub>2A</sub>AR to the endogenous agonist.

### **Disruption of disulfide bond I causes gain in affinity and function of A<sub>2A</sub>AR**

The C159S mutant receptor showed a significant increase in potency for the three adenosine derivatives NECA, CGS21680 and PSB-15826, but not for adenosine itself. This effect could be due to the higher expression level of this mutant in comparison to the wt A<sub>2A</sub>AR defined by ELISA, but the C159S might also be a gain-of-function mutation. It was previously demonstrated that mutations in the ECL2 could lead to constitutively active and gain-of-function mutants in the close homolog A<sub>2B</sub>AR [44,46]. The A<sub>2A</sub> C159S mutant receptor also gained affinity for the adenosine derivatives NECA, CGS21680 and PSB-15826 with 4-fold, 2.6-fold and 4-fold, respectively (Table 8). The disulfide bond Cys71<sup>2,69</sup>-Cys159<sup>45,43</sup> restricts the movement of the receptor and the charged amino acid residues Gln157 or Gln163, which are close to Cys159, were minimized for the natural ligand adenosine. However, for the C159S mutant receptor, the binding pocket might become wider than the wildtype pocket. Therefore, adenosine might stay longer in the meta binding site as compared to the orthosteric binding site due to stronger interactions (Fig 19a). Contrarily, for the larger agonists CGS21680 and PSB-15826 the breakage of the disulfide bridge results in flexible movement of the loop which probably form a cap which retains the compounds in the orthosteric binding site for a longer duration (Fig 19a). During this time, the residues in the loop region such as Lys150 or Lys153 might form interactions with the agonists CGS21680 and PSB-15826 thereby increasing their affinity and potency with the receptor (Fig 19a).

### **Disulfide bond II is critical for cell surface expression of A<sub>2A</sub>AR**

The mutation of Cys146 in A<sub>2A</sub>AR critically affected the cell surface expression of the receptor defined by ELISA, the identified data were supported by *Naranjo et al.* [70], and the agonist-induced cAMP accumulation assay displayed almost no activation at adenosine and PSB-15826 and extremely reduced efficacy at NECA and CGS21680. On the basis of the ELISA results, the reduced functionality of the C146S mutant receptor could be due to the low density of active receptors present at the cell surface. Binding studies versus [<sup>3</sup>H]NECA showed that the affinity of the C146S mutant receptor for CGS21680 did not change as compared to the wt A<sub>2A</sub>AR. However, competitive binding studies versus [<sup>3</sup>H]CGS21680 have not been possible for this mutant. The mutation of Cys146 could have shifted the equilibrium towards the inactive state, lowering the percentage of active state receptors.

NECA, which has higher affinity for the active state than CGS21680, can label more efficiently the low percentage of active state receptors, while CGS21680 cannot label all of them (narrow window between the total binding and the non-specific binding). However, the expression level ( $B_{\max}$  value) of the C146S mutant detected with [ $^3\text{H}$ ]NECA is similar to the wt  $A_{2A}\text{AR}$ , meaning that the amount of total binding sites in the membrane preparation is similar to the one of the wt receptor. We suggest that the disulfide bond Cys74<sup>3,22</sup>-Cys146<sup>45,30</sup> connecting the TMD3 and the ECL2 is critical for the receptor folding and its disruption might cause receptor aggregation and ER retention (Fig 19b), as it was proposed for other cysteine mutant GPCRs [63,87]. The small percentage of mutant receptors transported to the plasma membrane might have adopted a different stabilized conformation due to new interactions which are formed with the exchanged serine residue. The side chain of serine is sterically and electronically similar to the cysteine and can form a hydrogen bond with the nearby residue Asn144 or a salt bridge with His75 (Fig 19b). The competitive binding using [ $^3\text{H}$ ]NECA versus unlabeled adenosine derivatives (NECA, CGS21680 and PSB-15826) was not abolished, however the C146S mutant receptor lost affinity only for NECA. We hypothesize that during the ligand recognition process, the small molecule agonists, such as NECA and adenosine, could probably bind into a pocket in the the ECL2 close to the disulfide bond Cys74<sup>3,22</sup>-Cys146<sup>45,30</sup>. This so-called meta-binding site was described by Moro *et al.* [81]. They investigated  $A_{2A}\text{AR}$ s using a new molecular dynamics simulation approach, supervised molecular dynamics (SuMD), with diverse adenosine receptor ligands and detected for adenosine and NECA a meta binding site in the loop region, to which the affinity of the ligands was almost as strong as for the orthosteric binding site. Thus, the disruption of the disulfide bond Cys74<sup>3,22</sup>-Cys146<sup>45,30</sup> could have an impact on the meta binding site and this can probably explain the loss in affinity for NECA which we found for the C146S mutant receptor (Fig 19b) [81]. In contrast, large agonists, such as CGS21680 and PSB-15826, which are not likely to interact with the meta binding site, are not affected by the mutation of the cysteine residue (Table 8). They seem to bind directly to the orthosteric binding pocket.

### **The GPCR-conserved disulfide bond (III) is not required for activation and binding of $A_{2A}\text{AR}$ by adenosine derivatives**

The cell surface expression of the C166S mutant receptor and its overall density in the membrane suspension was moderately lower than the level obtained for the wt  $A_{2A}\text{AR}$ . In



addition to Cys74<sup>3.22</sup>-Cys146<sup>45.30</sup>, the conserved disulfide bond Cys77<sup>3.25</sup>-Cys166<sup>45.50</sup> could also be involved in the stabilization of receptor folding. The weak loss of potency observed for NECA, CGS21680 and PSB-15826 is most likely due to the lower expression level of the mutant in comparison to the wt A<sub>2A</sub>AR. On the other hand, the endogenous agonist adenosine lost 30-fold potency at the C166S mutant receptor, which cannot be explained by different expression levels. It might therefore be due to the mutation resulting in the disruption of the disulfide bond. As shown in Fig 19c, the location of two of the residues important for the interaction with the adenine core of nucleosidic agonists, Phe168 and Glu169, might be affected by the loss of the disulfide bond when Cys166 is mutated, since it is very close. Thus, the conserved disulfide bond Cys77<sup>3.25</sup>-Cys166<sup>45.50</sup> appears to be essential for the proper activation of the receptor by the endogenous ligand adenosine, as much as the Cys71<sup>2.69</sup>-Cys159<sup>45.43</sup> and Cys74<sup>3.22</sup>-Cys146<sup>45.30</sup> disulfide bonds. Minor variations in affinity were observed between the C166S mutant receptor and the wt A<sub>2A</sub>AR for the adenosine derivatives NECA, CGS21680 and PSB-15826. The adenosine derivatives are characterized by substitutions to the adenine core which interact with the A<sub>2A</sub>AR binding site, stabilizing its conformation and are able to compensate the effect of the conserved disulfide bond disruption. In particular, the loss in potency for adenosine (30-fold) and for NECA (3-fold) comparing the C166S mutant and the wt A<sub>2A</sub>AR confirms that the N-ethylcarboxamido group largely contributes to the stabilization of the ligand-receptor complex. This finding is supported by the results obtained for CGS21680 which are comparable to the wt A<sub>2A</sub>AR. Despite the fact that PSB-15826 has no substitutions at the ribose ring, it slightly lost potency (1.2-fold) and affinity (1.7-fold) as compared to the wt A<sub>2A</sub>AR because the adenine substitution compensates with other interactions (Fig 19c).

### **The 2-substitution length of adenosine derivatives affect affinity and activation of the double mutant receptor**

The double mutant receptor, in which the two suggested non-essential disulfide bonds (Cys71<sup>2.69</sup>-Cys159<sup>5.20</sup> and Cys74<sup>3.22</sup>-Cys146<sup>4.67</sup>) were disrupted, has a similar expression as the wt A<sub>2A</sub>AR. Functional studies showed that the potency and efficacy of this mutant receptor are affected by the length of the substitution in position 2 at the adenine moiety of the ligand. Small ligands as adenosine and NECA showed a considerable loss in potency in the double mutant receptor (253- and 87-fold, respectively) as compared to the wt A<sub>2A</sub>AR. On the other hand, 2-substituted adenosine derivatives as CGS21680 and PSB-15826 only

showed minor changes in potency in comparison to the wt  $A_{2A}AR$ . The affinity of the compounds at the double mutant receptor was affected as well. In the C146S-C159S mutant receptor, a considerable loss of affinity is shown for NECA (31-fold) in comparison to the wt  $A_{2A}AR$ . Similar to functional studies, the long substituted CGS21680 and PSB-15826 displayed only small variations in  $K_i$  values (Table 8). The disruption of two disulfide bonds in the double mutant receptor possibly results in highly flexible ECL1 and ECL2 (Fig 19d). The double disruption could influence the TMD2 and TMD3 of the receptor and furthermore, the residues in the orthosteric binding pocket. The high flexibility of the loop affects the interaction with the agonists in the binding site, as observed for adenosine and NECA. However, the flexible ECL2 of the double mutant receptor might be stabilized by the bulky substituent of CGS21680 and PSB-15826, resulting in similar potency and efficacy as the wt  $A_{2A}AR$ . Probably, as explained for the C159S mutant, the charged amino acids residues Lys150 or Lys153 form interactions with CGS21680 and PSB-15826 and maintain similar potency and affinity to the wt  $A_{2A}AR$  (Fig 19d).

A higher efficacy was observed at the double mutant receptor for adenosine and NECA in comparison to the wt  $A_{2A}AR$ . Small ligands might not be able to stabilize the flexible ECL2 of the double mutant receptor so the equilibrium between receptor conformations is more oriented toward an active form increasing the maximal effect of the small compounds (85% and 94% vs. 44% and 55% for the wt  $A_{2A}AR$ , respectively). A similar increased efficacy was observed in the loop exchange mutant  $hA_{2B}(ECL2\ hA_{2A})$  where the exchange of the ECL2 between the two AR subtypes induces a stabilization of a receptor conformation that couples more efficiently to the  $G_s$  protein [39].

## Conclusions

Functional studies indicated that the three disulfide bonds between ECL1 and 2 are essential for the proper function of the  $A_{2A}AR$  in response to the endogenous agonist adenosine. Inducing a simultaneous reduction of the extracellular disulfide bonds with DTT, we proved that the disulfide bond network is also relevant for the  $A_{2A}AR$  response to adenosine derivatives (NECA and CGS21680). However, when the disulfide bonds are individually disrupted, the receptors compensate the loss of the covalent bridge by forming new interactions involving the exchanged serine residue. Another possibility includes the dynamics of disulfide bonds, as it was suggested for the  $P2Y_{12}$  receptor [63]. Crystallographic studies on  $P2Y_{12}R$  were performed with agonist and antagonist, however, the conserved

disulfide bond is present only in the structure co-crystallized with the agonists 2MeSADP and 2MeSATP [63,88]. Mutagenesis studies of the two conserved cysteine residues did not cause any affinity loss or receptor aggregation. On the other hand, a second extracellular disulfide bond was found in the structure (Cys17-Cys270) and its disruption caused receptor aggregation, meaning that this observed disulfide bond was essential for the receptor's stability and conformation. Similar results were found in our study on A<sub>2A</sub>AR: the disruption of the conserved disulfide bond did not cause any dramatic changes in affinity and potency, except for adenosine, while the disruption of Cys74<sup>3,22</sup>-Cys146<sup>45,30</sup> caused decreased membrane transport.

Another hypothesis could also be that the cysteine residues are involved in different interactions, i.e. direct ligand binding or allosteric disulfide bonds in oxidative stress condition or they could be regulated by the post-translation modification of the close asparagine residue Asn154, which can be glycosylated [55].

In conclusion, all of the predicted disulfide bonds between ECL1 and 2 in A<sub>2A</sub>AR were found to be critical for the proper activation of the receptor when the endogenous agonist adenosine was used. The relevance of each cysteine residue in the ECL2 is ligand specific: while lower potencies at the mutant receptors were noticed for small agonists (adenosine and NECA), larger adenosine derivatives substituted in position 2 with a large residue (e.g. CGS21680) appear to be able to stabilize the flexible extracellular loops in the mutants that are lacking cysteine residues for disulfide formation and, therefore, they showed comparable potency for the mutant receptors. The conserved disulfide bond Cys77<sup>3,25</sup>-Cys166<sup>45,50</sup> is not essential for binding and activation of the receptor by adenosine derivatives while the Cys74<sup>3,22</sup>-Cys146<sup>45,30</sup> is essential for the receptor folding and activation. Further studies are required to understand which could be the possible roles of extracellular cysteine residues in ARs.

### 3. Characterization of the G protein coupled-receptor GPR143

#### 3.1 Albinism

Melanin-related agents in the retinal pigment epithelium (RPE) exert a strong influence on the development of neural retina, a cell layer containing photoreceptors, which is just at the back of the RPE. When melanin is reduced or absent, the neural retina develops abnormally. Mutations in multiple genes that decrease eye pigmentation all share the same developmental eye defects demonstrating that melanin-related agents are crucial for normal development of the visual system. The abnormalities are of great interest because they reveal how melanin-related agents control specific aspects of the developing visual system [89].

Albinism refers to a disease characterized by a group of inherited conditions, in particular little or no pigment in eyes, skin or hair. People affected by albinism inherited altered genes that do not make the usual amounts of melanin. There are different types of albinism and the amount of pigment in the eyes varies .

Ocular albinism is one form of albinism which affects primarily the eyes. There are multiple forms of ocular albinism that are clinically similar (Table 9). The most common variety corresponds to the ocular albinism type I.

**Table 9.** Description of the ocular albinism subtypes. The gene involved is listed together with the main information about the syndroms [90].

Name	Gene involved	Description
Ocular Albinism type I (OA1)	GPR143	Also known as Nettleship-Falls syndrome, it is the most common variety of ocular albinism. OA1 is usually associated with nystagmus. Males show more readily observable symptoms.
Ocular Albinism type II (OA2)	CACNA1F	Also known as Forsius-Eriksson syndrome or "Åland Island eye disease", mostly only affects males, though females are often carriers and can sometimes be symptomatic; it is frequently linked with protanopic dichromacy (a form of color blindness) and with night blindness (nyctalopia).
Ocular Albinism with sensorineural deafness (OASD)	? (Xp22.3)	It is associated with loss of hearing.

### 3.2 Ocular Albinism type I

Ocular Albinism type I (OA1) is an X-linked inherited disease characterized by severe reduction of visual acuity, nystagmus, strabismus, photophobia, iris translucency, hypopigmentation of the retina, foveal hypoplasia and misrouting of the optic tracts, resulting in loss of stereoscopic vision [89]. OA1 is not caused by impairment of melanin production but by reduced number of melanosomes [91], organelles in which melanin is synthesized and stored in retinal pigment epithelium (RPE) and skin melanocytes. The skin pigmentation in OA1 patients is usually not affected or slightly reduced, however subcellular abnormalities, such as the presence of giant melanosomes (“macromelanosomes” shown in Fig 20), reduction of melanosome number and alteration of melanosome motility, were found in both skin melanocytes and RPE [92,93]. The reason why the eyes are more affected than the skin in OA1 patients is still unclear however, several hypotheses about the role of GPR143 in the disease have been suggested.

This form of albinism appears to be caused by a defect in melanosome biogenesis. Ultrastructural analysis of the RPE cells suggests that the giant melanosomes may form by abnormal growth of single melanosomes, rather than the fusion of several, shedding light on the pathogenesis of ocular albinism [94].

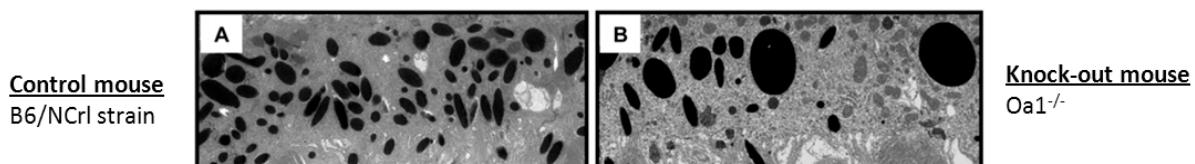


**Figure 20. Retinal pigment epithelium melanosomes from *Oa1* knock-out mice.** The ultrathin RPE sections from *Oa1*<sup>-/-</sup> (B) and their control B6/NCrl (A) mice show that knock-out mice have macromelanosomes in comparison with the control [95].

### 3.3 GPR143 receptor

The protein responsible for ocular albinism type I is GPR143, product of the *OAI* gene located on the distal short arm of the X chromosome [96]. Despite the low amino acid sequence conservation, GPR143 shares structural and functional similarities with different classes of G protein-coupled receptors (GPCRs; Schiaffino et al. 1999) but it still unclear to which family it belongs.

Furthermore, the receptor is highly expressed in pigmented cells such as melanocytes and RPE [96]. Unlike most of the GPCRs, GPR143 is not localized at the cell plasma membrane but is targeted to the membrane of melanosomes. The sorting mechanisms of GPR143 are still not clear but evidences show that it follows the lysosomal/melanosomal sorting pathway as other melanosomal proteins (e.g. tyrosinase, TYR, and tyrosinase-related protein 1, TRP1) [98]. Supporting this hypothesis, two sorting signals were found in the intracellular loop 3 and in the C-terminal tail of GPR143 which were demonstrated to be necessary and sufficient for its intracellular localization (Fig 21) [99]. These two sorting signals are recognized by non-melanocytic cells as well, indeed GPR143 is localized at the membrane of late endosomes and lysosomes in transfected non-pigmented cells [99,102,103].

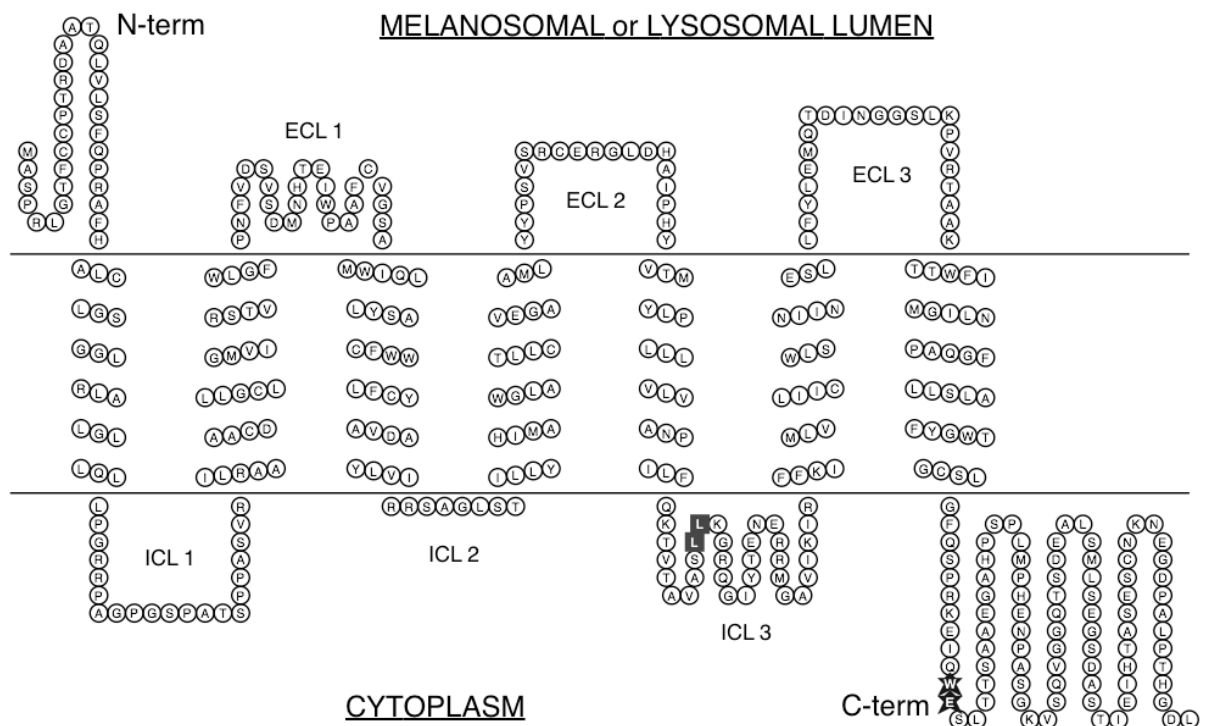


**Figure 21. 2D topology structure of GPR143 predicted by TMHMM Server [62,102].** The two sorting signals necessary and sufficient for GPR143 intracellular localization are highlighted (dileucin motif in the intracellular loop 3 and tryptophan-glutamic acid doublet in the C terminal tail) [99].

The endogenous GPR143 receptor was analyzed by Western blot (Fig 22) in healthy human melanocytes. It was extracted as a doublet of 45-48 kDa and a band migrating at 60 kDa corresponding to different patterns of glycosylation [100].

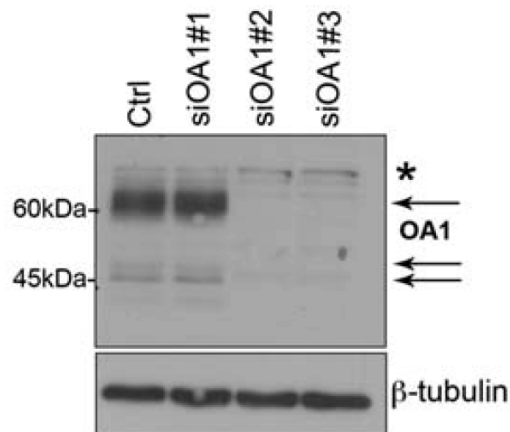


**Figure 22. Western blot showing GPR143 receptor as a doublet at 45-48 kDa and a large band at 60 kDa.** In the first well, the lysate of healthy human melanocytes was analyzed, while in the other samples three different oligonucleotides were tested to silence GPR143 expression [103].

There are three potential N-glycosylation sites in the sequence of mouse GPR143 (asparagine residues: 101, 106 and 263), but only two sites are conserved in the human GPR143 sequence (asparagine residues: 106 and 263). N106 seems to be the only or the first site which is actually glycosylated but the possibility that the other two sites may be glycosylated or that the first site is necessary for the second site to undergo glycosylation is not excluded [104]. Additional post-translational modifications in addition to N-glycosylation are feasible.

Several types of mutations were identified within the GPR143 gene in OA1 patients, including deletions, frameshifts, stop-codon insertion and a number of missense mutations. GPR143 mutants can be classified into two biochemical groups. The group I mutants displayed a glycosylation pattern completely overlapping the wildtype one and a cytoplasmic vesicular distribution, more concentrated in the perinuclear area and spread toward the periphery. The group II mutants showed an altered glycosylation pattern, characterized by the absence of the 60 kDa glycosylated form. These GPR143 mutants appear unable to undergo complete processing in the Golgi apparatus which could affect the correct folding of the receptor. They exhibited a fine reticular distribution, with staining of the nuclear membrane, consistent with protein accumulation in the endoplasmic reticulum (ER) [101,105].

The mutations belonging to the group I might affect important residues for the signaling activity of GPR143. In contrast, mutations of the group II (mainly concentrated within or close to the putative TM domain) appear to cause the retention of the GPR143 in the ER, preventing its proper glycosylation in the Golgi apparatus and its final targeting to the lysosomes/melanosomes [105].

### **3.4 Subcellular localization debate**

In contrast to canonical GPCRs, GPR143 is not localized to the cell surface but it is exclusively detectable on the membrane of intracellular organelles. However some controversy exists on the precise subcellular localization of the protein.

By double immunofluorescence in normal human melanocytes, the endogenous GPR143 was found to co-localize with the melanosomal matrix glycoprotein Pmel17 [97,106], which label melanosomes at early developmental stages [107]. The proteomic analysis of the purified early melanosome fraction obtained from the human melanoma line MNT1 confirmed that GPR143 is associated to these organelles [108]. In addition immunogold and immunoperoxidase assays in normal human melanocytes demonstrated that GPR143 is also present on melanosomes at later stages of maturation [97,100].

By contrast, studies on the mouse ortholog showed that the recombinant GPR143 linked to GFP in mouse melanocytes co-localized widely with LAMP1, lysosomal marker, but only modestly with tyrosinase-related protein 1 (TRP1), marker of mature melanosomes [104]. Then, upon density gradient fractionation of subcellular organelles, GPR143 was not found to peak at the dense fraction as tyrosinase and TRP1, suggesting that it is mostly an endo-lysosomal protein, with minimal or no co-localization with melanosomes [104].

The reason for these discrepancies might partially lie in the different techniques, markers and cell models utilized. In order to solve this issue, quantitative immunofluorescence and immunogold analyses of GPR143 distribution were performed in MNT1 cells, demonstrating that the receptor was similarly distributed along both the late endosomal/lysosomal and the melanosomal compartment [109].

Previous studies showed that GPR143 was ubiquitinated and this was essential for its targeting to the intraluminal vesicles of multivesicular bodies (MVBs) in non-melanocytic



and melanocytic cells. In pigmented cells, ubiquitination of GPR143 was likely to control the balance between down-regulation and delivery to melanosomes [110].

### 3.5 Intracellular signaling pathway and ligands

The endogenous GPR143 was found to co-precipitate with the  $G_{\alpha i}$ ,  $G_{\alpha o}$  and  $G_{\beta}$  subunits of heterotrimeric G proteins in melanocytes extracts [97]. Similar results were obtained in COS7 cells transfected with the wildtype GPR143, but not with the mutants carrying amino acid substitutions identified in OA1 patients [97]. In addition, the intracellular loop 3 and the C-terminal tail of GPR143 were able to bind  $G_{\alpha i}$ ,  $G_{\alpha q/11}$  and  $G_{\beta}$  by *in vitro* binding assay [97].

An agonist-independent or constitutive activity of GPR143 was demonstrated expressing the receptor with its putative G protein partners in a heterologous system. When GPR143 was expressed in COS7 cells together with  $G_{\alpha 15}$  (PLC $\beta$ -coupled G protein), the protein was able to induce a significant accumulation of inositol 1,4,5-trisphosphate compared to G proteins alone, GPR143 mutants and even unstimulated or ligand-activated canonical GPCRs [111].

GPR143 phosphorylation and its interaction with  $\beta$ -arrestin protein were demonstrated by co-localization and co-precipitation studies [111].

Topological orientation studies indicated that GPR143 had an odd number of transmembrane domains and the C terminal tail is oriented towards the cytoplasm. These findings underlined that putative ligands should bind from melanosome lumen [97,112].

In 2008 levodopa (L-DOPA) and dopamine (DOPA) were found to bind GPR143 at high concentrations (L-DOPA  $K_d$  9.35  $\mu$ M and DOPA  $K_d$  2.39  $\mu$ M) and activate the intracellular calcium release through  $G_{q/11}$  protein coupling in transfected CHO cells [113].

Since GPR143 was found to be expressed not only in pigmented cells but also in parts of the central nervous system (mainly in cerebral cortex and hypothalamus) and in some peripheral tissues (kidney, spleen and lung) [114], the role of DOPA and L-DOPA in the development of neural retina was investigated.

*Hiroshima et al.* studied the role of L-DOPA on GPR143 in the central nervous system, showing that the compound has a lower affinity for GPR143 than described before ( $K_d$  79.1  $\mu$ M) and does not cause calcium release in CHO cells but only in cells derived from RPE [115].

The association of GPR143 with L-DOPA and the role of its signaling is still an unclear issue however, recent evidences demonstrated that L-DOPA accumulated in RPE is critical for the proper development and differentiation of cells in the neural retina [116]. Those findings could explain the perturbed neural cell generation in different albinism types, such as tyrosinase-mutated albinism, in which the L-DOPA concentration in RPE is very low during the neural retinal development, or OA1, in which GPR143 is mutated and its signaling might be inhibited [117].

### **3.6 Tyrosinase**

Tyrosinase is the key regulatory enzyme of melanogenesis, catalyzing three distinct reactions in the melanogenic pathway: oxydation of L-tyrosine to L-DOPA, dehydrogeneation of L-DOPA to dopaquinone and dehydrogenation of a dihydroxyindole (Fig 23).

The structure of tyrosinase is highly conserved among different species and shows high homology with other tyrosinase-related proteins including tyrosinase-related protein 1 (TRP1) and tyrosinase-related protein 2 (TRP2). The N terminal domain of tyrosinase comprises a signal peptide (important for intracellular trafficking and processing), the EGF-like/cysteine-rich domain, two histidine-rich regions binding coppers with a cysteine-rich region between them (important catalytic domain), the hydrophobic transmembrane domain and the cytoplasmatic tail (Fig 24). The cytoplasmatic tail contains the dileucin motif for the melanosomal sorting, indeed a missense mutation in the *platinum* allele of the murine tyrosinase, which produces a truncated protein lacking the cytoplasmatic dileucin motif, results in improper targeting of tyrosinase and the albino phonotype (mice are a shade darker than albino) [118].

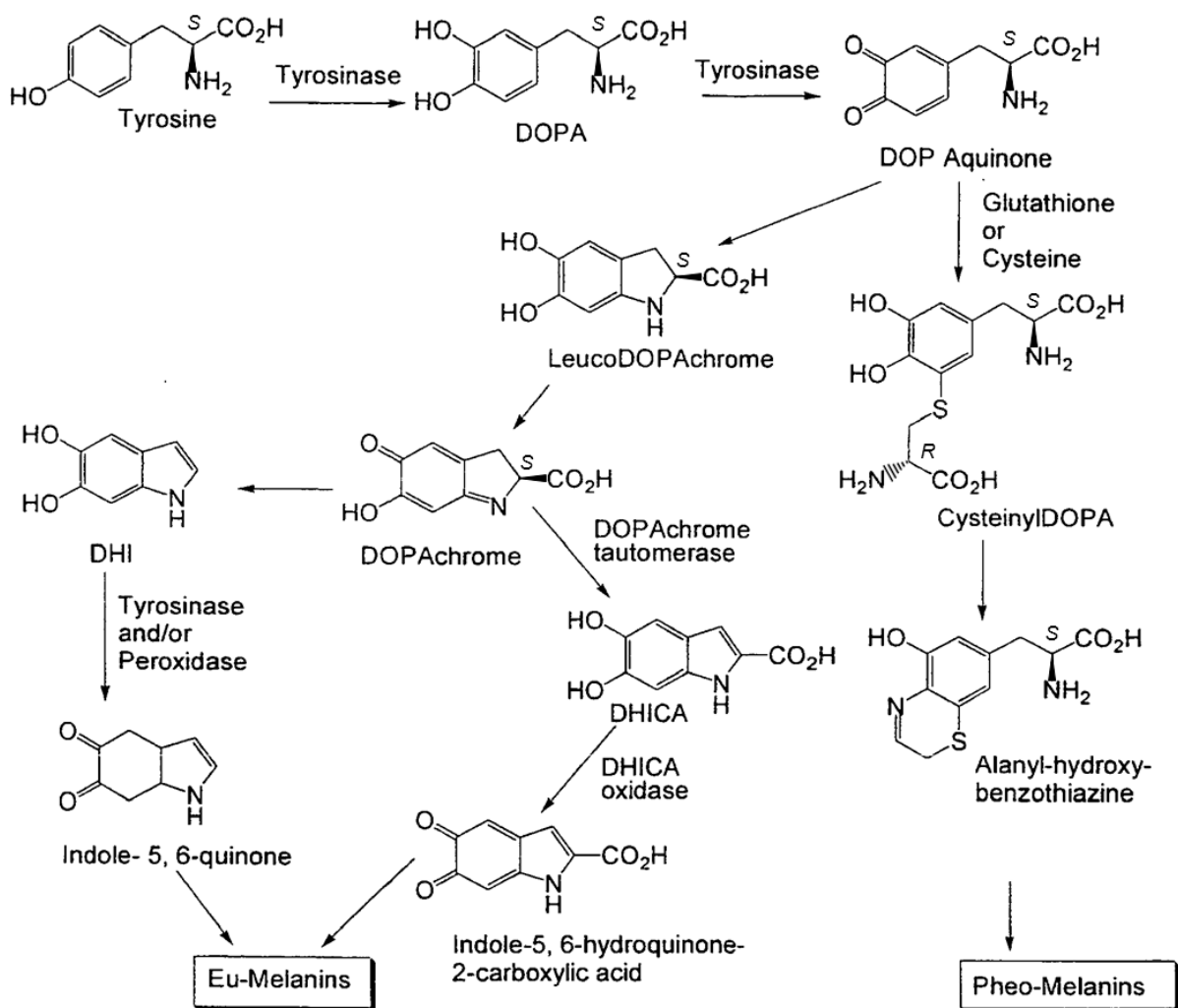


**Figure 23. Enzymatic activity of tyrosinase in the melanogenic pathway** (adapted from [119]). Melanin is produced by the oxidation of the amino acid tyrosine, followed by polymerization. In the skin there are two types of melanin: eumelanin and pheomelanin. Eumelanin can be brown or black melanin, which chemically differ from each other in their pattern of polymeric bonds. Pheomelanins differs from eumelanins in that the oligomer structure incorporates benzothiazine and benzothiazole units that are produced, when the amino acid L-cysteine is present.

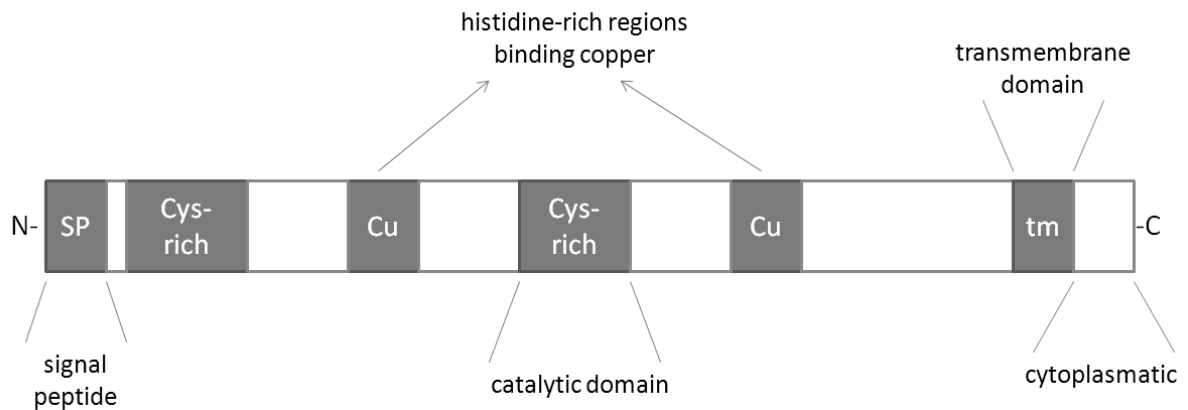


**Figure 24. Scheme of tyrosinase structure with the most important domains:** a signal peptide, the EGF-like/cysteine-rich domain, two histidine-rich regions binding coppers with a cysteine-rich region between them (catalytic domain), the hydrophobic transmembrane domain and the cytoplasmic tail [120].

Newly synthesized tyrosinase has a molecular mass of 55-58 kDa. Proteolytic cleavage of the transmembrane portion of the enzyme generates two soluble molecular forms: a 53 kDa unmodified protein or a 65 kDa glycosylated tyrosinase, which may be active in the melanosome or secreted into the extracellular environment. After glycosylation (N- and O-glycosylation) in the trans-Golgi complex, tyrosinase increases in size to 65-70 kDa or even 80 kDa [121,122]. In melanocytes and melanoma cells tyrosinase exists in both membrane-bound and soluble forms. Proteolytic cleavage of the membrane-bound enzyme near the C terminal tail produces a soluble form with equivalent activity [123].

Defects in tyrosinase gene lead to the tyrosinase negative oculocutaneous albinism type I (OCA1). In addition to mutations in hot spots (copper binding domains), the entire coding sequence of the gene is susceptible to mutations. These include missense, non-sense, frameshift and splicing abnormalities. If translated, mutant tyrosinase proteins are routed for degradation by proteasomes (due to the retention of misfolded proteins in the ER), rather than allowed to pass to the Golgi apparatus for glycosylation and further transport to premelanosomes [121].

L-DOPA seems to be involved in both tyrosinase and GPR143 signaling pathways and previous studies also showed that if GPR143 was silenced by iRNA (interference RNA), the melanin production in MNT-1 cells was modified *in vitro* [103].

### 3.7 GPR143 functions

Hypotheses about the role of GPR143 in the melanogenesis process have been suggested but a clear model of the receptor mechanism of action is still required. Understanding the function of GPR143 and which pathways it regulates may be instrumental for investigating how neurogenesis is regulated during optic development.

Several evidences demonstrated that macromelanosomes derive from an abnormal growth of single organelles, rather than from the fusion of different mature melanosomes [94]. Thus GPR143 seems to be involved in the regulation of melanosome biogenesis [104,124], functioning as stop signal for melanosome growth during melanogenesis. GPR143 mutations which affect its function would permit the continuous import of melanosomal proteins into melanosomes resulting in giant organelles because the downstream signaling pathway is compromised.

Based on its topological orientation into the melanosomal membrane [97,112], GPR143 ligands should bind from the organelle lumen and transduce information to the cytosol through activation of heterotrimeric G proteins. In this way, GPR143 could function as a “sensor” of melanosomal maturation inhibiting the organelle overgrowth [109].

Another role assigned to GPR143 is the ability to control the melanosome transport inside the cell regulating the microtubules-mediated motility [93]. Since GPR143 could be sensitive to the melanosomal maturation, it could transduce this information in the cytosol and through a signalling cascade trigger the undeveloped organelles close to the perinuclear region for a complete maturation.

*In vivo* studies with GPR143 and TYR double mutant mice demonstrated that GPR143 has a double function in two different stages of melanosome maturation: first, at early stages of organellogenesis GPR143 controls the rate of melanosome biogenesis (GPR143 mutation affects the number of melanosomes) and at final stages of melanosomal maturation (stage III and IV) GPR143 might regulate the organelle size, inhibiting the overgrowth [91]. This hypothesis was supported by the finding of a previously unknown function of GPR143: the regulation of transcription of genes involved in melanosome biogenesis [125]. GPR143 may regulate the expression of the microphthalmia-associated transcription factor (MITF), the key gene controlling the expression of several melanosomal proteins. In this way, GPR143 is included in a feedback loop since it was proved that MITF controls expression of GPR143 itself [125,126].

Recently, an additional evidence clarified the role of GPR143 in the melanogenesis process: in HeLa cells GPR143 signaling inhibits at the endosomal stage the lysosomal delivery of proteins and blocks the fusion of multivesicular bodies (MVBs) with lysosomes [127]. These findings are in agreement with the suggested role of GPR143 to be a sensor of melanosomal maturation, delaying the endosome-lysosome fusion in order to allow time for the delivery of melanin-synthesizing enzymes at later melanosome stages in order to synthesize and deposit melanin in Pmel-containing melanosomes.

The connection between GPR143 and the melanosomal biogenesis and maturation was suggested by several studies *in vitro* and *in vivo* but the mechanism by which the receptor perceives the maturation of the organelle is still an unsolved question [91,104,109,124].

### 3.8 Aim of the project

The role of GPR143 in the development of neural retina and in the Ocular albinism type I pathogenesis is still not clear. Several evidences obtained by *in vitro* experiments and *in vivo* observations suggested different hypotheses about GPR143 function but the reason why GPR143 mutations induce severe defects in the visual system while the skin is not affected is unknown.

As first, our investigation focused on the role of GPR143 and its intracellular signaling cascade. Besides the suggested  $G_{q/11}$  protein coupling after L-DOPA stimulation, GPR143 was found to co-precipitate with  $G_{\alpha_o}$ ,  $G_{\alpha_i}$  and  $G_{\beta}$  subunits of heterotrimeric G proteins in melanocyte extracts [97,113]. In addition, a GPR143 constitutive activity and co-localization with  $\beta$ -arrestin 2 and 3 were detected in transfected COS7 cells [111]. The purpose of our study was to find a **pharmacological tool suitable to analyze GPR143 function**, such as a compound able to activate or inhibit the receptor signaling. Due to its intracellular localization, it is problematic for compounds with different sizes and hydrophobicity levels to reach GPR143. Thus, we generated a double mutant receptor exchanging the two sorting signals necessary for melanosomal/lysosomal localization to alanine residues [99] in order to have the receptor expressed at the cell plasma membrane. Beyond the establishment of CHO cell lines expressing the wildtype and mutant GPR143, L-DOPA was the first compound tested for the activation of calcium,  $\beta$ -arrestin and cAMP downstream signaling pathways.

Since the  $\beta$ -arrestin recruitment assay was suitable for high-throughput screening, two compound libraries were tested against GPR143 searching for selective and valuable ligands.

The second part of the project was oriented toward GPR143 function as “sensor” of melanosomal maturation. The connection between GPR143 and the melanosomal biogenesis and maturation was suggested by several studies *in vitro* and *in vivo* but the mechanism by which the receptor perceives the maturation of the organelle is still an unsolved question [91,104,109,124]. The knowledge about the interaction between GPCRs and other proteins is getting more and more critical for the receptor folding, signaling and function [128]. Thus the purpose of our study was to investigate a hypothetical connection between **GPR143 and tyrosinase**, the main enzyme responsible for the melanin synthesis and thus for the melanosomal maturation. Taking advantage of the double mutant GPR143 expressed at the cell plasma membrane and through the optimization of several methodologies, such as immunoprecipitation, co-localization studies and Fluorescence Resonance Energy Transfer (FRET), we defined the physical interaction between GPR143 and tyrosinase in different cells systems.

The work shown in the following result sections is included in two manuscripts:

- **De Filippo E.**, Manga P. and Schiedel A.C. (*in preparation*). Identification of novel GPR143 ligands useful as pharmacological tools.
- **De Filippo E.**, Schiedel A.C. and Manga P. (*in preparation*). GPR143-tyrosinase interaction as a measure of melanosome maturation.

### **3.9 Part I: GPR143 ligands as pharmacological tools to analyze receptor function**

#### **3.9.1 Characterization of wildtype and mutant GPR143 in CHO cells**

The starting point of our research was to generate a cell-based system expressing GPR143 suitable for screening of compound libraries. The GPR143 intracellular localization and its topological orientation in the lysosomal/melanosomal membrane constituted a challenging issue for this purpose. The GPR143 amino acid sequence contains two sorting signals responsible for its intracellular localization and recognized by non-melanocytic cells as well [99]. Exchanging these two sequences with alanine residues (L223A-L224A and W329A-E330A), we generated a double mutant GPR143 which we assumed was transported at the cell plasma membrane and whose putative binding site was oriented toward the extracellular space.

GPR143 was found to co-localize and co-precipitate with  $\beta$ -arrestin, which is involved in agonist-mediated desensitization and signaling transduction of GPCRs. Thus, we established a  $\beta$ -arrestin cell line expressing either the wildtype (wt) or the mutant GPR143 in order to set up a  $\beta$ -arrestin recruitment assay, which was also suitable for high-throughput screening.

CHO cells were used as *in vitro* system for the expression of GPR143 and for the establishment of the  $\beta$ -arrestin recruitment assay, since these cells do not endogenously express the receptor of interest and untransfected CHO cells can be used to control the specificity of the ligand targeting.

The C terminus of wt and mutant GPR143 were linked to a ProLink (PL) tag, which is a  $\beta$ -galactosidase fragment, and the obtained constructs were transfected in CHO cells already containing the  $\beta$ -arrestin protein linked to the second  $\beta$ -galactosidase fragment, Enzyme Acceptor (EA) fragment.

Several plasmids were available from DiscoverX to link the GPCR of interest to the ProLink tag, such as PL1, PL2, ARMS1 and ARMS2. The ProLink2 (PL2) tag has higher affinity for EA than the original ProLink (PL1) tag (~3-fold greater) and is useful for weak protein-protein interactions. G-protein Receptor Kinase (GRK) phosphorylates GPCRs; facilitating recruitment of arrestins. The Arrestin Recruitment Modifying Sequence (ARMS) is a G protein receptor kinase (GRK) consensus phosphorylation site deduced from analysis of GPCRs which generate a high signal-background in the assay. We subcloned the wildtype and mutant GPR143 in the four vectors and transfected them in CHO cells. The expression of the



mutant receptor was firstly quantified in the four cell lines by RT-PCR using two set of primers designed to bind within the cDNA sequence of GPR143. The aim was to compare the relative copy number of receptor between four established cell lines, using as control the house keeping gene  $\beta$  actin.

The relative quantification of the samples was normalized to the control, set as 1 (Fig 25a). The highest expression of the mutant GPR143 was found in ARMS2 and ProLink2 (~20 and 15 fold higher than the control).

Before the compound test, we quantified the basal activity of the cell lines expressing GPR143 in the  $\beta$ -arrestin recruitment assay. We observed an higher recruitment of  $\beta$ -arrestin without any compound stimulation as compared to untransfected CHO cells (Fig 25b). Cells expressing GPR143 in ProLink2 and ARMS2 plasmids showed the highest basal activity for wildtype and mutant GPR143. This constitutive activity was correlated with the relative expression of the receptor measured by RT-PCR.

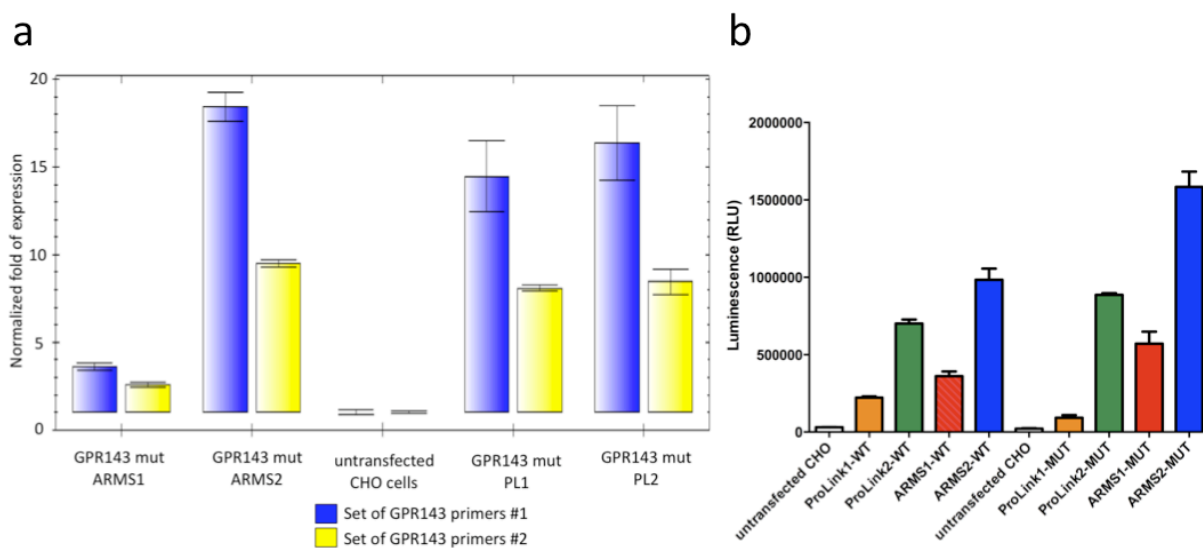


**Figure 25. GPR143 expression in CHO cells transfected with different ProLink vectors. (a)** Relative quantification of mutant GPR143 expression in stable transfected  $\beta$ -arrestin CHO cells by qPCR. The expression was normalized to the control, untransfected  $\beta$ -arrestin CHO cells. Two sets of primers were tested: H1-H2 shown in blue and H3-H4 shown in yellow (n=2). **(b)** Basal activity of CHO  $\beta$ -arrestin cell lines established with four ProLink vectors expressing GPR143 wildtype or double mutant. The cell lines with the higher constitutive activity in comparison to the control were the ones transfected with ProLink2 (green) and ARMS2 (blue) plasmids (n=2).

The CHO cells transfected with the ProLink2 and ARMS2 plasmids had the higher GPR143 expression among the four cell lines however, the modified ProLink tag of ARMS2 might increase aspecific signals. Thus, we decided to use the CHO cells transfected with the ProLink2 for further experiments.

Using an antibody anti-PL and a plasma membrane marker (E-cadherin), we detected the subcellular localization of the wt and mutant GPR143 in the stably transfected  $\beta$ -arrestin CHO cell lines (Fig 26). While the wt receptor is intracellularly expressed in the perinuclear region and in cytoplasmatic vesicles, the mutant GPR143 is also present at the cell surface co-localizing with the plasma membrane marker.

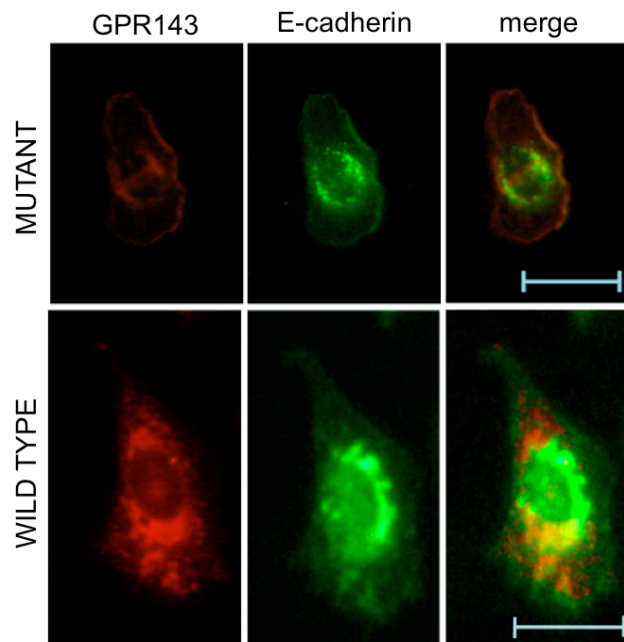


**Figure 26. Characterization of CHO  $\beta$  arrestin cells expressing wildtype (wt) or mutant GPR143.** The subcellular localization of GPR143 was detected by immunofluorescence. Cells were fixed and stained with monoclonal anti-ProLink antibody (against PL-tagged GPR143) and polyclonal anti-cadherin antibody (plasma membrane marker). Scale bars represent 10  $\mu$ m.

### 3.9.2 GPR143 stimulation with levodopa

The  $\beta$ -arrestin CHO cell lines expressing the wt or mutant GPR143 were used to investigate the potential levodopa (L-DOPA) activation of different signaling pathways. As previously described, we noticed that CHO cell lines expressing wt and mutant GPR143 when not stimulated showed a high basal activation in  $\beta$ -arrestin recruitment (Fig 27a) in comparison with untransfected  $\beta$ -arrestin CHO cells. Stimulation of GPR143 with L-DOPA (10  $\mu$ M) induced only a minor increase in  $\beta$ -arrestin recruitment as compared to the control and the calculated signal-to-noise ratio was 1.12 for the mutant GPR143 and 1.25 for the wt GPR143. The DiscoverX company, who designed the  $\beta$ -arrestin recruitment assay, suggested that a compound which stimulates a receptor obtaining a signal-to-noise ratio higher than 3 can be considered as a valuable agonist. A larger range of L-DOPA concentrations (until 100  $\mu$ M) was tested on the  $\beta$ -arrestin assay to obtain a dose-response curve however, any tendency or major gain in signaling response was detected (data not shown).

The intracellular calcium release associated with GPR143  $G_{q/11}$  protein coupling was also measured after L-DOPA stimulation. Any increase in intracellular calcium was observed in CHO cells expressing wt or mutant GPR143 after 10  $\mu$ M L-DOPA treatment as compared to the control (Fig 27b). Finally, the signaling pathways associated with  $G_i$  and  $G_s$  protein coupling were assessed. If L-DOPA would induce the coupling of GPR143 with  $G_i$  protein, a reduction in intracellular cAMP concentration would be expected however, no significant difference was measured after L-DOPA stimulation in comparison to the cAMP accumulation after forskolin treatment (Fig 27c). On the contrary, the coupling of GPR143 to  $G_s$  protein after L-DOPA stimulation would cause an increase of intracellular cAMP accumulation however, L-DOPA treatment of mutant GPR143 expressing cells did not induce any increment in cAMP concentration (Fig. 27c). In summary, L-DOPA cannot be considered a valuable pharmacological tool to study GPR143 function since the stimulation of the receptor by L-DOPA did not induce a significant activation of a precise signaling pathway.

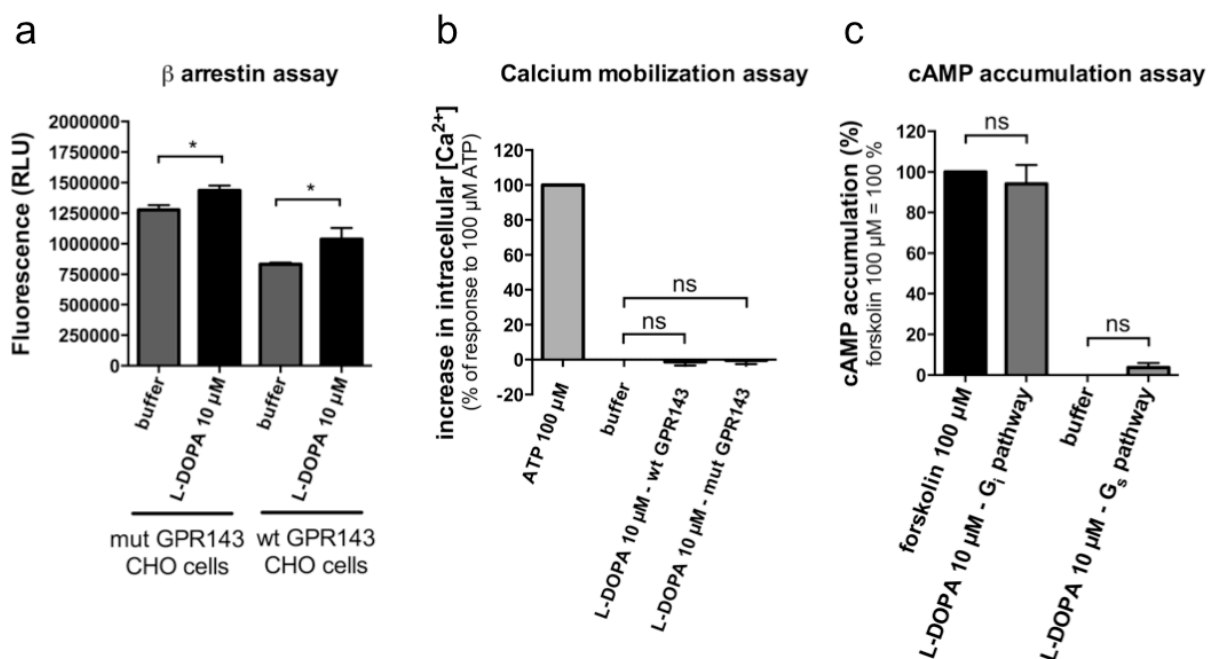
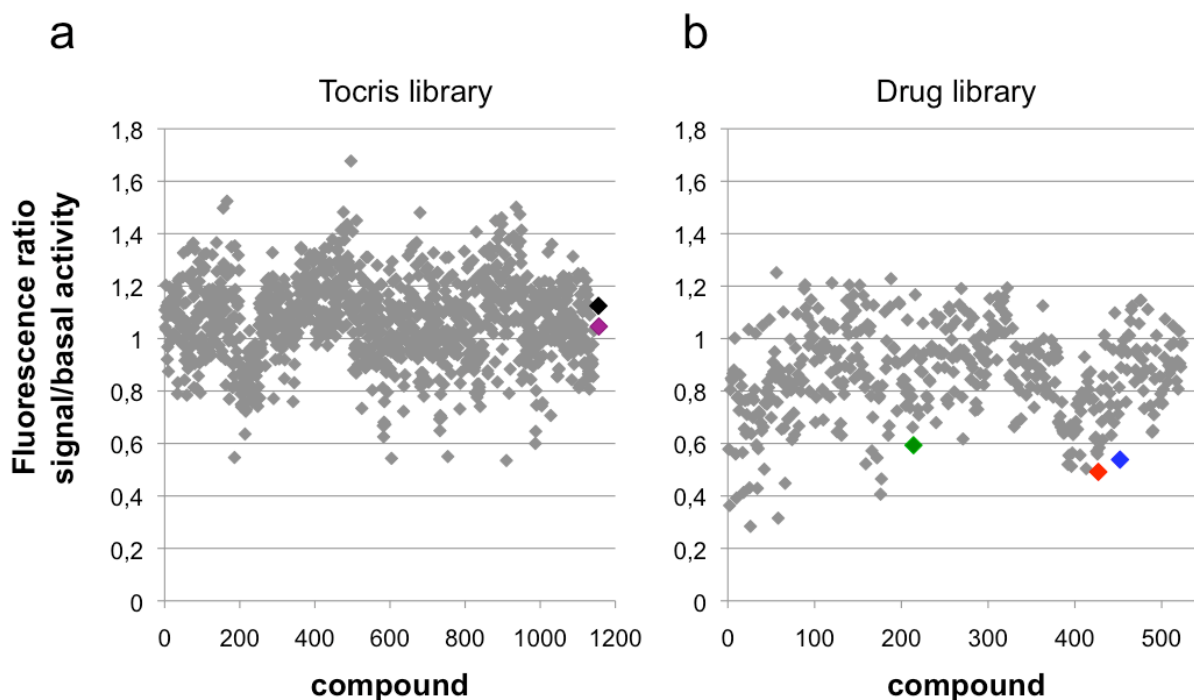


**Figure 27. Effect of L-DOPA on CHO cells expressing GPR143.** (a)  $\beta$  arrestin assay: L-DOPA was tested at 10  $\mu$ M final concentration on CHO cells expressing the wildtype or the mutant GPR143 and buffer was used as control. Experiments were performed in duplicates. (b) Calcium mobilization assay: data were normalized to the positive control (100  $\mu$ M ATP), set as 100%, and the buffer control was set at 0%. Experiments were performed in triplicates. (c) cAMP accumulation assay: data were normalized to the positive control (100  $\mu$ M forskolin), set as 100%, and to the negative control, buffer, set as 0%. Experiments were performed in triplicates. Data are mean  $\pm$  SEM of three independent experiments. Two-tailed  $t$ -test: <sup>ns</sup> not significantly different from the control, \*  $p < 0.05$ , \*\*  $p < 0.01$  and \*\*\*  $p < 0.001$ .

### 3.9.3 Compound library screening

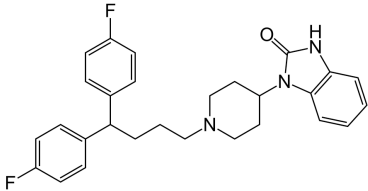
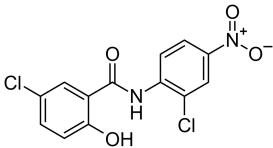
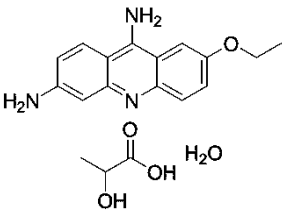
The  $\beta$ -arrestin recruitment assay optimized for GPR143 was used as high-throughput screening technique to test the Tocris and Drug library which taken together included about 1800 compounds. The goal of the screening was to find a pharmacological tool to investigate GPR143 function. Due to the high basal activity observed in CHO cells expressing GPR143, the investigation of compounds either increasing or decreasing the receptor activation was feasible. Each compound of the libraries was tested at 10  $\mu$ M final concentration and the corresponding signal-to-noise ratio was calculated (Fig 28). As comparison dopamine (DOPA) and L-DOPA values were added to the plot (black and magenta spots, respectively, Fig 28a). Any compound reached a signal-to-noise ratio equal or greater than 3 and the

compounds with the highest ratio ( $\geq 1.5$ ) produced non-reproducible values. On the other hand, about 40 compounds reached a signal-to-noise ratio equal or lower than 0.6 which was the threshold suggested by DiscoverX company for potential antagonists or inverse agonists. It was possible to confirm three hits compounds from the Drug library as potential inhibitors of GPR143 activity due to reproducible and consistent values (highlighted in Fig 28b, pimoziide in red, niclosamide in green and ethacridine lactate in blue). Additionally, the three compounds were tested against a different GPCR, the rat adenine receptor, with high constitutive activity and they did not alter its function (Table 10). The described hits are drugs currently on the market: pimoziide, an antipsychotic drug, niclosamide and ethacridine lactate, antiseptic compounds (Table 10). Dose-response curves were obtained with different compound concentrations using the  $\beta$ -arrestin assay (Fig 29). The compound potencies were in low micromolar range:  $2.72 \pm 1.17 \mu\text{M}$  for pimoziide,  $3.40 \pm 1.11 \mu\text{M}$  for niclosamide and  $26.1 \pm 1.03 \mu\text{M}$  for ethacridine lactate.



**Figure 28. High-throughput screening via  $\beta$  arrestin assay of (a) Tocris and (b) Drug libraries.** CHO cells expressing the mutant GPR143 were used. Each point represents a single compound ( $n=1$ ) tested at  $10 \mu\text{M}$  final concentration. Plotted values correspond to the signal-to-noise ratio (compound signal/baseline). Compounds are considered potential GPR143 agonists if the signal-to-noise ratio is higher than 3.0 and potential inverse agonists if it is lower than  $\leq 0.6$ . **(a)** Data corresponding to L-DOPA and DOPA ( $10 \mu\text{M}$ ) are shown in black and magenta, respectively. **(b)** Reproducible hit compounds are highlighted in red (pimoziide), green (niclosamide) and blue (ethacridine lactate).

**Table 10.** Hit compounds description. The structure and the principal effects of the hit compounds from the Drug library screening are listed. The signal-to-noise ratio of the compounds tested at 10  $\mu$ M final concentration on CHO cells expressing the human mutant GPR143 is specified. As control the compounds have been tested on CHO cells expressing the rat adenine receptor, which has an high basal activity as well. Data correspond to mean  $\pm$  SEM of three independent experiments performed in duplicates.

compound name	compound structure	compound description	signal-to-noise ratio $\pm$ SEM	
			human GPR143 CHO cells	rat adenine CHO cells
Pimozide		an antipsychotic drug used for schizophrenia and chronic psychosis, Tourette syndrome, resistant tics and paranoid personality disorder	0.6 $\pm$ 0.1	0.9 $\pm$ 0.1
Nicosamide		An antiseptic in the anthelmintic family especially effective against cestodes that infect humans	0.6 $\pm$ 0.1	1.0 $\pm$ 0.1
Ethacridine lactate		an aromatic organic compound based on acridine. Its primary use is as an antiseptic in solutions of 0.1%. It is also used as an agent for second trimester abortion.	0.6 $\pm$ 0.1	0.9 $\pm$ 0.1

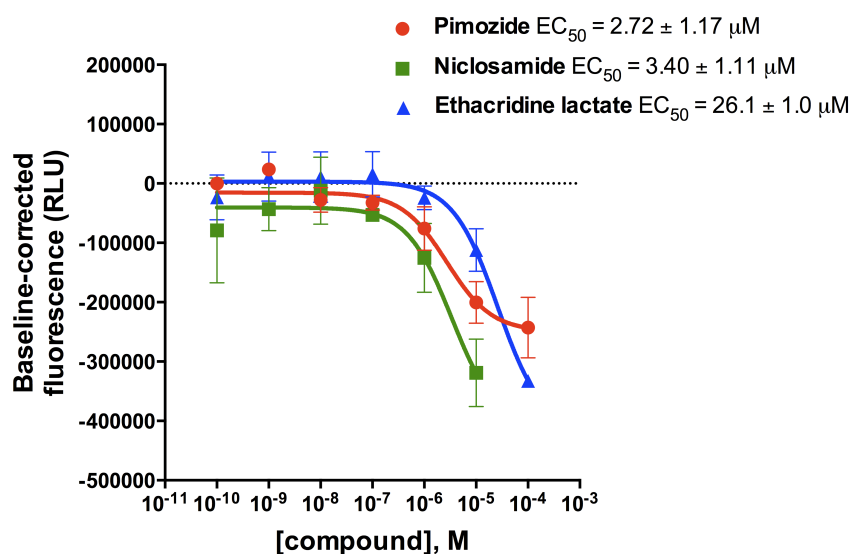


**Figure 29. Dose-response curves of hit compounds in  $\beta$ -arrestin assays.** CHO cells expressing the mutant GPR143 were stimulated with different concentrations of selected compounds: pimozide (red), niclosamide (green) and ethacridine lactate (blue). Data were baseline-corrected (signal-baseline) and correspond to mean  $\pm$  SEM of three independent experiments performed in duplicates.  $EC_{50}$  values are shown in the legend for each compound.

### 3.9.4 Validation of hit compounds

Since the effect of the three hit compounds from the library screening were specific for GPR143 (expressed in CHO cells), we tested them in an endogenous cell system, such as melan-a cells. In order to detect and measure pigmentation changes, cells were treated with compounds for three to five days and a previous cell viability assay was necessary to set the proper range of non-toxic compound concentrations.

After three days of cell treatment, pimozide was toxic at higher concentrations than 10  $\mu$ M, while niclosamide showed 40% of cell viability at 1  $\mu$ M. Ethacridine lactate displayed toxicity at concentrations higher than 100  $\mu$ M (Fig 30a).

The melanin assay was performed treating melan-a cells for five days with different compound concentrations. Propylthiouracil (PTU), a tyrosinase inhibitor, and 3-isobutyl-1-methylxanthine (IBMX), a phosphodiesterase inhibitor, were used as controls (Fig 30b). Niclosamide and pimozide treatment dramatically reduced cell pigmentation thus, niclosamide at 0.5  $\mu$ M reached 6% of the control melanin amount while pimozide decreased

the melanin content of 88% in comparison with DMSO. Ethacridine lactate induced a 39% reduction in pigmentation at 1  $\mu\text{M}$  and 85% at 5  $\mu\text{M}$  as compared to the control however, at the highest concentration (7.5  $\mu\text{M}$ ) the melanin accumulated in the cells was similar to the control.

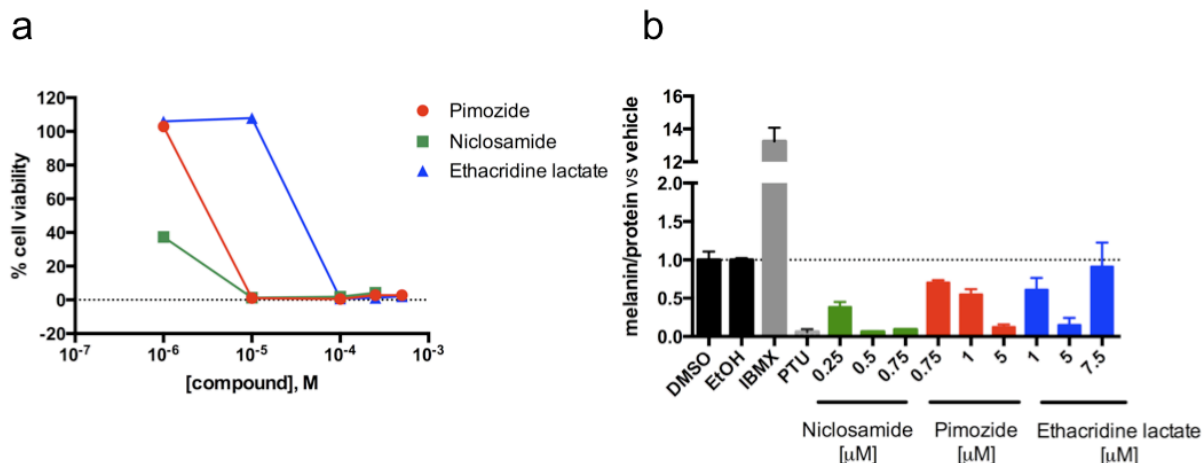


**Figure 30. Treatment of melan-a cells with the hit compounds. (a)** MTT assay for cell viability. Melan-a cells were treated with different concentrations of pimozide (in red), niclosamide (in green) and ethacridine lactate (in blue) for 72 hr and then the cell viability was measured by MTT assay. Data were normalized to the cell treatment with vehicles (DMSO or ethanol), set as 100%. Data represent one of four independent experiments performed in quadruplicates. **(b)** Melanin assay. Melan-a cells were treated with different concentrations of hit compounds (see Fig 30a) and then the amount of melanin produced was isolated and quantified. Data were normalized to the cell treatment with vehicles (DMSO and ethanol), set to 1. Propylthiouracil (PTU) and 3-isobutyl-1-methylxanthine (IBMX) were used as controls to decrease and increase, respectively, the pigmentation of the cells. Data correspond to mean  $\pm$  SEM from triplicate samples from one of five representative experiments.

### 3.9.5 Tyrosinase activity

In order to verify the target specificity of the hit compounds, the tyrosinase activation was analyzed in melan-a cell lysates. The tyrosine hydroxylase activity of tyrosinase was first examined in lysates of untreated melan-a cells (Fig 31a) incubated with different concentrations of the three hit compounds (50 and 100  $\mu\text{M}$ ). The purpose was to check the direct interaction of the compounds with tyrosinase, whether the reduction in pigmentation



observed in the melanin assays was caused by direct tyrosinase inhibition. As control, increasing concentrations of unlabeled L-tyrosine were used to compete with [<sup>3</sup>H]L-tyrosine. The tyrosinase activity in melan-a lysates treated with pimoziide, niclosamide and ethacridine lactate was comparable to the vehicle one, indicating that the compounds do not directly inhibit the tyrosine hydroxylase activity (Fig 31a).

Finally, the tyrosinase function was verified in lysates derived by melan-a cells treated for five days with the compounds and used in melanin assay (Fig 31b). A significant inhibition of tyrosinase activity was observed in melan-a cell treated with niclosamide as compared to the vehicle (ethanol). The enzyme activation in melan-a cells after pimoziide treatment was similar to the DMSO control. Ethacridine lactate induced a reduction in tyrosinase activity only at the highest concentrations (5 and 7.5 μM). Niclosamide and ethacridine lactate seemed to indirectly affect tyrosine hydroxylase activity, which could be a potential reason why the pigmentation was reduced in melan-a cells.

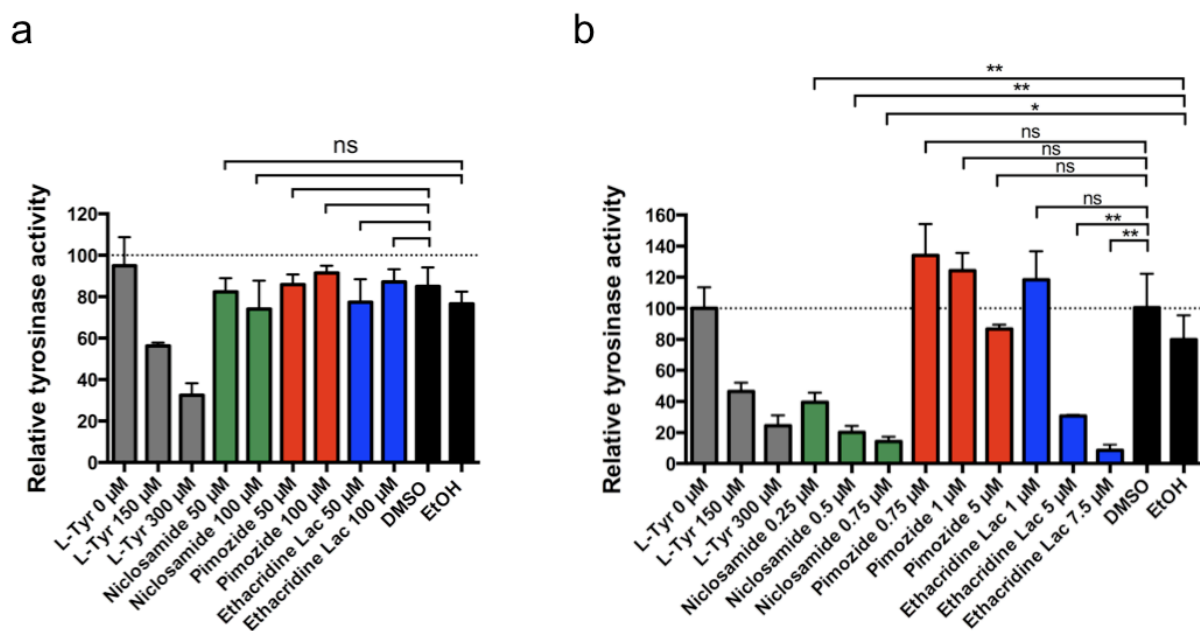


**Figure 31. Effect of hit compound treatment on tyrosinase activity. (a)** Tyrosinase assay performed treating melan-a cell lysates with different concentrations (50 and 100 μM) of hit compounds: pimoziide, niclosamide and ethacridine lactate. Data were normalized to the untreated melan-a lysates (L-tyr 0 μM), set as 100%. Positive controls correspond to L-tyrosine treatments (150 and 300 μM), since unlabeled L-tyrosine competes with [<sup>3</sup>H]L-tyrosine and the release of radioactive water decreases. The vehicles (DMSO and ethanol) were tested as control. **(b)** Tyrosinase assay performed with melan-a cell lysates from melanin assay. Melan-a cells were treated with different concentrations of hit compounds (see Fig 29b) for 5 days. The melanin was isolated from the cell

lysates, which were tested for tyrosinase activity. L-tyrosine (150 and 300  $\mu$ M) and the vehicles (DMSO and ethanol) were used as controls. The tyrosinase activity of untreated melan-a cells was set as 100%. Experiments were performed in triplicates. Data are mean  $\pm$  SEM of one experiment. Two-tailed *t*-test: <sup>ns</sup> not significantly different from the control, \*  $p < 0.05$ , \*\*  $p < 0.01$  and \*\*\*  $p < 0.001$ .

### 3.9.6 Discussion

Ocular Albinism type I (OA1) is a X-linked form of albinism characterized by optical anomalies typical of albinism however, the cutaneous changes in pigmentation are usually mild or absent [129]. Despite the fact that the skin of OA1 patients seems not to be affected, histological analysis showed that subcellular abnormalities are present in both skin melanocytes and retinal pigment epithelium (RPE) [92]. The RPE appears hypopigmented because melanin is concentrated in few giant melanosomes instead of being homogeneously dispersed in the cell and also the number of melanosomes is reduced [91].

GPR143 is the protein product of the *Oa1* gene and its mutations were found to be responsible for OA1 development [96]. GPR143 is mainly expressed in pigmented cells of the eye and skin however, recently its expression was also found in the central nervous system and in peripheral tissues [114]. Two sorting signals are present in GPR143 coding sequence which are necessary and sufficient for its intracellular localization [99]. GPR143 is localized to the membrane of melanosomes in pigmented cells and on lysosomes and early endosomes in non-melanocytic cells [99]. The pathophysiological role of GPR143 in pigmented cells is still unclear nevertheless, considering the subcellular consequences of GPR143 mutation, the suggested function for the receptor is the regulation of melanogenesis rate and melanosome maturation [104,124]. GPR143 shares structural and functional similarities with G protein-coupled receptors (GPCRs; Schiaffino et al. 1999) and a characteristic feature all GPCRs have in common is the coupling with heterotrimeric G proteins. Different types of G proteins and effectors were found to co-precipitate and co-localize with GPR143 in melanocytes, such as  $\beta$ -arrestin,  $G_{\alpha o}$ ,  $G_{\alpha i}$  and  $G_{\beta}$  subunits [97,113] and so far only levodopa, L-DOPA, was proposed to be the GPR143 endogenous agonist activating the the  $G_{q/11}$  protein associated pathway [113].

The aim of our investigation was to find a valuable pharmacological tool to study the function of GPR143 and clarify its role in the OA1 pathogenesis. The first step consisted in the validation of L-DOPA as GPR143 agonist. Exchanging the two sorting signal sequences into

alanine residues, we generated a double mutant GPR143 expressed at the cell plasma membrane and accessible by compounds from the extracellular space.

We established CHO cell lines expressing either the wildtype (wt) or the mutant GPR143 and optimized specific cell-based assays to test the activation of GPR143 through different downstream signaling pathways, such as the  $\beta$ -arrestin recruitment assay, calcium mobilization assay and cAMP accumulation assay. Performing the  $\beta$ -arrestin recruitment assay we observed that the  $\beta$ -arrestin CHO cell lines expressing GPR143 displayed a high constitutive activation in comparison with the untransfected  $\beta$ -arrestin CHO cells, as previously suggested by *Innamorati et al, 2006*.

L-DOPA was tested in the  $\beta$ -arrestin recruitment assay against the wt and the mutant GPR143 and only a slight increase in activation was observed at 10  $\mu$ M final concentration. The DiscoverX company, who designed the  $\beta$ -arrestin recruitment assay, suggested that a valuable agonist tested at 10  $\mu$ M should have a signal-to-noise ratio equal or greater than 3. L-DOPA displayed a signal-to-noise ratio of 1.12 for the mutant GPR143 and 1.25 for the wt GPR143. Since the compound was previously reported to have low affinity for the receptor ( $K_d$  9.35  $\mu$ M [113] and  $K_d$  79.1  $\mu$ M [115]), higher L-DOPA concentrations (until 100  $\mu$ M) were tested however, the signal-to-noise ratio did not increase. L-DOPA was tested on GPR143 expressing CHO cells for the activation of calcium signaling pathway through  $G_{q/11}$  protein coupling and for cAMP accumulation pathways through  $G_i$  and  $G_s$  protein coupling however no significant differences were observed from the controls.

A recent study showed that L-DOPA could not induce intracellular calcium increase in CHO cells transfected with GPR143, differently from the previous study by *Lopez et al. (2008)*, however calcium responses to L-DOPA were visible in ARPE-19 cells, derived from RPE which endogenously express GPR143 [115]. We observed that L-DOPA slightly induced  $\beta$ -arrestin recruitment in GPR143 expressing CHO cells but the calcium response was not detected, supporting the former findings [115]. An hypothesis could be that the participation of a third factor is necessary for the activation of GPR143 by L-DOPA and this additional component is present only in pigmented cells. An alternative might be that the observed calcium release in ARPE-19 cells after L-DOPA treatment is not a GPR143 specific effect, since some dopamine receptor subtypes are endogenously expressed in those cells, such as D1 and D5 subtypes, and their activation induces intracellular calcium increase [130,131]. Recent studies indicated that L-DOPA produced by RPE has a role in retinal development through

the activation of dopamine receptors present on neural retina cells however, the hypothetical L-DOPA targeting of dopamine receptors on RPE has never been approached yet [116]. RPE cells differentiate already during the first days of eye formation [89] and during this time tyrosinase produce L-DOPA, which is then secreted and taken up by retina neurons. The dopamine produced by L-DOPA in immature retina cells induce activation of dopamine receptors and play a role in retinal differentiation since early stages of development. A more focused investigation needs to address the link between GPR143 activation by L-DOPA and L-DOPA targeting of dopamine receptors in RPE and neural retina.

The  $\beta$ -arrestin recruitment assay resulted the best technique to analyze the function of GPR143 since it showed a slight activation of GPR143 after L-DOPA treatment and a GPR143 constitutive activity which was previously observed [111]. The  $\beta$ -arrestin recruitment assay was suitable for high-throughput screening thus, we decided to screen two compound libraries in order to find more valuable ligands for GPR143. In addition the receptor basal activity displayed in the assay opened the opportunity to investigate not only potential agonists but also potential inverse agonists which decrease the activity of the receptor. The wt and mutant GPR143 exhibited similar behaviour when L-DOPA was tested in the  $\beta$ -arrestin recruitment assay and calcium mobilization assay, as they both showed high basal activity and comparable signal-to-noise ratios. For this reason we decided to test the compounds against the mutant GPR143, which is accessible to all compounds independently to their size and hydrophobicity level.

Two compound libraries were screened against GPR143: the Tocris library, which contains a collection of small molecules biologically active at most of the important biological targets (GPCRs, ion channels, kinases, transporters) and the drug library including important drugs available on the market. The screening resulted in three reproducible hit compounds, which decreased the constitutive activation of GPR143 with a signal-to-noise ratio close to 0.6, as was suggested by the DiscoverX company for potential antagonists or inverse agonists.

The hit compounds were drugs currently on the market and their potency at GPR143 were in the low micromolar range. The hit compounds were pimozide, an antipsychotic drug active on dopamine receptors [132], nicosamide, an oral antihelminthic drug lately discovered to be active against cancer cells [133], and ethacridine lactate, antiseptic and abortifacient. The specificity of the compound effects observed in the  $\beta$ -arrestin recruitment against GPR143 was proven by testing them against CHO cells expressing a GPCR with high constitutive

activity, the rat adenin receptor. The compound treatment did not induce any decrease in  $\beta$ -arrestin recruitment on rat adenin receptor expressing cells, indicating that the displayed effect on GPR143 is specific for the receptor.

In order to investigate the effect of the compounds in pigmented cells endogenously expressing GPR143, melan-a cells derived from murine melanocytes were tested with different concentrations of compounds and then the accumulated melanin content was quantified. The cell viability assay indicated the nontoxic concentration range of each compound for a long-term (three days) cell treatment. The results of the melanin assay showed that the treatment with the three hit compounds induced a dose-dependent reduction in melan-a cell pigmentation.

The melanin synthesis in melanocytes and RPE is controlled by tyrosinase, an enzyme responsible for the tyrosine hydroxylation in L-DOPA and its oxidation to dopaquinone. Thus, we checked if the reduction in melan-a cell pigmentation was due to the inhibition of tyrosinase activity by the compounds. Treating melan-a lysates with different concentrations of compounds, we observed that the three compounds did not directly inhibit tyrosinase thus, the enzyme activity was comparable to the vehicle treatments. On the other hand, analyzing the melan-a lysates derived from compound treatment for the melanin assay, a strong inhibition of tyrosinase activity was displayed by niclosamide and ethacridine lactate. These two compounds did not directly influence tyrosinase but the pigmentation reduction was due to an inhibitory effect on the enzyme. On the contrary, the reduction in pigmentation in melan-a cells derived by pimozide treatment was not due to the inhibition of tyrosinase activity. Since we proved that pimozide was selectively inhibiting GPR143 constitutive activity, this compound might be able to inactivate GPR143 inducing a reduction in melanocyte pigmentation.

In a previous study GPR143 was inactivated by interference RNA in pigmented MNT-1 cells and the melanosome morphology and composition was analyzed when GPR143 expression was silenced [103]. It was found that the number of mature melanosomes and melanin content was reduced of 50% as compared to the control cells. After 5 days of GPR143 silencing, abnormal enlarged pigmented structures appeared in the cells however the pigmentation and the number of melanosomes did not increase [103]. We suggest that pimozide decrease GPR143 function and this condition could resemble the cell phenotype of OA1, in which GPR143 is mutated and non-functional. An alternative explanation is that pimozide targets

dopamine receptors on melanocytes, since this compound has high affinity for different dopamine receptor subtypes such as D2, D3 and D4 [134]. A few studies demonstrated that melanocytes and RPE express dopamine receptors and dopamine agonists could decrease tyrosinase activity in hair follicular melanocytes reducing the pigmentation of the cultured cells [135,136]. The possibility that pimoziide targets a different receptor than GPR143 in melan-a cells and activates a signaling pathway causing the melanin content reduction cannot be excluded. However, we proved that tyrosinase activity was not inhibited when cells were treated with pimoziide indicating that the reduction in pigmentation is not due to direct tyrosinase regulation.

In summary, the  $\beta$ -arrestin recruitment assay was a cell-based technique optimized to analyze the GPR143 function and was used to confirm its high constitutive activation. L-DOPA slightly increased the GPR143 activity but it cannot be considered a valuable pharmacological tool to investigate the receptor's role as its signal-to-noise ratio is close to the control one. Further studies are necessary to address the specificity of the L-DOPA target in the RPE clarifying its role in the neural retina development. In addition, the compound library screening resulted in three hits which were able to decrease GPR143 constitutive activity and might be used as scaffolds to develop GPR143 high affinity ligands. One of these hit compounds, pimoziide, is a promising candidate to study GPR143 function in an endogenous system since it is able to reduce the pigmentation of melanocytes without interfering with tyrosinase activity. We proved that pimoziide can selectively decrease GPR143 basal activity in CHO cells, however the underlying mechanism of action in an endogenous cell system needs to be investigated.

### 3.10 Part II: investigation of GPR143-tyrosinase interaction

#### 3.10.1 Characterization of GPR143 in COS7 and melan-a cells

With mutations in the amino acid sequence of the sorting signals (L223A-L224A and W329A-E330A) we generated a double mutant GPR143 receptor which does not follow the lysosomal/melanosomal sorting pathway and it can be transported to the plasma membrane of COS7 cells. The cell surface expression of the mutant GPR143 can be helpful to singularly investigate its role in pigmented and non-pigmented cells.

The wildtype (wt) and mutant GPR143 were transiently expressed in COS7 cells and characterized by immunostaining and western blot. The wt GPR143 was intracellularly expressed, localized in vesicles close to the perinuclear region (Fig 32a, upper panels), while the mutant GPR143 was more distributed in vesicles in cell periphery and it colocalized with cadherin at the cell plasma membrane (Fig 32a, lower panels).

The Western Blot analysis performed with lysates of GPR143 transiently transfected COS7 cells showed the proper glycosylation pattern of the receptor [100] which consisted of a doublet of 45 and 48 kDa and a thicker band at 60 kDa (Fig 32b).

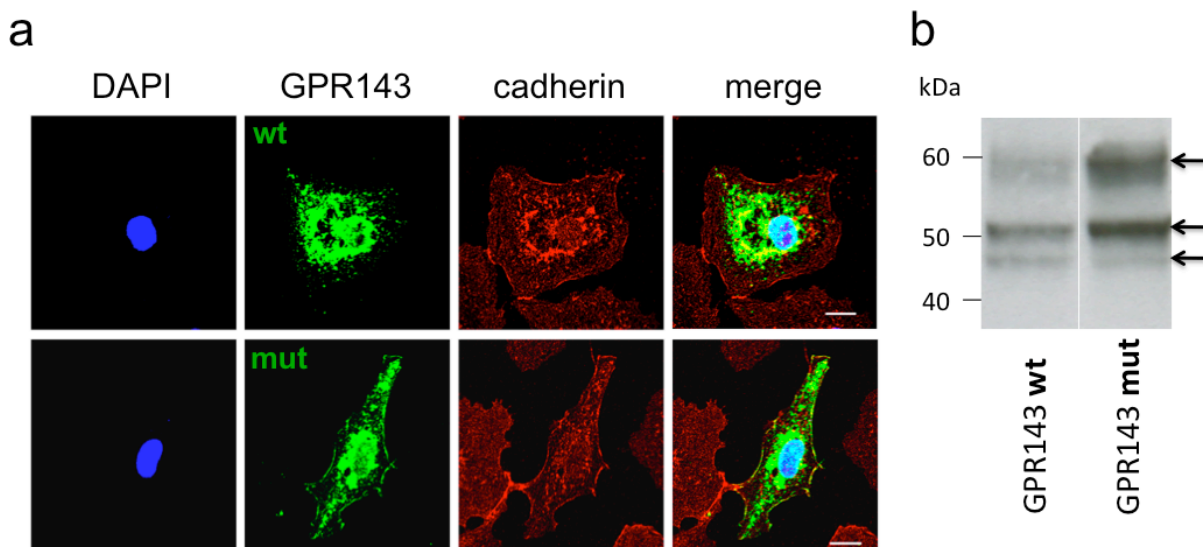


**Figure 32. Characterization of COS7 cells expressing wildtype (wt) or double mutant GPR143.**

(a) Subcellular localization of wt and mutant GPR143 detected by immunofluorescence. Transfected COS7 cells were fixed and stained with monoclonal anti-ProLink antibody (against PL tagged-GPR143), polyclonal anti-cadherin antibody (plasma membrane marker) and DAPI (nuclei). Scale bars represent 20 μm. (b) Immunoblot of protein extracts from transfected COS7 cell. The anti-ProLink antibody was used to detect GPR143. Each lane was loaded with 30 μg of total amount of protein.

Furthermore, the glycosylation of GPR143 was analyzed with Peptide-N-Glycosidase F (PNGase F) and endoglycosidase H (Endo H) in order to report the extent of oligosaccharide processing in the exogenous cell system. While PNGase F treatment caused the loss of the 60 kDa band, Endo H did not cause any oligosaccharide cleavage (Fig 33) meaning that the 60 kDa band corresponds to a complex oligosaccharide, which is processed in the Golgi apparatus. This finding confirmed that GPR143 was carried through the endoplasmic reticulum (ER) to the Golgi and then sorted to the proper subcellular organelles.

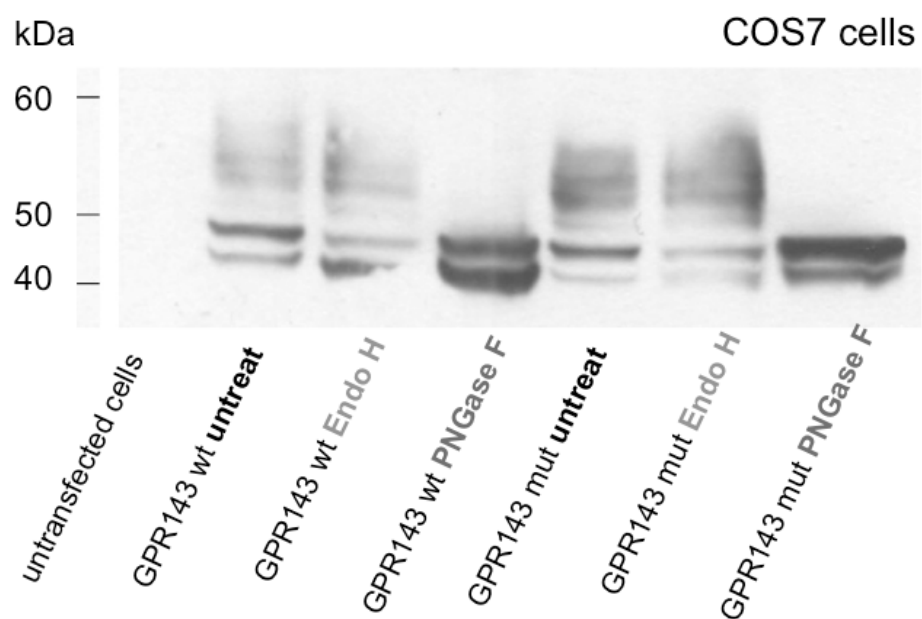


**Figure 33. Glycosylation study of GPR143 expressed in COS7 cells.** The wildtype and mutant GPR143 were treated with different endoglycosidases (Endo H and PNGase F) reacting at different levels of the glycosylation pattern. GPR143 was subjected to complex glycosylation in the Golgi apparatus and to different post-translational modifications apart from N-glycosylation. Each lane of the SDS-PAGE was loaded with 50  $\mu$ g of total protein amount from the lysate, after treatment with the corresponding enzyme.



### **3.10.2 Colocalization of GPR143 and tyrosinase in COS7 and melan-a cells**

Tyrosinase contains sorting signals in the C-terminal tail responsible for its lysosomal localization in heterologous systems [118], thus we investigated the colocalization in COS7 cells of tyrosinase and GPR143, as both proteins should follow the lysosomal sorting pathway in non-melanocytic cells.

When the wt GPR143 was expressed together with tyrosinase, colocalization was detectable in the perinuclear region of the cell, where ER and Golgi apparatus are located, and only in a few vesicles in the cell periphery (Fig 34a). On the other hand, in double transfected COS7 cells where the mutant GPR143 was present and localized at the cell surface, tyrosinase was also partially localized at the plasma membrane overlapping with the mutant GPR143 (Figure 2a, lower panels).

The validation of the observed colocalization between tyrosinase and GPR143 was performed in a pigmented cell system, melan-a cells, a mouse melanocyte cell line. Since the amino acid sequence alignments displayed high identity and similarity between human and mouse GPR143 and tyrosinase (Appendix 1, also shown in [109]), melan-a cells were transfected with GPR143-YFP and its colocalization with the mouse endogenous tyrosinase was investigated. The localization of the two proteins in melan-a cells was similar to the one in COS7 cells. The wt GPR143 was localized in vesicles in the cell periphery which appeared different but often close to the vesicles containing the endogenous tyrosinase (Fig 34b). The mutant GPR143 and the endogenous tyrosinase were localized at the plasma membrane in melan-a cells and the vesicles containing tyrosinase were mostly grouped at the cell periphery close to the cell surface (Fig 34b).

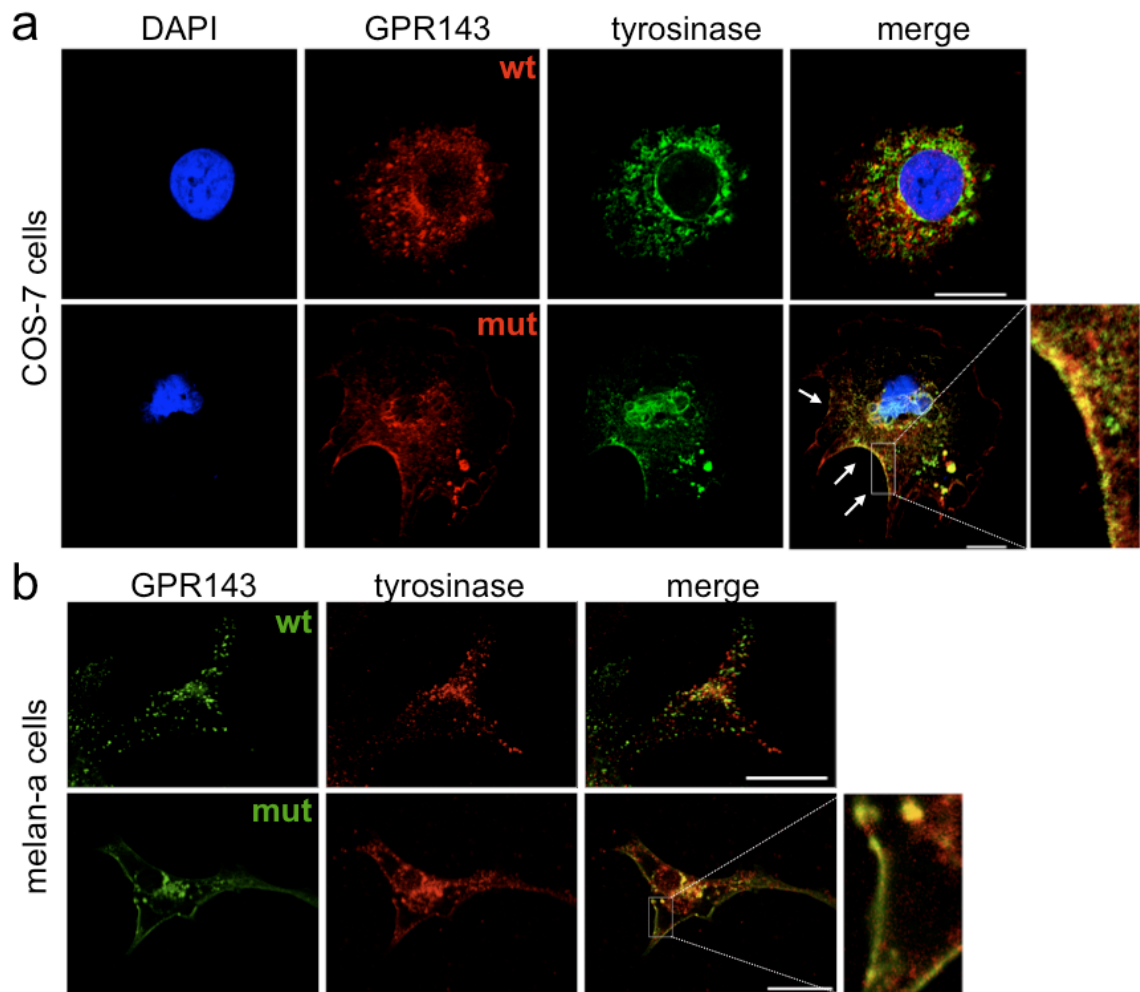


**Figure 34. Colocalization of GPR143 and tyrosinase by immunofluorescence in COS7 (a) and melan-a (b) cells.** (a) COS7 cells were double transfected with GPR143 (wt or mutant) and TYR-EGFP, fixed and stained with monoclonal anti-ProLink antibody (against PL tagged-GPR143) and DAPI (nuclei). (b) Melan-a cells transfected with GPR143-EYFP (wt or mutant) were fixed and stained with  $\alpha$ PEP7 (against endogenous tyrosinase). Magnification of plasma membrane regions are shown as insets. Scale bars represent 20  $\mu$ m.

### 3.10.3 Immunoprecipitation of GPR143 and tyrosinase

Since the previous colocalization studies suggested a direct interaction between GPR143 and tyrosinase, the hypothetical physical interaction between these two proteins was investigated by immunoprecipitation (IP) in lysates of transfected cells. In double transfected COS7 cells GPR143-PL was pulled down by the anti-ProLink antibody and the fractions derived by the IP (washing and elution) were analyzed by Western Blot detecting either GPR143 or

tyrosinase (Fig 35a). The lysate fractions were loaded in the SDS-PAGE as control since they were not incubated with the antibody.

GPR143 was identified in the lysates of the double transfected COS7 cells (two bands of 50-60 kDa) but not in untransfected cells. The GPR143 lower band is overlapping with one of the anti-ProLink antibody bands (~50 kDa) corresponding to the heavy antibody chain, visible in the untransfected COS7 cells as well, however the higher GPR143 band is clearly detectable in both washing and elution fractions.

Tyrosinase was detected in the blot by a different species antibody. Thus, the antibody chains were not visible. The bands corresponding to different glycosylation patterns of tyrosinase (70-84 kDa + EGFP 27 kDa) were detected in the lysate and elution fractions of the double transfected COS7 cells, indicating that the enzyme was interacting and pulled down together with GPR143.

Comparable results were obtained pulling down tyrosinase using the anti-GFP antibody in double transfected COS7 cells (Appendix 2). Both wt and mutant GPR143 were able to interact with tyrosinase since no differences were detected between the two transfected cell lines.

Furthermore, IP studies were also performed in melan-a cells transfected with GPR143-EYFP pulling down the mouse endogenous tyrosinase with  $\alpha$ -PEP7 (Fig 35b). A broad band representing tyrosinase was detected above 75 kDa and it was present in the lysates and elutions of all samples, including the untransfected melan-a cells.

A doublet corresponding to GPR143 (45-60 kDa + EYFP 27 kDa) was observed below 75 kDa in the lysates and elutions of the transfected melan-a cells, confirming the interaction between GPR143 and endogenous tyrosinase.

The  $\alpha$ -PEP7 was loaded as control in GPR143- and tyrosinase-detecting blots since the samples were treated differently (for GPR143: 37 °C 30 min and for tyrosinase: boiled 2 min) and as consequence the antibody chains were running differently in the SDS-PAGE (Appendix 2). GAPDH was detected to check the specificity of the IP and the amount of protein loaded for each fraction. The protein amount was similar for the three cell lines (slightly lower in untransfected cells) and the absence of GAPDH in the elution indicates that the precipitation is specific for GPR143 and tyrosinase (Appendix 2).

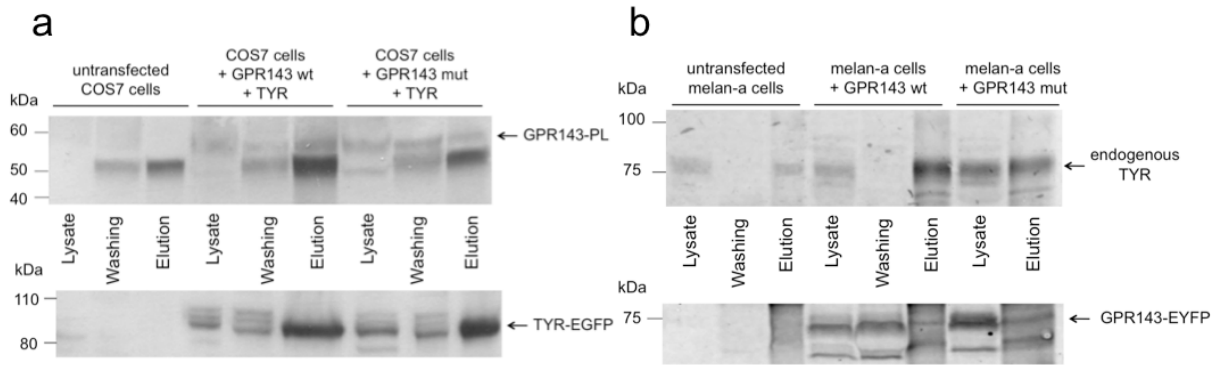


**Figure 35. Western blotting detection of proteins obtained through immunoprecipitation (IP).**

**(a)** Immunoblots of IP performed with anti-ProLink antibody in COS7 cell lysates transfected with GPR143-PL (wt or mutant) and TYR-EGFP. Untransfected COS7 cells lysates were used as control. Each lane was loaded with 30  $\mu$ l of total volume. The upper blot was stained with the monoclonal anti-ProLink antibody against the PL tagged-GPR143 and the lower blot with polyclonal anti-GFP antibody against the EGFP tagged-TYR. **(b)** Immunoblots of IP performed with  $\alpha$ PEP7 antibody in melan-a cells transfected with GPR143-EYFP (wt or mutant). Untransfected melan-a cells were used as control. Each lane was loaded with equal volume of solution ( $\sim$  30  $\mu$ l). The upper blot was stained with  $\alpha$ PEP7 (against endogenous tyrosinase) and the lower blot with the monoclonal anti-GFP antibody against the EYFP tagged-GPR143. As additional controls, GAPDH was detected in each fraction and the antibody used for precipitation ( $\alpha$ PEP7) was loaded in each blot.

### 3.10.4 Fluorescence Resonance Energy Transfer (FRET)

FRET is a technique which allows insight into protein interaction thus we established a cell system to study the direct interaction of GPR143 and tyrosinase. We linked EYFP and ECFP to the C-terminal end of GPR143 and TYR, respectively, generating GPR143-EYFP and TYR-ECFP fusion proteins. Since previous evidences showed that GPR143 is a 7-transmembrane protein [112] and tyrosinase is a single membrane-spanning enzyme, both characterized by the N-terminal end oriented toward the cytosol, the fluorescent proteins (EYFP and ECFP) should be located on the same side of the phospholipidic membrane. The constructs were transiently transfected together or singularly in COS7 cells and the cells were analyzed by confocal microscopy after fixation.

Sensitized emission is one method to evaluate FRET efficiency in which the excitation of the donor fluorophore (ECFP) leads to the emission of the acceptor molecule (EYFP), if the proteins are close enough (1-10 nm) for the energy transfer to occur (Fig 36a). Images of the

transfected cells were simultaneously acquired in the three channels (YFP, CFP and FRET), as Figure 37 shows. The Nikon A1 software was used to calculate the correction parameters (see the formulas in Methods section) by means of single transfected COS7 cells (wt or mutant GPR143-EYFP or TYR-ECFP, see Fig 38) and the FRET efficiency value of each point in a point-to-point manner, thus the FRET efficiency distribution view was obtained (last right panels, Fig 37). The transition from purple to red indicates the increase in FRET efficiency from 0 to 100% which corresponds to the intensity of protein interaction. When the wt GPR143 was expressed together with tyrosinase, the FRET signal was observed in several vesicles in the cell periphery, in addition to the perinuclear region (Fig 37). On the other hand, the FRET signal was found at the cell plasma membrane when tyrosinase was co-expressed with the mutant GPR143. In this case the FRET efficiency in some regions of the plasma membrane was spanning between 20 and 100% (white arrows in Fig 37).

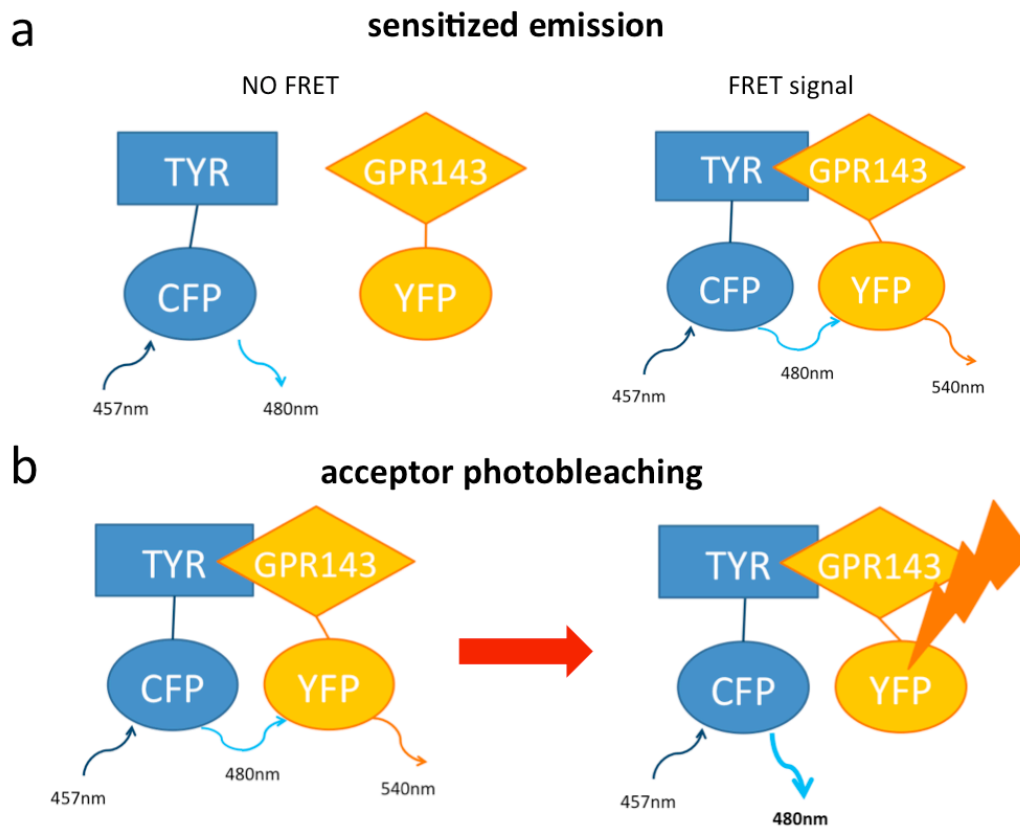


**Figure 36. Fluorescence Resonance Energy Transfer (FRET) detection methods. (a)** The sensitized emission FRET consists in the excitation of the single donor fluorophore (i.e. CFP) and in the detection of the acceptor (YFP) emission. If the two proteins are not close enough ( $< 10$  nm) to each other, FRET does not occur. **(b)** The acceptor photobleaching methods consists in bleaching the acceptor using a high intensity laser and monitor the donor emission spectrum. If the FRET occurs, bleaching the acceptor results in an increased donor emission.

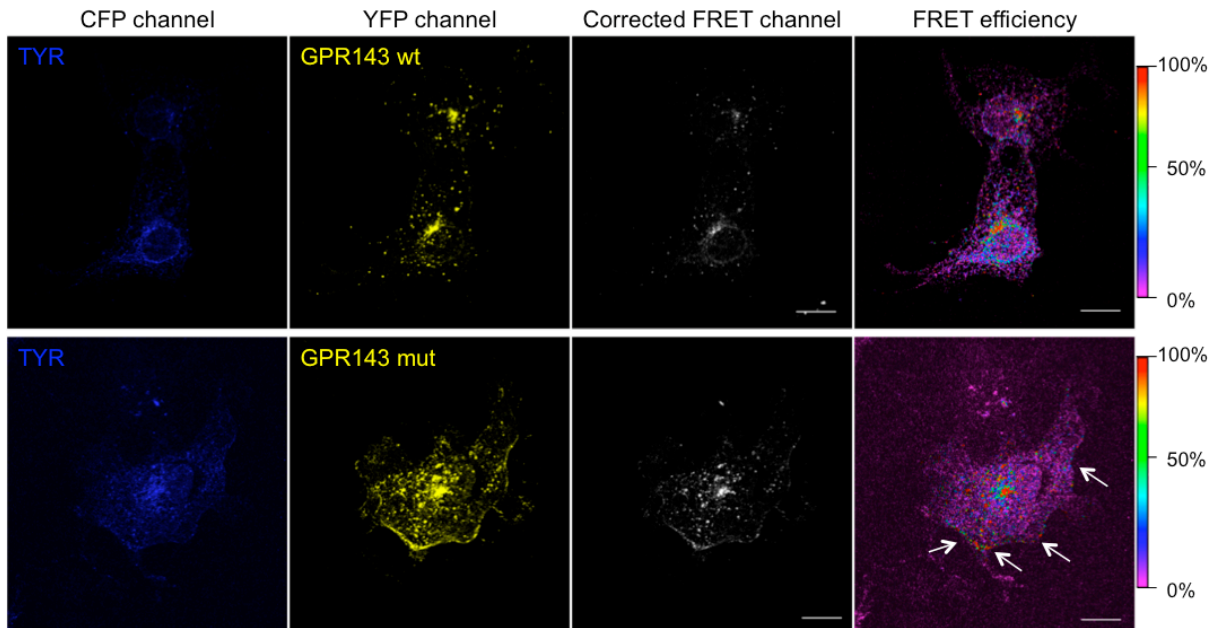


**Figure 37. FRET images of COS7 cells transfected with GPR143-EYFP (wt or mutant) and TYR-ECFP.** Sensitized emission method was used to detect interaction of GPR143 (YFP channel) and TYR (CFP channel). FRET signal, corrected by CoA and CoB parameters, and FRET efficiency (color scale on the far right) are shown. White arrows indicate the plasma membrane regions where FRET signal is localized. Controls are shown in Fig 38. Scale bars represent 20  $\mu\text{m}$ .

To further validate the interaction of GPR143 and tyrosinase we used the acceptor photobleaching method, a simple and quantitative FRET technique which measures the donor “de-quencing” in presence of an acceptor (Fig 36b). During FRET the donor fluorescence is channeled to the acceptor, thus it is partially quenched. Photobleaching the acceptor irreversibly eliminates the quenching effect and the level of donor fluorescence increases. The FRET efficiency can be measured subtracting the donor fluorescence before to after the acceptor bleaching and normalizing this value to the donor intensity after the bleaching (see Methods section). The photobleaching of the acceptor was delimited to some regions of interest (ROI) which correspond to some vesicles in the cell periphery where the wt GPR143 and TYR were present and parts of the plasma membrane where the mutant GPR143 and TYR colocalize.

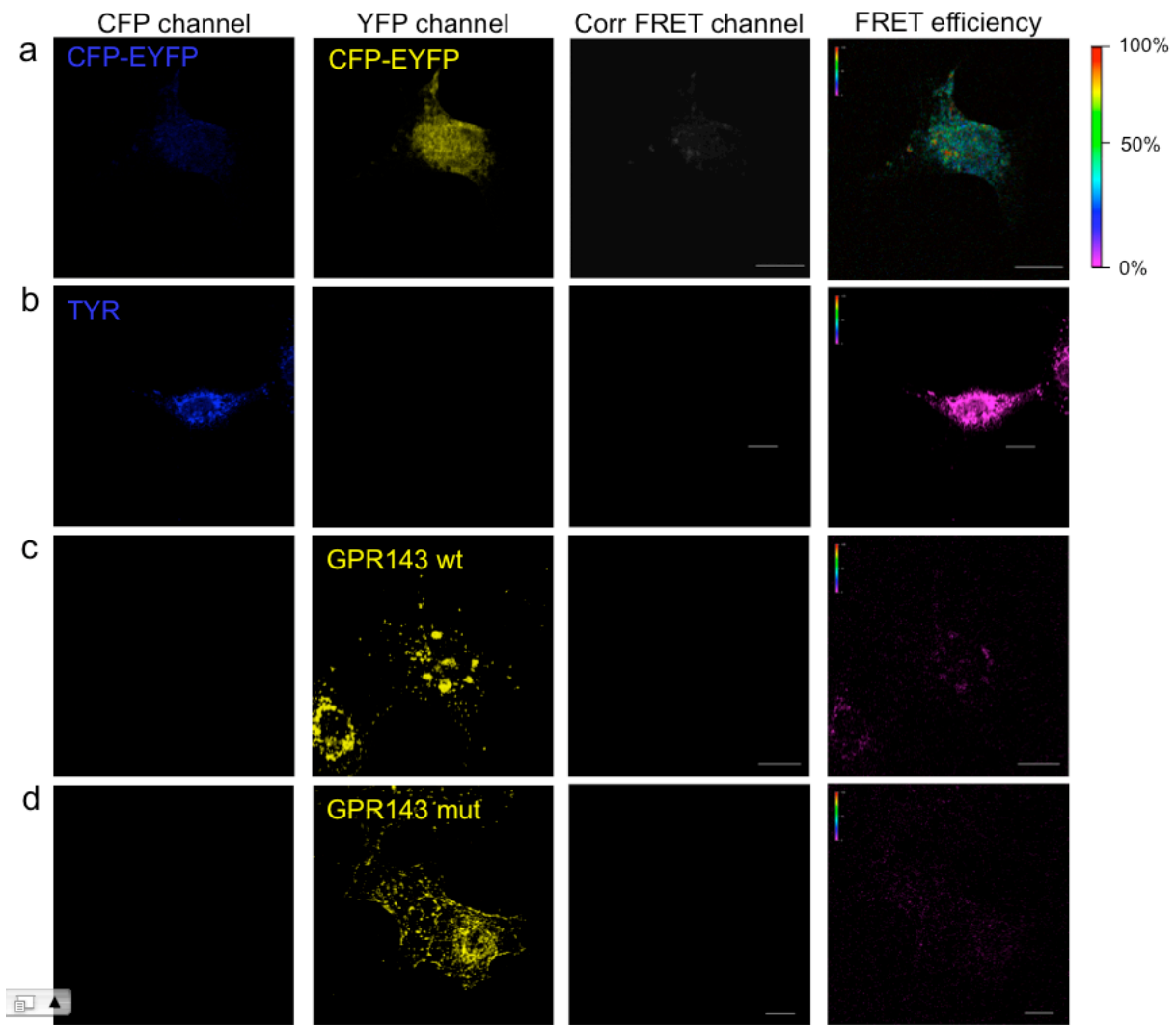


**Figure 38.** Control FRET images of COS7 cells transfected either with (a) ECFP-EYFP fusion protein or (b) TYR-ECFP or (c) wt GPR143-EYFP or (d) mutant GPR143-EYFP. Sensitized emission method was used to detect interaction of GPR143 (YFP channel) and TYR (CFP channel). FRET signal, corrected by CoA and CoB parameters, and FRET efficiency (color scale on the far right) are shown. Scale bars represent 20  $\mu\text{m}$ .

Images were captured before and after the photobleaching, displaying the fluorescence in the CFP and YFP channels (Fig 39). The fluorescence of the ROI were used to calculate the ratio of emission intensity after to before the photobleaching and the FRET efficiency (Fig 40). The intensity of the ECFP emission increased when GPR143-EYFP and TYR-ECFP were expressed together indicating that the pair of fluorophores were involved in a resonance energy transfer before the acceptor photobleaching (Fig 40a). The FRET efficacy of the double transfected COS7 cells resulted  $21.8 \pm 4.5\%$  for the wt GPR143 with TYR and  $16.3 \pm$

3.4% for the mutant GPR143 with TYR (Fig 40b), which was significantly different from the negative controls (single transfected COS7 cells) and comparable to the positive control (ECFP-EYFP fusion protein:  $28.4 \pm 4.4\%$ ).

Taken together we were able to show with IP and two different methods that GPR143 and TYR are directly interacting with each other in several regions and this interaction depends on the localization of GPR143.

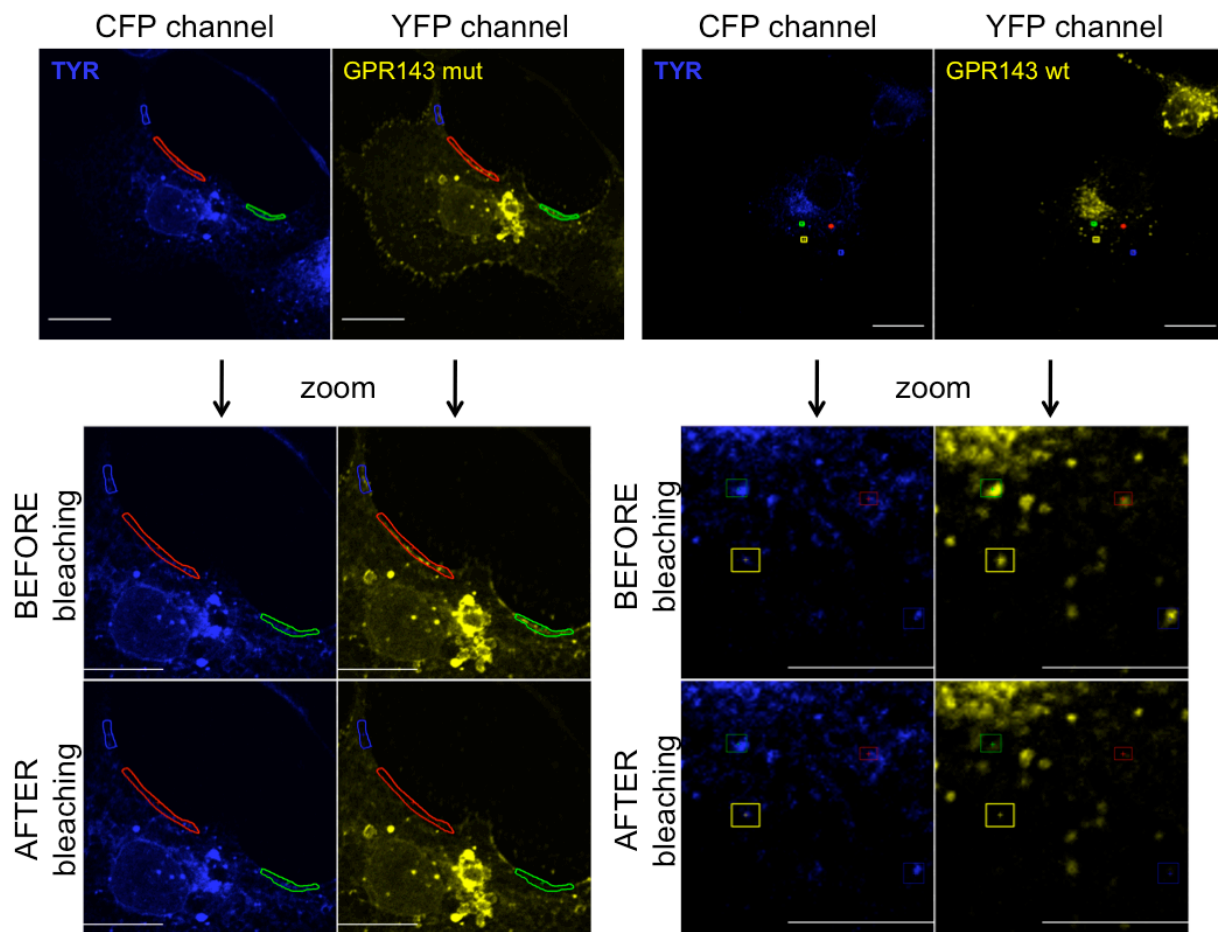


**Figure 39. FRET acceptor photobleaching in COS7 cells transfected with GPR143-EYFP (wt or mutant) and TYR-ECFP.** The EYFP photobleaching was performed and detected in delimited regions (highlighted and zoomed in the pictures). Images of GPR143 (YFP channel) and TYR (CFP channel) fluorescence are shown before and immediately after the acceptor photobleaching. Scale bars represent 20  $\mu\text{m}$ .



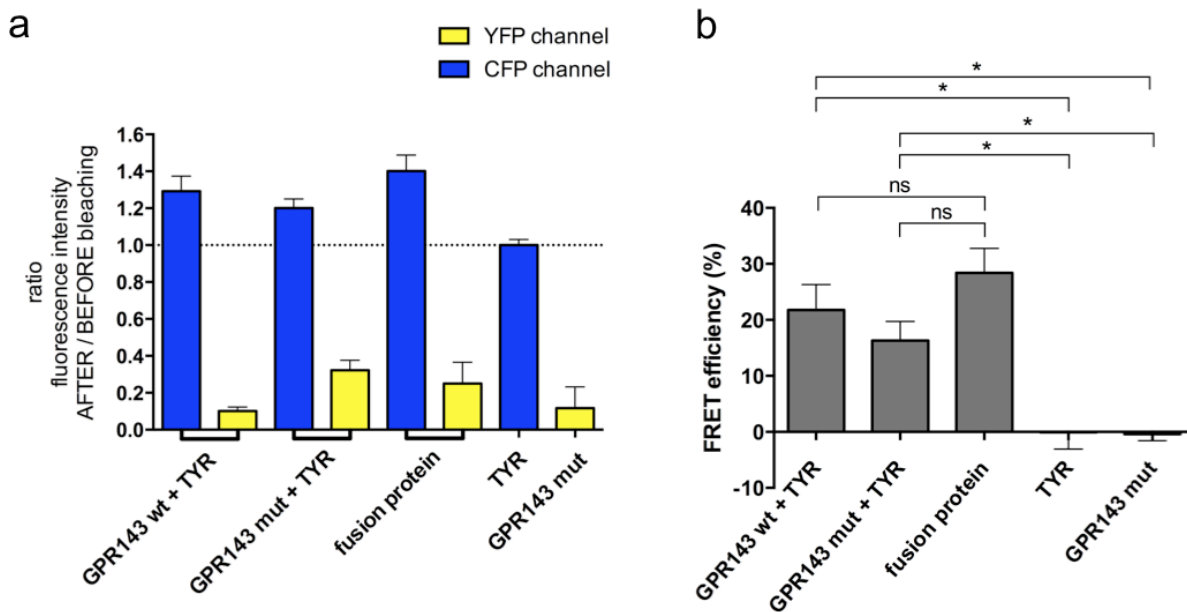


**Figure 40. Quantification analysis of FRET acceptor photobleaching in COS7 cells expressing GPR143-EYFP (wt or mutant) and TYR-ECFP.** (a) Ratio of emission intensity after bleaching to that before bleaching is plotted for both the CFP and YFP channels. Single transfected COS7 cells and the fusion protein ECFP-EYFP are used as controls. Data represent means  $\pm$  SEM of four (double transfected cells) or two (controls) different cells (two independent experiments). For wt GPR143, the photobleaching and the relative quantification was performed in limited intracellular spots, while for mutant GPR143, small portions of plasma membrane were photobleached and analyzed (see ROI in Fig 39). (b) FRET efficiency was quantified for COS7 cells double transfected with GPR143-EYFP (wt or mutant) and TYR-ECFP. Single transfected cells and ECFP-EYFP fusion protein were tested as controls. Results are expressed as means  $\pm$  SEM of four (double transfected cells) or two (controls) different cells (two independent experiments). The unpaired *t*-test was performed: \*  $p < 0.05$ , *ns* not significantly different from the control. Efficacy values refer to the limited regions described in Fig 39a.

### 3.10.5 Discussion

GPR143 is a peculiar G protein-coupled receptor (GPCR) with an undisclosed function in pigmented cells whose mutation was found to be responsible for a X-linked form of albinism, the Ocular Albinism type I (OA1) [129]. Hypotheses about GPR143 function include to be a sensor of melanosome maturation and to delay the fusion of multivesicular bodies (MVBs) to lysosomes [104,127]. The mechanism used by GPR143 to recognize the melanosome maturation is still an unsolved question, however the suggested purpose of the lysosomal

fusion delay was the delivery of melanosomal proteins and this hypothesis gave us an indication for further studies. Since in the last decade the interaction between GPCRs and proteins was found to be important for their regulation and function [128], our investigation focused on the association between GPR143 and tyrosinase, the leading enzyme responsible for the melanosome maturation. Previous evidences showed that the function of tyrosinase is not influenced by GPR143 mutation, indeed in GPR143 knockout mice tyrosinase is expressed and functional in macromelanosomes [91]. However when tyrosinase is knocked out or not transported to the melanosomes (membrane-associated transporter protein, Matp, knockout mice), macromelanosomes are not formed and GPR143 stops the maturation of the organelles in stage II [91]. Those findings underline a possible connection between GPR143 and tyrosinase or tyrosinase products.

We first generated a double mutant GPR143 replacing the two sorting signals necessary for its intracellular localization with alanine residues [99]. The wildtype (wt) and the mutant GPR143 were transiently expressed in COS7 cells and for this purpose the proper DNA concentration was researched in order not to overexpress the proteins, indeed in a former study the wt GPR143 was found at the plasma membrane in COS7 cells due to high over expression [111]. The characterization of the receptors showed that the wt receptor is intracellularly localized in the ER, Golgi apparatus and in vesicles which correspond to endosomes and lysosomes (data not shown), in agreement with previous studies [97,101]. On the other hand, the mutant GPR143 was mainly expressed at the cell plasma membrane. The glycosylation study revealed that both wt and mutant receptors were properly processed in the Golgi apparatus and were subjected to highly complex post-translation modifications.

Colocalization studies in transfected COS7 and melan-a cells showed that wt GPR143 and tyrosinase converged in some spots but they are mainly localized in close proximity vesicles. However, mutant GPR143 and tyrosinase were found to colocalize at the plasma membrane and in vesicles close to cell surface. The accuracy of the results was confirmed in melan-a cells, where the endogenous mouse tyrosinase was found to colocalize with the mutant GPR143.

Different arguments about the role of GPR143 in tyrosinase transport could derive from these findings. An hypothesis might be that GPR143 triggers the delivery of tyrosinase to the membrane where it is located, thus if mutant GPR143 localizes at the plasma membrane, tyrosinase is delivered to the same compartment. A similar interpretation was already

suggested by *Cortese et al. (2005)* who proposed that GPR143 controls the membrane delivery to melanosomes. However, this explanation is not in agreement with some evidences observed in pigmented cells of OA1 patients, in which tyrosinase is delivered to melanosomes even if GPR143 is not functional or retent in the ER, creating macromelanosomes full of melanin [91]. On the other hand, considering that melanosomal and lysosomal markers are mixed in the same vesicles when GPR143 is knockout and the two pathways are not separated [103], tyrosinase could be delivered to the lysosomes and produce macro-organelles containing melanin. A different interpretation for our findings could involve the direct interaction of GPR143 with tyrosinase. Thus, mutant GPR143 might transport the enzyme from the Golgi apparatus through vesicles to the plasma membrane.

As further step, the hypothetical direct interaction between GPR143 and tyrosinase was investigated. The immunoprecipitation studies in COS7 and melan-a cells showed that the two proteins are pulled down together from the cell lysates using antibodies either against GPR143 or tyrosinase. The double mutation in GPR143 does not influence the interaction with tyrosinase. The physical interaction of GPR143 and tyrosinase was supported by two different FRET techniques which demonstrated the close promity of the two proteins in several intracellular vesicles in COS7 cells, where the wt GPR143 was transfected, and at the plasma membrane, when the mutant GPR143 was present. The FRET efficiency obtained by analyzing the interaction of GPR143 and tyrosinase was comparable with the signal obtained by the fluorophores fusion protein. In addition, the obtained values of FRET efficacy are in the same order of significance of values showed in other studies involving the same fluorophore pair (ECFP-EYFP) [137–139], thus they can be considered accurate and reliable.

*Cortese et al.* demonstrated that at early stages of melanogenesis (stage I-II) GPR143 controls the rate of melanosome biogenesis while at final stages of maturation (stage III-IV) it regulates the organelle size and protein content [91]. Considering the results of our investigation and the information gained so far about GPR143 regulation, we propose an hypothetical model for the biological relevance of the receptor in pigmented cells (Fig 41). GPR143, after being processed in the Golgi apparatus, is transported to the early endosomes which evolve in premelanosomes due to an enrichment of melanosomal proteins [107]. Controlling the early segregation of the melanosomal and lysosomal pathway [127], GPR143 might regulate the rate of melanosomal biogenesis (Fig 41a). At later stages of melanosomal biogenesis GPR143 controls the maturation of the organelles through either perceiving the

presence of tyrosinase or controlling the delivery of melanin-related proteins (MRP), including tyrosinase, to the organelles (Fig 41a). When MRP are delivered to the melanosomes, the melanin synthesis begins and the maturation occurs. GPR143 might interact with tyrosinase and its downstream signaling changes, blocking the delivery of MRP to the mature organelles which are released to the cell periphery (Fig 41a). Then, GPR143 can be ubiquitinated and recycled [110]. Melanin-containing melanosomes are resistant to lysosome fusion [103,140] thus, the activity of GPR143 would not be required anymore.

The GPR143 regulation of early stages of melanogenesis could be associated to the receptor constitutive activity and its binding to the  $G_{\alpha i3}$  subunit (Fig 41a), since the introduction of a constitutively active  $G_{\alpha i3}$  protein in GPR143 knockout mice corrected the abnormal rate of melanosomal biogenesis [141]. Additional factors have been associated to the downstream pathway of GPR143, such as  $\beta$ -arrestin [111] which might regulate GPR143 signaling after the perception of melanosome maturation (Fig 41a). Over a decade ago, it was demonstrated that GPCRs are involved in biased signaling through arrestin proteins which activate a G protein-independent signaling pathway [142]. Therefore, later stages of melanosome maturation could be regulated by the arrestin recruitment after GPR143 binding to tyrosinase, which could switch off its basal activity (Fig 41a).

Most of OA1-associated mutations lead to ER retention of GPR143 while some others produce an unfunctional receptor [105]. When GPR143 is not functional (Fig 41b), the lysosomal and melanosomal pathways in pigmented cells are not segregated [103] which might be caused by an enhanced fusion of immature melanosomes and lysosomes due to the absence of GPR143 [103,127]. Part of these endosomes containing melanosomal and lysosomal markers, including an non-functional GPR143, could be targeted by the vesicles delivering MRP, such as tyrosinase and TRP1 (Fig 41b). GPR143 might not perceive the maturation of the organelles, due to loss in signaling function after tyrosinase interaction and the presence of lysosomal markers on the melanosomes induces a continuous delivery of MRP generating macromelanosomes.

In summary, we provided evidence of a direct interaction between GPR143 and tyrosinase through different methods. The colocalization of these two proteins in COS7 and melan-a cells and the FRET studies showed that the subcellular localization of TYR partially depends on GPR143. In addition, the physical interaction between GPR143 and TYR was suggested by IP studies in COS7 and melan-a cells. The results of our investigation improve the view

about GPR143 mechanism of action and open the scenario to new possible prospects about the role of GPR143 in the melanosomal biogenesis. These findings have important implications in the clarification of the physiopathology of Ocular Albinism type I, since GPR143 mutations were found to be responsible for the disease but the receptor role in the ocular and neurodevelopmental process is still unsolved.

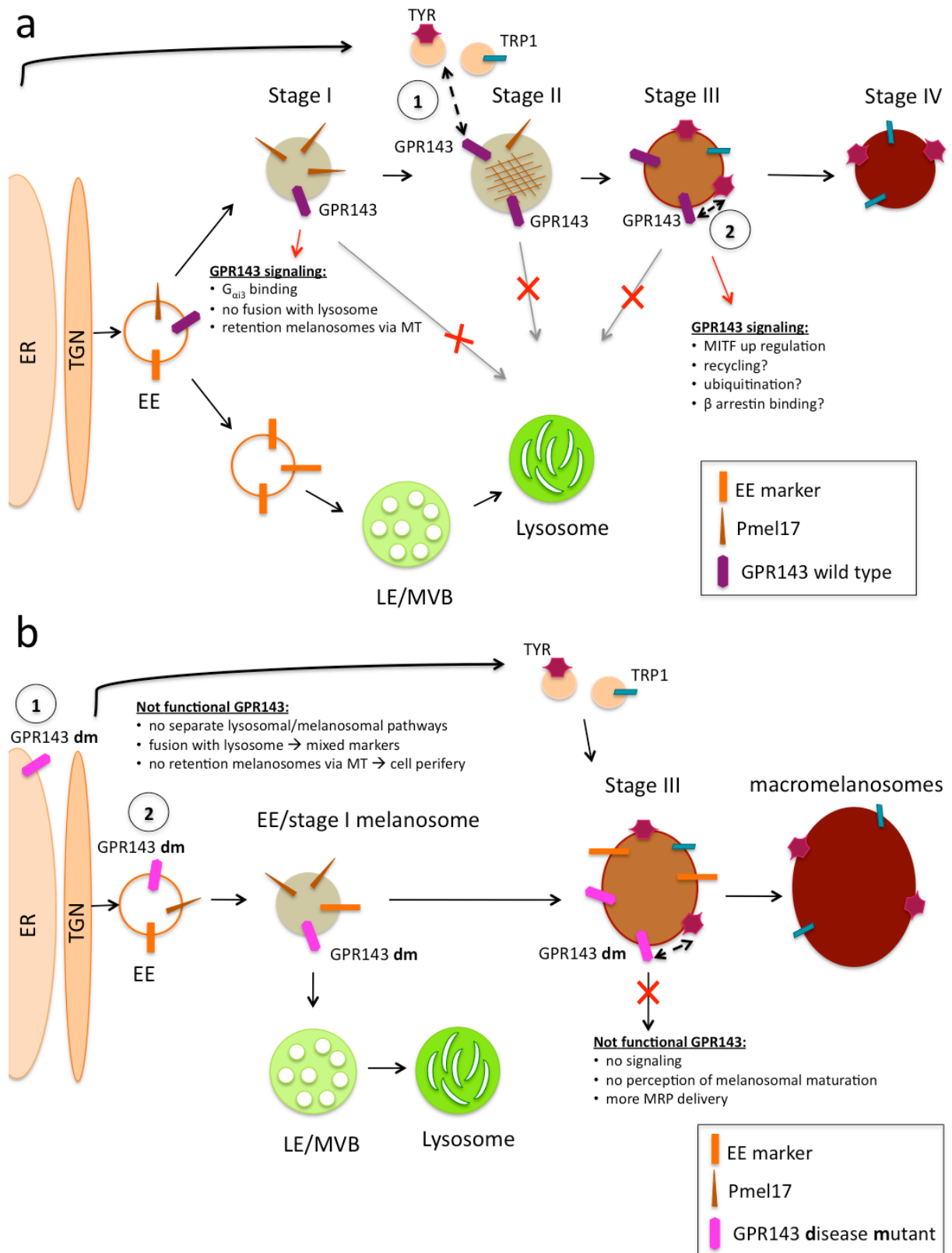


**Figure 41. Proposed hypothetical model for the role of GPR143 in the regulation of melanosome biogenesis.** (a) GPR143 first has a role at early stages of the organellogenesis controlling the rate of melanosomal biogenesis, inhibiting the fusion with lysosomes and holding the organelles in the perinuclear region through microtubules (MT) action. Then, GPR143 might control the delivery of

tyrosinase-containing vesicles to melanosomes (1) or perceive the maturation of the melanosomes through interaction with tyrosinase (2). EE early endosomes, LE late endosomes, MVB multivesicular body, TYR tyrosinase, TRP1 tyrosinase-related protein 1, TGN trans-Golgi network, stages I-IV refer to the maturation steps of melanosomes. **(b)** Mutations in GPR143 are associated with Ocular Albinism type I and could cause (1) GPR143 ER retention or (2) a functional problem in its signaling. In any of the two cases, there might be not a complete segregation between lysosomal and melanosomal pathway with marker mixing. The melanosomes are dispersed in the cell periphery, a reduced number of stage II melanosomes are present and the delivery of melanin-related proteins to melanosomes is continuous since the sensor of the organelle maturation, GPR143, is not functional. “*GPR143 dm*” refers to disease mutations in GPR143.

## 4. Summary

The present thesis deals with the characterization of G protein-coupled receptors (GPCRs) and their interaction with modulators on a molecular level. We focused on the structural and functional investigation of different types of GPCRs: the well known, previously crystallized adenosine A<sub>2A</sub> receptor and its closely related, but much less investigated relative, the adenosine A<sub>2B</sub> receptor, both of which are promising drug targets, and the underexplored orphan receptor GPR143, an intracellular GPCR which is involved in Ocular Albinism type I. Our goal was to study the impact of structural changes of GPCRs on ligand binding, signaling, and ligand selectivity as well as their allosteric modulation by interaction with other proteins. The results of our studies do not only expand the knowledge of basic biological processes, but they will also contribute to design of potent and selective receptor ligands which have potential as novel therapeutics. The most important results are summarized below.

### 1. Adenosine receptors

The human A<sub>2A</sub> and A<sub>2B</sub> adenosine receptors (ARs) are the closest homologs among the four AR subtypes. However, the endogenous ligand adenosine and its derivatives NECA and CGS21680 show significantly higher affinity for A<sub>2A</sub>AR than for the A<sub>2B</sub>AR subtype. The largest differences in sequences were found in the loop regions, especially in the extracellular loop 2 (ECL2). We created a chimeric receptor exchanging the ECL2 of the human A<sub>2A</sub>AR for the one of the human A<sub>2B</sub>AR generating the hA<sub>2A</sub>(ECL2-hA<sub>2B</sub>) mutant receptor. Ligand binding and receptor activation of the loop mutant receptor was compared to that of the wildtype (wt) human A<sub>2A</sub> and A<sub>2B</sub>AR.

- We found that the ECL2 in A<sub>2A</sub> and A<sub>2B</sub> receptors is involved in ligand recognition and subtype selectivity. Adenosine lost its affinity (22-fold) and potency in cAMP accumulation studies (70-fold) at the loop mutant (hA<sub>2A</sub>(ECL2-hA<sub>2B</sub>)) as compared to the wt A<sub>2A</sub>AR, indicating that the ECL2 plays an important role in the binding of and interaction with the endogenous agonist adenosine (Fig 42).
- Competitive binding studies versus [<sup>3</sup>H]CGS21680 showed that compounds with an extended substituent in the 2-position of adenosine (CGS21680 and PSB-15826) displayed a loss in affinity at the loop mutant in comparison with the wt A<sub>2A</sub> receptor. Therefore we could confirm that the A<sub>2A</sub> ECL2 is involved in binding of large 2-substituents of adenosine derivatives.



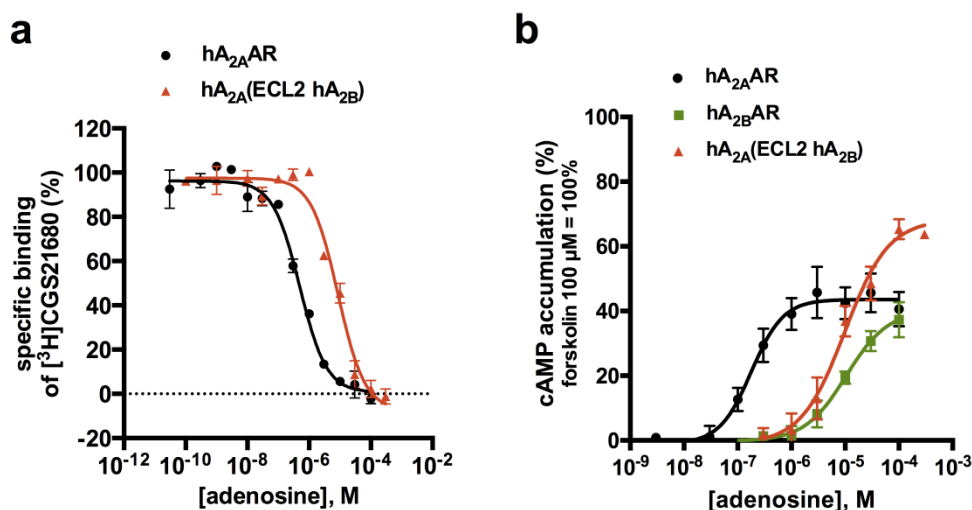


**Figure 42. Adenosine binding (a) and activation (b) at the wildtype human A<sub>2A</sub>AR and hA<sub>2A</sub>(ECL2-hA<sub>2B</sub>) receptor. (a)** Competition binding studies versus [<sup>3</sup>H]CGS21680 using adenosine. **(b)** Adenosine-induced cAMP accumulation assay at CHO cells stably expressing wild type A<sub>2A</sub>AR, wildtype A<sub>2B</sub>AR and hA<sub>2A</sub>(ECL2 hA<sub>2B</sub>) receptor.

- In addition, we verified that the ECL2 of the A<sub>2A</sub> and A<sub>2B</sub>AR is associated with conformational changes. Binding studies versus the A<sub>2A</sub> antagonist [<sup>3</sup>H]MSX-2 revealed a marked biphasic behaviour corresponding to the active and inactive receptor species in the hA<sub>2A</sub>(ECL2-hA<sub>2B</sub>) mutant. The ECL2 exchange appeared to stabilize the active conformation of the receptor for agonists such as NECA and CGS21680.

The investigation of the role of extracellular cysteine residues of the human A<sub>2A</sub>AR for ligand binding and receptor activation constituted a further part of this study. Cysteine mutant receptors were generated (Cys146Ser, Cys159Ser, Cys166Ser and Cys146Ser-Cys159Ser) and various agonists including the endogenous ligand adenosine were tested. The results obtained in binding and functional studies were supported by molecular modeling based on recently published crystal structures.

- The three disulfide bonds between ECL1 and 2 (Cys71<sup>2.69</sup>-Cys159<sup>45.43</sup>, Cys74<sup>3.22</sup>-Cys146<sup>45.30</sup> Cys77<sup>3.25</sup>-Cys166<sup>45.50</sup>) were found to be essential for the proper activation of the A<sub>2A</sub>AR in response to the endogenous agonist adenosine since all cysteine A<sub>2A</sub> mutant receptors displayed significantly reduced potency for adenosine as compared to the wt A<sub>2A</sub>AR, reaching EC<sub>50</sub> values in the micromolar range, similar to those determined for the wt A<sub>2B</sub>AR.

- The C159S mutant receptor showed a significant increase in potency for the three adenosine derivatives NECA, CGS21680 and PSB-15826 which could be due to the higher expression level of this mutant in comparison to the wt  $A_{2A}$ AR or to the gain in affinity for the adenosine derivatives (in contrast to adenosine itself) at the loop mutant receptor. Disruption of the disulfide bond I (Cys71<sup>2.69</sup>-Cys159<sup>45.43</sup>) generated a mutant receptor characterized by higher affinity and potency for adenosine derivatives than the wt  $A_{2A}$ AR as it was already observed in ECL2 mutant of the close homolog, the  $A_{2B}$ AR (Peeters *et al.* (2012) and (2014)).
- The mutation of Cys146 in the  $A_{2A}$ AR critically affected the cell surface expression of the receptor shown by ELISA. We suggest that the disulfide bond II (Cys74<sup>3.22</sup>-Cys146<sup>45.30</sup>) is critical for receptor folding, and its disruption might cause its ER retention (Fig 43).
- The disulfide bond III (Cys77<sup>3.25</sup>-Cys166<sup>45.50</sup>) conserved in most class A GPCRs appears to be essential for the proper activation of the receptor by the endogenous ligand adenosine. However, only minor variations in affinity and potency were observed at the C166S mutant for adenosine derivatives NECA, CGS21680 and PSB-15826 as compared to the wt  $A_{2A}$ AR (Fig 43). This indicates that the GPCR-conserved disulfide bond is not required for  $A_{2A}$ AR activation by adenosine derivatives.

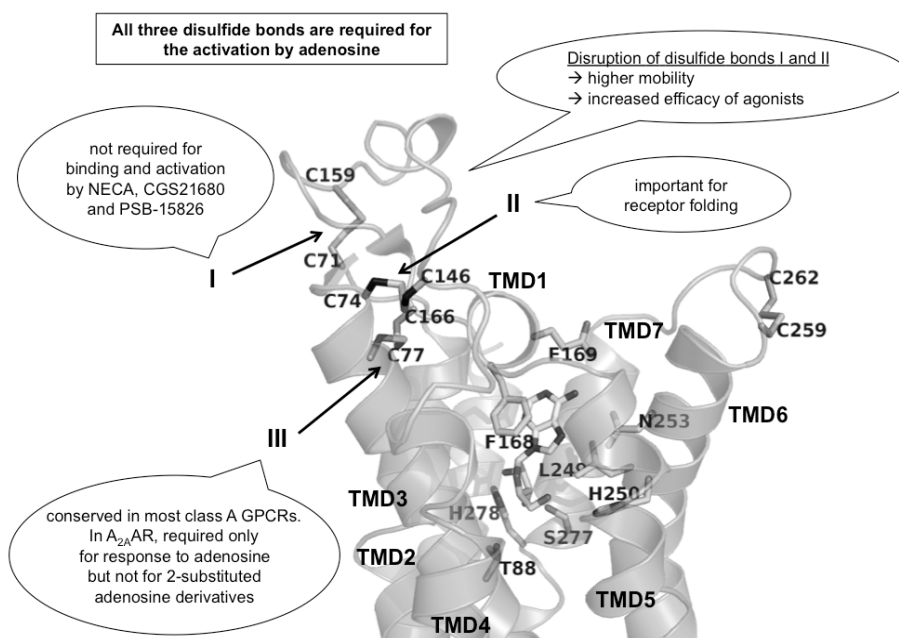


**Figure 43. Binding of adenosine at the  $A_{2A}$ AR.** The disulfide bonds have been numbered from I to III based according to increasing numbers of the cysteine residues. A summary of the main findings is shown.

- The length of the 2-substituent of the adenosine derivatives affected their binding and activation at the double mutant receptor, in which the two non-conserved disulfide bonds I and II (Cys71<sup>2.69</sup>-Cys159<sup>5.20</sup> and Cys74<sup>3.22</sup>-Cys146<sup>4.67</sup>) were disrupted. Small ligands such as adenosine and NECA showed a considerable loss in affinity and potency in the double mutant receptor as compared to the wt A<sub>2A</sub>AR. On the other hand, the 2-substituted adenosine derivatives CGS21680 and PSB-15826 only showed minor changes in receptor binding and activation in comparison to the wt A<sub>2A</sub>AR (Fig 43). The flexible ECL2 of the double mutant receptor is stabilized by the bulky substituents of CGS21680 and PSB-15826, resulting in similar potency and efficacy than for the wt A<sub>2A</sub>AR.

## 2. Ocular Albinism type I and GPR143

Despite its recent “de-orphanization”, the role of GPR143 in the development of neural retina and in the Ocular Albinism type I pathogenesis is still unclear. Our investigation focused on the function of GPR143 and its intracellular signaling cascade, and the purpose of our study was to identify pharmacological tools suitable to analyze GPR143 function, i.e. compounds able to activate or inhibit receptor signaling.

- GPR143 is an intracellular receptor, and thus we generated a double mutant GPR143 receptor which is expressed in the plasma membrane. Then we established CHO cell lines expressing either the wildtype (wt) or the mutant GPR143 to perform pharmacological studies.
- Levodopa (L-DOPA) was proposed to be the endogenous GPR143 agonist by *Lopez et al. (2008)*. We tested it using an engineered CHO cell line allowing to monitor agonist-induced  $\beta$ -arrestin recruitment with a luminescence readout based on a  $\beta$ -galactosidase complementation assay (DiscoverRx company). We found that the cell line showed high basal activation, and L-DOPA displayed only a small effect with a low signal-to-noise ratio. L-DOPA was also tested for activation of the calcium signaling pathway through G<sub>q/11</sub> protein coupling and for cAMP accumulation pathways through G<sub>i</sub> and G<sub>s</sub> protein coupling, however no significant differences from controls were observed. GPR143 might be already completely activated in the artificial cell system indicating a high constitutive activity. Thus, L-DOPA could not induce a further significant activation of the receptor. Since GPR143 activation by L-DOPA previously had only been observed in

ARPE-19 cells derived from retinal pigment epithelium which endogenously express GPR143, a second hypothesis could be that the participation of a third factor is required for activation of GPR143 by L-DOPA, and this additional component may be only present in pigmented cells. An alternative might be that the observed calcium release in ARPE-19 cells after L-DOPA treatment is not a GPR143-specific effect, but mediated by other natively expressed receptors that may be directly or indirectly activated by L-DOPA.

- In order to find more valuable tools to analyze GPR143 function, we screened two compound libraries using the  $\beta$ -arrestin recruitment assay. The screening campaign resulted in three reproducible hit compounds, which decreased GPR143 activation with potencies in the low micromolar concentration range (Fig 44).
- Pimozide, an antipsychotic drug active on dopamine receptors (Fig 44), was found to be a promising candidate to study GPR143 function in an endogenous system since it selectively reduced GPR143 basal activity and decreased melanocyte pigmentation without interfering with tyrosinase activity. Pimozide might be used as a scaffold for optimization to develop high affinity GPR143 ligands.

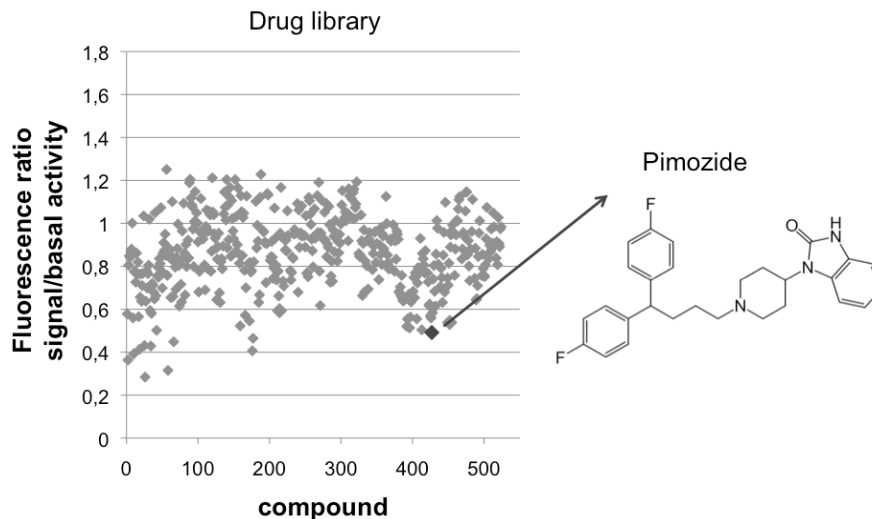


**Figure 44. High throughput screening of the Tocris compound library by  $\beta$ -arrestin recruitment assay.** Each point represents a single compound tested at 10  $\mu$ M final concentration. The reproducible hit compound, pimozide, which decreases GPR143 constitutive activity is indicated in green.

As a second part of the project, the connection between GPR143 and melanosomal maturation was investigated through studying the possible interaction between GPR143 and tyrosinase, the main enzyme responsible for the melanin synthesis and thus for melanosomal maturation.

- Colocalization studies in transfected COS7 and melan-a cells showed that when the wt GPR143 and tyrosinase are expressed together, they are mainly localized in vesicles in close proximity. However, tyrosinase was found to colocalize at the cell plasma membrane with the mutant GPR143 receptor (Fig 45).

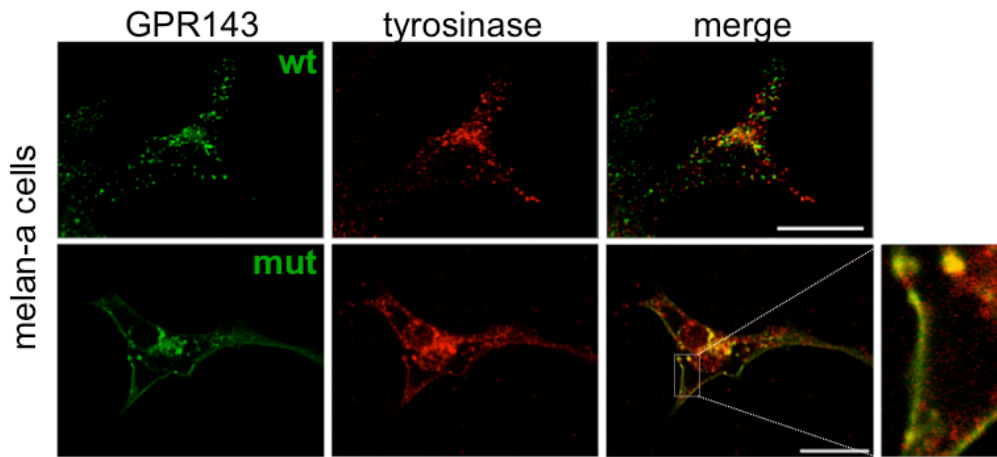


**Figure 45. Colocalization studies of tyrosinase and wildtype or mutant GPR143.** Melan-a cells were transfected with GPR143, fixed and the localization of endogenous tyrosinase and GPR143 was detected by staining with antibodies. Scale bars = 20  $\mu\text{m}$ .

- The interaction between GPR143 and tyrosinase was demonstrated by immunoprecipitation studies in COS7 and melan-a cells. In addition, the physical interaction of GPR143 and tyrosinase was supported by two different FRET techniques.
- A hypothesis involves GPR143 triggering the delivery of tyrosinase to the membrane where it is located, thus if the mutant GPR143 localizes at the plasma membrane, tyrosinase is delivered to the same compartment. Another hypothesis for these findings could be that GPR143 directly interacts with tyrosinase, and in this way the mutant GPR143 escorts the enzyme from the Golgi apparatus through vesicles, where they converge, to the plasma membrane.
- We provide evidence for a direct interaction between GPR143 and tyrosinase through different methods. Our results are critical for understanding the GPR143 mechanism of action in melanosomal biogenesis. GPR143 might control the maturation of melanosomes by perceiving the presence of tyrosinase or by controlling the delivery of melanin-related proteins, including tyrosinase, to the organelles. These findings have important implications for the clarification of the pathophysiology of Ocular Albinism type I, since GPR143 mutations were found to be responsible for the disease.

## 5. Materials

### 5.1 Chemicals and tested compounds

ADA	Roche, 10102105001
Adenosine	Sigma, A9251
ATP	Roth, 987-65-5
Agarose	Roth, 2267.2
Amaya kit for Nucleofector device	Lonza, Walkersville, MD
Ampicillin sodium salt	Applichem, A0839
BAY60-6583	Dr. Thomas Krahn, Bayer AG
BSA, albumin fraction V	Applichem, A1391
Bromophenol blue	Applichem, 3640
Calcium chloride dihydrate	Fluka, 21097
cAMP	Enzo Life Science, 80-0056
CGS21680	Tocris, 1063
DMSO	Applichem, A3608
DMSO for cell culture	Applichem, A3672
EDTA	Roth, 8040.3
Ethacridine lactate	Selleckchem, S4196
Ethanol	ZVE Universität Bonn, 123974
FCS	Sigma, F-0804
Forskolin	Applichem, 66575-29-9
Fura-2 AM	Molecular probes, F1221
G418	Calbiochem, 345810
Glacial acetic acid	Merk, 1.00063.1011
D-(+)-Glucose	Sigma, G-7012
Glycerine	Applichem, A1123,1000

HEPES	Sigma, H-3375
Hydrochloric acid, 37%	Applichem, A 0659
IBMX	Fluka, 58620
Isopropanol	ZVE Universität Bonn, 123903
jetPRIME transfection kit	Polyplus Transfection, Darmstadt, Germany
L-Glutamine	Cambrex Bioscience
LB-Agar	Invitrogen, 22700-041
LB-powder medium	Applichem, A0954,901
Lipofectamine	Invitrogen, 11668019
Magnesium chloride	Sigma, M-8266
Magnesium sulphate	Sigma, M-2643
2-Mercaptoethanol	Applichem, A4338
Monopotassium phosphate	Sigma, P-9791
Mycophenolic acid	Tocris, 1505
MSX-2	Synthesis in AK Prof. Dr. C.E. Müller
NECA	Sigma, E-2387
Niclosamide	Sigma, N3510
Oregon Green 488 BAPTA-1, AM	Molecular probes, O6807
Paraformaldehyde	Applichem, 3813,025
Pen-Strep solution	Gibco, 15140
Pimozide	Sigma, P1793
Pluronic F-127	Sigma, P2443
Polybrene	Aldrich, 10,768-9
Poly(ethyleneimine) in 50% (w/v) water	Sigma Aldrich, P 3143-1L
Potassium chloride	Fluka, 60128
PSB-15826	Synthesis in AK Prof. Dr. C.E. Müller

PTU	Sigma, P7629
Ro20-1724	Hoffmann La Roche
Scintillation cocktail	Luma safe scintillation cocktail, Perkin Elmer, 3087
Sodium acetate	Applichem, 4555,025
Sodium butyrate	Fluka, 19364
Sodium chloride	Sigma, P-9541
Sodium hydrogen carbonate	Sigma, S-5761
Sodium hydroxide	Fluka, 71689
Trypsin	Lonza, 17-160
TRIS	Roth, AE15.3
Triton X-100	Sigma, X-100
Xanthine	Applichem, 6665,001

## 5.2 Instruments

Analytical balance	Sartorius CP225D
Autoclave	VX-95, Systec
Bacterial shaker	Innova 4200, New Brunswick Scientific
Cell incubator	Haeraeus HERAcell 240 and Inc 246, Memmert
Centrifuge	Allegra 21 R, Beckman Coulter Avanti J-201, Beckman
Cell culture flask	Cell Star – Greiner Bio-One
Hamilton syringe	Syringes 705, Roth
Harvester	Brandell M24, 48, Gaithersburg, MD, USA
Heater	Thermomixer comfort, Eppendorf
Homogenizer	RW 16 basic, IKA Labortechnik, Germany



Laminar airflow workbenches	NUNC Safe flow 1.2 and NUNC BIOFLOW
LSC-counter	Tricarb 2900 TR, Canberra Packard/Perkin Elmer
Microplates	Greiner Bio-One
Multipette	Eppendorf Multipette Plus
Microwave	Microwave 800, Severin
pH meter	WTW pH Electrode SenTix 41
Photometer	Beckman DU, 530 Life Science
Safe-lock tubes	Eppendorf
Softwares	GraphPad Prism, version 5
	Microsoft Excel and Word
	QuantityOne, version 4.4.0
	NIS ELEMENT viewer for Nikon microscope
	ClustalW2, European Bioinformatics Institute
	Clone Manager, version 9
Sterile filters	Fitropur 0.22 $\mu$ m, Sarstedt
Thermocycler	Biometra TPersonal
Vortexer	IKA Labortechnik MS1
Water bath	GFL 1083
Western blot equipment	BioRad and Invitrogen

### 5.3 Cell lines and culture media

CHO cells	Dulbecco's Modified Eagle-F12 Medium (DMEM-F12) medium supplemented with 10% fetal calf serum (FCS), 100 U/ml penicillin G and 100 $\mu$ g/ml streptomycin (if transfected, 0.2 mg/ml G418)
$\beta$ -arrestin CHO cells	F12 medium supplemented with 10% fetal calf serum (FCS), 100 U/ml penicillin G, 100 $\mu$ g/ml streptomycin and 0.8

	mg/ml hygromycin B (if transfected, 0.2 mg/ml G418)
COS7 cells	Dulbecco's Modified Eagle Medium (DMEM) supplemented with 10% fetal calf serum (FCS), 100 U/ml penicillin G and 100 µg/ml streptomycin (if transfected, 0.2 mg/ml G418)
GP+envAM12 packaging cells	HXM medium which consists of DMEM, 10% FCS, 100 U/ml penicillin G, 100 µg/ml streptomycin, 1% ultraglutamine, 0.2 mg/ml hygromycin B, 15 µg/ml hypoxanthine, 250 µg/ml xanthine and 25 µg/ml mycophenolic acid
Melan-a cells	80% RPMI-20% DMEM medium supplemented with 10% FCS, 1% sodium pyruvate, 1% glutamate, 5 U/ml penicillin, 5 µg/ml streptomycin, 1% non-essential amino acids and 200 nM 12- <i>O</i> -tetradecanoyl phorbol 13-acetate

#### 5.4 Radioligands

<i>Radioligand</i>	<i>Specific activity/Concentration</i>	<i>Company</i>
[ <sup>3</sup> H]MSX-2	84 Ci/mmol	Amersham Life Science, UK
[ <sup>3</sup> H]cAMP	34 Ci/mmol	Amersham Life Science, UK
[ <sup>3</sup> H]CGS21680	36.05 Ci/mmol	Perkin Elmer Life Science
[ <sup>3</sup> H]NECA	17 Ci/mmol	Amersham Life Science, UK

#### 5.5 Buffers

##### *Hanks buffer salt solution (HBSS), pH 7.3 (buffer for cAMP assay and calcium assay)*

Hepes (20 mM), NaCl (130 mM), glucose (5.5 mM), MgSO<sub>4</sub> (0.83 mM), MgCl<sub>2</sub>.6 H<sub>2</sub>O (0.5 mM), CaCl<sub>2</sub>.2H<sub>2</sub>O (1.4 mM), NaHCO<sub>3</sub> (4.17 mM), KCl (5.36 mM), KH<sub>2</sub>PO<sub>4</sub> (0.4 mM) and Na<sub>2</sub>HPO<sub>4</sub> (0.3 mM) were dissolved in autoclaved water and the pH was adjusted to 7.4 using 1 N NaOH.

##### *Lysis buffer pH 7.3 (buffer for cAMP assay)*

Na<sub>2</sub>EDTA (4 mM) were dissolved in 1 L of water and the pH was adjusted to 7.4 using HCl (37%). Then 0.01% Triton X-100 was added.

### ***Phosphate buffered saline (PBS), pH 7.4 (washing buffer for cells)***

NaCl (137 mM), KCl (2.7 mM), Na<sub>2</sub>HPO<sub>4</sub> (4.3 mM) and KH<sub>2</sub>PO<sub>4</sub> (1.47 mM) were dissolved in 1 L of water. HCl (37%) was used to adjust the pH to 7.4.

### ***Tris-acetate-EDTA buffer (TAE), pH 8 (buffer for DNA agarose gel electrophoresis)***

TRIS (40 mM) was dissolved in 1 L of water. The pH was adjusted to 8 using acetic acid, then Na<sub>2</sub>EDTA (2 mM) was added.

### ***Tris-acetate-EDTA buffer (TAE), pH 8***

TRIS (40 mM) was dissolved in 1 L of water. The pH was adjusted to 8 using acetic acid, then Na<sub>2</sub>EDTA (2 mM) was added.

### ***Fura-2 stock solution***

Calcium-sensitive dye Fura-2 AM (50 µg) were dissolved in 49.9 µl DMSO to get a stock solution of 1 mM. Then it was aliquoted into Eppendorf vials and kept at -20 ° C.

## **5.6 Antibodies**

Mouse monoclonal anti-HA	Covance, Munich, Germany
Mouse monoclonal anti-ProLink/PK	PathHunter DiscoverX, Birmingham, UK
Rabbit polyclonal anti-pan Cadherin E	Abcam, Cambridge, UK
Mouse monoclonal anti-GPF	Covance, Freiburg, Germany
Rabbit polyclonal anti-eGFP	Thermo Scientific, Darmstadt, Germany
Rabbit antiserum αPEP-7	Dr. V. J. Hearing, National Cancer Institute
Goat anti-rabbit-AlexaFluor488	Jackson Immuno Research, Hamburg, Germany
Donkey anti-mouse-AlexaFluor594	Jackson Immuno Research, Hamburg, Germany
Donkey anti-rabbit-DyLight649	BioLegend, San Diego, CA
Goat anti-mouse-HRP	Jackson Immuno Research, Hamburg, Germany

Donkey anti-rabbit-HRP	Jackson Immuno Research, Hamburg, Germany
Goat anti-mouse IRDye 800CW	Odyssey, LI-COR, Lincoln, NE
Goat anti-rabbit IRDye 680	Odyssey, LI-COR, Lincoln, NE

## 5.7 Mutagenesis primers

The base pairs in bold capital letters indicate the mutated region of the gene coding sequence. The primers used to generate the chimera A<sub>2A</sub>(ECL2 A<sub>2B</sub>) receptor by Gibson assembly are color coded as shown in Fig 43, indicating the annealing regions.

f-hOA1-L223A-L224A	5'-gactgcagtgccctct <b>GCAGCT</b> aaaggaagacaaggca-3'
r-hOA1-L223A-L224A	5'-tgccttgcttccctt <b>AGCTGC</b> agaggccactgcagtc-3'
f-hOA1-W329A-E330A	5'-caggaaggagatccag <b>GCGGCA</b> tactgaccacctc-3'
r-hOA1-W329A-E330A	5'-gagtggtcagtgat <b>TGCCGC</b> ctggatctccttctg-3'
hA <sub>2A</sub> (ECL2 hA <sub>2B</sub> ) 1-f	5'-ggaattgatccgcccgcaccggt <b>accatgcccatcatgggctcctcggtgtac</b> -3'
hA <sub>2A</sub> (ECL2 hA <sub>2B</sub> ) 1-r	5'- <b>tgtctt</b> actgttccaacctagcatgggagtcaggccgatg-3'
hA <sub>2A</sub> (ECL2 hA <sub>2B</sub> ) 2-f	5'- <b>ctcccatgctaggttgaac</b> agfaaagacagtgccaccaacaactgcacagaacc-3'
hA <sub>2A</sub> (ECL2 hA <sub>2B</sub> ) 2-r	5'- <b>ccatgtagttcatggggaccac</b> attctcaaagagacacttcacaaggcagcagc-3'
hA <sub>2A</sub> (ECL2 hA <sub>2B</sub> ) 3-f	5'- <b>aagtgtctctt</b> gagaatgtggtcccatgaactacatggtgtactcaac-3'
hA <sub>2A</sub> (ECL2 hA <sub>2B</sub> ) 3-r	5'-gggagagggggcgaattccggatcct <b>caggacactcctgctccatcctgggccag</b> -3'
f-hA <sub>2A</sub> C146S	5'-ggttgaacaac <b>TCC</b> ggtcagccaaagg-3'
r-hA <sub>2A</sub> C146S	5'-ccttggtgacc <b>GGA</b> gttgtccaacc-3'
f-hA <sub>2A</sub> C159S	5'-gaaccactcccagggc <b>TCC</b> ggggagggccaagtgg-3'
r-hA <sub>2A</sub> C159S	5'-ccactggcctcccc <b>GGA</b> gcctgggagtggttc-3'
f-hA <sub>2A</sub> C166S	5'-gaggccaagtggcc <b>TCT</b> ctcttgaggatgtg-3'
r-hA <sub>2A</sub> C166S	5'-cacatcctcaaagag <b>AGA</b> ggccacttggccctc-3'

## 5.8 Materials for molecular biology

Deoxyribonuclease I – Amplification grade' kit	Invitrogen
DNA Clean and Concentrator kit	Zymo Research
Gel DNA Recovery kit	Zymo Research
Gel Red-Nucleic acid stain	Biotium
HiPure Plasmid Filter Midiprep kit	Invitrogen
Lambda DNA/HindIII	Thermo Scientific
PerfectPure RNA cultured cell	5 Prime
PhiX174 DNA-HaeIII digest	Thermo Scientific
Plasmid Miniprep-Classic kit	Zymo Research
Q5® High-Fidelity DNA Polymerase	NEB Biolabs
QuantiTect Reverse Transcription kit	Qiagen
Real Master Mix SYBR Rox kit	5 Prime
Restriction enzymes	NEB Biolabs
T4 DNA Ligase	NEB Biolabs

## **6. Methods**

### **6.1 Cell culture**

#### **6.1.1 General conditions and handling**

The cell lines are handled under sterile conditions (laminar air flow hood) using disposable sterile plastic pipettes and flasks. Different sizes of tissue flasks (25 cm<sup>2</sup>, 75 cm<sup>2</sup>, 175 cm<sup>2</sup>) are used depending on the aim of the culture. Incubation of cells occurs in a humidified incubator with a 5% CO<sub>2</sub> at 37°C. Adherent cells are detached by a 0.01% trypsin/0.6 mM EDTA solution and counted using a haemocytometer (depth: 0.100 mm, Neubauer improved).

#### **6.1.2 Transient transfection**

Lipofection is a technique used to inject genetic material into a cell using liposomes, which are vesicles that can easily merge with the cell membrane since they are both made of a phospholipid bilayer. Lipofectamine reagent contains lipid subunits which can form liposomes in an aqueous environment entrapping DNA. Lipofectamine is a cationic liposome formulation, which complexes with negatively charged nucleic acid molecules to allow them to overcome the electrostatic repulsion of the cell membrane. The DNA-containing liposomes (with positive charge on their surfaces) can fuse with the negatively charged plasma membrane of living cells. In a 25 cm<sup>2</sup> flask 1.5 million cells were seeded thus, their confluency was 80-90% at the time of transfection. Before the transfection (2 h), the cell medium was changed in medium without antibiotics. 600 µl of Optimem medium were mixed to 25 µl of Lipofectamine 2000 reagent and incubate 5 min at RT in order to form liposomes. After mixing 10 µg of plasmidic DNA to Optimem medium to reach a final volume of 625 µl, the lipofectamine suspension was added and mixed to the DNA solution, incubated 20 min at RT and finally transferred to the cells. One day after the cells were splitted (1:10 dilution) and seeded in normal medium. The day after the cell medium was changed in selection medium containing antibiotic for the only survival of cells that have incorporated the plasmid.

Another transfection reagent used for transfection of COS7 cells was the jetPRIME transfection kit according to the manufacturer's recommendations. Finally, melan-a cells were transfected using the DNA electroporation method with the Nucleofector device following manufacturer's instructions of Amaxa kit.

### 6.1.3 Stable transfection

Taking advantage of viruses, genes can be delivered to target cells using the retroviral transfection procedure. The concept of virus-based gene delivery is to engineer the virus so that it can express the gene of interest and retain its ability to deliver the gene to target cells. The use of competent retrovirus is not feasible, since the infected cells will die. Therefore, genetically engineered viruses are used in which only genes responsible for viral RNA encapsulation, reverse transcription and integration are kept [143].

Packaging cells (i.e. GP<sup>+</sup>envAM12, derived from mouse fibroblast) used for virus assembly are already transfected with two plasmids, one contains the *env* gene responsible for the viral envelop and the second one contains *gag* and *pol* genes of murine leukemia virus (MuLV) that are responsible for the group-specific antigen on capsids and the viral polymerase, respectively. The presence of hygromycin B, hypoxanthine, xanthine and mycophenolic acid in the culture medium causes a selective pressure on cells so they do not lose the three genes. The packaging cells are then transfected with a third plasmid that contains the packaging signal sequence ( $\Psi$ ) necessary for the proper insertion of the RNA into the virion and the gene of interest cloned into the multi cloning site. Both of these genes are flanked by LTRs where the viral promoters and transcriptional enhancers are located. In order to increase the infectivity of viruses, a co-transfection with a vector encoding the glycoprotein G of the vesicular stomatitis virus (VSV-G) is done so the retrovirus will not only infect by binding to specific receptors but rather by binding to phospholipids unspecifically [143].

GP<sup>+</sup>envAM12 packaging cells were seeded in DMEM medium containing 10% FCS, 100 U/ml penicillin G and 100 µg/ml streptomycin into a flask 24 h before the transfection. The cells were then transfected with the receptor DNA (6.75 µg) and the vesicular stomatitis virus G protein DNA (VSV-G, 3.75 µg) using Lipofectamine 2000. After 15 h of incubation, the medium was removed and replaced by 3 ml of DMEM medium containing 10% FCS, 100 U/ml penicillin G and 100 µg/ml streptomycin, including 5 mM sodium butyrate. The packaging cells were incubated at 32 °C with 5% CO<sub>2</sub> for 48 h. Then the supernatant of the GP<sup>+</sup>envAM12 cells was filtered, mixed with 6 µl of polybrene solution (4 mg/ml) and then incubated with CHO cells for 2.5 h at 37 °C. After 48 h the cells were selected using 0.8 mg/ml of G418. After two weeks, the concentration of G418 was reduced to 0.2 mg/ml.

## 6.2 Membrane preparation

Stably transfected CHO cells were cultured in dishes until confluency. In order to increase the exogenous protein expression, valproic acid was added (final concentration: 0.5 mg/ml) one day before harvesting [144]. Then cells were washed with sterile PBS and scraped off using ice-cold Tris buffer. The cell suspension was homogenized and centrifuged 10 min at 1000 x g to remove unbroken cells and nuclei. The supernatant was centrifuged at 30 000 g for 60 min. The pellet was resuspended in ice-cold 50 mM Tris-HCl buffer (pH 7.4) and stored at -80 °C until required. Protein concentrations were determined with the Bradford method [107].

## 6.3 Molecular biology

### 6.3.1 Cloning

#### 6.3.1.1 Polymerase Chain Reaction (PCR)

All the PCRs were carried out with the Q5 High Fidelity Polymerase to obtain an optimal cloning result with as less faults as possible. The optimal working condition for this enzyme is 72°C. The annealing temperature ( $T_A$ ) of the primers depends on their sequence. It was chosen to be 2-5 °C below the melting temperature. In some cases DMSO can be added to the PCR mixture (with a final concentration of 2%) since it enhanced the PCR amplification of GC rich regions. The amplification was carried out on a Thermoblock.

Reaction mixture for PCR:

Template DNA	≈ 10 ng
Primer forward	5 pmol/μl – final concentration 0.3 μM
Primer reverse	5 pmol/μl – final concentration 0.3 μM
Q5 High Fidelity Polymerase	1 U/μl
10X Q5 Buffer	5 μl
dNTPs mix	final concentration 0.2 mM
PCR grade water until final volume of 50 μl	



PCR program (step 2-4 repeated 20-30 times):

Step 1: long denaturation	94 °C	4 minutes
Step 2: denaturation	94 °C	1 minute
Step 3: annealing	$T_m - 2-5$ °C	1 minute
Step 4: elongation	72 °C	1 minute/1000bp
Step 5: final elongation	72 °C	10 minutes
Step 6: storage	4 °C	

### 6.3.1.2 Analysis and separation of PCR products

1% agarose gel in TAE buffer containing GelRed-Nucleic acid stain was used to analyze the PCR products and plasmids. Gels were run at 100 V for about 25 min. Lambda DNA/HindIII and phiX174 DNA-HaeIII digest served as markers. The bands corresponding to the expected size were excised from the gel and the DNA was extracted and purified using the Gel DNA Recovery kit according to the manufacturer's protocol.

### 6.3.1.3 Enzymatic digestion

Different enzymes were used corresponding to the restriction site present in the construct. In some cases a double digestion was feasible. The digestion was carried out at 37 °C for 1 h. The general reaction mixture was carried out on a Thermoblock and consisted in the following reagents. After the digestion the PCR product was purified using DNA Clean and Concentrator kit according to manufacturer's protocol. On the other hand, the digested vector was analyzed through an agarose gel together with a negative control (not digested vector) and then extracted with Gel DNA Recovery kit.

PCR product or vector	0.5-1 µg
Restriction enzyme(s)	1 U/µg of DNA
10X Suggested buffer	1:10 dilution
10X BSA (if needed)	1:10 dilution
PCR grade water until final volume of 20-30 µl	

#### 6.3.1.4 Ligation

The digested PCR product was ligated into the corresponding digested vector, which carries an antibiotic resistance, used afterwards to select the bacteria containing the plasmid. The insert/vector molar ratio is usually 4:1. The ligation was performed with the following protocol:

Digested vector	50 ng
Digested PCR product	150 ng
T4 DNA Ligase	1 $\mu$ l (~ 400 U)
10X Ligase buffer	1:10 dilution
ATP	Final concentration 10 mM
PCR grade water until final volume of 20-50 $\mu$ l	

The ligation mixture was incubated for 16 h at 16 °C or 30 min at RT. As negative control a ligation without the insert was simultaneously carried out.

#### 6.3.1.5 Production of competent *E.coli* with Calcium Chloride

Untransformed Top10 *E.coli* bacteria (50  $\mu$ l from a bacterial glycerol stock) were inoculated in 4 ml of LB medium without any antibiotic and cultivated overnight at 37 °C on a shaker (220 rpm). The culture was then inoculated in 40 ml of LB medium and after 45 min of incubation, the absorption of the bacteria suspension was measured at 550 nm until the OD<sub>550</sub> reached 0.5. Then the bacterial suspension was centrifuged (1700 g, 20 min, 4 °C), the pellet was resuspended in 20 ml of sterile cooled 0.1 M CaCl<sub>2</sub> solution and incubated 30 min on ice. Bacteria were then centrifuged again, resuspended in 2 ml of CaCl<sub>2</sub> solution and 0.5 ml of sterile glycerol was added. Aliquots of 100  $\mu$ l were prepared and stored at –80 °C.

#### 6.3.1.6 Transformation of chemocompetent bacteria

Aliquots of chemocompetent bacteria were thawed from –80 °C on ice for 30 min. The ligation mixture or 10-50 ng of plasmidic DNA were added to the bacterial suspension,

carefully mixed and incubated 30 min on ice. The heat shock to produce rearrangements in the bacterial membrane was performed at 42 °C for 30 sec and then back on ice for 2 min. 200 µl of LB medium were then added and the bacterial suspension was incubated 1 h at 37 °C on a shaker (300 rpm) in order to let the bacteria recover. The complete mixture was transferred on an agar plate containing the selective antibiotic and incubated overnight at 37 °C.

#### **6.3.1.7 Colony screening and MiniPreps**

One day after the bacteria transformation with a ligation mixture, grown clones on the agar plates were checked for the right insertion. Several colonies were randomly picked up from the agar plate and cultivated in 4 ml of LB medium supplemented with the selective antibiotic overnight at 37 °C on a shaker. The next day plasmids were isolated from the bacterial culture using Plasmid Miniprep Classic kit. The isolated plasmids are then loaded on an agarose gel together with a negative control (vector without insert) to check their size. The negative control band should have a lower molecular weight than the vector ligated with the insert. The positive plasmids were then digested with the same restriction enzymes used for the insertion of the PCR product into the vector and the digestion mix is afterward loaded into a second agarose gel where the insert should be cut out from the vector. Sequencing of the positive clones is then performed by GATC Biotech, provider of DNA sequencing and bioinformatics for industry and academic research.

#### **6.3.1.8 Plasmid preparation by Midipreps**

When high amount of plasmidic DNA is needed (i.e. for mammalian cell transfection), a large scale plasmid isolation should be performed. 50 µl of bacterial or glycerol culture was inoculated in 4 ml of LB medium with the selective antibiotic and incubated 6-7 h at 37 °C on the shaker. The bacterial culture was then amplified to a 100 ml culture and cultivated overnight. The day after MidiPreps were performed using HiPure Plasmid Filter Midiprep kit according to manufacturer's protocol.

### 6.3.1.9 Site-directed mutagenesis

The site-directed mutagenesis can be performed by PCR in order to introduce specific and intentional changes in the DNA sequence of a gene. The gene of interest has to be subcloned in a small plasmid (i.e. pUC19 contains  $\approx 2700$  bp) to obtain as less fault as possible. The first step is a common PCR reaction with small changes, followed by a DNA purification using DNA Clean and Concentrator kit according to manufacturer's protocol.

Mutagenesis PCR program (step 2-4 repeated 30 times):

Step 1: long denaturation	94 °C	4 minutes
Step 2: denaturation	94 °C	1 minute
Step 3: annealing	$T_m - 2-5$ °C	1 minute
Step 4: elongation	72 °C	10 minutes
Step 5: final elongation	72 °C	10 minutes
Step 6: storage	4 °C	

The original wildtype DNA differs from the new synthesized molecule in the methylation. For this reason the wildtype DNA is then digested by a methylation sensitive *DpnI* restriction enzyme. *DpnI* is a Type II restriction enzyme which specifically cleaves DNA containing methylated adenine (<sup>m</sup>A) in the recognition sequence G<sup>m</sup>ATC. The general reaction mixture and digestion program were the following:

Purified DNA derived from mutagenesis PCR	10 $\mu$ l
DpnI	1 $\mu$ l ( $\approx 20$ U)
10X NEB Buffer 4	2 $\mu$ l
PCR grade water until final volume of 20 $\mu$ l	7 $\mu$ l

The reaction was carried out at 37 °C for 90 min then the enzyme was inactivated at 80 °C for 20 min. The final mixture was transformed into chemocompetent bacteria and transferred on agar plate containing the selective antibiotic. The plasmids isolated from the colonies were sequenced to confirm the presence of the mutation.

### 6.3.1.10 Gibson assembly master mix

The technique allows for the successful assembly of multiple DNA fragments, regardless of fragment length or end compatibility. Gibson Assembly efficiently joins multiple overlapping DNA fragments in a single-tube isothermal reaction [75]. The Gibson Assembly Master Mix includes three different enzymatic activities that perform in a single buffer:

- The exonuclease creates a single-stranded 3' overhang that facilitates the annealing of fragments that share complementarity at one end.
- The polymerase fills in gaps within each annealed fragment.
- The DNA ligase seals nicks in the assembled DNA.

The result is a double-stranded DNA molecule that can serve as template for PCR, RCA or a variety of other molecular biology applications, including direct transformation (a short overview is shown in Fig 46). The method has been successfully used to assemble oligonucleotides, DNA with varied overlaps (15–80 bp) and fragments hundreds of kilobases long.

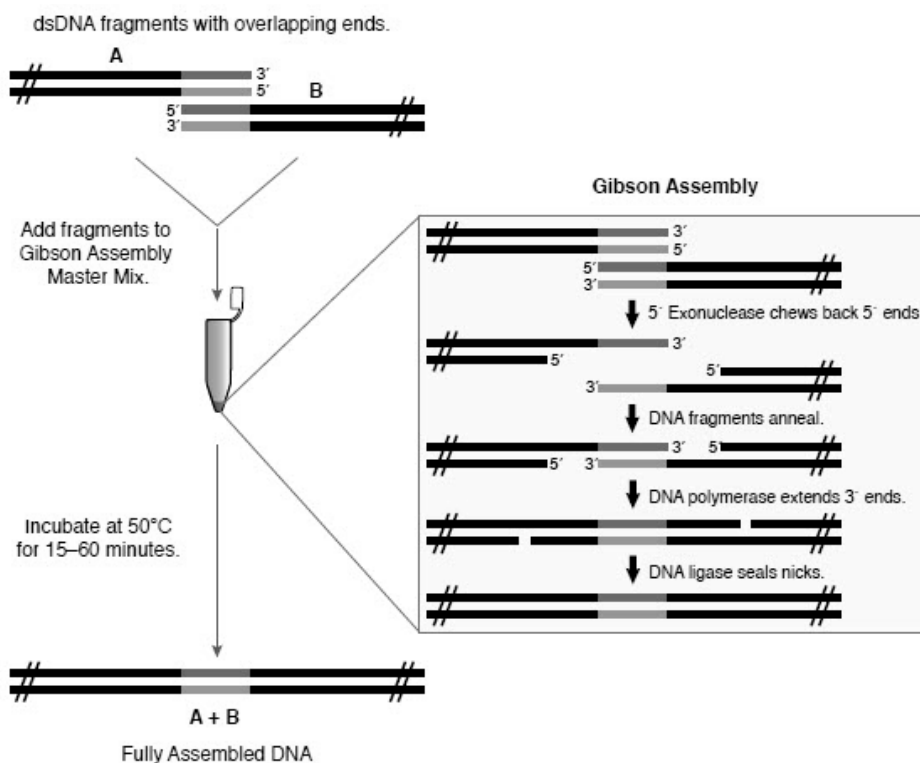


**Figure 46. Gibson assembly technique.** Overlapping DNA segments can be assembled in a single double stranded DNA molecule using the Gibson Assembly master mix, which contains three enzymes (exonuclease, DNA polymerase and DNA ligase) working at the same temperature [145].

The Gibson Assembly Master Mix was used to generate a human A<sub>2A</sub>(ECL2 A<sub>2B</sub>)AR chimera where the human A<sub>2A</sub> ECL2 was exchanged with the human A<sub>2B</sub> ECL2. For this purpose, three sets of primers were designed to create three PCR products with specific overlapping regions (see Material, Mutagenesis primers). Figure 47 shows the final plasmid product with the annealing regions of the primers.

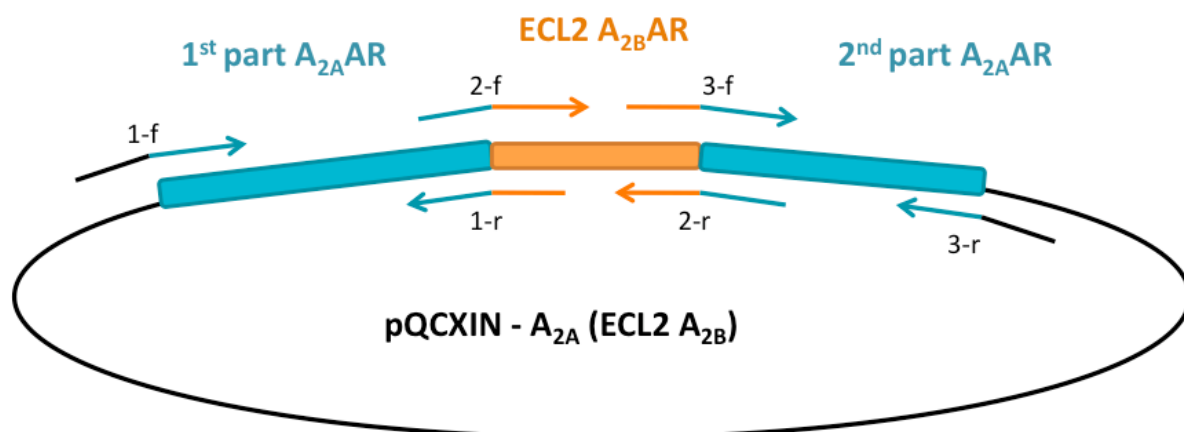


**Figure 47. Final chimera human A<sub>2A</sub>(ECL2 human A<sub>2B</sub>)AR in pQCXIN plasmid generated by Gibson Assembly reaction.** The three sets of primers created for the reaction are indicated (forward and reverse 1-3). The colors correspond to the annealing regions. The “f” and “r” refer to forward and reverse primer, respectively.

### 6.3.2 Quantitative PCR (qPCR)

#### 6.3.2.1 mRNA extraction

The mRNA extraction was performed using 5 Prime – PerfectPure RNA cultured cell kit.

Cells were seeded in a 6 well-plate and cultivated until they reached 80-90% confluency. The cells were then washed with PBS, scraped off and transferred in sterile RNase-free tubes. After centrifugation, the pellet was resuspended in lysis buffer and kept on ice. The lysate was transferred into the purification column where the mRNA binds and centrifuged until it completely passed through the column. The mRNA bound to the column was washed with washing buffer 1 and 2 and then eluted with the elution buffer. The mRNA concentration was determined by spectral absorption at 260 nm using a 1 cm quartz cuvette, knowing that 1 OD<sub>260</sub> unit corresponds to 40 µg/mL solution of single stranded RNA. The extracted mRNA is stored at -80 °C.

### **6.3.2.2 DNaseI digestion**

In order to remove the genomic DNA contamination, the mRNA solutions were treated with Deoxyribonuclease I. The DNA digestion was performed using Deoxyribonuclease I – Amplification grade kit. 1 µg of mRNA sample was mixed to 1 U of DNaseI (stock: 1 U/µl) and reaction buffer and incubated 15 min at RT. Then, 25 mM EDTA was added to the reaction mix and incubated 10 min at 65 °C for the inactivation of the enzyme.

### **6.3.2.3 Reverse transcription**

The mRNA was transcribed in cDNA to be then quantified using the qPCR. The reverse transcription was performed using QuantiTect Reverse Transcription kit. The first step consisted in an additional genomic DNA digestion, mixing the DNaseI digested mRNA with gDNA Wipeout buffer and incubating them 2 min at 42 °C. The second step included the reverse transcription which was performed at 42 °C for 30 min mixing the mRNA sample from the first step, the reverse transcriptase, the Quantiscript buffer and RT primers. The enzyme was then inactivated for 3 min at 95 °C.

### **6.3.2.4 Real Time PCR**

The quantification of a gene expression was performed using Real Master Mix SYBR Rox kit. The cDNA was diluted and mixed to the Real Master Mix buffer containing the intercalant dye Syber Green and to specific primers (5 pmol/µL) for the gene of interest. As positive control, the quantification of a housekeeping gene, such as the β actin gene, was performed at the same time. As negative control, a sample without primers was included. For each sample a negative control using not retro-transcribed mRNA was also added.

The PCR process goes through three main phases as the number of cycles and the amount of product generated increase. Initially, when the amount of product is small and enzyme and reagents are not limiting, product generation is exponential and the reaction is closest to 100% efficiency. This exponential growth is hard to detect initially through real-time fluorescence because the amount of product is small. During the linear phase products continue to accumulate (Fig 48), but the reaction efficiency begins to fall and reagents become limiting. Finally, in the plateau phase of the reaction, accumulation of product ceases as the reaction is exhausted.

Relative quantification determines the changes in steady-state mRNA levels of a gene across multiple samples and expresses it relative to the levels of an internal control RNA or of a background control. Therefore, relative quantification does not require standards with known concentrations and calculations are based on the comparison of the distinct cycle determined by various methods, i.e. crossing points (Cp) and cycle threshold values (Ct) at a constant level of fluorescence (Fig 48) [146].

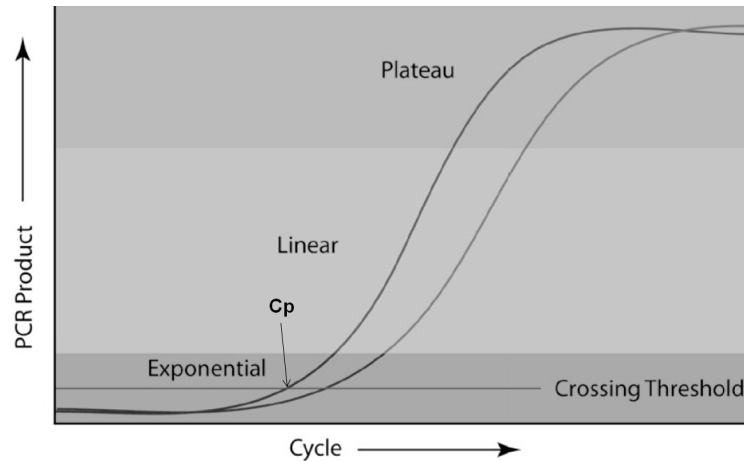


**Figure 48. Schematic graph of a typical qPCR cycle** (adapted from [146]).

#### 6.4 Immunohistochemistry

Transfected cells were cultured on coverslips in 12-well plates and fixed with a cold 1:1 methanol/acetone solution for 20 min at -20 °C. Cells were then washed with PBS and blocked 1 h with 1% BSA/PBS solution. Cells were incubated in the dark 60 min with the first antibody and then 30 min with the secondary antibody, both diluted in 1% BSA/PBS. In between and after antibody incubations, cells were washed with PBS. Nuclei staining was carried out using DAPI. At last coverslips were mounted using ProLong Gold antifade reagent (Invitrogen, Darmstadt, Germany) and stored in the dark at 4 °C. A Nikon A1 Spectral confocal microscope (Pharmaceutical Institute, University of Bonn, Germany) and Carl Zeiss LSM 700 (Ronald O. Perelman Department of Dermatology and Department of Cell Biology, New York) were used for imaging.



## 6.5 Bradford protein assay

The Bradford assay is a spectroscopic analytic procedure for the detection and quantification of total amount of proteins. When mixed with a protein solution, the acidic dye reagent (Coomassie Brilliant Blue G-250) changes color from brown to blue in proportion to the amount of protein present in the sample. The difference between the two forms of the dye is greatest at 595 nm thus, that is the optimal wavelength to measure the Coomassie dye-protein complex. Development of color has been associated with the presence of certain basic amino acids (primarily arginine, lysine and histidine) in the protein. The number of Coomassie dye ligands bound to each protein molecule is approximately proportional to the number of positive charges found on the protein.

Protein determination was made by comparison to the color response of protein standards, prepared as a series of known dilutions (0.5–3 mg/ml in PBS) of BSA (Fig 49). Afterward, 200  $\mu$ l of Bradford reagent was mixed to 1  $\mu$ l of the cell lysate and the absorbance was measured at 595 nm.

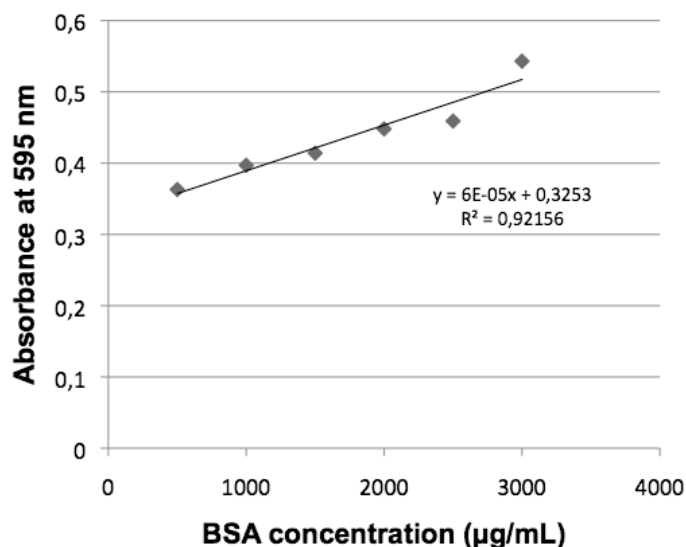


**Figure 49.** Example of BSA standard curve for Bradford protein assay. Absorbance measured at 595 nm.

## 6.6 Western Blot

A known amount of protein (~ 30  $\mu$ g) was mixed with loading buffer (3X loading buffer for GPR143: 0.2 M Tris-HCl pH 6.8, 12% Glycerin, 42% SDS, 15% Mercaptoethanol, 0.03% (w/v) Bromphenolblue – 4X loading buffer for tyrosinase: 0.25 M Tris-HCl pH 6.8, 15%

Glycerin, 8% SDS, 20% Mercaptoethanol, 0.04% (w/v) Bromphenolblue) and separated in 10% SDS-PAGE gel and then transferred onto a nitrocellulose membrane (PROTRAN – Nitrocellulose Transfer Membrane – Whatman, Sigma, Taufkirchen, Germany) or polyvinylidene difluoride membrane (Immobilon, Millipore, Waltham, MA). The Precision Plus Protein Kaleidoscope Prestained Protein Standard was used as marker. The membrane was blocked 1 hour in a 5% powdered milk/PBS-Tween solution (for COS7 lysates) or StartingBlock (TBS) Blocking buffer (for melan-a lysates, Thermo Fisher Scientific, Grand Island, NY). Afterward, the membrane was incubated with the primary antibody overnight at 4 °C or 1 hour at RT, washed 1 h with PBS-Tween, incubated with secondary antibody and washed again. The detection was performed with ECL kit (GE Healthcare, Amersham, Arlington, IL – Dassel, Germany) according to the manufacturer's instructions. Western blots of melan-a lysates were detected with Odyssey (LI-COR, Lincoln, NE) using the following secondary antibodies: ODYSSEY goat anti-rabbit IRDye 680 and ODYSSEY goat anti-mouse IRDye 800CW.

## **6.7 Immunoprecipitation**

Two days after DNA transfection, COS7 and melan-a cells were scraped off the dishes and lysed on ice with lysis buffer (20 mM HEPES pH 7.2, 1% NP-40, 10% glycerol and protease inhibitor cocktail (Sigma, Taufkirchen, Germany). The lysate was centrifuged 15 min at 21000 g and the protein concentration was determined with BCA Protein assay reagent kit (Thermo Fisher Scientific, Grand Island, NY) or with Bradford reagent. The protein samples were mixed with loading buffer containing 2% SDS (or 14% SDS for GPR143) and boiled for 2 min (or warmed at 37 °C for 30 min for GPR143). For immunoprecipitation samples, 1 mg of lysate was mixed to 2 µg of antibody and incubated overnight at 4 °C on a rotating wheel. Protein A-agarose beads (50 µl of suspension for each sample - Thermo Fisher Scientific, Grand Island, NY) were washed twice with lysis buffer and then pre-incubated 1 h in 0.1% BSA/lysis buffer. Then, beads were washed in lysis buffer twice and incubated with the lysate-antibody for 2 hours at 4 °C on a rotating wheel. After the beads were washed four times, the proteins were eluted in loading buffer containing 2% SDS (or 14% SDS for GPR143) and boiled for 2 min (or warmed at 37 °C for 30 min for GPR143). Immunoprecipitated proteins were separated in a 10% SDS-PAGE, transferred to a membrane and detected with antibodies (see Western Blot).

## 6.8 Glycosylation studies

The glycosylation studies were performed using two enzymes: Peptide N-Glycosidase (PNGase F) and endoglycosidase H (Endo H).

PNGase F is an amidase which cleaves N-linked oligosaccharides between the innermost GlcAc and asparagine residues of high mannose, hybrid and complex oligosaccharides from N-linked glycoproteins.

Endo H is a highly specific endoglycosidase which cleaves asparagine-linked mannose rich oligosaccharides, but not highly processed complex oligosaccharides from glycoproteins. It is commonly used to monitor post-translational modification in the Golgi apparatus. Most proteins destined for the cell surface are translated by ribosomes in the rough endoplasmic reticulum (ER) and translocated into the Golgi. Upon entering the ER a molecule containing 14 sugar subunits is linked en bloc to an asparagine in a selective manner by the enzyme oligosaccharyl transferase. This oligosaccharide molecule moves through the different compartments of the Golgi apparatus. Endoglycosidase H is able to cleave each structure of this oligosaccharide as it is processed until the enzyme Golgi alpha-mannosidase II removes two mannose subunits. Since all later oligosaccharide structures are resistant to Endo H cleavage the enzyme is widely used to report the extent of oligosaccharide processing a protein has undergone (Fig 50).

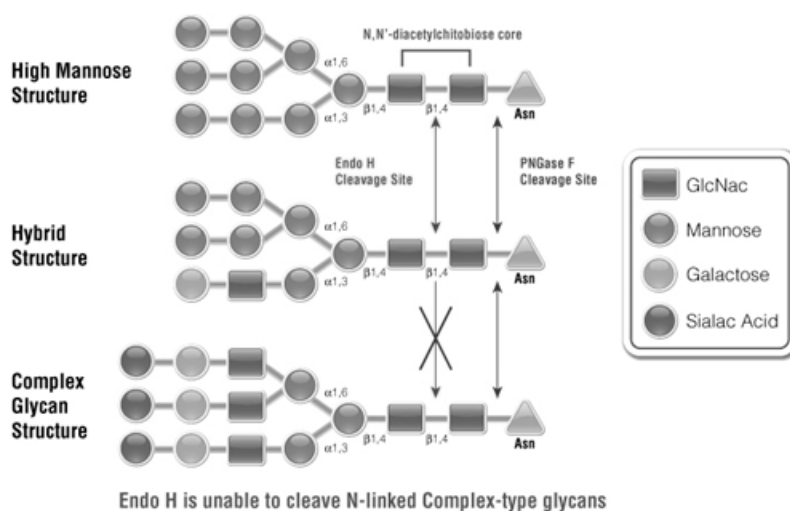


**Figure 50. Peptide N-Glycosidase (PNGase F) and endoglycosidase H (Endo H) cleavage sites [147].**

Cells were transiently transfected and after 48 h of incubation they were detached and sonicated (3 times for 10 sec). 50  $\mu$ g of total lysates were mixed with proper buffers, following the manufacturer's instruction. The reaction mixture was incubated 1 h at 37 °C. Thereafter, each reaction was mixed with loading buffer, the proteins were separated into a 10% SDS-PAGE and transferred to a membrane (see Western Blot).

## **6.9 Fluorescence Resonance Energy Transfer (FRET)**

Fluorescence Resonance Energy Transfer (FRET) methods are able to detect interactions between proteins in living or fixed cells. The FRET process involves a transfer of energy from one fluorophore in the excited state (donor) to a second fluorophore (acceptor) [148]. For an efficient FRET, there must be an overlap between the donor fluorescence emission spectra and the acceptor fluorescence excitation spectra (Fig 51a). In addition, FRET occurs only if the two fluorophores are within 2-10 nm distance to each other (Fig 51b). The two proteins of interest are linked to the fluorophores and expressed in a cell system [148]. The FRET experiment measures the amount of acceptor protein emission after excitation of the donor. In this project we used YFP (Yellow Fluorescent Protein) as acceptor fluorophore linked to GPR143 receptor and CFP (Cyan Fluorescent Protein) as donor fluorophore linked to tyrosinase (TYR).

FRET detection methods include sensitized emission and acceptor bleaching. The sensitized emission technique is based on measuring the FRET signal, exciting only the donor and filtering the emission of the acceptor, from a series of cell sample and control images. Images of the donor and the FRET signal are collected and corrected for background intensity, noise and contributions that do not arise directly from the FRET signal. On the other hand, the principle of the acceptor photobleaching is that in the absence of the acceptor no FRET occurs. If the acceptor is photobleached in a defined region of the sample where FRET signal is present, the result consists in an increased intensity of the donor signal [148].

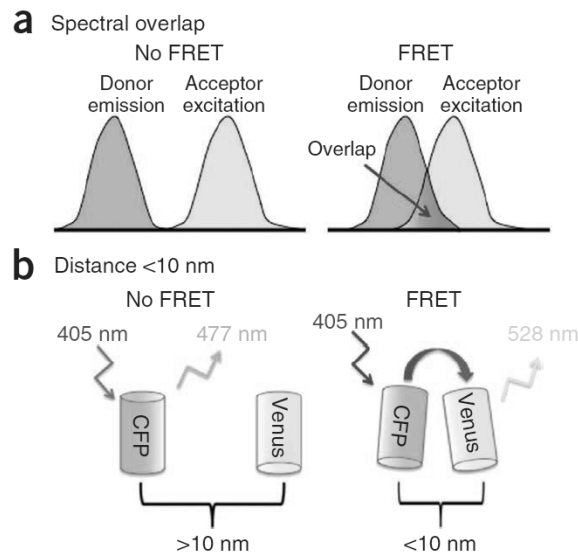


**Figure 51. Schematic representation of the Fluorescence Resonance Energy Transfer (FRET) mechanism of action.** (a) The donor emission energy must be absorbed by the acceptor thus, the excitation spectra of the acceptor have to overlap with the emission spectra of the donor. (b) The FRET occurs only if the fluorophores are within 10 nm of one another. The represented donor is CFP (Cyan Fluorescent Protein) and the acceptor is Venus (a variant of Yellow Fluorescent Protein). Adapted from [148].

The GPR143 coding sequence was cloned into the pEYFP-N1 vector using KpnI and AgeI restriction enzymes, while the TYR was cloned into the pECFP-N1 plasmid using HindIII and BamHI. The fusion protein ECFP-EYFP was created by cloning ECFP into the pEYFP-N1 plasmid using KpnI and AgeI restriction enzymes. COS7 cells ( $10^5$  cells well<sup>-1</sup>) were seeded on sterile glass coverslips in 12 well-plates and transfected with different combinations of DNA plasmids. After 48 h cells were fixed with an ice-cold 1:1 methanol/acetone solution for 20 min and mounted on slides using Mowiol 4-88 medium (Roth, Karlsruhe, Germany). A Nikon A1 Spectral confocal microscope operating with an argon laser was used for imaging. Cells were examined with a 60X oil immersion objective. NIS Element Advanced Research software 4.0 was used for image analysis.

For the sensitized emission method, different optical configurations were set up: “Dd channel” for excitation and emission of the donor chromophore (ECFP, excitation filter: 457 nm, emission filter: 482/35 nm), “Aa channel” for excitation and emission of the acceptor chromophore (EYFP, excitation filter: 514 nm, emission filter: 540/30 nm) and “FRET

channel” for the excitation of the donor and emission of the acceptor chromophore (excitation filter: 457 nm, emission filter: 540/30 nm).

For each image, parameters (high voltage, offset and laser intensity) were adjusted in order to limit the spectral bleed through and to avoid the pixel over-saturation. The laser intensity was equalized in both FRET and donor channel, while the high voltage was equalized in both FRET and acceptor channel. The FRET calibration was performed with single transfected cells expressing either GPR143-YFP or TYR-CFP. Correction parameters,  $C_{oA}$  (1) and  $C_{oB}$  (2) were calculated by the software using the following formulas:

$$(1) \quad C_{oA} = \frac{Da_{ACCEPTOR}}{Aa_{ACCEPTOR}}$$

$$(2) \quad C_{oB} = \frac{Dd_{DONOR}}{Dd_{DONOR}}$$

where  $Aa$  corresponds to the channel where the excitation and the emission of acceptor is measured,  $Dd$  corresponds to the channel of excitation and emission of the donor and  $Da$  corresponds to the channel of the excitation of the donor and emission of the acceptor.  $X_{DONOR/ACCEPTOR}$  coefficients are average intensities of the donor/acceptor-only images.

The corrected FRET signal (3) and the FRET efficiency (4) were calculated for each image using the following formulas:

$$(3) \quad FRET_{CORR} = Da_{FRET} - (Dd_{FRET}C_{oB}) - (Aa_{FRET}C_{oA})$$

$$(4) \quad FRET_{EFFICIENCY} = \frac{FRET_{CORR}}{Dd_{FRET}} 100$$

where  $X_{FRET}$  members are average intensities of assigned FRET image components.

For the acceptor photobleaching method, images were captured before and after the photobleaching of acceptor molecules in a specific region of the cell. If any interactions leading to energy transfer were present, photobleaching of the acceptor will lead to an increase of donor fluorescence, as it is no longer quenched by the acceptor. Acceptor photobleaching was performed with a high-intensity laser pulse at 514 nm. Images in the  $Aa$

and Dd channels were captured simultaneously before and after the photobleaching. FRET efficiency (5) was calculated using the following formula:

$$(5) \quad FRET_{EFFICIENCY} = \frac{I_A - I_B}{I_A} 100$$

where  $I_A$  is the CFP intensity emission after bleaching and  $I_B$  is the CFP intensity emission before bleaching.

### 6.10 Enzyme-linked immunosorbent assay (ELISA)

The cell surface expression of adenosine receptors in CHO cells was verified by enzyme-linked immunosorbent assay (ELISA). 200000 cells/well were seeded in 24-well plates 24 h before the assay. Cells were washed with PBS, blocked 5 min with 1% BSA/PBS and then incubated with a HA antibody solution, diluted 1:1000 in 1% BSA/PBS, for 1 h at room temperature. After washing with PBS, cells were fixed with a cold 1:1 (v/v) methanol/acetone solution for 15 min at -20 °C, washed and blocked again at the same conditions described above. The horseradish peroxidase-coupled secondary antibody was diluted 1:5000 in 1% BSA/PBS and incubated 1 h with the cells at room temperature. Finally, the cells were washed with PBS and incubated 50 min with 300  $\mu$ l of ABTS substrate (Thermo scientific Pierce, Rockford, USA). 170  $\mu$ l of the substrate was transferred in a 96-well plate and the absorbance was measured at 405 nm. Independent experiments were performed in triplicates.

### 6.11 MTT assay

Melan-a cells (5000 cells/well) were seeded in a 96-well plate and cultivated overnight in the incubator. The compounds dissolved in DMSO and ethanol were diluted in the medium (80% RPMI-20% DMEM medium), added to the cells and incubated 72 h at 37 °C with 10% CO<sub>2</sub>. The reagent is composed by a tetrazolium compound [3-(4,5-dimethylthiazol-2-yl)-5-(3-carboxymethoxyphenyl)-2-(4-sulfophenyl)-2H-tetrazolium] which needs to be mixed with an electron coupling reagent (phenazine methosulfate). The mixed reagents were applied on the cells (100  $\mu$ l) after the supernatant disposal and the cells were incubated for 1 h at the same conditions described above. The absorbance was then read at 490 nm. The cells treated with the vehicles were used as control and set as 100% cell viability. Independent experiments

were performed in quadruplicates.

### **6.12 Melanin assay**

Melan-a cells were seeded in 10 cm<sup>2</sup> dishes (60000 cells/dish) and cultivated overnight at 37 °C with 10% CO<sub>2</sub>. Different concentrations of compounds (pimozide, niclosamide and ethacridine lactate) were added in each dish and incubated for 5 days at the same conditions described above. At the third day the cell medium was disposed and exchanged with fresh medium containing the compounds. Cells were treated with vehicles (DMSO and ethanol) as negative control, while propylthiouracil (PTU, 300 µM final concentration) and 3-isobutyl-1-methylxanthine (IBMX, 150 µM final concentration) were used as agents to decrease and increase, respectively, the pigmentation of melan-a cells. Afterwards, cells were washed with PBS, scraped off the dishes with lysis buffer (1% Triton X-100, 50 mM Tris-HCl pH 7.5, 300 mM NaCl, 5 mM EDTA and protease inhibitor) and centrifuged 20 min 14000 g at 4 °C. The supernatant was transferred in a fresh tube and the protein concentration was determined using the Pierce BCA protein assay kit (Thermo Fisher Scientific, Grand Island, NY). The cell pellet was washed twice with a solution 1:1 ethanol/ether and let it dry under the fume hood. A water solution of 2 N NaOH was added to the dried pellets and warmed up to 80 °C in order to dissolve the melanin. A fixed volume of melanin solution (100-200 µl) was transferred to a 96-well plate and the absorbance was read at 490 nm. Independent experiments were performed in triplicates.

### **6.13 Tyrosinase activity in cell lysates**

Melan-a cell lysates were used to test the activation of tyrosinase [149]. The reaction mixture contained 1 mM cold tyrosine, 0.3 µCi/sample [<sup>3</sup>H]-tyrosine, 1 mM L-DOPA, 30 µg of protein lysate and the proper compound concentration. Lysates derived either from melan-a cells treated with compounds for the melanin assay, in this case no compound was added in the reaction mixture, or from the lysis of untreated melan-a cells. The reaction was incubated at 37 °C for 60 min then separated on a Dowen column. The radioactivity contained in the eluted tritium water released during the enzymatic hydroxylation of tyrosine to L-DOPA was quantified in a liquid scintillation analyser. Data were normalized to the tyrosinase



hydroxylase activity in absence of compounds, set as 100%. Independent experiments were performed in triplicates.

## 6.14 Functional assays

### 6.14.1 $\beta$ -arrestin recruitment assay

The  $\beta$  arrestin assay is a cell-based method developed by DiscoverX to detect GPCR activation after ligand stimulation. The assay is based on Enzyme Fragment Complementation (EFC) and it is carried out using a particular cell line where an enzyme, the  $\beta$ -galactosidase, is splitted into two inactive fragments: the Enzyme Acceptor (EA) part is linked to the  $\beta$  arrestin and the ProLink (PL) part is linked to the GPCR of interest. If a ligand binds and activates the receptor, the  $\beta$  arrestin is recruited near the GPCR since this protein is involved in the receptor recycling. The recruitment causes the complementation of the enzyme, which is at this point active and can hydrolyze a substrate creating chemoluminescence (Fig 52).

The  $\beta$  arrestin assay is performed with an engineered CHO cell line containing the  $\beta$  arrestin protein linked to the EA fragment. This cell line is transfected with the GPCR gene of interest linked to the ProLink tag.

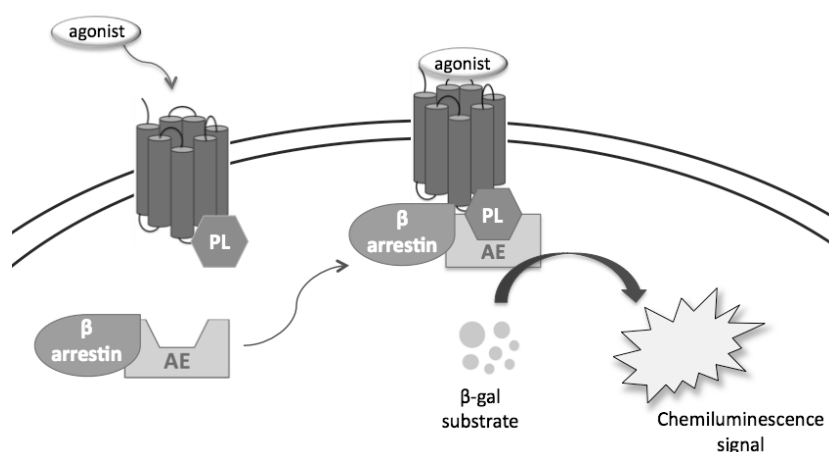


**Figure 52. General working principle of  $\beta$ -arrestin assay.**

The day before the assay, CHO  $\beta$  arrestin cells (20000 cells/well) were seeded in a 96-well plate in 90  $\mu$ l of F12 medium with 10% FCS, 100 U/ml penicillin G and 100  $\mu$ g/ml streptomycin and cultivated overnight. Then, 10  $\mu$ l of diluted compounds were added to the

cell plate and incubated at 37 °C for 90 min. F12 medium was used as negative control. The final DMSO concentration in each well was 1%. Afterwards, the PathHunter detection reagent (DiscoverX, Birmingham, UK) was added to the cell plate (50 µl/well), incubated 1 h at room temperature in the dark and finally chemoluminescence was detected. The high-throughput screening was performed adding 1 µl of 1 mM DMSO diluted compound in 99 µl of F12 medium in each well, in order to test the compounds at 10 µM and keep the 1% DMSO final concentration.

#### 6.14.2 Calcium mobilization assay

Among fluorescence-based assays, measurement of transient calcium mobilization from intracellular stores in response to the activation of  $G\alpha_q$  protein coupled GPCRs is considered a standard approach for the pharmacological characterization of receptors.

Cells expressing the GPCR of interest are pre-loaded with a fluorescent calcium indicator dye which crosses the cell membrane (Oregon Green or Fluo-4). Once inside the cell, the lipophilic blocking groups of the dye are cleaved by esterases resulting in a negatively charged fluorescent dye that stays inside the cell. If the receptor is activated by a stimulus, calcium is released from the endoplasmic reticulum and binds to the dye causing the enhancement of fluorescence (Fig 53).

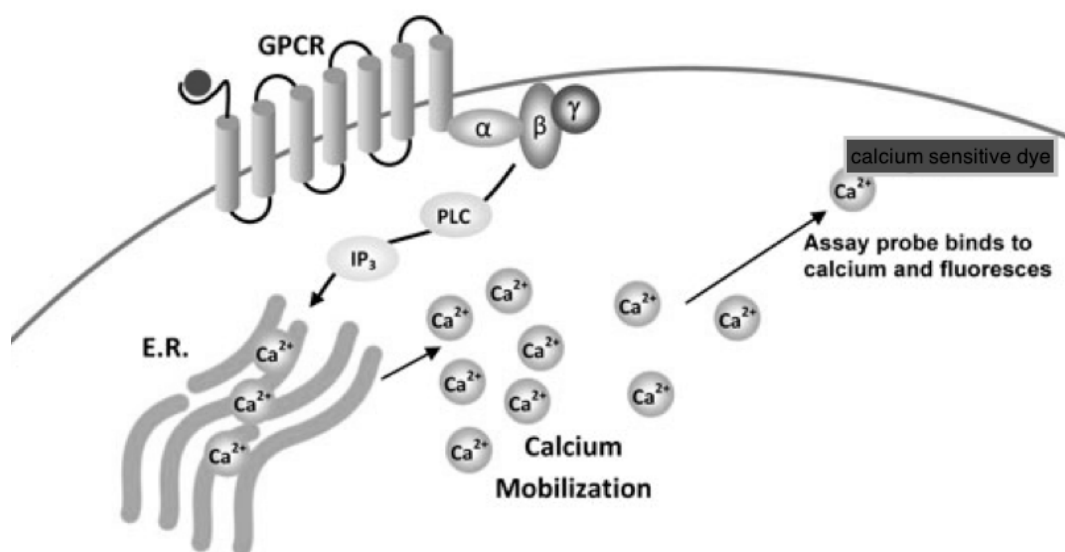


Figure 53. General working principle of the calcium mobilization assay (adapted from [150]).

CHO  $\beta$  arrestin cells expressing the wt or the mutant GPR143 receptor were seeded in one 175cm<sup>2</sup> flask and cultivated until they reach 80-90% of confluency. The cells were detached with trypsin, transferred to a falcon tube containing medium and placed into a 37 °C incubator for 45 min allowing them to recover. Afterward, cells were centrifuged and the pellet resuspended in Hank's Balanced Salt Solution (HBSS). The calcium sensitive dye was added (Fluo-4 AM, 3  $\mu$ M diluted in DMSO) together with Pluronic F-127 (60  $\mu$ M final concentration), a detergent permeabilizing the cell membrane to permit the dye-uptake from the cells. Cells were incubated 1 h at room temperature in the dark on a rotating wheel. The reagent plate was prepared with the compound dilutions, negative control (HBSS) and positive control (100  $\mu$ M ATP). Then, the cells were centrifuged at lowest velocity and the pellet was washed three times with buffer (HBSS). The cells were seeded in a 96-well plate with clear flat bottom and incubated under light exclusion for 30 minutes allowing the cells to settle down in the wells. The cell and reagent plates were placed into the microplate reader which measured the fluorescence intensity at a wavelength of 520 nm following excitation at 480 nm.

### **6.14.3 cAMP accumulation assay**

Receptor activation through G<sub>i</sub> or G<sub>s</sub> proteins is evaluated by analyzing the activity of cellular adenylate cyclase.

CHO cells (200000 cells/well) were seeded in 24-well plates 24 h before performing the assay. Cells are then washed and incubated 2 h at 37 °C and 5% CO<sub>2</sub> with HBSS. If adenosine receptors were analyzed the HBSS was supplemented with 1 U/ml of adenosine deaminase (ADA). Where adenosine was tested as an agonist, ADA was omitted. Cells were then incubated 15 min with the phosphodiesterase inhibitor Ro20-1724 (final concentration 40  $\mu$ M) at 37 °C and 5% CO<sub>2</sub>.

To detect the G<sub>i</sub> protein signaling pathway, different concentrations of compounds in 5% DMSO/HBSS buffer (final DMSO concentration: 1%) were added and, after a 5 min incubation at 37 °C, forskolin (10  $\mu$ M final concentration) was added in every well. The supernatant was removed after an incubation of 15 mins at 37 °C. On the other hand, to detect the G<sub>s</sub> protein signaling pathway, different dilutions of compounds in 5% DMSO/HBSS

buffer were added to the cells and incubated 15 min at the same conditions described above. The supernatant was then removed and 500  $\mu$ l of hot lysis buffer (90 °C) were added.

Cyclic AMP levels were quantified by incubation of an aliquot with cAMP binding protein and [ $^3$ H]cAMP. The assay is based on competition between unlabelled cAMP and a fixed amount of [ $^3$ H]cAMP for binding to a protein which has high affinity for cAMP. The amount of labelled protein-cAMP complex formed is inversely related to the amount of unlabelled cAMP present in the assay sample. Measurement of the protein-bound radioactivity enables the amount of unlabelled cAMP in the sample to be calculated.

After one hour of mixing on ice, the cAMP amount in the lysates was determined by competitive radioligand binding experiments [151]. 50  $\mu$ l of lysate was incubated with 30  $\mu$ l of [ $^3$ H]cAMP solution in lysis buffer (final radioligand concentration 3 nM) and 40  $\mu$ l of cAMP binding protein (50  $\mu$ g/vial) [151]. For the cAMP standard curve, 50  $\mu$ l of different cAMP concentrations were measured instead of the cell lysate. Total binding was obtained mixing radioligand solution and cAMP binding protein to lysis buffer, and the background was defined in the absence of binding protein. For experiments in reducing conditions, cells were preincubated for 2 h with a final concentration of 10 mM dithiothreitol (DTT). The mixture was incubated 60 min on ice and then filtered through GF/B glass fiber filters using a Brandel harvester. The filters were then washed with ice-cold Tris buffer (50 mM, pH 7.4), transferred into vials and incubated for 6 h with 2.5 ml of scintillation cocktail. The vials were then counted in liquid scintillation counter. Independent experiments were performed in duplicates. Amounts of cAMP were calculated by linear regression from a standard curve and normalized to the maximal effect induced by 100  $\mu$ M forskolin (set as 100%).

#### Analysis of data

- Average of the cpm for samples in the absence of unlabeled cAMP is calculated ( $C_0$  – Total binding).
- $C_0/C_x$  is also determined for each concentration of cAMP and unknowns in the assay.
- The cpm of known amounts of cAMP (40, 20, 10, 5 and 2.5 pmol) are measured in order to calculate a calibration curve.
- $C_0/C_x$  was plotted against pmoles of standard cAMP; a straight line should be obtained with an intercept of 1.

## Scheme of pipetting

Unknown sample		Background		Total binding	
Cell lysate	50 $\mu$ l	Lysis buffer	90 $\mu$ l	Lysis buffer	50 $\mu$ l
[ <sup>3</sup> H]cAMP	30 $\mu$ l	[ <sup>3</sup> H]cAMP	30 $\mu$ l	[ <sup>3</sup> H]cAMP	30 $\mu$ l
Binding protein	40 $\mu$ l	Total volume of 120 $\mu$ l in each vial		Binding protein	40 $\mu$ l
Total volume of 120 $\mu$ l in each vial				Total volume of 120 $\mu$ l in each vial	

### 6.15 Radioligand binding

Competition experiments were performed with [<sup>3</sup>H]CGS21680 (2-*p*-[2-carboxyethyl]phenethylamino)-5'-N-ethylcarboxamidoadenosine), [<sup>3</sup>H]MSX-2 (3-(3-hydroxypropyl)-7-methyl-8-(*m*-methoxystyryl)-1-propargylxanthine) and [<sup>3</sup>H]NECA (5'-N-ethylcarboxamidoadenosine) in a final volume of 400  $\mu$ l. The vial contained 10  $\mu$ l of dissolved compound in DMSO, 90  $\mu$ l of Tris buffer (50 mM, pH 7.4), 100  $\mu$ l of MgCl<sub>2</sub> solution (final concentration: 10 mM, only for CGS21680 and NECA), 100  $\mu$ l of radioligand solution (final radioligand concentration: 5 nM [<sup>3</sup>H]CGS21680, 1 nM [<sup>3</sup>H]MSX-2 and 3 nM [<sup>3</sup>H]NECA) and 100  $\mu$ l of membrane preparation (70-150  $\mu$ g/vial), which was previously incubated with 2 U/mg of adenosine deaminase for 20 min. Total binding was measured in absence of test compound, while nonspecific binding was determined in the presence of 50  $\mu$ M NECA in experiments with [<sup>3</sup>H]CGS21680 and [<sup>3</sup>H]MSX-2 and 100  $\mu$ M N<sup>6</sup>-((*R*)-(2-phenylisopropyl)adenosine (*R*-PIA) in experiments with [<sup>3</sup>H]NECA. After an incubation time (1 h for [<sup>3</sup>H]CGS21680, 3 h for [<sup>3</sup>H]NECA and 30 min for [<sup>3</sup>H]MSX-2 experiments), the assay mixture was filtered through GF/B glass fibre filters using a Brandel harvester (Brandel, Gaithersburg, USA). Filters used for binding with [<sup>3</sup>H]MSX-2 were pre-soaked in 0.3% Polyethylenimine solution for 30 min. When adenosine was tested, adenosine deaminase was omitted and membranes were washed with 50 mM Tris buffer (pH 7.4) four times more to remove as much endogenous adenosine as possible. After harvesting, the filters were washed with ice-cold Tris buffer (50 mM, pH 7.4), transferred into vials and incubated for 6 h with 2.5 ml of scintillation cocktail. The vials were then counted in liquid scintillation counter. Independent experiments were performed in duplicates.

## 6.16 Molecular Docking

The molecular docking studies and the following models of the A<sub>2A</sub> cysteine mutant receptors have been performed by Dr. Vigneshwaran Namasivayam (University of Bonn).

The recent X-ray structure of the human A<sub>2A</sub>AR bound to the agonist CGS21680 (4UHR.pdb) was obtained from the RCSB Protein Data Bank [152]. The agonist structure PSB-15826 was docked into the binding pocket of the A<sub>2A</sub>AR using AutoDock 4.2 [153]. As an initial step, the crystallographic waters and co-crystallized ligand were removed from the X-ray structure. The hydrogen atoms were added and protonated using Protonate in Molecular Operating Environment (MOE 2014.08) [154]. The AutoDockTools package was applied to calculate the partial charges, generate the docking input files and analyze the docking results [153]. Three-dimensional energy scoring grids of size 60 × 60 × 60 points with a spacing of 0.375 Å were computed. To define the binding pocket for the docking procedure, the grids were centered based on the co-crystallized ligand. In the final step, PSB-15826 was docked into the binding site using the search algorithm Lamarckian Genetic Algorithm and the default scoring function, which is a hybrid scoring function (semi-empirical and free-energy) implemented in AutoDock4.2. The putative binding mode of PSB-15826 was selected on the basis of the lowest binding energy and visual inspection of the interactions. For obtaining the comparison with the binding conformation of NECA, adenosine, the X-ray crystal structures (PDB ID 2YDO and 2YDV) were downloaded from RCSB and superimposed on the structure obtained with CGS21680 [52]. For the mutant receptors, we generated a receptor model by substituting the residues using the protein builder and minimization modules of MOE 2014.08.

## 7. References

- [1] International Human Genome Sequencing Consortium. Initial sequencing and analysis of the human genome. *Nature* 2001;409:860–921.
- [2] Fredriksson R, Lagerstrom MC, Lundin L, Schioth HB. The G-protein coupled receptors in the human genome form five main families. Phylogenetic analysis, paralogon groups, and fingerprints. *Mol Pharmacol* 2003;63:1256–72.
- [3] Venkatakrisnan AJ, Deupi X, Lebon G, Tate CG, Schertler GF, Babu MM. Molecular signatures of G-protein-coupled receptors. *Nature* 2013;494:185–94.
- [4] Kolakowski LFJ. GCRDb: a G-protein-coupled receptor database. *Recept Channels* 1994;2:1–7.
- [5] Stevens RC, Cherezov V, Katritch V, Abagyan R, Kuhn P, Rosen H, et al. The GPCR Network: a large-scale collaboration to determine human GPCR structure and function. *Nat Rev Drug Discov* 2013;12:25–34.
- [6] Rosenbaum DM, Rasmussen SGF, Kobilka BK. The structure and function of G-protein-coupled receptors. *Nature* 2009;459:356–63.
- [7] Marinissen MJ, Gutkind JS. G-protein-coupled receptors and signaling networks: emerging paradigms. *Trends Pharmacol Sci* 2001;22:368–76.
- [8] Rajagopal S, Rajagopal K, Lefkowitz RJ. Teaching old receptors new tricks: biasing seven-transmembrane receptors. *Nat Rev Drug Discov* 2010;9:373–86.
- [9] DeWire SM, Ahn S, Lefkowitz RJ, Shenoy SK.  $\beta$ -arrestins and cell signaling. *Annu Rev Physiol* 2007;69:483–510.
- [10] Palczewski K, Kumasaka T, Hori T, Behnke C, Motoshima H, Fox B, et al. Crystal structure of rhodopsin: a G protein-coupled receptor. *Science* 2000;289:739–45.
- [11] Katritch V, Cherezov V SR, Katritch V, Cherezov V, Stevens RC. Structure-function of the G protein-coupled receptor superfamily. *Annu Rev Pharmacol Toxicol* 2013;53:531–56.
- [12] Yang J, Zhang Y. GPCR-EXP: a database of experimentally solved GPCR structure 2015. <http://zhanglab.ccmb.med.umich.edu/GPCR-EXP/>.
- [13] Berman HM, Westbrook J, Feng Z, Gilliland G, Bhat TN, Weissig H, et al. The Protein Data Bank. *Nucleic Acids Res* 2000;28:235–42.
- [14] Hollenstein K, Kean J, Bortolato A, Cheng RKY, Doré AS, Jazayeri A, et al. Structure of class B GPCR corticotropin-releasing factor receptor 1. *Nature* 2013;499:438–43.
- [15] Siu FY, He M, de Graaf C, Han GW, Yang D, Zhang Z, et al. Structure of the human glucagon class B G-protein-coupled receptor. *Nature* 2013;499:444–9.
- [16] Wu H, Wang C, Gregory KJ, Han GW, Cho HP, Xia Y, et al. Structure of a class C GPCR metabotropic glutamate receptor 1 bound to an allosteric modulator. *Science* 2014;344:58–64.
- [17] Doré AS, Okrasa K, Patel JC, Serrano-Vega M, Bennett K, Cooke RM, et al. Structure of class C GPCR metabotropic glutamate receptor 5 transmembrane domain. *Nature* 2014;511:557–62.

- [18] White JF, Noinaj N, Shibata Y, Love J, Kloss B, Xu F, et al. Structure of the agonist-bound neurotensin receptor. *Nature* 2012;490:508–13.
- [19] Egloff P, Hillenbrand M, Klenk C, Batyuk A, Heine P, Balada S, et al. Structure of signaling-competent neurotensin receptor 1 obtained by directed evolution in *Escherichia coli*. *Proc Natl Acad Sci USA* 2014;111:E655–62.
- [20] Wang C, Wu H, Evron T, Vardy E, Han GW, Huang X-P, et al. Structural basis for Smoothed receptor modulation and chemoresistance to anticancer drugs. *Nat Commun* 2014;5:4355.
- [21] Weierstall U, James D, Wang C, White TA, Wang D, Liu W, et al. Lipidic cubic phase injector facilitates membrane protein serial femtosecond crystallography. *Nat Commun* 2014;5:3309.
- [22] Bortolato A, Doré AS, Hollenstein K, Tehan BG, Mason JS, Marshall FH. Structure of Class B GPCRs: new horizons for drug discovery. *Br J Pharmacol* 2014;171:3132–45.
- [23] Ballesteros JA, Weinstein H. Integrated methods for the construction of three-dimensional models and computational probing of structure-function relations in G protein-coupled receptors. *Methods Neurosci* 1995;25:366–428.
- [24] Abbracchio MP, Burnstock G, Verkhratsky A, Zimmermann H. Purinergic signalling in the nervous system: an overview. *Trends Neurosci* 2009;32:19–29.
- [25] Velasquez S, Eugenin EA. Role of Pannexin-1 hemichannels and purinergic receptors in the pathogenesis of human diseases. *Front Physiol* 2014;5:1–12.
- [26] Fredholm B, Abbracchio M, Burnstock G, Daly J, Harden T, Jacobson K, et al. Nomenclature and classification of purinoceptors. *Pharmacol Rev* 1994;46:143–56.
- [27] Brunschweiler A, Müller CE. P2 receptors activated by uracil nucleotides - an update. *Curr Med Chem* 2006;13:289–312.
- [28] Fredholm BB, IJzerman AP, Jacobson KA, Linden J, Müller CE. International union of basic and clinical pharmacology. LXXXI. Nomenclature and classification of Adenosine Receptors - An update. *Pharmacol Rev* 2011;63:1–34.
- [29] Linden J, Thai T, Figler H, Jin X, Robeva AS. Characterization of human A(2B) adenosine receptors: radioligand binding, western blotting, and coupling to G(q) in human embryonic kidney 293 cells and HMC-1 mast cells. *Mol Pharmacol* 1999;56:705–13.
- [30] Müller CE, Jacobson KA. Recent developments in adenosine receptor ligands and their potential as novel drugs. *Biochim Biophys Acta* 2011;1808:1290–308.
- [31] Milne GR, Palmer TM. Anti-inflammatory and immunosuppressive effects of the A2A adenosine receptor. *ScientificWorldJournal* 2011;11:320–39.
- [32] Leone RD, Lo Y-C, Powell JD. A2AR antagonists: next generation checkpoint blockade for cancer immunotherapy. *Comput Struct Biotechnol J* 2015;13:265–72.
- [33] Popoli P, Pepponi R. Potential therapeutic relevance of adenosine A2B and A2A receptors in the central nervous system. *CNS Neurol Disord Drug Targets* 2012;11:664–74.
- [34] Wilson CN, Nadeem A, Spina D, Brown R, Page CP, Mustafa SJ. Adenosine receptors and asthma. *Handb Exp Pharmacol* 2009;193:329–62.



- [35] Hajiahmadi S, Panjehpour M, Aghaei M, Shabani M. Activation of A2b adenosine receptor regulates ovarian cancer cell growth: involvement of Bax/Bcl-2 and caspase-3. *Biochem Cell Biol* 2015;1–9.
- [36] Melani A, Pugliese AM, Pedata F. Adenosine receptors in cerebral ischemia. *Int Rev Neurobiol* 2014;119:309–48.
- [37] Antonioli L, Blandizzi C, Csóka B, Pacher P, Haskó G. Adenosine signalling in diabetes mellitus-pathophysiology and therapeutic considerations. *Nat Rev Endocrinol* 2015;11:228–41.
- [38] Fredholm BB, Ijzerman AP, Jacobson KA, Klotz K, Linden J. International Union of Pharmacology. XXV. Nomenclature and Classification of Adenosine Receptors. *Pharmacol Rev* 2001;53:527–52.
- [39] Seibt BF, Schiedel AC, Thimm D, Hinz S, Sherbiny FF, Müller CE. The second extracellular loop of GPCRs determines subtype-selectivity and controls efficacy as evidenced by loop exchange study at A2 adenosine receptors. *Biochem Pharmacol* 2013;85:1317–29.
- [40] Thimm D, Schiedel AC, Sherbiny FF, Hinz S, Hochheiser K, Bertarelli DCG, et al. Ligand-specific binding and activation of the human adenosine A2B receptor. *Biochemistry* 2013;52:726–40.
- [41] Beukers MW, van Oppenraaij J, van der Hoorn PPW, Blad CC, den Dulk H, Brouwer J, et al. Random mutagenesis of the human adenosine A2B receptor followed by growth selection in yeast. Identification of constitutively active and gain of function mutations. *Mol Pharmacol* 2004;65:702–10.
- [42] Beukers MW, den Dulk H, van Tilburg EW, Brouwer J, Ijzerman AP. Why are A(2B) receptors low-affinity adenosine receptors? Mutation of Asn273 to Tyr increases affinity of human A(2B) receptor for 2-(1-Hexynyl)adenosine. *Mol Pharmacol* 2000;58:1349–56.
- [43] Matharu AL, Mundell SJ, Benovic JL, Kelly E. Rapid agonist-induced desensitization and internalization of the A(2B) adenosine receptor is mediated by a serine residue close to the COOH terminus. *J Biol Chem* 2001;276:30199–207.
- [44] Peeters MC, Li Q, van Westen GJP, Ijzerman AP. Three “hotspots” important for adenosine A(2B) receptor activation: a mutational analysis of transmembrane domains 4 and 5 and the second extracellular loop. *Purinergic Signal* 2012;8:23–38.
- [45] Peeters MC, van Westen GJP, Guo D, Wisse LE, Müller CE, Beukers MW, et al. GPCR structure and activation: an essential role for the first extracellular loop in activating the adenosine A2B receptor. *FASEB J* 2011;25:632–43.
- [46] Peeters MC, Li Q, Elands R, van Westen GJP, Lenselink EB, Müller CE, et al. Domains for activation and inactivation in G protein-coupled receptors - a mutational analysis of constitutive activity of the adenosine A2B receptor. *Biochem Pharmacol* 2014;92:348–57.
- [47] Liu R, Groenewoud NJA, Peeters MC, Lenselink EB, IJzerman AP. A yeast screening method to decipher the interaction between the adenosine A2B receptor and the C-terminus of different G protein  $\alpha$ -subunits. *Purinergic Signal* 2014;10:441–53.

- [48] Liu R, Nahon D, le Roy B, Lenselink EB, Ijzerman AP. Scanning mutagenesis in a yeast system delineates the role of the NPxxY(x)<sub>5</sub>,6F motif and helix 8 of the adenosine A<sub>2</sub>B receptor in G protein coupling. *Biochem Pharmacol* 2015;95:290–300.
- [49] Jaakola V, Griffith MT, Hanson MA, Cherezov V, Ellen YT, Lane JR, et al. The 2.6 angstrom crystal structure of a human A<sub>2</sub>A adenosine receptor bound to an antagonist. *Science* 2008;322:1211–7.
- [50] Liu W, Chun E, Thompson AA, Chubukov P, Xu F, Katritch V, et al. Structural basis for allosteric regulation of GPCRs by sodium ions. *Science* 2012;337:232–6.
- [51] Doré AS, Robertson N, Errey JC, Ng I, Hollenstein K, Tehan B, et al. Structure of the adenosine A<sub>2</sub>A receptor in complex with ZM241385 and the xanthines XAC and caffeine. *Structure* 2011;19:1283–93.
- [52] Lebon G, Warne T, Edwards PC, Bennett K, Christopher J, Leslie AGW, et al. Agonist-bound adenosine A<sub>2</sub>A receptor structures reveal common features of GPCR activation. *Nature* 2011;474:521–5.
- [53] Xu F, Wu H, Katritch V, Han GW, Jacobson KA, Gao Z-G, et al. Structure of an agonist-bound human A<sub>2</sub>A adenosine receptor. *Science* 2011;332:322–7.
- [54] Lebon G, Edwards PC, Leslie AGW, Tate CG. Molecular determinants of CGS21680 binding to the human adenosine A<sub>2</sub>A receptor. *Mol Pharmacol* 2015;87:907–15.
- [55] Schiedel AC, Hinz S, Thimm D, Sherbiny F, Borrmann T, Maass A, et al. The four cysteine residues in the second extracellular loop of the human adenosine A<sub>2</sub>B receptor: role in ligand binding and receptor function. *Biochem Pharmacol* 2011;82:389–99.
- [56] Sherbiny FF, Schiedel AC, Maass A, Müller CE. Homology modelling of the human adenosine A<sub>2</sub>B receptor based on X-ray structures of bovine rhodopsin, the beta<sub>2</sub>-adrenergic receptor and the human adenosine A<sub>2</sub>A receptor. *J Comput Aided Mol Des* 2009;23:807–28.
- [57] Peeters MC, van Westen GJP, Li Q, Ijzerman AP. Importance of the extracellular loops in G protein-coupled receptors for ligand recognition and receptor activation. *Trends Pharmacol Sci* 2011;32:35–42.
- [58] Congreve M, Andrews SP, Dore AS, Hollenstein K, Hurrell E, Langmead CJ, et al. Discovery of 1,2,4-Triazine Derivatives as Adenosine A<sub>2</sub>A antagonists using structure based drug design. *J Med Chem* 2012;55:1898–903.
- [59] Kim J, Jiang Q, Glashofer M, Yehle S, Wess J, Jacobson KA. Glutamate residues in the second extracellular loop of the human A<sub>2</sub>a adenosine receptor are required for ligand recognition. *Mol Pharmacol* 1996;49:683–91.
- [60] Jaakola V-P, Lane JR, Lin JY, Katritch V, Ijzerman AP, Stevens RC. Ligand binding and subtype selectivity of the human A<sub>2</sub>(A) adenosine receptor: identification and characterization of essential amino acid residues. *J Biol Chem* 2010;285:13032–44.
- [61] De Zwart M, Vollinga RC, Beukers MW, Slegers DF, von Frijtag Drabbe Künzel JK, de Groote M, et al. Potent antagonists for the human adenosine A<sub>2</sub>B receptor. Derivatives of the triazolotriazine adenosine receptor antagonist ZM241385 with high affinity. *Drug Dev Res* 1999;48:95–103.

- [62] TOPO2. Transmembrane protein display software. Johns, SJ <http://www.sacs.ucsf.edu/TOPO2/>.
- [63] Zhang K, Zhang J, Gao Z-G, Zhang D, Zhu L, Han GW, et al. Structure of the human P2Y<sub>12</sub> receptor in complex with an antithrombotic drug. *Nature* 2014;509:115–8.
- [64] Avlani VA, Gregory KJ, Morton CJ, Parker MW, Sexton PM, Christopoulos A. Critical role for the second extracellular loop in the binding of both orthosteric and allosteric G protein-coupled receptor ligands. *J Biol Chem* 2007;282:25677–86.
- [65] Unal H, Jagannathan R, Bhat MB, Karnik SS. Ligand-specific conformation of extracellular loop-2 in the angiotensin II type 1 receptor. *J Biol Chem* 2010;285:16341–50.
- [66] Klco JM, Wiegand CB, Narzinski K, Baranski TJ. Essential role for the second extracellular loop in C5a receptor activation. *Nat Struct Mol Biol* 2005;12:320–6.
- [67] De Graaf C, Foata N, Engkvist O, Rognan D. Molecular modeling of the second extracellular loop of G-protein coupled receptors and its implication on structure-based virtual screening. *Proteins* 2008;71:599–620.
- [68] Rader AJ, Anderson G, Isin B, Khorana HG, Bahar I, Klein-Seetharaman J. Identification of core amino acids stabilizing rhodopsin. *Proc Natl Acad Sci U S A* 2004;101:7246–51.
- [69] Goddard WA, Kim S-K, Li Y, Trzaskowski B, Griffith AR, Abrol R. Predicted 3D structures for adenosine receptors bound to ligands: comparison to the crystal structure. *J Struct Biol* 2010;170:10–20.
- [70] Naranjo AN, Chevalier A, Cousins GD, Ayettey E, McCusker EC, Wenk C, et al. Conserved disulfide bond is not essential for the adenosine A<sub>2A</sub> receptor: Extracellular cysteines influence receptor distribution within the cell and ligand-binding recognition. *Biochim Biophys Acta* 2015;1848:603–14.
- [71] Ni F, So S-P, Cervantes V, Ruan K-H. A profile of the residues in the second extracellular loop that are critical for ligand recognition of human prostacyclin receptor. *FEBS J* 2008;275:128–37.
- [72] Ott TR, Troskie BE, Roeske RW, Illing N, Flanagan CA, Millar RP. Two mutations in extracellular loop 2 of the human GnRH receptor convert an antagonist to an agonist. *Mol Endocrinol* 2002;16:1079–88.
- [73] Ahn KH, Bertalovitz AC, Mierke DF, Kendall DA. Dual role of the second extracellular loop of the cannabinoid receptor 1: ligand binding and receptor localization. *Mol Pharmacol* 2009;76:833–42.
- [74] Olah ME, Jacobson KA, Stiles GL. Role of the second extracellular loop of adenosine receptors in agonist and antagonist binding. Analysis of chimeric A<sub>1</sub>/A<sub>3</sub> adenosine receptors. *J Biol Chem* 1994;269:24692–8.
- [75] Gibson DG, Young L, Chuang R-Y, Venter JC, Hutchison CA, Smith HO. Enzymatic assembly of DNA molecules up to several hundred kilobases. *Nat Methods* 2009;6:343–5.
- [76] Yan L, Burbiel JC, Maass A, Müller CE. Adenosine receptor agonists: from basic medicinal chemistry to clinical development. *Expert Opin Emerg Drugs* 2003;8:537–76.

- [77] Katritch V, Kufareva I, Abagyan R. Structure based prediction of subtype-selectivity for adenosine receptor antagonists. *Neuropharmacology* 2011;60:108–15.
- [78] Luthin DR, Linden J. Comparison of A4 and A2A binding sites in striatum and COS cells transfected with adenosine A2A receptors. *J Pharmacol Exp Ther* 1995;272:511–8.
- [79] Murphree LJ, Marshall MA, Rieger JM, Macdonald TL, Linden J, M DPLJ, et al. Human A2A adenosine receptors: high-affinity agonist binding to receptor-G protein complexes containing Gbeta4. *Mol Pharmacol* 2002;61:455–62.
- [80] Varani K, Gessi S, Merighi S, Iannotta V, Cattabriga E, Spisani S, et al. Effect of low frequency electromagnetic fields on A2A adenosine receptors in human neutrophils. *Br J Pharmacol* 2002;136:57–66.
- [81] Sabbadin D, Moro S. Supervised Molecular Dynamics (SuMD) as a helpful tool to depict GPCR-ligand recognition pathway in a nanosecond time scale. *J Chem Inf Model* 2014;54:372–6.
- [82] Takezako T, Unal H, Karnik SS, Node K. Structure-function basis of attenuated inverse agonism of ARBs for active-state AT1 receptor. *Mol Pharmacol* 2015;88:488–501.
- [83] Scarselli M, Li B, Kim S-K, Wess J. Multiple residues in the second extracellular loop are critical for M3 muscarinic acetylcholine receptor activation. *J Biol Chem* 2007;282:7385–96.
- [84] Hillmann P, Ko G, Spinrath A, Raulf A, Ku I Von, Wolff SC, et al. Key determinants of nucleotide-activated G protein-coupled P2Y2 receptor function revealed by chemical and pharmacological experiments, mutagenesis and homology modeling. *J Med Chem* 2009;52:2762–75.
- [85] O'Malley MA, Naranjo AN, Lazarovab T, Robinson AS. Analysis of adenosine A2A receptor stability: effects of ligands and disulfide bonds. *Biochemistry* 2010;49:9181–9.
- [86] Mazzoni MR, Giusti L, Rossi E, Taddei S, Lucacchini A. Role of cysteine residues of rat A2A adenosine receptors in agonist binding. *Biochim Biophys Acta* 1997;1324:159–70.
- [87] Scholl DJ, Wells JN. Serine and alanine mutagenesis of the nine native cysteine residues of the human A1 adenosine receptor. *Biochem Pharmacol* 2000;60:1647–54.
- [88] Zhang J, Zhang K, Gao Z, Paoletta S, Zhang D, Won G, et al. Agonist-bound structure of the human P2Y12 receptor. *Nature* 2014;509:119–22.
- [89] Jeffery G. The albino retina: an abnormality that provides insight into normal retinal development. *Trends Neurosci* 1997;20:165–9.
- [90] The National Organization for Albinism and Hypopigmentation. NOAH <http://www.albinism.org/site/c.flKYIdOUlhJ4H/b.9194783/k.C775/Welcome.htm>.
- [91] Cortese K, Giordano F, Surace EM, Venturi C, Ballabio A, Tacchetti C, et al. The ocular albinism type 1 (OA1) gene controls melanosome maturation and size. *Invest Ophthalmol Vis Sci* 2005;46:4358–64.
- [92] Garner A, Jay BS. Macromelanosomes in X-linked ocular albinism. *Histopathology* 1980;4:243–54.

- [93] Palmisano I, Bagnato P, Palmigiano A, Innamorati G, Rotondo G, Altimare D, et al. The ocular albinism type 1 protein, an intracellular G protein-coupled receptor, regulates melanosome transport in pigment cells. *Hum Mol Genet* 2008;17:3487–501.
- [94] Incerti B, Cortese K, Pizzigoni A, Surace EM, Varani S, Coppola M, et al. Oa1 knock-out: new insights on the pathogenesis of ocular albinism type 1. *Hum Mol Genet* 2000;9:2781–8.
- [95] Young A, Jiang M, Wang Y, Ahmedli NB, Ramirez J, Benjamin E, et al. Specific interaction of Gai3 with the Oa1 G-protein coupled receptor controls the size and density of melanosomes in retinal pigment epithelium. *PLoS One* 2011;6.
- [96] Bassi MT, Incerti B, Easty DJ, Sviderskaya F V, Ballabi A. Cloning of the murine homolog of the Ocular Albinism type 1 (OA1) gene: sequence, genomic structure and expression analysis in pigment cells. *Genome Res* 1995;1:880–5.
- [97] Schiaffino MV, Addio M, Alloni A, Baschiroto C, Valetti C, Cortese K, et al. Ocular albinism: evidence for a defect in an intracellular signal transduction system. *Nat Genet* 1999;23:108–12.
- [98] Winder AJ, Wittbjør A, Rosengren E, Rorsman H. The mouse brown (b) locus protein has dopachrome tautomerase activity and is located in lysosomes in transfected fibroblasts. *J Cell Sci* 1993;166:153–66.
- [99] Piccirillo R, Palmisano I, Innamorati G, Bagnato P, Altimare D, Schiaffino MV. An unconventional dileucine-based motif and a novel cytosolic motif are required for the lysosomal and melanosomal targeting of OA1. *J Cell Sci* 2006;119:2003–14.
- [100] Schiaffino MV, Baschiroto C, Pellegrini G, Montalti S, Tacchetti C, De Luca M, et al. The ocular albinism type 1 gene product is a membrane glycoprotein localized to melanosomes. *Proc Natl Acad Sci U S A* 1996;93:9055–60.
- [101] Shen B, Rosenberg B, Orlow SJ. Intracellular distribution and late endosomal effects of the Ocular Albinism type 1 gene product: consequences of disease-causing mutations and implications for melanosome biogenesis. *Traffic* 2001;2:202–11.
- [102] Krogh A, Larsson B, Heijne G von, Sonnhammer ELL. Predicting transmembrane protein topology with a hidden Markov model: Application to complete genomes. *J Mol Biol* 2001;305:567–80.
- [103] Giordano F, Bonetti C, Surace EM, Marigo V, Raposo G. The ocular albinism type 1 (OA1) G-protein-coupled receptor functions with MART-1 at early stages of melanogenesis to control melanosome identity and composition. *Hum Mol Genet* 2009;18:4530–45.
- [104] Samaraweera P, Shen B, Newton JM, Barsh GS, Orlow SJ. The mouse ocular albinism 1 gene product is an endolysosomal protein. *Exp Eye Res* 2001;72:319–29.
- [105] Addio M, Pizzigoni A, Bassi MT, Baschiroto C, Valetti C, Incerti B, et al. Defective intracellular transport and processing of OA1 is a major cause of ocular albinism type 1. *Hum Mol Genet* 2000;9:3011–8.
- [106] Schiaffino MV, Dellambra E, Cortese K, Baschiroto C, Bondanza S, Clementi M, et al. Effective retrovirus-mediated gene transfer in normal and mutant human melanocytes. *Hum Gene Ther* 2002;13:947–57.

- [107] Raposo G, Tenza D, Murphy DM, Berson JF, Marks MS. Distinct protein sorting and localization to premelanosomes, melanosomes, and lysosomes in pigmented melanocytic cells. *J Cell Biol* 2001;152:809–23.
- [108] Kushimoto T, Basrur V, Valencia J, Matsunaga J, Vieira WD, Ferrans VJ, et al. A model for melanosome biogenesis based on the purification and analysis of early melanosomes 2001:1–6.
- [109] Schiaffino MV, Tacchetti C. The ocular albinism type 1 (OA1) protein and the evidence for an intracellular signal transduction system involved in melanosome biogenesis. *Pigment Cell Res* 2005;18:227–33.
- [110] Giordano F, Simoes S, Raposo G. The ocular albinism type 1 (OA1) GPCR is ubiquitinated and its traffic requires endosomal sorting complex responsible for transport (ESCRT) function. *PNAS* 2011;108:11906–11.
- [111] Innamorati G, Piccirillo R, Bagnato P, Palmisano I, Schiaffino MV. The melanosomal/lysosomal protein OA1 has properties of a G protein-coupled receptor. *Pigment Cell Res* 2006;19:125–35.
- [112] Sone M, Orlow SJ. The ocular albinism type 1 gene product, OA1, spans intracellular membranes 7 times. *Exp Eye Res* 2007;85:806–16.
- [113] Lopez VM, Decatur CL, Stamer WD, Lynch RM, McKay BS. L-DOPA is an endogenous ligand for OA1. *PLoS Biol* 2008;6:e236.
- [114] Fukuda N, Naito S, Masukawa D, Kaneda M, Miyamoto H, Abe T, et al. Expression of ocular albinism 1 (OA1), 3, 4- dihydroxy- L-phenylalanine (DOPA) receptor, in both neuronal and non-neuronal organs. *Brain Res* 2015;1602:62–74.
- [115] Hiroshima Y, Miyamoto H, Nakamura F, Masukawa D, Yamamoto T, Muraoka H, et al. The protein Ocular albinism 1 is the orphan GPCR GPR143 and mediates depressor and bradycardic responses to DOPA in the nucleus tractus solitarii. *Br J Pharmacol* 2014;171:403–14.
- [116] Roffler-Tarlov S, Liu JH, Naumova EN, Bernal-Ayala MM, Mason CA. L-Dopa and the albino riddle: content of L-Dopa in the developing retina of pigmented and albino mice. *PLoS One* 2013;8:e57184.
- [117] Ilia M, Jeffery G. Retinal cell addition and rod production depend on early stages of ocular melanin synthesis. *J Comp Neurol* 2000;420:437–44.
- [118] Simmen T, Schmidt A, Hunziker W, Beermann F. The tyrosinase tail mediates sorting to the lysosomal compartment in MDCK cells via a di-leucine and a tyrosine-based signal. *J Cell Sci* 1999;53:45–53.
- [119] Jones K, Padmapriya A, Blume G. Aqueous composition comprising active ingredients for the de-pigmentation of the skin. Patent., 1999.
- [120] Vijayasaradhi S, Xu Y, Bouchard B, Houghton AN. Intracellular sorting and targeting of melanosomal membrane proteins: identification of signals for sorting of the human brown locus protein, GP75. *J Cell Biol* 1995;130:807–20.
- [121] Slominski A, Tobin DJ, Shibahara S, Wortsman J. Melanin pigmentation in mammalian skin and its hormonal regulation. 2004:1155–228.

- [122] Winder AJ, Wittbjør A, Rosengren E, Rorsman H. Fibroblasts expressing mouse c locus tyrosinase produce an authentic enzyme and synthesise pheomelanin. *J Cell Sci* 1993;104:467–75.
- [123] Wittbjør A, Dahlbäck B, Odh G, Rosengren A, Rosengren E, Rorsman H. Isolation of human tyrosinase from cultured melanoma cells. *Acta Derm Venereol* 1989;69:125–31.
- [124] Shen B, Samaraweera P, Rosenberg B, Orlow SJ. Ocular Albinism type 1: more than meets the eye. *Pigment Cell Res* 2001;14:243–8.
- [125] Falletta P, Bagnato P, Bono M, Monticone M, Schiaffino MV, Bennett DC, et al. Melanosome-autonomous regulation of size and number: the OA1 receptor sustains PMEL expression. *Pigment Cell Melanoma Res* 2014;27:565–79.
- [126] Vetrini F, Auricchio A, Du J, Angeletti B, Fisher DE, Ballabio A, et al. The Microphthalmia Transcription Factor (Mitf) controls expression of the Ocular Albinism type 1 gene: link between melanin synthesis and melanosome biogenesis. *Mol Cell Bio* 2004;24:6550–9.
- [127] Burgoyne T, Jolly R, Martin-Martin B, Seabra MC, Piccirillo R, Schiaffino M V., et al. Expression of OA1 limits the fusion of a subset of MVBs with lysosomes - a mechanism potentially involved in the initial biogenesis of melanosomes. *J Cell Sci* 2014;127:700–700.
- [128] Brady AE, Limbird LE. G protein-coupled receptor interacting proteins: emerging roles in localization and signal transduction. *Cell Signal* 2002;14:297–309.
- [129] King RA, Hearing VG, Creel DJ, Oetting WS. Albinism. *Metabolic and Molecular Bases of Inherited Disease*. Ed 8. Scriver, C.R., Beaudet, A.L., Sly, W.S., Valle, D., McGraw-Hill, New York: 1995, p. 4353–92.
- [130] Guha S, Baltazar GC, Tu L-A, Liu J, Lim JC, Lu W, et al. Stimulation of the D5 dopamine receptor acidifies the lysosomal pH of retinal pigmented epithelial cells and decreases accumulation of autofluorescent photoreceptor debris. *J Neurochem* 2012;122:823–33.
- [131] So CH, Verma V, Alijaniaram M, Cheng R, Rashid AJ, Dowd BFO, et al. Calcium signaling by dopamine D5 receptor and D5-D2 receptor hetero-oligomers occurs by a mechanism distinct from that for dopamine D1-D2 receptor hetero-oligomers. *Mol Pharmacol* 2009;75:843–54.
- [132] Seeman P. Atypical antipsychotics: mechanism of action. *Can J Psychiatry* 2002;47:27–38.
- [133] Pan J-X, Ding K, Wang C-Y. Niclosamide, an old antihelminthic agent, demonstrates antitumor activity by blocking multiple signaling pathways of cancer stem cells. *Chin J Cancer* 2012;31:178–84.
- [134] Brunton L, Chabner B, Knollman B. Goodman and Gilman's *The Pharmacological Basis of Therapeutics* (12th ed.). New York: McGraw-Hill Professional. 2010.
- [135] Nguyen-Legros J, Versaux-Botteri C, Vernier P. Dopamine receptor localization in the mammalian retina. *Mol Neurobiol* 1999;19:181–204.
- [136] Burchill S, Thody A. Dopaminergic inhibition of tyrosinase activity in hair follicular melanocytes of the mouse. *J Endocrinol* 1986;111:233–7.

- [137] Gu Y, Di W, Kelsell D, Zicha D. Quantitative fluorescence resonance energy transfer (FRET) measurement with acceptor photobleaching and spectral unmixing. *J Microsc* 2004;215:162–73.
- [138] Wilson MC, Meredith D, Halestrap AP. Fluorescence resonance energy transfer studies on the interaction between the lactate transporter MCT1 and CD147 provide information on the topology and stoichiometry of the complex in situ. *J Biol Chem* 2002;277:3666–72.
- [139] Karpova T, Baumann C, He L, Wu X, Grammer A, Lipsky P, et al. Fluorescence resonance energy transfer from cyan to yellow fluorescent protein detected by acceptor photobleaching using confocal microscopy and a single laser. *J Microsc* 2003;209:56–70.
- [140] Lopes VS, Wasmeier C, Seabra MC, Futter CE. Melanosome maturation defect in Rab38-deficient retinal pigment epithelium results in instability of immature melanosomes during transient melanogenesis. *Mol Biol Cell* 2007;18:3914–27.
- [141] Young A, Wang Y, Ahmedli NB, Jiang M, Farber DB. A constitutively active Gai3 protein corrects the abnormal retinal pigment epithelium phenotype of Oa1 <sup>-/-</sup> mice. *PLoS One* 2013;8:4–13.
- [142] Shukla AK, Singh G, Ghosh E. Emerging structural insights into biased GPCR signaling. *Trends Biochem Sci* 2014;39:594–602.
- [143] Hu W-S, Pathak VK. Design of retroviral vectors and helper cells for gene therapy. *Pharmacol Rev* 2000;52:493–511.
- [144] Backliwal G, Hildinger M, Kuettel I, Delegrange F, Hacker DL, Wurm FM. Valproic acid: a viable alternative to sodium butyrate for enhancing protein expression in mammalian cell cultures. *Biotechnol Bioeng* 2008;101:182–9.
- [145] New England BioLabs. NEB <https://www.neb.com/>.
- [146] VanGuilder HD, Vrana KE, Freeman WM. Twenty-five years of quantitative PCR for gene expression analysis. *Biotechniques* 2008;44:619–26.
- [147] Promega Corporation. Promega [www.promega.com](http://www.promega.com).
- [148] Broussard JA, Rappaz B, Webb DJ, Brown CM. Fluorescence resonance energy transfer microscopy as demonstrated by measuring the activation of the serine/threonine kinase Akt. *Nat Protoc* 2013;8:265–81.
- [149] Pomerantz SH. The Tyrosine Hydroxylase Activity of Mammalian Tyrosinase. *J Biol Chem* 1966;241:161–9.
- [150] Enzo Life Science I. Enzo Life Science [enzolifesciences.com](http://enzolifesciences.com).
- [151] Nordstedt C, Fredholm BB. A modification of a protein-binding method for rapid quantification of cAMP in cell-culture supernatants and body fluid. *Anal Biochem* 1990;189:231–4.
- [152] Bank RPD. RCSB Protein Data Bank - RCSB PDB
- [153] Morris GM, Huey R, Lindstrom W, Sanner MF, Belew RK, Goodsell DS, et al. AutoDock4 and AutoDockTools4: Automated docking with selective receptor flexibility. *J Comput Chem* 2009;30:2785–91.
- [154] Computing GC, Inc. Molecular Operating Environment (MOE) 2014.09 2014.



## 8. Appendices

### Appendix 1

Alignments of human and mouse GPR143 and tyrosinase. Conserved amino acids are indicated with a straight line, double dots (:.) and single dots (.) indicate conserved and semi-conserved amino acids, respectively. Alignments are performed using EMBOSS Needle.

#### Human and mouse GPR143 amino acid sequences: 79% identity and 85% similarity

hGPR143	1	MASPRLGTFCCPTRDAATQLVLSFQPRAFHALCLGSGGLRRLALGLLQLLP	50
mGPR143	1	MASPRLGIFCCPTWDAATQLVLSFQPRVHFALCLGSGTLRLVLGLLQLLS	50
hGPR143	51	GRRPAGPGSPATSPASVIRLRAAAACDLLGCLGMVIRSTVWLGFNPFVD	100
mGPR143	51	GRRSVGHRAPATSPAASVHILRAATAADLLGCLGIVIRSTVWIIAYPEFIE	100
hGPR143	101	SVSDMNHTEIWPAAFVCGSAMWIQLLYSACFWWLFCYAVDAYLVIRRSAG	150
mGPR143	101	NISNVNATDIWPATFCVGSAMWIQLLYSACFWWLFCYAVDVYLVIRRSAG	150
hGPR143	151	LSTILLYHIMAWGLATLLCEGAAMLYYPSVSRCEGLDHAIPHYVTMYL	200
mGPR143	151	RSTILLYHIMAWGLAVLLCEGAVMLYYPVSRCEGLDHAIPHYVTTYL	200
hGPR143	201	PLLLLVANPILFQKTVTAVASLLKGRQGIYTENERRMGAVIKIRFFKIM	250
mGPR143	201	PLLLLVANPILFHKTVTSVASLLKGRKGVYTENERLMGAVIKTRFFKIM	250
hGPR143	251	LVLII CWLSNIINESLLFYLEMQTDINGGSLKPVRTAAKTTWFIMGILNP	300
mGPR143	251	LVLII ACWLSNIINESLLFYLEMQPDIHGSLKRIQNAARTTWFIMGILNP	300
hGPR143	301	AQGFLLSLAFYGTGCSLGFQSPRKEIQWESLTTSAAEGAHPSPL---MP	347
mGPR143	301	AQGLLSLAFYGTGCSLDVHPPKMVIQWETMTASAAEGTYQTPVRSCVP	350
hGPR143	348	HENPASGKVSQVGGQTSDEALSMLSEGS DASTIEIHTASESCNKNEG DPA	397
mGPR143	351	HQNPR--KVVCVGGH TSDEVLISLSEDS DASTVEIHTATGSCNIKEVD SI	398
hGPR143	398	LPTHGDL 404	
mGPR143	399	SQAQGEL 405	

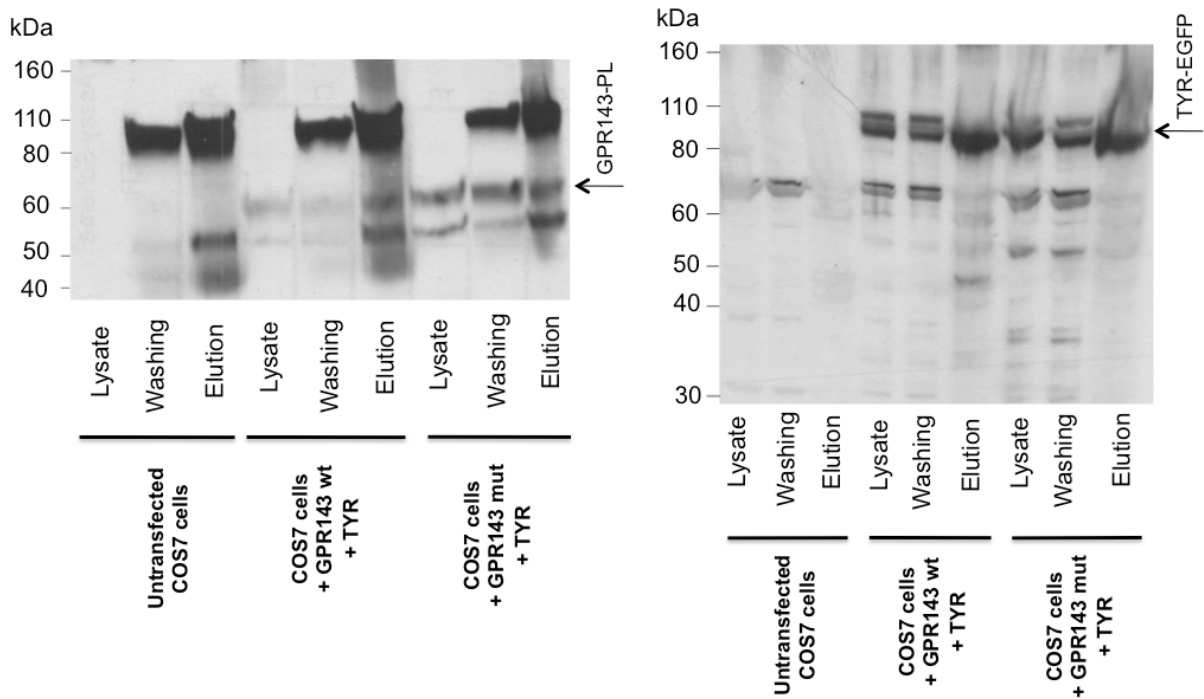
#### Human and mouse tyrosinase amino acid sequences: 86% identity and 92% similarity

mTyr	1	MFLAVLYCLLWSFQISDGHFPRACASSKNLLAKECCPPWMDGSPCGQLS	50
hTyr	1	MLLAVLYCLLWSFQTSAGHFPRACVSSKNLMEKECCPPWSDRSPCGQLS	50
mTyr	51	GRGSCQDILLSSAPSGPQFPFKGVDDRESWPSVIFYNRTCQCSGNFMGFNC	100
hTyr	51	GRGSCQNILLSNAPLGPQFPFTGVDDRESWPSVIFYNRTCQCSGNFMGFNC	100
mTyr	101	GNSKFGFGGPNCTEKRVLIRRNIFDLSVSEKNKFFSYLTLAKHTISSVYV	150
hTyr	101	GNCKFGFWGPNCTERRLLVRRNIFDLSEKPEKDFAYLTLAKHTISSDYV	150

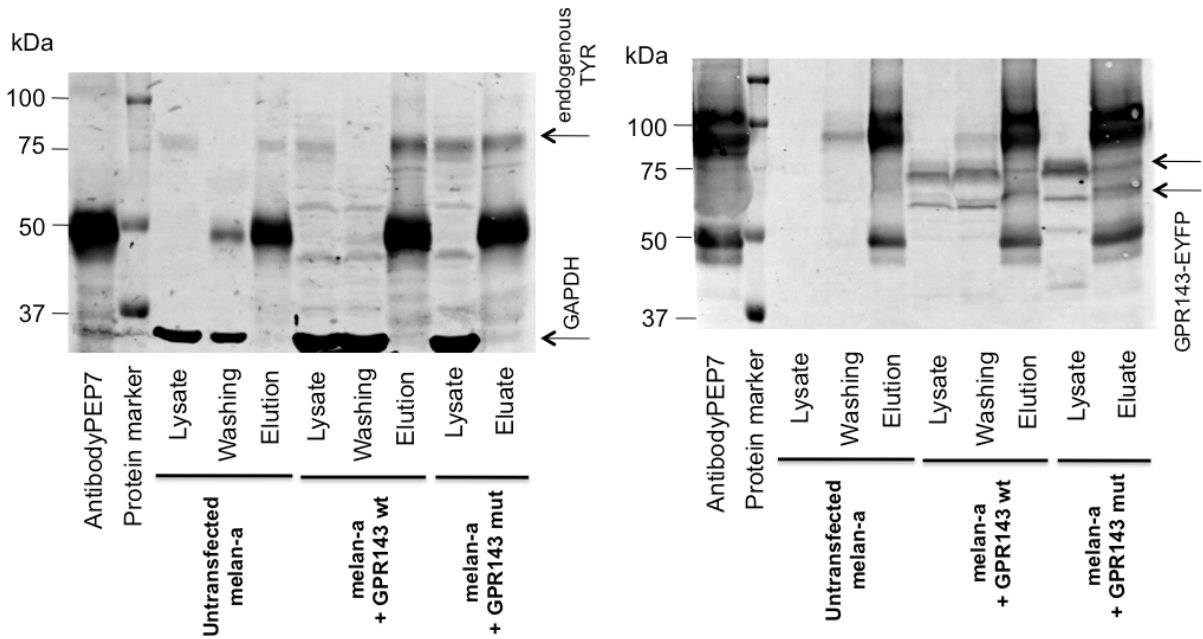
mTyr	151	IPTGTYGQMNGSTPMFNDINIYDLFVVMHYVSRDTLLGGSEIWRDIDF	200
hTyr	151	IPIGTYGQMKNKNGSTPMFNDINIYDLFVVMHYVSM DALLGGSEIWRDIDF	200
mTyr	201	AHEAPGF L PWHRLFLLLWEQEIRELTGDENFTVPYWDWRDAENC DICTDE	250
hTyr	201	AHEAPAF L PWHRLFLLRWEQEIQKLTGDENFTIPYWDWRDAEKDC DICTDE	250
mTyr	251	YLGGRHPENPNLLSPASFFSSWQIICSRSEEYN SHQVLC DGTPEGPLLRN	300
hTyr	251	YMGGQHPTNP NLLSPASFFSSWQIVCSRLEEYN SHQSLCNGTPEGPLRRN	300
mTyr	301	PGNHDKAKTPRLPSSADVEFCLSLTQYESGSM DRTANF SFRNTLEVFASP	350
hTyr	301	PGNHDKSRTPRLPSSADVEFCLSLTQYESGSM DKAANF SFRNTLEGFASP	350
mTyr	351	LTGIADPSQSSMHNALHIFMNGTMSQVQGSAN DP I FLLH HAFVDSIFEQW	400
hTyr	351	LTGIADASQSSMHNALHIY MNGTMSQVQGSAN DP I FLLH HAFVDSIFEQW	400
mTyr	401	LRRHRPLLEVYPEANAPIGHNRDSYMPFIPLYR NGDFFITSKDLGYDYS	450
hTyr	401	LRRHRPLQEVYPEANAPIGHNRDSYMPFIPLYR NGDFFISSKDLGYDYS	450
mTyr	451	YLQESDPGFYRNIIEPYLEQASRIWPWLLGAALV GAVIAAALSGLSSRLC	500
hTyr	451	YLQSDPDSFQDYIKSYLEQASRIWSWLLGAAMV GAVLTALLAGLVSLLC	500
mTyr	501	LQKKKKKKQPQEERQPLLMDKDDYHSLLYQSHL	533
hTyr	501	---RHKRKQLPEEKQPLLMEKEDYHS-LYQSHL	529

## Appendix 2

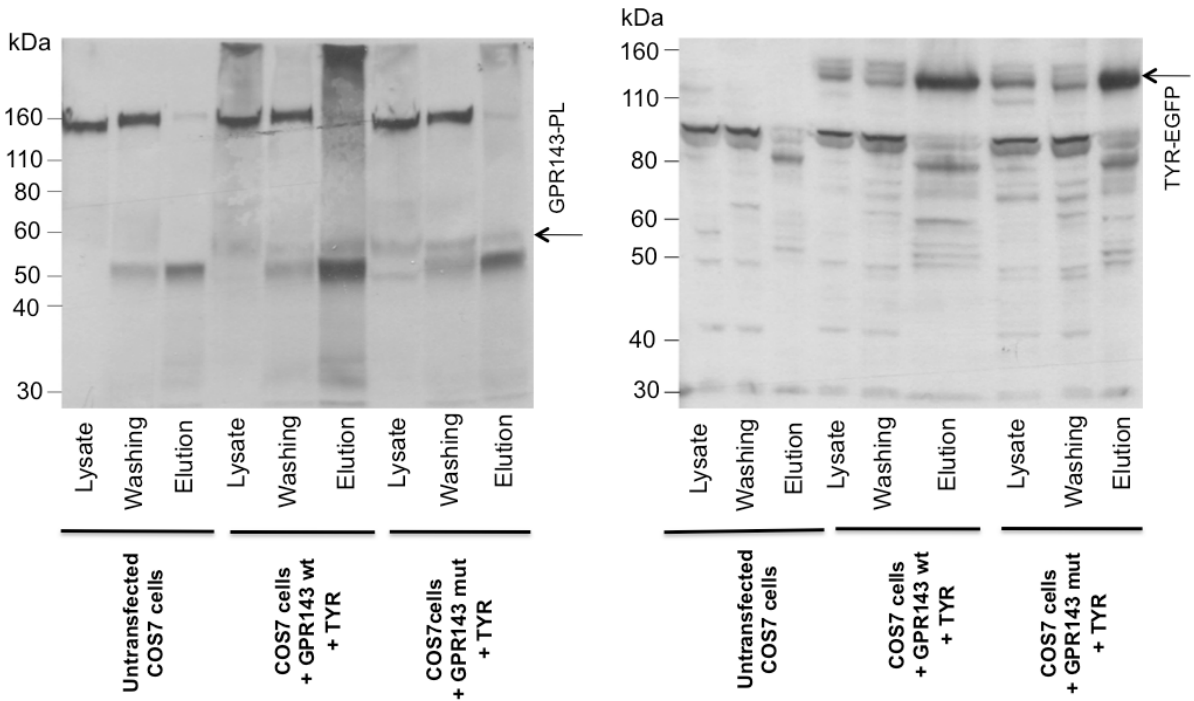
### Immunoprecipitation Western Blots - COS7 cells transfected with GPR143-PL and TYR-EGFP - Immunoprecipitation realized with anti-GFP antibody



**Immunoprecipitation Western Blots - melan-a cells transfected with GPR143-EYFP - Immunoprecipitation realized with anti-PEP7 antibody (against tyrosinase)**



**Immunoprecipitation Western Blots - COS7 cells transfected with GPR143-PL and TYR-EGFP – Immunoprecipitation realized with anti-ProLink antibody**



## 9. Abbreviations

ADA	Adenosine deaminase
ADP	Adenosine diphosphate
AMP	Adenosine monophosphate
ARs	Adenosine receptors
ARPE-19 cells	Arising retinal pigment epithelia cell (from a 19-years old man)
ATP	Adenosine triphosphate
BAY60-6583	2-[6-amino-3,5-dicyano-4-[4 (cyclopropylmethoxy)phenyl]pyridin-2-ylsulfanyl]acetamide
B <sub>max</sub>	Measure of receptor density in membranes
BSA	Bovine serum albumin
CADO	2-chloroadenosine
cAMP	Cyclic adenosine-3',5'-monophosphate
CCPA	2-Chloro-N6-cyclopentyladenosine
cDNA	Complementary DNA
eCFP	(enhanced) Cyan fluorescent protein
CGS21680	(2- <i>p</i> -[2-carboxyethyl]phenethylamino)-5'-N-ethylcarboxamidoadenosine
CHO cells	Chinese Hamster Ovary cells
Ci	Curie (1 Ci = 37 GBq)
CI-IB-MECA	1-[2-chloro-6-[[3-iodophenyl)methyl]amino]-9H-purin-9-yl]-1-deoxy-N-methyl-β- <i>D</i> -ribofuranuronamide
COS7 cells	CV-1 (simian) in Origin and carrying the SV40 genetic material
CPA	N6-cyclopentyladenosine
cpm	Counts per minute
DAPI	4',6-diamidino-2-phenylindole
DMEM	Dulbecco's Modified Eagle Medium
DMSO	Dimethylsulfoxide

DNA	Deoxyribonucleic acid
dNTP	Deoxynucleoside triphosphate
DOPA	Dopamine
DTT	Dithiothreitol
EC <sub>50</sub>	50% effective concentration
ECL	Extracellular loop
<i>E. coli</i>	<i>Escherichia coli</i>
EDTA	Ethylene diamine tetracetic acid
EE	Early endosome
EGF	Epidermal growth factor
ELISA	Enzyme-linked immunosorbent assay
ER	Endoplasmatic reticulum
f	forward
FCS	Fetal calf serum
FRET	Fluorescent Resonance Energy Transfer
G418	Geneticin
GAPDH	Glyceraldehyde 3-phosphate dehydrogenase
GF/B	Glass fiber filter type B
eGFP	(enhanced) Green fluorescent protein
GPCRs	G protein-coupled receptors
h	Human
HA	Haemoagglutinin (tag)
HBSS	Hank buffer salt solution
HEPES	4-(2-hydroxyethyl)-1-piperazine ethanesulfonic acid
HTS	High throughput screening
IBMX	Isobutylmethylxanthine

IC <sub>50</sub>	50% inhibitory concentration
ICL	Intracellular loop
IP	Immunoprecipitation
K <sub>D</sub>	Dissociation binding constant
kDa	Kilo Dalton
K <sub>i</sub>	Inhibition constant
LB medium	Luria-Bertani medium
L-DOPA	Levodopa
min	Minutes
MITF	Microphthalmia-associated transcription factor
MNT-1 cells	Human melanoma cell line
mRNA	Messenger ribonucleic acid
MRP	Melanin-related proteins
MSX-2	(3-(3-hydroxypropyl)- 7-methyl-8-(m-methoxystyryl)-1-propargylxanthine)
MTT	3-(4,5-dimethylthiazol-2-yl)-2,5-diphenyltetrazolium bromide
MVBs	Multivesicular bodies
NECA	5'-N-ethylcarboxamidoadenosine
OA1	Ocular Albinism type I
PCR	Polymerase chain reaction
PBS	Phosphate buffered saline
PDB ID	Protein Data Bank identification code
PEI	Polyethyleneimine
PL	ProLink (tag)
Pmel17	Premelanosome protein 17
PSB-15826	2-(4-(4-fluorophenyl)piperazin-1-yl)ethylthioadenosine
PTU	Propylthiouracil

qPCR or RT-PCR	Quantitative or reverse transcription polymerase chain reaction
Ro20-1724	4-(3-butoxy-4-methoxyphenyl)methyl-2-imidazolidone
ROI	Region of interest
RPE	Retinal pigment epithelium
<i>R</i> -PIA	( <i>R</i> )-N <sup>6</sup> -phenylisopropyladenosin
rpm	Rotations per minute
RPMI	Roswell Park Memorial Institute medium
RT	Room temperature
rv	reverse
SDS-PAGE	Sodium dodecyl sulfat – Poly Acrylamide Gel Electrophoresis
SEM	Standard error of the mean
siRNA	Silencing RNA
TAE buffer	Tris-Acetate-EDTA buffer
T <sub>m</sub>	Melting temperature
TMD	Transmembrane domain
TRP1/2	Tyrosinase-related protein 1 or 2
TRIS	2-amino-2-hydroxymethyl-propane-1,3-diol (tris(hydroxyl methyl)amino methane)
Triton X-100	t-octylphenoxy polyethoxy ethanol
TYR	Tyrosinase
UK432097	2-(3-(1-(pyridin-2-yl)piperidin-4-yl)ureido)ethyl-6-N-(2,2-diphenylethyl)-5'-N-ethylcarboxamido adenosine-2-carboxamide
wt	Wildtype
XAC	Xanthine amine congener
eYFP	(enhanced) Yellow fluorescent protein
ZM241385	4-(2-[7-amino-2-(2-furyl)[1,2,4]triazolo[2,3-a][1,3,5]triazin-5-ylamino]ethyl)phenol

## 10. Curriculum vitae

### Publications

**De Filippo E.**, El-Tayeb A., Schiedel A.C. and Müller C.E. (*in preparation*). Characterization of human adenosine A<sub>2A</sub> receptor chimera.

**De Filippo E.**, Namasivayam V., Zappe L., El-Tayeb A., Schiedel A.C. and Müller C.E. Role of extracellular cysteine residues in the adenosine A<sub>2A</sub> receptor. *Purinergic Signalling* (2016)

**De Filippo E.**, Schiedel A.C. and Manga P. GPR143-tyrosinase interaction as a measure of melanosome maturity. *Submitted*.

**De Filippo E.**, Manga P. and Schiedel A.C. (*in preparation*). Identification of novel GPR143 ligands useful as pharmacological tools.

### Poster presentations

**De Filippo E.**, Danish A., Manga P., Schiedel A. C. *Establishment of a high throughput screening assay suitable for the G protein-coupled receptor 143*. “Horizons in Molecular Biology” International PhD Student Symposium. 8-11 October, 2012 – Göttingen, Germany.

**De Filippo E.**, Manga P., Schiedel A. C. *Human GPR143 and its interaction partners*. 18<sup>th</sup> Meeting European Society for Pigment Cell Research (ESPCR 2013). 9-12 September, 2013 – Lisbon, Portugal – Universidade Nova de Lisboa.

**De Filippo E.**, Mobarec J. C., Kolb P., Schiedel A. C. *Cloning and expression optimization in HEK293 cells for ligand screening*. GLISTEN GPCR spring conference - 28-30 April, 2014 - Biomedical Research Park, Barcelona, Spain.

**De Filippo E.**, Seibt B. F., Schiedel A. C. , Müller C. E. *A<sub>2A</sub>/A<sub>2B</sub> adenosine receptor subtype-selectivity is defined by the extracellular loop 2*. Purines 2014 - Nucleotides, nucleosides and nucleobases – International Conference on Signalling, Drugs and Targets. 23-27 July 2014 – University of Bonn, Germany.



**De Filippo E.**, Seibt B. F., Schiedel A. C., Müller C. E. *Role of the extracellular loop 2 in A<sub>2A</sub> and A<sub>2B</sub> adenosine receptors*. Adenosine receptors: present and future challenges. 2-3 March, 2015 – Uppsala University, Sweden.

**De Filippo E.**, Manga P., Schiedel A. C. *Switching off G-protein coupled receptor 143 (GPR143)*. 40<sup>th</sup> Congress of the Federation of European Biochemical Societies (FEBS). 4-9 July, 2015 – Berlin.

**De Filippo E.**, Namasivayam V., Zappe L., Schiedel A. C., Müller C. E. *Are extracellular disulfide bonds essential for adenosine A<sub>2A</sub> receptor function?* Biochemical Society conference. GPCRs: Beyond Structure Towards Therapy – 16-18 September, 2015 - Monash University Prato, Italy.

## **Workshops**

- Course for protection against ionizing radiation | September 2014 | University of Bonn
- Lenti- and Retroviral vectors and viral gene transfer | November 2012 | University of Bonn, Prof. A. Pfeifer
- Haemophilia A therapeutics: from plasma-derived products to personalized cell-based therapies | March 2013 | University of Bonn, Prof. J. Oldenburg
- Databases, molecular biology tools and visualization of 2D and 3D models | November 2013 | University of Bonn, PD Dr. A. Schiedel
- Research Ethics workshop | July 2012 | German Reference Center for Ethics in the Life Sciences (DRZE) and Institute of Science and Ethics (IWE)
- Communication and presentation skills workshop | July 2012 | Zweirat – Beratung and Training, R. Koetter
- Microscopy and Quantitative Histology workshop | December 2015 | Prof. Dr. Daniel A. Peterson, University of Bonn

## 11. Acknowledgments

Foremost, I am deeply grateful to my supervisor Prof. Dr. Christa E. Müller. I would like to thank you for providing me the opportunity and funding to work in your stimulating group. I am grateful for your patient and scientific discussion which made you a great mentor. She taught me how good science is done. Your support and guidance made my PhD thesis possible.

Furthermore, I would like to thank my co-supervisor PD Dr. Anke C. Schiedel. Working with you has been a great pleasure for me. You have been a steady influence during my PhD career, you supported me with care and discussions with you always led to new ideas. Your enthusiasm and dedication for research was contagious and motivational for me even during tough times. I appreciate all your contributions of time, advice and funding which made my PhD experience stimulating and productive.

I would like to thank Prof. Dr. rer. nat. Evi Kostenis for her time and acceptance to act as co-examiner in my PhD examination committee.

I would like to acknowledge PD Dr. Stefan Goertz for his time and acceptance to act as external co-examiner in my PhD examination committee.

I would like to deeply thank Prof. Prashiela Manga for providing me the opportunity to spend two amazing months at the New York University working in her hearty group. I appreciate your scientific advices, enthusiasm and proofreading of many papers.

I would like to thank NRW International Graduate Research School BIOTECH PHARMA and Bonn International Graduate School of Drug Sciences (BIGS DrugS) for PhD fellowships, interesting workshops and for introducing me into an international scientific environment.

I would like to acknowledge Dr. Vigneshwaran Namasivayam for taking care of the molecular modeling in my thesis and for his kind help in paper revision. In addition, I am grateful to Dr. Ali El-Tayeb for providing me a great compound of his library which upgraded my thesis work.

I am deeply grateful to Dr. Dominik Thimm for his excellent scientific advices. I was really inspired by your creativity and dedication.

I would like to thank Dr. Sonja Hinz for her useful suggestions during FRET experiments and good discussions.

I am really grateful to my office colleagues Azeem Danish and Muhammad Rafehi for the fantastic and friendly atmosphere.

I want to thank present and past members of the AK Müller group: it was a pleasure for me to get to know and to collaborate with many great and skillful people. Thank you for the amazing time inside and outside the lab. A particular thanks to Clara Schoeder for her effort in teaching me German and to Lukas Zappe for helping me to finish my project.

I am really grateful to Genevieve Torres and Martha Vega for teaching me incredible techniques and for the incommensurate help during my stay at the New York University. A particular thank goes to Omotayo Arowojolu and all other Manga lab members for the amazing and fun time at the institute and in the city.

I would like to thank Dr. Ralf Mayer and the colleagues of 7<sup>o</sup> semester for giving me the opportunity to learn and encouraging me to do my best.

I really appreciated the lovely support of Prof. Barbara Gatto who made my connection with Dr. Anke Schiedel possible.

This PhD thesis would not have been possible without the infinite support of my parents. Thanks for always encouraging and endorsing me. I would like to thank my entire family for their immense love.

Finally, I would like to express my sincere love and gratitude to all my friends in Bonn and Italy. In particular, I would like to acknowledge Alberto, Anna and Martina for the emotional support, entertainment and care they provided being like a second family to me.